Universität Hamburg

DER FORSCHUNG | DER LEHRE | DER BILDUNG

External injection of electron beams into plasma-wakefield accelerators

**Dissertation zur Erlangung des Doktorgrades im Fachbereich Physik
an der Fakultät für Mathematik, Informatik und Naturwissenschaften
der Universität Hamburg**

Vorgelegt von

Sarah Schröder

aus Heidelberg

Hamburg 2021

Betreuer	Dr. Jens Osterhoff
Gutachter der Dissertation	Prof. Dr. Brian Foster
	Dr. Jens Osterhoff
	Prof. Dr. Olle Lundh
Zusammensetzung der Prüfungskommission	Dr. Jens Osterhoff
	Prof. Dr. Brian Foster
	Prof. Dr. Erika Garutti
	Prof. Dr. Gudrid Moortgat-Pick
	Prof. Dr. Daniela Pfannkuche
Vorsitzende der Prüfungskommission	Prof. Dr. Daniela Pfannkuche
Vorsitzender des Promotionausschusses	Prof. Dr. Wolfgang Hansen
Dekan der Fakultät für Mathematik Informatik und Naturwissenschaften	Prof. Dr. Heinrich Graener
Datum der Disputation	6th August, 2021

Abstract

Plasma wakefields enable $\mathrm{GeV\,m^{-1}}$-level acceleration gradients, making them a promising avenue to reduce the size and the associated costs of future particle accelerators. High-energy physics facilities in particular place stringent demands on beam quality and energy efficiency, which necessitates precise control of the beam acceleration. Injecting an external electron bunch with predefined and controllable properties into beam-driven plasma wakefields is ideally suited to investigate the beam–plasma interaction in detail. This cumulative dissertation was carried out at the FLASHForward facility, and is driven by the overarching goal of advancing the understanding of this beam–plasma interaction from an experimental perspective and thereby promoting the precise control of the acceleration process.

Initial studies dealt with the preparation of the wake-driving as well as the injected electron bunch in both the transverse as well as the longitudinal plane for the interaction with the plasma. A new method for measuring transverse beam parameters has been implemented based on beam-jitter measurements in beam-position monitors, thereby enabling non-invasive fast-feedback control for the tedious process of matching the transverse phase space to the focusing forces prevalent in plasma wakes, which is essential for efficient and high-quality acceleration. Crucial acceleration parameters such as the transformer ratio, the energy transfer efficiency as well as the resulting energy spectrum of the accelerated bunch are strongly related to the detailed wakefield shape, which can be changed via beam loading and requires the ability to precisely shape the current profiles of both the wake-driving bunch and the accelerated bunch. To achieve this, a device of three finely adjustable collimators was implemented in the FLASHForward beam line, enabling current-profile modifications at the femtosecond-level through energy collimation in a dispersive section of an electron bunch with a strongly correlated longitudinal phase space. With the capabilities of these new tools, an operating point with an acceleration gradient of $1.3\ \mathrm{GeV\,m^{-1}}$ was accomplished at which the energy spread as well as the charge of the injected bunch was preserved while achieving an energy-transfer efficiency of 42%. The characteristic shape of the plasma wakefield can also be used to reduce a remaining correlated energy spread, which has been demonstrated with a dechirping strength of $1.8\ \mathrm{GeV\,mm^{-1}\,m^{-1}}$. To achieve unprecedented control over plasma-based accelerators, new developments are required to diagnose the acceleration process, with the shape of the wakefields being of major interest. As the backbone of this work, a new method was invented to measure the longitudinal wakefield that effectively acts on the wake-driving and the externally injected electron bunch over the entire interaction length. This novel sampling method for beam-driven plasma wakefields enables femtosecond-resolved insights into the acceleration process and now permits it to be optimised routinely.

Kurzfassung

Plasma-Nachlauffelder ermöglichen Beschleunigungsgradienten in der Größenordnung von $GeV\,m^{-1}$ und sind damit ein vielversprechender Ansatz um Teilchenbeschleuniger zukünftig kompakter bauen zu können und so deren Kosten zu reduzieren. Beschleunigeranlagen der Hochenergiephysik haben besonders hohe Anforderungen die Energieeffizienz als auch die Strahlqualität betreffend, eine präzise Steuerung der Beschleunigung ist daher unerlässlich. Das Einsetzen eines externen Elektronenbündels in strahlgetriebene Plasma-Nachlauffelder mit vom anschließenden Beschleunigungsprozess unabhängig einstellbaren Eigenschaften ist ideal geeignet, um die Wechselwirkung zwischen dem Elektronenbündel und dem Plasma im Detail zu untersuchen. Die vorliegende kumulative Dissertation wurde an der FLASHForward-Anlage durchgeführt und ist motiviert durch das übergeordnete Ziel, das Verständnis über die Strahl-Plasma-Wechselwirkung aus experimenteller Sicht zu verbessern und die präzise Steuerung des Beschleunigungsprozesses zu ermöglichen.

Erste Studien befassen sich mit der Vorbereitung der transversalen und longitudinalen Eigenschaften der Elektronenbündel. Für eine effiziente und qualitativ hochwertige Beschleunigung, muss der transversale Phasenraum der Elektronenbündel an die im Plasma vorherrschenden Fokussierungskräfte angepasst werden. Es wurde ein neues Verfahren zur Bestimmung der transversalen Strahlparameter implementiert, was die Einstellung des Strahlfokus auf den Plasmakanaleingang durch eine schnelle Bewertung erleichtert. Die Optimierung der Beschleunigungseffizienz, des Transformationsverhältnisses als auch des resultierenden Energiespektrums kann mittels Verformen der beschleunigenden Felder durch die Anpassung der Ladungslast, also der Stromprofile beider Elektronenbündel, erreicht werden. Hierfür wurde ein Gerät mit fein einstellbaren Kollimatoren konzipiert und in einen dispersiven Abschnitt der Strahllinie implementiert, welches erlaubt das Stromprofil von Elektronenbündel mit einem stark korrelierten longitudinalen Phasenraum effektiv mit Femtosekunden-Präzesion zu modifizieren. Mit Hilfe dieser neuen Werkzeuge konnte schließlich ein Arbeitspunkt gefunden werden, bei dem Elektronenbündel mit einem Gradienten von $1.3\,GeV\,m^{-1}$ beschleunigt wurden, während die Energiebreite als auch die Ladung des beschleunigten Elektronenbündels erhalten werden konnte, und gleichzeitig eine Energieübertragungseffizienz von etwa 42% erreicht wurde. Die charakteristische Form des longitudinalen Plasma-Nachlauffeldes kann außerdem genutzt werden, um den korrelierten longitudinalen Phasenraum eines eingehenden Elektronenbündels zu korrigieren, was mit einer Stärke von $1.8\,GeV\,mm^{-1}\,m^{-1}$ demonstriert wurde. Um die Steuerung von plasmabasierten Teilchenbeschleuniger zu verbessern, müssen auch die zur Verfügung stehende Diagnostiken weiterentwickelt werden. Kern dieser Arbeit ist die Erfindung einer neuen Methode um die beschleunigenden Felder, die über die gesamte Wechselwirkungslänge effektiv auf die Elektronenbündel einwirken, zu messen und ermöglicht femtosekunden-aufgelöste Einblicke in den Beschleunigungsprozess und begleitet nun dessen routinemäßige Optimierung.

List of publications

The thesis in hand substantially builds upon two first-authored and three co-authored publications. While the two first-authored publications form the backbone of this thesis, the co-authored publications are contentual closely connected to them. The latter represent projects led by others that are a direct result of the work done within the scope of this thesis or for which significant contributions have been made. The publications and the respective description of contributions can be found in *Appendix A*.

First-authored core publications:

- **S. Schröder**, C.A. Lindstrøm, S. Bohlen, G. Boyle, R. D'Arcy, S. Diederichs, M.J. Garland, P. Gonzalez, A. Knetsch, V. Libov, P. Niknejadi, K. Põder, L. Schaper, B. Schmidt, B. Sheeran, G. Tauscher, S. Wesch, J. Zemella, M. Zeng and J. Osterhoff, *High-resolution sampling of a beam-driven plasma wakefield*, Nat. Commun. **11**, 5984 (2020) [1]

- **S. Schröder**, K. Ludwig, A. Aschikhin, R. D'Arcy, M. Dinter, P. Gonzalez, S. Karstensen, A. Knetsch, V. Libov, C.A. Lindstrøm, F. Marutzky, P. Niknejadi, A. Rahali, L. Schaper, A. Schleiermacher, B. Schmidt, S. Thiele, A. de Zubiaurre Wagner, S. Wesch and J. Osterhoff, *Tunable and precise two-bunch generation at FLASHForward*, J. Phys.: Conf. Ser.1596 012002 (2020) [2]

Co-authored core publications:

- C. A. Lindstrøm, R. D'Arcy, M.J. Garland, P. Gonzalez, B. Schmidt, **S. Schröder**, S. Wesch, and J. Osterhoff, *Matching small beta functions using centroid jitter and two beam position monitors*, Phys. Rev. Accel. Beams **23**, 052802 (2020) [3]

- C. A. Lindstrøm, J. M. Garland, **S. Schröder**, L. Boulton, G. Boyle, J. Chappell, R. D'Arcy, P. Gonzalez, A. Knetsch, V. Libov, G. Loisch, A. Martinez de la Ossa, P. Niknejadi, K. Põder, L. Schaper, B. Schmidt, B. Sheeran, S. Wesch, J. Wood, and J. Osterhoff, *Energy-Spread Preservation and High Efficiency in a Plasma-Wakefield Accelerator*, Phy. Rev. Lett. **126**, 014801 (2021) [4]

- R. D'Arcy, S. Wesch, A. Aschikhin, S. Bohlen, C. Behrens, M. J. Garland, L. Goldberg, P. Gonzalez, A. Knetsch, V. Libov, A. Martinez de la Ossa, M. Meisel, T.J. Mehrling, P. Niknejadi, K. Põder, J.-H. Röckemann, L. Schaper, B. Schmidt, **S. Schröder**, C. Palmer, J.-P. Schwinkendorf, B. Sheeran, M.J.V. Streeter, G. Tauscher, V. Wacker, and J. Osterhoff *Tunable Plasma-Based Energy Dechirper*, Phys. Rev. Lett. **122**, 034801 (2019) [5]

Other co-authored articles have been published but are not further discussed in depth in this thesis:

- R. D'Arcy, A. Aschikhin, S. Bohlen, G. Boyle, T. Brümmer, J. Chappell, S. Diederichs, B. Foster, M. J. Garland, L. Goldberg, P. Gonzalez, S. Karstensen, A. Knetsch, P. Kuang, V. Libov, K. Ludwig, A. Martinez de la Ossa, F. Marutzky, M. Meisel,T.J. Mehrling, P. Niknejadi, K. Põder, P. Pourmoussavi, M. Quast, J.-H. Röckemann, L. Schaper, B. Schmidt, **S. Schröder**, J.-P. Schwinkendorf, B. Sheeran, G. Tauscher, S. Wesch, M. Wing, P. Winkler, M. Zeng and J. Osterhof, *FLASHForward: plasma wakefield accelerator science for high-average-power applications*, Phil. Trans. R. Soc. A377, 20180392 (2019)

- V. Libov, A. Aschikhin, J. Dale, R. D'Arcy, K. Ludwig, A. Martinez de la Ossa, T. Mehrling, J.-H. Röckemann, L. Schaper, B. Schmidt, **S. Schröder**, S. Wesch, J. Zemella, J. Osterhoff *FLASHForward X-2: Towards beam quality preservation in a plasma booster*, Nucl. Instrum. Methods Phys. Res., A 909, 80-83 (2018)

- A. Knetsch, B. Sheeran, L. Boulton, P. Niknejadi, K. Põder, L. Schaper, M. Zeng, S. Bohlen, G. Boyle, T. Brümmer, J. Chappell, R. D'Arcy, S. Diederichs, B. Foster, M.J. Garland, P. Gonzalez Caminal, B. Hidding, V. Libov, C.A. Lindstrøm, A. Martinez de la Ossa, M. Meisel, T. Parikh, B. Schmidt, **S. Schröder**, G. Tauscher, S. Wesch, P. Winkler, J. Wood and J. Osterhoff, *Controlled density-downramp injection in a beam-driven plasma-wakefield accelerator* Phys. Rev. Accel. Beams **24**, 101302 (2021)

- R. D'Arcy, A. Aschikhin, C. Behrens, S. Bohlen, J. Dale, L. Di Lucchio, M. Felber, B. Foster, L. Goldberg, J.-N. Gruse, Z. Hu, G. Indorg, A. Knetsch, O. Kononenko, V. Libov, S. Karstensen, K. Ludwig, A. Martinez De La Ossa, F. Marutzky, T. Mehrling, P. Niknejadi, C.A.J. Palmer, P. Pourmoussavi, M. Quast, P. Winkler, J.-H. Röckemann, L. Schaper, J. Schaffran, H. Schlarb, B. Schmidt, **S. Schröder**, J.-P. Schwinkendorf, B. Sheeran, M. J. V. Streeter, G. Tauscher, J. Thesinga, V. Wacker, S. Weichert, S. Wesch, S. Wunderlich, J. Zemella and J. Osterhoff, *FLASHForward - Future-oriented wakefield-accelerator research and development at FLASH*, Proceedings of the 8th International Particle Accelerator Conference (2017)

Contents

CHAPTER 1

High-gradient particle acceleration

The development of high-energy particle accelerators has undoubtedly laid the foundation for groundbreaking discoveries in particle physics that have fundamentally changed our scientific understanding of matter in the last century. With the invention of the cathode ray tube [6] in 1897, the first elementary particle, the electron [7], was discovered and a vigorous debate about the sub-structure of atoms [8–10] was sparked. This was just the beginning of an intensive and thoroughly successful search for the fundamental building blocks of matter and the associated interaction forces—supported by the constant further development of increasingly powerful particle accelerators. The subsequently discovered particles were incrementally embedded into a theoretical framework: the Standard Model of particle physics [11]. Theoretical predictions of particles and their interaction via the fundamental electromagnetic, weak and strong forces of nature could be reliably deduced and lead to new discoveries. The last missing particle in the Standard Model, the Higgs boson, which gives the particles mass, was observed experimentally in 2012 [12, 13] (48 years after its theoretical prediction [14, 15]) in the most powerful particle accelerator ever built: the 27 km-circumference circular Large Hadron Collider [16]. Despite this undisputed success of the Standard Model, many mysteries about the universe persist, such as the description of gravitation, the nature of dark matter and dark energy as well as the prevalence of matter over antimatter (to mention only some of them). Particle physicists' urge to answer these questions has manifested itself over the past decades in a vivid discussion about the construction of a new (even larger) particle collider [17, 18].

Continuous developments in accelerator research have not only paved the way for discoveries in particle physics, but have also created new research fields. Originally regarded as the limiting factor for the maximum attainable particle energy, the energy emitted in the form of photons in circular accelerators, the synchrotron radiation [19], turned out to be an excellent X-ray source [20] for studying the structure of materials at the molecular level. The invention of Free-Electron-Lasers (FELs) [21] now enables the spatio-temporal resolution of the transient dynamics in molecules and atoms on their natural time scale of femtoseconds. The unparalleled brilliance of FEL X-ray pulses particularly enriched the combined efforts to investigate phenomena across chemistry, physics and biophysics [22]. Storage-ring-based X-ray radiation sources just recently reached a zeptosecond time-resolution [23] while FELs are on their way to give unique insights to chemical bonds and reactions of individual molecules [24–26]. With this wealth of scientific applications, particle accelerators contribute to a Nobel Prize in Physics on average every three years (1939–2018) [27]. Moreover, despite

the outstanding role accelerators play in science, only 1% of the more than 30,000 particle accelerators worldwide are dedicated to research [28]. Accelerators are valued tools, especially for a variety of industrial and medical applications. Their applications range from ion implantation in chip technology to sterilisation or cutting tools through to medical diagnostic and cancer therapy devices [29, 30]. The value of advances in accelerator technology to society seems evident.

The sheer size and cost of particle accelerators, however, make them impractical and unaffordable for all but the largest organisations. Depending on the target energy and the application, the size of a particle accelerator ranges from a few meters up to several kilometres. The associated construction costs range from several millions up to tens of billions of Euros [28], the latter being unaffordable for average national economies. Today's largest accelerator facilities therefore rely on close international partnerships and, in addition to these fruitful global collaborations, all kinds of measures are taken to reduce costs, e.g. by reusing and repurposing existing accelerators and the corresponding infrastructure. However, the costs associated with these large machines are often dictated not only by the construction, but also by the operating expenses. Enhancing the energy efficiency of accelerators in operation is a further crucial aspect for reducing the footprint of future facilities and requires special attention in a society that is increasingly sensitised to ecological and social impacts [18]. The greatest opportunities for future accelerator facilities arose from new technologies, and so there is currently an increased research activity to develop a novel acceleration method which can achieve both reduction in size of the machines and an increase in overall efficiency in operation. Such a novel high-gradient accelerator technology could accelerate particles in much smaller devices to a given energy, or accelerate particles over a given distance to unprecedented energies. A whole new future is conceivable in which small particle accelerators are available for mobile use or in which the energy in scientific facilities such as colliders and FELs is significantly increased, which would have a transformative effect across natural, material and life sciences, promising further outstanding discoveries.

Various approaches are being pursued for a new high-gradient particle-acceleration technology, including plasma-based acceleration [31, 32], to which this work is dedicated. In this plasma-based approach, charge-density waves are excited in the plasma that can sustain electric fields with an acceleration gradient of up to hundreds of $\mathrm{GeV\,m^{-1}}$ [33], which is several orders of magnitude larger than that in conventional technologies. The basic concept of particle acceleration using plasma has been successfully demonstrated [34, 35] and, following these successes, a vast research activity has developed in which various acceleration schemes were proposed—each of which has advantages and disadvantages for a particular applications. The work in hand deals specifically with the scheme of beam-driven plasma wakefield acceleration of an externally injected electron bunch—a concept which is mostly relevant for future high-energy high-power applications such as colliders or FELs, since the plasma-wave driver itself (an ultra-relativistic electron beam) is available with high average power and advantageous wall-plug efficiency. Following the demonstration of the basic concepts [36–39], the research focus is rightly shifting towards beam-quality preservation of the accelerated bunch as well as precision control and overall stabilisation of the acceleration process.

The work in hand contributes to this comprehensive common goal, driven by the overarching vision of being able to control and understand the acceleration process with unparalleled precision. Chapter 1 briefly introduces the basic concept of particle acceleration, motivates

the need for high-gradient acceleration technologies, and explains the fundamentals of beam-driven plasma wakefield acceleration. Chapter 2 describes the experimental setup on which this work was carried out. The experimental results are finally discussed in Chapter 3. In Section 3.1, the preparation of the bunches for an optimised interaction with the plasma is investigated. A new technique was implemented to position the beam focus precisely at the entrance of the plasma channel for efficient plasma-wave excitation (Sec. 3.1.1). Furthermore, an advanced collimator device was designed and commissioned (Sec. 3.1.2) to generate two well-synchronised consecutive electron bunches out of one—the leading bunch driving the plasma-wave, the trailing bunch being accelerated in the wave. The ability gained to adjust the current profiles with femtosecond precision with this device enabled precise control of the beam–plasma interaction and, above all, led to the invention of a robust technique for measuring the effective longitudinal electric fields that are experienced by the bunches throughout the interaction with the plasma (Sec. 3.4). Armed with this new level of tunability of the acceleration process, an acceleration condition was established in which the energy spread as well as the charge of the accelerated bunch were preserved and acceleration efficiencies of up to 42% were achieved simultaneously (Sec. 3.2).

1.1 Particle acceleration

The secrets of our universe are hidden in both the largest and smallest structures of matter, and answering the everlasting question of our origin requires research into both. Telescopes search the depths of our universe for new phenomena on the large scale, particle accelerators explore the physics on the very smallest scale, with both having extraordinarily large experiments in common. Telescopes must be big in order to collect enough light from objects millions of light years away and to achieve the required resolution, while the immense size of a particle accelerator is largely due to the technological limitation on the acceleration gradients that must be overcome. The basic concepts of conventional particle acceleration and plasma wakefield acceleration are introduced below, only outlining the fundamentals required to understand the research discussed in this thesis. A more rigorous treatment can be found e.g., in the References [40–44].

1.1.1 The pursuit of ever higher beam energies

The principle of resolving an object in its details is based on a trivial requirement: the probe must be smaller than the object. For an electromagnetic wave probe, the wavelength must be small compared to the object. Visible light (400–700 nm), for instance, is used in optical microscopes to image biological objects, e.g. cells. Resolving sub-atomic structures, however, requires wavelengths in the order of $\lambda < 10^{-15}$ m (e.g. charge radius of a proton [45]) or even smaller. Electromagnetic waves of such short wavelengths, i.e. X-rays, emerge when charged particles are deflected, which is referred to as Bremsstrahlung [46] (or synchrotron radiation if generated in synchrotrons). Since energy conservation must be guaranteed during this radiation, the energy of the emitted photon E_γ is in any case smaller than the kinetic energy of the deflected particle ($E_{kin} \geq E_\gamma$). The wavelength of the emitted photon is related to its energy via:

$$\lambda = \frac{h}{p} = \frac{hc}{E},$$

(1.1)

where h is the Planck constant, c the speed of light, E and p the photon energy and momentum respectively. Particles themselves can also be used as a probe and, according to de Broglie, have an attributed wavelength λ_{dB} [47], for the determination of which Equ. (1.1) also applies, where p and E are then the particle's momentum and energy respectively. This relation (Equ. 1.1) shows how the resolution limit is fundamentally linked to the particle energy. Reaching wavelengths of order $\lambda < 10^{-15}$ m necessitates a particle energy well above 10^{-10} J, i.e. 10^9 eV or in other words: an electron must have passed through a total electric potential of 10^9 V. That is exactly what particle accelerators are needed for.

The exploration of the fundamental constituents of matter does not only rely on investigating today's extant matter, but must also search for short-living particles that may have formed the early stages of our universe and are yet undiscovered. For this, the equivalence of energy and mass $E = mc^2$ postulated by Albert Einstein [48, 49] confronts accelerator physicists with a clear mandate: the heavier the particles they are looking for, the higher the energy that has to be provided. The minimum collision energy—or centre-of-mass energy—needed to produce a particle of rest mass m_0 through the pair-production channel, where a particle and its anti-particle are produced (in order to conserve quantum numbers, momentum and energy), is given by:

$$W \geq 2m_0c^2. \tag{1.2}$$

The heaviest known boson, the Higgs boson, has a mass of 125 GeV c^{-2} and the heaviest known quark, the top quark, has a mass of 173 GeV c^{-2}. In order to discover new particles beyond these masses, beam energies of hundreds of GeV up to the TeV-scale must be provided in future colliders.

1.1.2 Relativistic charged particles in an electromagnetic field

The electromagnetic force is the only known long-range force that also has a relative strength that is many orders of magnitude stronger than gravity. This makes it the only candidate to accelerate particles efficiently, or to be more precise: to accelerate *charged* particles efficiently. Accelerator physics is therefore predominantly concerned with the dynamics of charged particles in the presence of electromagnetic fields.

A first mathematical framework for the interplay of currents or free point-like charged particles with electromagnetic fields was formulated by Maxwell [50]; a more generalised description, however, is given by the Lagrangian formalism. The Lagrange function for a particle with coordinate $\mathbf{r}(t)$, velocity $\mathbf{v}(t)$, charge q and mass m in an externally applied electromagnetic field that is expressed in terms of a vector potential $\mathbf{A}(\mathbf{x},t)$ and scalar potential $\phi(\mathbf{x}, t)$ is given by:

$$\mathcal{L}(\mathbf{r}, \mathbf{v}, t) = -mc^2\sqrt{1 - \frac{\mathbf{v}(t)^2}{c^2}} + \frac{q}{c}\mathbf{v}(t) \cdot \mathbf{A}(\mathbf{r}, t) - q\Phi(\mathbf{r}, t). \tag{1.3}$$

The electric ($\mathbf{E}$) and magnetic ($\mathbf{B}$) field relate to the vector potential $\mathbf{A}$ and the scalar potential ϕ via:

$$\mathbf{E} = -\nabla\phi - \frac{1}{c}\frac{\partial \mathbf{A}}{\partial t}, \tag{1.4}$$

$$\mathbf{B} = \nabla \times \mathbf{A}. \tag{1.5}$$

Solving the Euler-Lagrange equation[1] and substituting Equs. (1.4) and (1.5) results in the equation of motion [51, 52]:

$$\mathbf{F} = \frac{d\mathbf{p}}{dt} = q\mathbf{E} + q(\mathbf{v} \times \mathbf{B}), \qquad (1.6)$$

where $\mathbf{F}$ is the well-known Lorentz force, $\mathbf{p} = \gamma_{rel}m\mathbf{v}$ is the relativistic momentum of the particle with the Lorentz factor $\gamma_{rel} = \sqrt{1 - (\mathbf{v}/c)^2}$. Since $\mathbf{v} \perp (\mathbf{v} \times \mathbf{B})$, the magnetic field cannot perform any work $\int \mathbf{F}d\mathbf{s} = \int \mathbf{F} \cdot \mathbf{v}\,dt = 0$ on the particle and consequently cannot be used for energy gain. In contrast, the longitudinal component of an electric field exerts a force in the direction of motion of a charged particle and is thus suitable for energy gain, which for a charge q in an electric field along the path s is given by:

$$\Delta E = q \int\limits_{s_1}^{s_2} \mathbf{E} \cdot d\mathbf{s} = qU, \qquad (1.7)$$

where U is the total electric potential that has been traversed. Particle acceleration to high energies but in a compact manner therefore requires either high potentials (linear accelerator) or the applied potential must be passed through several times (circular accelerator).

Magnetic fields, on the other hand, act transversely to the direction of propagation of a charged particle ($\mathbf{v} \times \mathbf{B}$) and are therefore used to guide the particles through the usually complex structure of an accelerator—the *beam line*.

Another important implication of Equ. (1.6) is the so-called *Panowsky-Wenzel theorem* [53], which relates in the co-moving frame ($\xi = z - ct$) the transverse change in the longitudinal component of the Lorentz force, F_z, to the longitudinal change in the transverse component of the Lorentz force, $F_\perp$, through[2]:

$$\nabla_\perp F_z = \partial_\xi F_\perp. \qquad (1.8)$$

Thus, if the acceleration force is transversely constant ($\nabla_\perp F_z = 0$), then the focusing force is also not dependent on the longitudinal coordinate ($\partial_\xi F_\perp = 0$). Both will later turn out to be indispensable properties for a stable high-quality acceleration process.

Particle guidance through the accelerator

Particle accelerators are typically complex in structure. The ideal path of a particle through the accelerator, *the nominal orbit*, is given by the physical centre of the beam line elements, and the interesting beam dynamics deals with small deviations from this orbit. It is therefore advisable to introduce a coordinate system whose origin follows the nominal orbit—the

---

1   The Euler-Lagrange equation ensures for any mechanical system a vanishing variation of the integral $\int_{t_0}^{t_1} \mathcal{L}(\mathbf{r}, \mathbf{v}, t)dt$ along a real path:
$\frac{d}{dt}\frac{\partial \mathcal{L}}{\partial \mathbf{v}} - \frac{\partial \mathcal{L}}{\partial \mathbf{r}} = 0$

2   This can be seen wit Equs. (1.4) and (1.5) and the definition of a pseudo-potential $\Psi = (\phi - A_z) \neq 0$:
$F_z = qE_z \approx -q\partial_\xi(\phi - A_z) = -\partial_\xi \Psi$
$F_\perp = q(E_\perp + (v_b \times B)_\perp) \approx q(-\nabla_\perp(\phi - A_z)) = -\nabla_\perp \Psi$

Frenet-Serret coordinate system[1] [54, 55]. This can be pictured as a transverse Cartesian coordinate system that exists at every orbit position in the beam line perpendicular to its tangent vector (see Fig. 1.1). The transverse motion of the particle through the accelerator is then described by the x–x' (and y–y' respectively) *trace space* with:

$$x' = \frac{p_x}{p_s} = \frac{dx}{dt} \Big/ \frac{ds}{dt} = \frac{dx}{ds},$$ (1.9)

where x denotes the coordinate in the transverse planes at the distance s travelled along the nominal orbit, and p_x and p_s are the corresponding transverse and longitudinal momentum respectively.
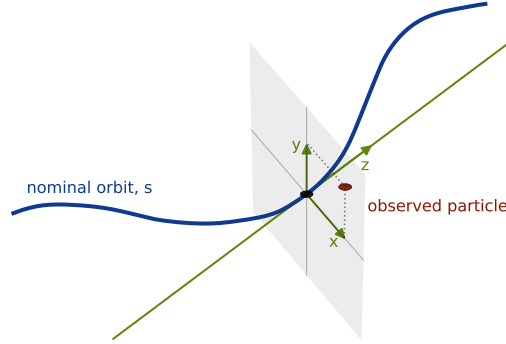

Figure 1.1: Frenet-Serret coordinate system. The coordinate of a particle in an accelerator is given by its s-position along the nominal orbit and the transverse position in a Cartesian coordinate system orthogonal to this orbit.

The performance of an accelerator crucially depends on its ability to keep the particles—and especially the accumulation of many equally charged particles of finite *divergence* ($\langle x'^2 \rangle \neq 0$)—in the vicinity of the nominal orbit. This task is accomplished with different types of magnets. Assuming only *transverse magnetic fields*, small deviations from the nominal orbit and the longitudinal momentum of the particle to be much larger than its transverse momentum (*paraxial approximation*, $p_s \gg p_x$), the magnetic field component $B_y(x)$ [and correspondingly for $B_x(y)$] can be expanded through:

$$B_y(x) = B_{y0} + \frac{dB_y}{dx}x + \frac{1}{2!}\frac{d^2 B_y}{dx^2}x^2 + ...$$ (1.10)

Great efforts are being made to produce magnets, the fields of which only have components of one of the terms of this multi-pole expansion (and the equivalent for the other transverse plane). As such, different magnet types that fulfil different tasks along the beam line can be realised. The x-independent action of a dipole (first term) bends the particles through the structure of a linear accelerator (linac) or constrains them onto the orbit of a circular machine. The linear x-dependent action of a quadrupole (second term) makes it a well-suited element to keep (focus) the particles close to the nominal orbit. Sextupoles (third term) and higher-order magnetic devices are typically used to correct for higher-order beam distortions.

---

[1] Particle position vector: $\mathbf{r}(s) = \mathbf{r}_0(s) + x\hat{x}(s) + y\hat{y}(s)$
     Unit vector tangential to reference orbit: $\hat{s}(s) = \frac{d\mathbf{r}_0(s)}{ds}$
     Unit vectors perpendicular to reference orbit: $\hat{x}(s) = -\rho(s)\frac{d\hat{s}(s)}{ds}$; $\hat{y}(s) = \hat{x}(s) \times \hat{s}(s)$; ρ: beam line curvature

Solving the equation of motion

Assuming only horizontally (x) deflecting dipoles and quadrupoles for beam deflection as well as focusing, the equation of motion of a charge q with a momentum p is given by a set of linear differential equations, also known as *Hill's equation* [40, 41]:

$$x''(s) + K_x(s)x(s) = \frac{1}{\rho(s)}\frac{\Delta p}{p_0} \tag{1.11a}$$

$$y''(s) + K_y(s)y(s) = 0 \tag{1.11b}$$

$$z'(s) = -\frac{1}{\rho(s)}x(s)\frac{\Delta p}{p_0}, \tag{1.11c}$$

where $K(s)$ are the magnet strengths ($K_x(s) = q/p\,\partial_x B(s) + 1/\rho^2(s)$, $K_y(s) = -e/p\partial_x B(s)$), $\rho(s)$ the beam line curvature and $\Delta p = p - p_0$ the momentum deviation from the reference particle that follows the nominal orbit and z the path length difference between the particle's trajectory and the nominal orbit. For the reference particle ($p = p_0 \to \Delta p = 0$), the equations (1.11a) and (1.11b) are both homogeneous differential equations. Due to the generally complex arrangement of different magnets in an accelerator and the associated s-dependency of the restoring force $K(s)$, Hill's equation cannot be directly solved in an analytic manner. However, the individual beam-line elements (magnets, drifts) typically have in good approximation an s-independent restoring force K and Hill's equation becomes a linear differential equation of the second order with the well-known solution of a harmonic oscillator, $x = A\cos(\phi + \phi_0)$. It is therefore useful to parameterise the dynamics through the entire beam line into sections of static magnetic fields by using a *matrix formalism*. For each beam-line component of static magnetic field, an associated 6×6 *transfer matrix* $\underline{\underline{R}}$ is derived from the basic equations of motion, which takes into account the entire physics within the device and transfers the state of the particle in front of the device to its state at the end, $\underline{\underline{R}} : x_0 \mapsto x_1$ where $x_i = (x, x', y, y', z, \frac{\Delta p}{p_0})^T$ is the column vector describing the particle's state. After traversing an arrangement of many beam-line components, called a *lattice*, the final state of the particle is given by the matrix multiplication:

$$\mathbf{x}_1 = \underline{\underline{R}} \cdot \mathbf{x}_0 = \underline{\underline{R}}_n \cdot ... \cdot \underline{\underline{R}}_2 \cdot \underline{\underline{R}}_1 \cdot \mathbf{x}_0. \tag{1.12}$$

With beam deflections only in the x-plane, the beam line has a midplane symmetry about $y = 0$ and the particle motion in x and y is decoupled. The transfer matrix reduces to:

$$R_i = \begin{bmatrix} R_{11} & R_{12} & 0 & 0 & 0 & R_{16} \\ R_{21} & R_{22} & 0 & 0 & 0 & R_{26} \\ 0 & 0 & R_{33} & R_{34} & 0 & 0 \\ 0 & 0 & R_{43} & R_{44} & 0 & 0 \\ R_{51} & R_{52} & 0 & 0 & 1 & R_{56} \\ 0 & 0 & 0 & 0 & 0 & 1 \end{bmatrix}, \tag{1.13}$$

where R_{21}, R_{43} represent the focal length of the magnets in x and y respectively, R_{16}, R_{26} the momentum dispersion and the angular dispersion in the x-plane respectively and R_{56} the longitudinal dispersion.

Dispersion

The trajectory of particles with a momentum different from the reference particle $\Delta p/p \neq 0$ satisfies the inhomogeneous Hills equation (Equ. 1.11a), the solution of which is given by the linear superposition of the homogenous solution $x(s)$ and a momentum-dependent displacement $x_D(s)$:

$$x_g(s) = x(s) + x_D(s) = x(s) + D(s)\frac{\Delta p}{p}, \tag{1.14}$$

where $D(s)$ is the so-called *dispersion function*. Off-momentum particles no longer follow the nominal orbit but a dispersive trajectory x_D and the path length becomes a function of momentum that is determined by the transfer matrix element R_{56}, $\Delta z = R_{56}\Delta p/p$.

This difference in path length is commonly used for subsequent *bunch compression* (see Fig. 1.2) in order to achieve particle bunches with picosecond length and with peak currents at the kA-level, which is difficult to achieve at low energies due to Coulomb repulsion. A monotonic correlation of the longitudinal phase space (z–p_z), also called *chirp*, is impressed on the particle bunch. In the dispersive environment of a magnetic chicane, particles of different energies follow a path of different length. Particles with higher energies follow a longer path, particles with lower energy follow a shorter path, which consequently leads to the compression of a bunch with a monotonically correlated longitudinal phase space. A typical energy spread in high-energy physics accelerators is on the order of percent or permille.
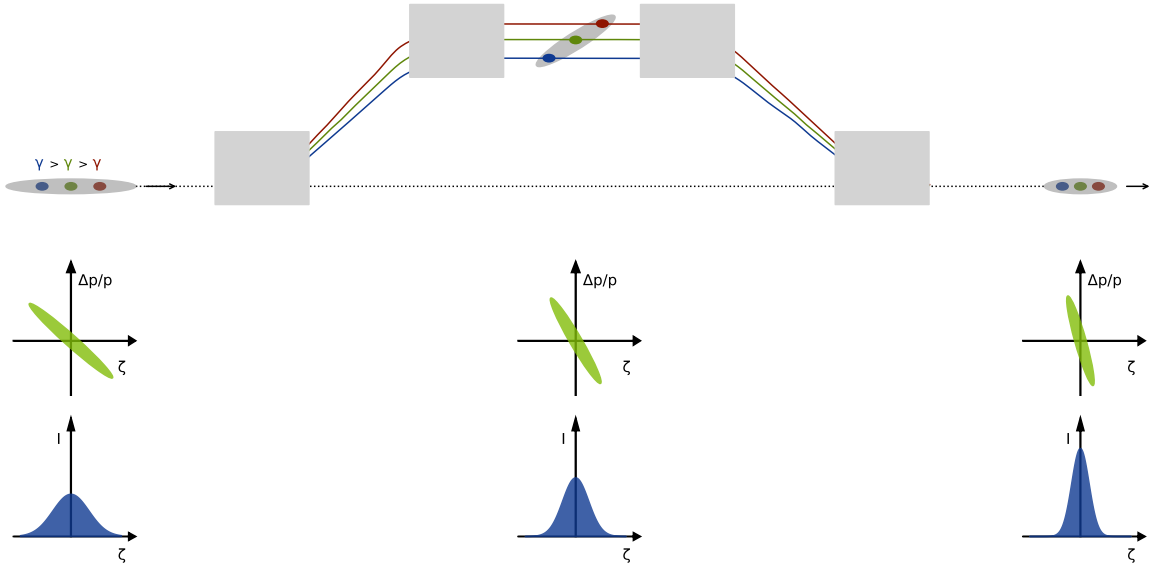

Figure 1.2: Bunch compression in a dispersive section. A particle bunch with a longitudinally correlated energy spread $\Delta p/p$ enters a C-shaped magnet chicane. Particles with higher momentum (blue), the bunch tail, are deflected less than those with a lower momentum (red), the bunch head. The head traverses the chicane on a longer trajectory than the bunch tail, which thus catches up with the bunch head—the bunch is consequently compressed. (Scheme adapted from [56])

Chromaticity

The momentum dependence of the magnet restoring force, $K = q/p \, \partial_x B$, leads to a transverse–longitudinal coupling of the beam dynamics, called *chromaticity*. Particles of higher energy are focused more weakly than those particles with lower energies. For a bunch of finite energy distribution, chromaticity therefore leads to a smeared beam focus. Chromatic bunch deterioration can be compensated by the use of sextupoles but inserts an irreversible non-linearity into the beam dynamics, the discussion of which is beyond the scope of this thesis.

Beam dynamics

Using the transfer-matrix formalism described above, the trajectory of a single particle can be determined along an arbitrarily complex beam-line lattice without the need to directly solve the Hill's Equ. (1.11). However, in order to obtain information about the properties of a collection of many particles, the *particle beam*, this technique has to be expanded. Assuming no transverse deflection ($1/\rho(s) = 0$) and a mono-energetic particle beam ($\Delta p/p = 0$), the Ansatz for a solution of the homogeneous Hill equation (Equ. 1.11a) of a particle beam is:

$$x(s) = \sqrt{\varepsilon \beta(s)} \cos(\phi(s) + \phi_0), \tag{1.15}$$

which represents a transverse oscillation about the orbit, termed *betatron oscillation*. This transverse motion of the beam is marked out by the envelope $\sqrt{\varepsilon \beta(s)}$, where ε is a beam property, called *emittance*, which is determined by the initial conditions of beam generation and remains constant throughout beam transportation. The s-dependent beta function $\beta(s)$ is determined by the field strengths of the focusing devices along the beam line and eventually determines the transverse beam size, making it a very important parameter of beam dynamics. Beam dynamics is concerned with the development of x and x' within the particle ensemble, so that it is useful to express the solution of Hill's equation in the x–x' trace space, where:

$$x'(s) = \frac{dx}{ds} = -\sqrt{\frac{\varepsilon}{\beta(s)}} \left[\alpha(s) \cos\left(\phi(s) + \phi_0\right) + \sin\left(\phi(s) + \phi_0\right) \right], \tag{1.16}$$

with the new variable:

$$\alpha(s) = -\frac{\beta'(s)}{2}. \tag{1.17}$$

Substituting the relation for the trigonometric functions $\cos(\phi(s) + \phi_0)$ from Equ. (1.15) and its derivative into Equ. (1.16) and rearranging leads to:

$$\gamma(s)x^2(s) + 2\alpha(s)x(s)x'(s) + \beta(s)x'^2(s) = \varepsilon, \tag{1.18}$$

with $\gamma(s) = (1 + \alpha^2(s))/\beta(s)$. This function describes an ellipse in the x–x' plane, the area of which is given by the emittance ε. As the particle beam traverses the beam line, the shape of the trace-space ellipse changes but its area remains constant. As a result, linear beam optics is fully described by the parameters $\beta(s)$ and $\alpha(s)$[1]. In a single-pass system such as a linac, the Courant-Snyder parameters [57] α, β, γ of the magnet structure must be *matched*

---

1   For beams of a finite energy distribution, the dispersion $D(s)$ and its derivative $D'(s)$ must be considered.

to the x–x' distribution of the input beam such that the bunch-density contours coincide with the ellipse corresponding to the particle trajectories [58].

Assuming a Gaussian beam profile, the 2D trace-space beam ellipse can be also formulated by a matrix equation $\mathbf{X}^T \Sigma^{-1} \mathbf{X} = 1$, with $\mathbf{X} = (x, x')^T$ and the *sigma matrix*:

$$\Sigma = \left[\begin{array}{cc} \sigma_{11} & \sigma_{21} \\ \sigma_{21} & \sigma_{22} \end{array} \right] = \left[\begin{array}{cc} \langle x^2 \rangle & \langle xx' \rangle \\ \langle xx' \rangle & \langle x'^2 \rangle \end{array} \right] = \varepsilon \left[\begin{array}{cc} \beta & -\alpha \\ -\alpha & \beta \end{array} \right] \tag{1.19}$$

The trace-space of the particle beam can then be tracked through the course of a magnetic structure $\underline{\underline{R}}$ via $\Sigma_2 = \underline{\underline{R}} \Sigma_1 \underline{\underline{R}}^T$. The area of the ellipse is given by $\pi (\det \Sigma)^{1/2} = \pi \varepsilon$ with the emittance (identical equations apply to the y–y' trace space.):

$$\varepsilon_x = \sqrt{\langle x^2 \rangle \langle x'^2 \rangle - \langle xx' \rangle^2}. \tag{1.20}$$

So far, only sections of exclusively focusing devices have been considered. Such focusing sections are usually interleaved with sections of acceleration for which the emittance is no longer a constant. Therefore the *normalised emittance* $\varepsilon_N = \gamma_{rel} \beta_{rel} \varepsilon$ with $\beta_{rel} = v/c$ is introduced, which is proportional to the area in the x–p_x phase space and is invariant under energy change.

1.1.3 Particle beams for high-energy applications

Achieving high particle energies is only part of the challenges in developing an accelerator. Special measures must also be taken to achieve high event rates in particle colliders or a sufficient quality of the radiation in light sources.

In a particle collider, head-on collisions of individual particles within the beam are required. If the two beams are brought to collision, the probability of such a particle-particle interaction, however, is actually relatively low due to the low particle density in the beam compared to e.g., a solid. The rate at which a certain physics event happens in a particle collider is given by the product of the event cross-section and the so-called *luminosity*, which is therefore regarded as a measure of the collider performance. The luminosity is proportional to the product of the colliding beam densities per unit time. Assuming Gaussian-shaped particle beams with cross-section σ_x, σ_y and a total number of N particles each, the luminosity is given by:

$$\mathcal{L} = H_D \frac{1}{4\pi} \frac{N^2}{\sigma_y \sigma_x} f_{rev} n_b \ \propto \ \frac{P_{wall} \, \eta \, N}{\sqrt{\beta_x \varepsilon_x} \sqrt{\beta_y \varepsilon_y}}, \tag{1.21}$$

where n_b denotes the number of equally spaced bunches that collide with a frequency f_{rev}. The factor H_D takes beam–beam effects that typically increase the luminosity by a factor 1.5–2 into account [59]. The luminosity can also be determined in a more technical manner as a function of beam power P_{wall}, energy efficiency η, normalised transverse beam emittance $\varepsilon_{x/y}$ and beta function $\beta_{x/y}$. In general, low-beta insertion into the Interaction Point (IP) and a high beam current is the first approach to increasing luminosity, but is severely limited due to beam-beam interactions [60] and smearing of the beam focus at the IP due to chromatic effects. These causes for the reduction in luminosity have to be assessed more critically in single-pass colliders (i.e. linear collider), where each particle has only one chance of collision. In summary, enhancing the performance of a collider requires special attention to small beam emittances, narrow beam-energy distributions, and high energy efficiencies.
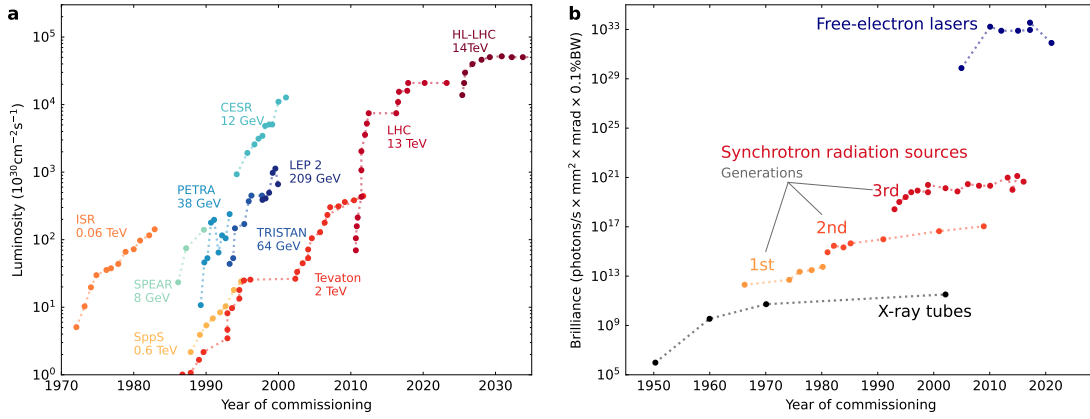
Figure 1.3: Development of achieved luminosity in colliders and brilliance in X-ray sources. a, The luminosity, the measure of event rate, is an essential parameter for the performance of a particle collider. While the energy of a collider typically corresponds to the design value right from the start, the luminosity typically increases over the life time of the collider by many orders of magnitude towards the intended design value. **b**, In X-ray light sources, the decisive parameter for the machine performance is the brilliance, which has made a big leap through fundamentally new technologies from the X-ray tube to the synchrotrons and ultimately to the free-electron lasers. (Data from Ref. [28])

Accelerator-based light sources such as synchrotrons or free-electron lasers have similar demands on the particle beam to achieve high-quality radiation that is expressed through a performance parameter called *brilliance*:

$$B = \left[\frac{\text{photons}}{s \cdot \text{mrad}^2 \cdot \text{mm}^2 \cdot 0.1\%\text{BW}} \right] \propto \frac{I}{\varepsilon_x \varepsilon_y \delta}. \tag{1.22}$$

Since the particle beam is ultimately the source of the radiation, its parameters also determine the properties of the generated radiation. The particle-beam emittance $\varepsilon_{x/y}$ defines the cross-section and the divergence of the radiation, the energy distribution δ determines the radiation bandwidth (BW), the beam current I defines the maximum radiation intensity. Therefore, small beam emittances and a narrow energy distribution are key for coherent and monochromatic X-rays.

Both the luminosity of colliders and the brilliance of X-ray light sources have improved over many orders of magnitude in the last few decades—supported by the constant development of new technologies (see Fig. 1.3). In high-performance machines envisaged for the future, particle beams with parameters of pC charge, kA-level peak currents, ‰-level energy spread, μm-level emittances and an average power in excess of tens of MW average beam power will be pursued. These parameters depend largely on the exact application, but give a rough estimate of what must be supported by a new technology for energy-frontier particle accelerators.

1.1.4 The scale of particle colliders

The most challenging accelerators to build are those used in high-energy physics research centres. Accelerator research therefore plays a pivotal role for the long-term vitality of high-energy physics that ultimately need to extend the energy frontier for colliders. The

permanent urge in particle physics for ever higher beam energies is thus also a permanent urge for new accelerator technologies. Despite continuous advances and groundbreaking inventions, particle accelerators developed into ever larger machines that now reach a size of tens of kilometres.

Accelerating a particle to a certain energy requires that it traverses a correspondingly high electric potential (see Equ. 1.7). The achievable particle energy that can be obtained with the most trivial approach of building an accelerator—applying a direct current potential—depends on the achievable high voltage of rectifiers or generators [62, 63], but is limited to energies up to the MeV-scale due to voltage breakdown. Through successive alternating fields with a suitable phase structure, high particle energies can be achieved without the correspondingly high voltage being required. By bending the particles with magnetic fields on a circular orbit, the same accelerator structure can be run through several times, taking into account the connection between magnetic field strength, particle orbit and the needed phase structure of the acceleration field with the steadily increasing particle energy. With the help of such circular machines (cyclotron, betatron, synchrotron), the energy limit has recently been increased by many orders of magnitude (see Fig. 1.4). The energy gain per revolution that can be achieved in a circular machine is eventually limited by the power loss caused by syn-

Figure 1.4: Particle accelerator energies over the years. Since the first particle accelerators in the 1930s, their energy has continuously increased over many orders of magnitude—supported by many technological advances. Linear accelerators (blue) in particular, however, lag far behind this development. (For reasons of comparability, the energy is plotted as the laboratory energy of a particle that collides with a proton at rest.) (Data from [61])

chrotron radiation, which scales with $\propto \gamma_{rel}^4/R$. This scaling has striking consequences: the minimum radius of a circular machine is not only determined by the maximum achievable bending magnetic fields, but especially by the gamma factor $\sim E/(mc^2)$. As a result, acceleration of light particles such as electrons or positrons to energies above 100 GeV becomes ineffective in circular machines and must be done in a linac where again the achievable *acceleration gradient* is the major limitation for a compact design. Today's high-energy linacs use Radio-Frequency (RF)-waves that are coupled into metallic cavities [64, 65]. A limit to the achievable field gradients in these cavities results from ionisation processes at lattice imperfections of the metal that lead to plasma breakdown when the electric field is raised. Nonetheless, a multi-GeV electron-positron collider with a centre-of-mass energy equal to that of the Higgs particle (a "Higgs factory") has the highest priority for future initiatives of the "European Strategy for Particle Physics" [18] due to the unique scientific insights expected from it. Concrete construction plans for the two most discussed future electron—positron colliders, the International Linear Collider (ILC) [66] and Compact Linear Collider (CLIC) [67], have been in place for many years now. The realisation of such a
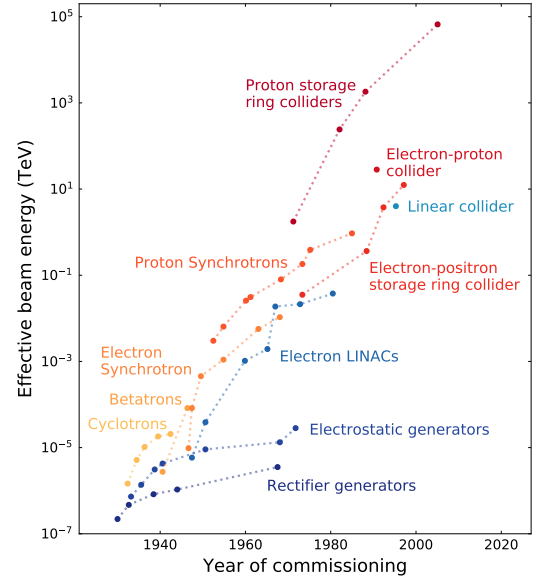
collider, however, is still uncertain due to its large costs. The impressive increase in particle energies over several orders of magnitude in the last century (see Fig. 1.4) was achieved by constant developments in acceleration technology. Despite the great efforts, the growing demand for higher-energy beams has outpaced the progress of conventional accelerator technologies and calls for a paradigm shift. Various approaches are being pursued in order to reduce the size and the related construction cost of such a high-energy collider in the future:

- *Improving resistance to material breakdown in conventional RF technology.* Many different techniques such as deliberate doping [68, 69], special heat treatment [70] or surface coating [71] are investigated. Todays' state-of-the-art super-conducting cavities manufactured in collaboration with industry achieve a maximum field amplitude of about $45\,\mathrm{MV\,m^{-1}}$ [69].

- *Increasing RF pulse frequency.* Newly developed cavities operating at the X-band [72] frequency can sustain electric fields on the order of $120\,\mathrm{MV\,m^{-1}}$ [73].

  Increasing the frequency beyond the radio-frequency range requires non-metallic resonators. Dielectric structures can be operated with optical pulses and have a breakdown damage threshold on the $\mathrm{GV\,m^{-1}}$-scale [74].

- *Change cavity medium.* A more visionary concept is to change the medium that sustains the accelerating electric fields. Dielectric structures are one example. Another approach is to use plasma, which is not bound by electric and material breakdown limitations and therefore can support extraordinary high electric fields—hundreds of $\mathrm{GV\,m^{-1}}$ have been experimentally demonstrated [75].

1.2 Plasma-based acceleration

In plasma-based particle-acceleration schemes, the plasma acts as a mediator for the energy transfer from an ultra-intense beam (particle or laser) to the accelerated particles. The energy is first transferred to the plasma in the form of an excited plasma wave and can then be extracted from the wave by an injected particle bunch. Plasma is not subject to material breakdown and therefore permits electric fields that are orders of magnitude greater than in conventional metallic RF resonators. Aside from these exceptionally high accelerating fields, plasma-based acceleration also allows for high acceleration efficiency—both of which make this technology a promising approach for future particle accelerators.

1.2.1 Fundamental characteristics of plasmas

Plasma is often referred to as the fourth state of matter. This definition follows the analogy to the transition of the states of matter through continuous supply of energy. Heating a solid results in a liquid, further heating results in a gas, and as even more energy is imparted, plasma is eventually created. In this state, the energy supplied exceeds the binding energy of the electrons in the gas molecules[1], the electrons are stripped off and form a gas of charged particles: agile free electrons and positively charged (heavy) nuclei.

---

1 Typical energies required for plasma creation [76]:
   Hydrogen (H_2, dissociation and ionisation): $15\,\mathrm{eV} \approx 17\,500\,\mathrm{K}$
   Argon (Ar, first ionisation level): $14\,\mathrm{eV} \approx 16\,300\,\mathrm{K}$

For use in the laboratory, plasma must be generated in a controlled manner. A common method for this is impact or radiation ionisation, in which energetic particles or radiation impart the energy to the plasma that is required for ionisation [77]. Such an ionisation process is triggered, for example, by a high voltage pulse (known as discharge ionisation), whereby the free electrons that are initially present in the gas gain kinetic energy and cause an ionisation avalanche through collision.

On a macroscopic scale, the plasma is neutral (i.e. quasi-neutral). Local deviations from quasi-neutrality are counteracted rapidly by a non-local collective dynamic of the free charges, driven by the long-range Coulomb force ($\propto r^{-2}$). In other words, the individual charged particles interact simultaneously with many other free charges in the area to restore global neutrality. In an ideal plasma, depending on its density as well as temperature, these macroscopic dynamics dominate over microscopic fluctuations such as collisions, which is a fundamental difference to the dynamics in ordinary gases. The plasma reacts to a charge displacement with an oscillation of the lighter plasma electrons around the equilibrium state of charge neutrality [78], which (assuming collision-free dynamics) is described by an undamped harmonic oscillator with the so-called *plasma frequency ω_p* [79, 80]:

$$\omega_p = \sqrt{\frac{n_p e^2}{\varepsilon_0 m_e}}, \tag{1.23}$$

where n_p is the unperturbed electron density of the plasma; ε_0, e, m_e are the natural constants of the permittivity, the electron charge and mass respectively. The plasma frequency is generally also a measure of the time scale ω_p^{-1} on which the plasma electrons react to any charge disturbance. Notably, the only variable in the plasma frequency is the plasma density, which is therefore the fundamental parameter that determines the dynamics in a plasma. Beyond that, the plasma temperature can change this dynamics in plasmas to the extent that a strong thermal movement can counteract the shielding tendency. In the following theoretical discussions in this work a "cold" plasma, in which these effects are neglected, is assumed throughout. The dynamics of the plasma electrons relevant to the acceleration process occur at much higher energies than the thermal energy, which justifies this approximation.

The idea of using relativistic plasma waves "to approach the problem of constructing accelerators for very high currents and super-high energies of the order of 10^{12} eV and even more" was independently formulated by *Veksler* [31] and *Budker* [32] in 1956 for the first time. It wasn't until two decades later that this idea received greater attention after Tajima and Dawson [33] proposed a plasma-based accelerator in 1979, in which an intense laser pulse excites a wave of plasma electrons via radiation pressure, with the wave propagating at a phase velocity equal to the corresponding laser group velocity. The resulting charge separation leads to enormous electromagnetic fields inside the wake, the longitudinal acceleration gradient of which can reach 100 GeV m^{-1}.

A rough estimate for these large field strengths can be derived from a simplified model of an electrostatic one-dimensional plasma wave $\mathbf{E} \sim \mathbf{E}_0 e^{ik_p z}$ that propagates at a phase velocity equal to the speed of light ($k_p = \omega_p/c$). The electric field prevalent in the plasma wave can be derived through Gauss' law:

$$\nabla \cdot \mathbf{E} = \frac{\varrho}{\varepsilon_0}. \tag{1.24}$$

The maximum fields are reached when the disturbance of the charge density is maximal, i.e. when the charge is fully separated: $\varrho = n_p e$. The state of full charge separation is also referred to as the *wave-breaking limit*, whose longitudinal electric field strength is given by:

$$E_z = \frac{1}{k_p}\frac{\rho}{\epsilon_0} = \sqrt{\left(\frac{m_e c^2}{\varepsilon 0}\right)}\sqrt{n_p} \approx 10\sqrt{\frac{n_p}{10^{16}\,[\mathrm{cm}^{-3}]}}\,\mathrm{GV\,m^{-1}}. \qquad (1.25)$$

This formula represents the scale for the accelerating fields that are supported in plasma. According to this approximation, plasma densities in the range of 10^{16}–10^{18} cm^{-3} facilitate accelerating fields on the order of 10–100 GV m^{-1}, which are typical plasma densities used in plasma-based particle accelerators. This simplified 1D treatment of the wave dynamics in plasma serves as a basis for understanding the fundamentals of plasma oscillations [81]. However, the validity of this approach is limited to very broad beams ($\sigma_{x,y} \gg k_p$) that excite the plasma waves, which is generally not the case. The following sections provide a more general and rigorous treatment of the theoretical framework that is required to understand the studies conducted in the context of this work—without any claim of completeness. A more detailed discussion of the underlying physics can be found in various References, e.g. [43, 82].

1.2.2 Plasma wake excitation using an electron bunch

The excitation of a relativistic plasma wave requires a particle beam that traverses the plasma with a velocity close to the speed of light. In principle, this beam can be of any particle species that causes a charge-displacement perturbation in the plasma. For practical reasons, readily available charged particle beams (electrons or protons) or photons (laser light with $\omega_\gamma \gg \omega_p$) are the common choices [83].

In this work an ultra-relativistic ($\sim$1 GeV), intense ($\sim$kA) and ultra-short [$\sim$200 fs root-mean-square (rms)] electron bunch is used. The plasma electrons are expelled from the propagation axis of the incident electron bunch by means of its space-charge repulsion force. If the particle bunch is shorter than the characteristic time scale on which the plasma can neutralise a charge disturbance ($\sigma_z < \omega_p^{-1}$), a co-propagating plasma-electron density wave is efficiently formed in its wake, which supplies large-amplitude *wakefields* that can be used to accelerate particles.

For perturbations of small amplitude and assuming that the ions are infinitely heavy (i.e. immobile), the plasma dynamics can be described by the electron density instead of a distribution function. The dynamics correspond to a laminar flow of the plasma electrons, which is described by the *density continuity equation*:

$$\partial_t n_1 + n_p \nabla \cdot \mathbf{v}_p = 0, \qquad (1.26)$$

where n_1 is the perturbed plasma density, n_p the original background plasma density and $\mathbf{v}_p$ the fluid velocity, i.e. the velocity of the plasma electrons. In the *approximation of non-relativistic plasma electron motion*, the forces induced by the electric fields dominate and the Lorentz equation (Eq. 1.6) reduces to:

$$\partial_t \mathbf{v}_p = -\frac{e}{m}\mathbf{E}, \qquad (1.27)$$

where $\mathbf{E}$ is the total electric field of the traversing electron bunch and the perturbed plasma. Substitution of this relation for the fluid momentum $\partial_t \mathbf{v}_p$ into the time derivative (∂_t) of the

continuity equation (Eq. 1.26) and using Gauss' law (Eq. 1.24) to determine the divergence of the electric field $\nabla \mathbf{E}$ for the total charge distribution $\varrho = -en_1 + \varrho_b$, the equation for the density perturbation is given by:

$$\partial_t^2 n_1 + \omega_p^2 n_1 = \omega_p^2 \varrho_b \tag{1.28}$$

It is found that the plasma response is described by an oscillator with frequency ω_p that is driven by the charge distribution of the traversing electron bunch (ϱ_b), the *drive bunch*.

Due to the linear nature of the calculus for small perturbations, the wakefields driven by an electron bunch of arbitrary charge distribution can be found by the linear superposition of the individual particle solutions [84, 85], which is the approach pursued here; a more detailed calculation is given in Ref. [86]. A charge density of a total charge q with radial extent $\delta(\mathbf{r}) = 1/(2\pi r)\delta(r)$, which traverses the plasma with velocity v_b in the z-direction

$$\varrho_b = q\delta(\mathbf{r})\delta(z - v_b t) = q\delta(\mathbf{r})\delta(\xi), \tag{1.29}$$

stimulates a sinusoidal longitudinal oscillation of the plasma electrons with the plasma frequency ω_p in its wake ($\xi > 0$)

$$n_1 = \frac{\omega_p e}{v_b} q\delta(\mathbf{r})\sin(\omega_p \xi). \tag{1.30}$$

A new variable ξ was introduced through an algebraic (Gallilean) coordinate transformation that measures the distance behind the drive bunch in the co-moving frame or "wake frame" $(x, y, z, t)^T \mapsto (\xi = z - v_\phi t, x, y, s = z)^T$. This proves to be a useful description [87], since the development of the drive bunch takes place on a much larger time scale than the dynamics of the plasma wave $\partial_s \ll \partial_\xi$ and the drive bunch is thus often assumed to be stationary. This so-called *quasi-static approximation* is widely used to simplify analytic calculations or to speed up numerical simulations. The plasma dynamics then depends on ξ only and the phase velocity of the density wake is dictated by the velocity of the drive bunch v_b.

An expression for the electromagnetic field in such a plasma density wave can be derived starting from the wave equation for the electric field:

$$\left(\frac{1}{c^2}\partial_t^2 - c^2\nabla^2\right)\mathbf{E} = -\mu_0\partial_t\mathbf{j} - \frac{c^2}{\varepsilon_0}\nabla\left(\nabla \cdot \mathbf{E}\right) \tag{1.31}$$

In the quasi-static approximation and assuming an ultra-relativistic bunch $v_b \approx c$, the longitudinal and transverse plane of the axially symmetric system can be disentangled: $\nabla^2 \mapsto \nabla_\perp^2 + \partial_z^2 = \nabla_\perp^2 + 1/c^2\partial_t^2$ and the left-hand side of the wave equation reduces to $-\nabla_\perp^2\mathbf{E}$. Substituting the relations for the current density $\partial_t\mathbf{j} = -n_p e\partial_t\mathbf{v} = n_p e^2\mathbf{E}/m$ and the divergence of the electric field $\nabla \cdot \mathbf{E} = (-en_1 + \varrho_b)/\varepsilon_0$, the wave equation after rearranging becomes:

$$\left(\nabla_\perp^2 - k_p^2\right)\mathbf{E} = \nabla\left(\frac{-en_1}{\varepsilon_0} + \frac{\varrho_b}{\varepsilon_0}\right) \tag{1.32}$$

For a vanishing divergence of the electron bunch density ($\nabla\varrho_b = 0$) and using the previously obtained solution for the perturbed plasma density n_1 (see Eq. 1.30), the longitudinal wakefield E_z is given by:

$$E_z = -2qk_p^2 K_0(k_p r)\cos\left(\omega_p \xi\right), \tag{1.33}$$

where K_0 is the zeroth-order modified Bessel function of the second kind. The transverse focusing forces can be determined analogously using the wave function for the magnetic fields or by using the Panowsky-Wenzel theorem (see Eq. 1.8):

$$E_\perp = -2qk_p^2 K_1(k_p r)\sin\left(\omega_p \xi\right),\tag{1.34}$$

where K_1 is the first-order modified Bessel function of the second kind.

The obtained fields show phases of longitudinally accelerating and decelerating forces and radially focusing and defocusing forces, with the amplitude largely depending on the beam density. For high-quality acceleration, it is necessary to be in the phase of the wake that is both focusing and accelerating, which is the case for the last quarter of the wake phase. However, it is found that the longitudinal field has a radial dependence and (according to the Panowsky-Wenzel theorem) the radially focusing force has a longitudinal dependence, both of which are highly undesirable features for stable transport of an electron bunch of finite length and width.

The wakefield driven by an arbitrary, continuous bunch charge distribution $\varrho_b(r,\theta,z_c t)$ is ultimately given by the integration:

$$E_z(r,\xi) = (-2k_p^2)\int\limits_{-\infty}^{+\infty} d\xi' \int\limits_0^\infty r'dr' \int\limits_0^{2\pi} d\theta' \varrho_b(r',\theta',\xi') \times K_0(k_p|\mathbf{r}-\mathbf{r}'|)\cos\left(k_p(\xi-\xi')\right)\tag{1.35}$$

Solving this equation for a radially flat-top and longitudinally Gauss-shaped electron bunch $\varrho(\xi) = qn_b e^{-\xi^2/2\sigma_z^2}$, the maximum wake amplitude scales as [88]:

$$E_z \propto q\frac{n_b}{n_p}k_p^2\sigma_r^2\ln\left(\frac{1}{k_p\sigma_r}\right)\tag{1.36}$$

The above calculation represent the so-called *linear regime* of plasma wakefield acceleration and serves as an excellent basis for understanding the dynamics in plasma waves. The underlying assumption was a small perturbation in the plasma density ($n_1 \ll n_p$, $n_b \ll n_p$) so that individual particle trajectories do not cross. For this, the electric field amplitude must be well below the wave-breaking field limit and the fluid velocity must not be relativistic ($v_p \ll c$). For wide beams ($\delta(\mathbf{r}) = 1$, $\nabla_\perp = 0$), i.e. in the 1D approximation, all these conditions are equivalent and simultaneously satisfied [88], and the plasma oscillation is described by a harmonic oscillator (see Eq. 1.30). In multi-dimensions and for a narrow drive bunch, the density wave is anharmonic and the electron flow is inherently turbulent [89, 90]. These turbulent dynamics become more severe as the charge density perturbation (i.e. drive bunch charge density) increases. The tipping point at which the linear theory breaks down [91] for an electron bunch was found to occur at a normalised charge per unit length $\Lambda = n_b/n_0 k_p^2\sigma_r^2 > 1$ [88]. The plasma dynamics must then be described by the kinetic motion of the plasma electrons and the so-called *non-linear regime* applies.

By virtue of its strong space charge, an ultra-intense electron bunch completely expels the plasma electrons from its axis of propagation, while the ions of the plasma are assumed to remain stationary[1]. An ion column forms behind the drive bunch, which attracts the

---

1   This assumption breaks down at the point when the drive bunch is so intense that the ions are attracted on-axis.
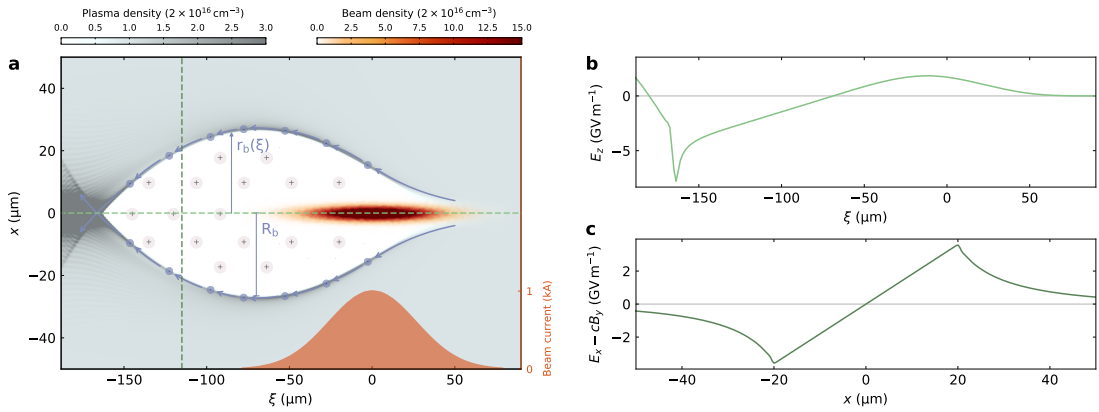
Figure 1.5: Plasma wake excitation in the non-linear regime of beam-driven plasma wakefield acceleration. a, By means of space charge, an ultra-intense electron bunch (red) creates a cavity-like structure of distinct charge separation in its wake: the positively charged ions remain unchanged while the lighter plasma electrons are ejected. After the electron beam has propagated over a distance of about λ_p, the ejected electrons are attracted back to the axis by the ion column (quasi-static Particle-In-Cell (PIC) simulation, $n_p = 2 \times 10^{16}$ cm^{-3}). **b**, Longitudinal field along the propagation axis of the drive bunch. **c**, Transverse field at a suitable location for bunch injection, which shows a linear dependence on deviation from the axis and is cylindrically symmetric. This is ideal for aberration-free focusing.

just radially ejected electrons back to the axis (see Figure 1.5a). These ejected electrons accumulate in a thin, high-density electron sheath that overshoots the beam-propagation axis after the drive bunch has propagated over a plasma wavelength λ_p. A cavity-like structure void of electrons and surrounded by weakly interacting neutral plasma is formed, which co-propagates in the wake of the drive bunch. The distinct charge separation with positively charged ions surrounded by a high-density electron layer creates a longitudinal electric field in excess of GV m^{-1} as well as MT m^{-1} focusing fields (see Figures 1.5b and 1.5c). By using a one-dimensional fluid theory, partial aspects of this non-linear regime could initially be understood [92]. However, to understand and examine the kinematics in this regime in greater detail the three-dimensionality must be retained, which typically requires computationally intensive numerical PIC simulations.

W. Lu et al. formulated a phenomenological, predictive theory [93, 94] that proves to be an excellent approach to gaining a basic understanding. The core idea behind this theoretical approach is to describe the source term of the wake through the trajectory of the electrons within the thin sheath that surrounds the cavity-like structure, i.e. through the cavity radius as a function of ξ, $r_b(\xi)$ (see Figure 1.5a). The non-linear 3D plasma wakefields are thus sourced by the currents in the thin electron sheath. This proves to be a valid approach in the ultra-relativistic limit when the drive bunch is very intense. The radius of the ion column then exceeds one skin depth at its maximum ($R_b \gg k_p^{-1}$) and the electron sheath is narrow compared to the ion column. For such intense drivers, the trajectory of the ejected electrons forms a sphere and the equation of motion for the sheath electrons is given by a second-order ordinary differential equation:

$$r_b \frac{d^2 r_b}{d\xi^2} + 2 \left(\frac{dr_b}{d\xi} \right)^2 + 1 = \frac{4\lambda(\xi)}{r_b^2}, \tag{1.37}$$

where $\lambda(\xi)$ describes the charge per unit length of the drive bunch or an injected bunch. The resulting accelerating field within this cavity is intimately related to the motion of the sheath electrons and found to be completely defined in terms of the local radius of the ion channel r_b and the slope of the sheath $dr_b/d\xi$:

$$E_z \approx \frac{1}{2} r_b \frac{dr_b}{d\xi} \tag{1.38}$$

An estimate for the focusing force can be found through Gauss' law (Eq. 1.24) for a uniform cylinder of a fully blown-out ion column $n_i = n_p$:

$$E_r = \frac{1}{2} \frac{en_p}{\varepsilon_0} r. \tag{1.39}$$

The accelerating field E_z is found to have no radial and the focusing field E_r to have no longitudinal dependence, respectively, as also expected from the Panowsky-Wenzel Theorem (see Equ. 1.8). In addition, the focusing field grows linearly with the deviation from the axis of propagation (see Figure 1.5c). Both the accelerating and the focusing field are cylindrically symmetric, which simultaneously enables aberration-free focusing in both transverse planes and acceleration. Such an ability of linear focusing during acceleration is essential to preserve beam emittance and makes this so-called non-linear regime (or blowout regime) critical to preserve beam quality during high-gradient acceleration [95, 96].

Throughout the preceding mathematical discussion of wake excitation we have assumed a non-evolving drive bunch, which of course is only valid to a limited extent and only on short time scales. The continuous transfer of energy from the bunch to the plasma undoubtedly affects the bunch. After a certain duration of interaction, parts of the drive bunch are no longer relativistic and consequently can no longer drive the wake. *Drive bunch energy depletion* constitutes the fundamental limit of wake excitation. In addition, successive longitudinal slices of the drive bunch experience a different focusing field which only gradually builds up from the front of the drive bunch. Successive slices of the drive bunch experience different focusing forces and thus also different betatron oscillations, so that the bunch head deteriorates and thus changes the driven wakefields. This effect is known as *head erosion* and represents another limit of stable wake excitation [97–99].

1.2.3 External injection of an electron bunch into a plasma wake

The generation of strong accelerating fields is only the first step of building a plasma accelerator. The energy that was transferred from the drive bunch to the plasma through wake excitation must now be extracted by another electron bunch that is injected into the accelerating phase of the wake. There are different injection mechanisms that primarily differ in where the injected electrons originate from. Internal injection mechanisms trap electrons from the plasma background, external injection mechanisms use pre-accelerated electron bunches from an external particle source. The latter method has the advantage that the properties of the injected bunch are easily controllable, typically more reproducible and independent of the acceleration process. The external injection mechanism is also particularly relevant for high-energy applications where the bunch is gradually accelerated in multiple successive acceleration stages into which the identical bunch must be injected externally [100]. The present work deals with the external injection method.

A relativistic electron bunch, which follows the similarly relativistic propagating drive bunch (with distance $< \lambda_p$), will experience the wakefields detailed in the previous section. Since both the wake and the injected bunch propagate near the speed of light, they stay in phase for a long distance[1] over which the injected bunch experiences the same wakefield. The energy gain that can be achieved throughout the plasma–beam interaction is only one important aspect. In view of accelerators that must provide high luminosity or high brightness, the maximum number of particles that can be accelerated, the resulting beam quality of the accelerated bunch (i.e. emittance, energy spread) as well as the overall efficiency of the device are of utmost importance (Sec. 1.1.3). These parameters are fundamentally determined by the interaction of the injected bunch with the wake.

Acceleration to high beam energies is generally associated with a lower beam quality as a result of possibly self-reinforcing instabilities and the necessity for a longer acceleration distance. Mitigation of such instabilities therefore requires special attention, and preserving beam quality within a single accelerator module is the ultimate goal. The great challenge of achieving this goal in plasma-based accelerators stems from the small dimensions of the plasma cavities and their transient nature [101] requiring the energy to be efficiently extracted within the first wake oscillation.

On the one hand, the small dimensions of the plasma cavity (33–330 µm for $n_p \sim 10^{16}$–10^{18} cm^{-3}) enable strong wakefields and thus high acceleration gradients as well as simultaneous aberration-free beam focusing. On the other hand, these strong fields make the system very sensitive to misalignment and constitute a major challenge for bunch injection. The strong transverse forces require a μm-level control on the straightness of the bunches and on the offset of the injected bunch relative to the wake. The matching conditions for the beta function of the injected bunch scales with the strength of the transverse fields and requires mm-level beta functions. In addition to the challenges that arise from the radial focusing force, the ξ-dependence of the accelerating field also affects the energy spectrum of the injected bunch of finite length and requires sub-femtosecond-level synchronisation between the wake and the injected bunch. In plasma accelerators and in stark contrast to an idealised conventional accelerator, the functional separation of acceleration, deflection and focusing is abolished—it happens simultaneously and with very strong fields, which makes the control of the acceleration process a great deal more difficult. The most important aspects to be considered for optimal bunch injection into beam-driven plasma wakefields are examined in more detail below.

Beam matching

The oscillation of the bunch envelope in the linear focusing forces of the non-linear plasma wake can be found to be a Hill's-like equation:

$$\frac{d^2\sigma}{dz^2} + \left(\frac{k_p^2}{2\gamma_{rel}} - \frac{\varepsilon^2}{\sigma^4} \right) \sigma = 0, \tag{1.40}$$

---

1   In principle, the accelerated bunch cannot indefinitely stay in phase with the wake due to the small difference in velocities. This limitation is given by the so-called dephasing length. For ultra-relativistic particle bunches, however, the fundamental limit of the acceleration process is the energy depletion of the drive bunch.

and allows for propagation of the injected bunch in matched conditions, where the transverse bunch size does not change [96]. Such a stationary solution ($d\sigma/dz = 0$) is found for a beta function:

$$\beta_{matched} = \frac{\sqrt{2\gamma_{rel}}}{k_p} = \sqrt{2\gamma_{rel}}\frac{c}{\omega_p}. \tag{1.41}$$

If the phase-space ellipse of the injected bunch is not properly matched into the focusing fields of the wake, the beam can undergo several focal waists throughout the acceleration process within the plasma [102, 103]. This so-called *beam pinching* results in an increase of the beam envelope and as a consequence also in the degradation of the beam emittance.

For a 1 GeV beam passing through a plasma with an electron density of 10^{16} cm^{-3}, the matched beta function is on the order of few millimetres—careful beam focusing at the plasma channel entrance is required! In principle, these conditions can be relieved by adiabatic matching using plasma density ramps [104–108], which is, however, very difficult to control and has therefore not yet routinely been used in experiments.

Beam loading and acceleration efficiency

Injecting a bunch of significant charge generally changes the dynamics of the wake by means of the added space charge and thus also the acceleration process. The description of the *effective acceleration fields* that ultimately act on the injected bunch must therefore take into account its own effect on the wakefield shape, which is typically referred to as *beam loading.*

In the linear regime, the effective fields are described by the superposition of the wake driven by the drive bunch and the wake driven by the injected bunch, $E_z = E_z^{wake} + E_z^{bunch}$ (see Figure 1.6). In the 1D approximation of wide and ultra-short bunches ($\sigma_r \gg c/\omega_p, \delta(\mathbf{r}) = 1, \nabla_\perp = 0$) the wake functions of both bunches are given by a sinusoid $E_z = E_0 cos(\omega_p t - k_p z + \phi)$. In this idealised case, the entire energy stored in the wake can theoretically be extracted by the injected bunch, such that the wakes destructively interfere and vanish behind the injected bunch[1] (see Figure 1.6a). This way, an energy-transfer efficiency in excess of 100% can be achieved but only at the expense of an energy spread also in excess of 100%. In order to achieve the beam quality required in high-energy physics experiments, the increase in energy spread during acceleration must be kept to a minimum. For this, *S. Van der Meer* suggested specialised shaping of the current profile of the injected bunch such that the field is flattened E_{flat} over the extent of the injected bunch (see Figure 1.6b) [109]. The suitable shape of the injected bunch for field flattening of a specific wakefield is obtained by solving Eq. (1.35) on the charge distribution, demanding a constant wakefield along the length of the injected bunch—which turns out to be a triangular shape [110–112]. The current profile required to flatten the wakefield depends on the phase of bunch injection and thus on the desired acceleration gradient, but ultimately also determines the energy-transfer efficiency that can be achieved $\eta = \Delta\mathcal{E}/\mathcal{E}_0 = 1 - E_{flat}/E_0$. Optimal bunch shaping can therefore be used to preserve the energy spread, but there is a trade-off between acceleration gradient and efficiency or loadable bunch charge. The energy-transfer efficiency only reaches

---

[1]   This idealised 100% efficiency is not even theoretically possible in RF cavities where a short bunch excites a wake function with higher-order modes. On the other hand, the energy that is not extracted from an RF cavity can be recycled, which is much more difficult in plasmas where the remaining energy may dissipate through instabilities [85].
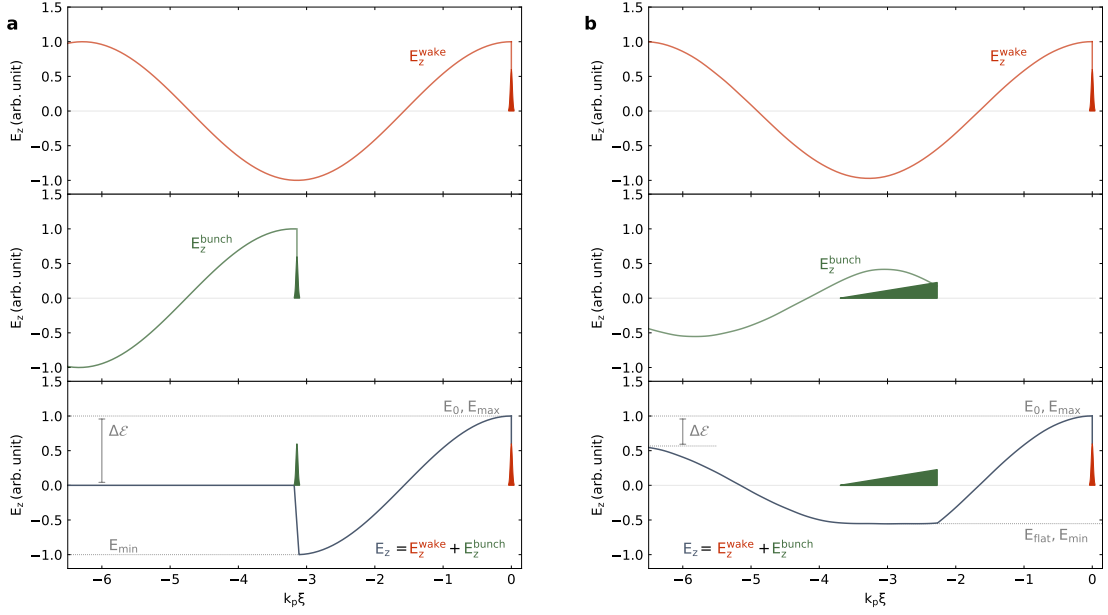
Figure 1.6: Beam loading in the linear regime. The effective wakefield (blue), $E_z = E_z^{wake} + E_z^{beam}$ is described by the superposition of the wakefield driven by the drive bunch (red), E_z^{wake}, and the wakefield driven by the injected bunch (green), E_z^{bunch}. **a,** For ultra-short bunches, the injected bunch can extract the entire energy stored in the initial wake such that the wake vanishes behind it. However, the "first" particle of the injected bunch experiences maximum acceleration and the "last" particle experiences no acceleration at all. The achievable acceleration efficiency is thus undesirably linked to the resulting energy spread. **b,** Shaping the current profile of the injected bunch, the wakefield can be flattened over the length of the injected bunch (E_{flat}), whereby the energy spread of the injected bunch is preserved. However, this reduces the maximum achievable acceleration gradient and efficiency, $\eta = \Delta\mathcal{E}/\mathcal{E}_0 = 1 - E_{flat}/E_0$. (Plot adapted from Ref. [85, 114])

$\sim$100% for zero accelerating field, while for the maximum accelerating field the efficiency approaches $\sim$0% [85]. The discussed special one-dimensional case is suitable to illustrate the intrinsic dependencies between the resulting energy spectrum, the energy-transfer efficiency, acceleration gradient and the current profile of the injected bunch, which is fundamental to plasma wakefield acceleration. This description, however, cannot be generalised to multiple dimensions [113].

In addition to the intrinsic wakefield shape, there are also other factors that induce an energy spread during acceleration, such as the phase slippage of the injected bunch and the radial dependence of the wakefield. While the former can be avoided by using ultra-relativistic bunches and by keeping the acceleration length well below the dephasing length, the latter only applies to the linear regime. Indeed, this is one of the reasons why the preservation of bunch quality depends on operating in the blowout regime in which the acceleration field is independent of r, the focusing forces are linear in r, and above all these characteristics do not change when the wake is loaded [114].

In the physical picture of the non-linear regime, the influence of the injected electron bunch on the wake must be considered in terms of its space-charge force, which changes the trajectory of the electrons in the sheath surrounding the plasma cavity [114, 115]. The

transverse electric field of the injected bunch counteracts the attractive force of the ions within the cavity and the trajectory of the sheath electrons at the location of the injected bunch ($\xi_0 - \Delta\xi < \xi < \xi_0$) is directed slightly away from the axis (see Figure 1.7a). The required charge per unit length $\lambda(\xi) = \int_{\xi_0}^{\xi_0 + \Delta\xi} r n_b dr$ that must be loaded into the wake for energy spread preservation can be found by solving Eq. (1.37) under the assumption of a constant field E_{flat} within the injected bunch. The bunch shape is again found to be trapezoidal (see Figure 1.7b) and the maximum charge that can be loaded under the requirement of perfect field flattening is found to be:

$$Q_{inj} = \frac{\pi}{16} \frac{R_b^4}{E_{flat}}. \tag{1.42}$$

The total accelerating force ($F = qE$), or equivalently the energy absorbed per unit length, is given by $Q_{inj} E_{flat} = \frac{\pi R_b^4}{16}$. This relation illustrates the trade-off between the bunch charge that can be accelerated and the achievable accelerating gradient. In stark contrast to the linear regime, the energy-transfer efficiency of the accelerator does not depend on the field E_{flat} as long as the charge profile is chosen appropriately [114].
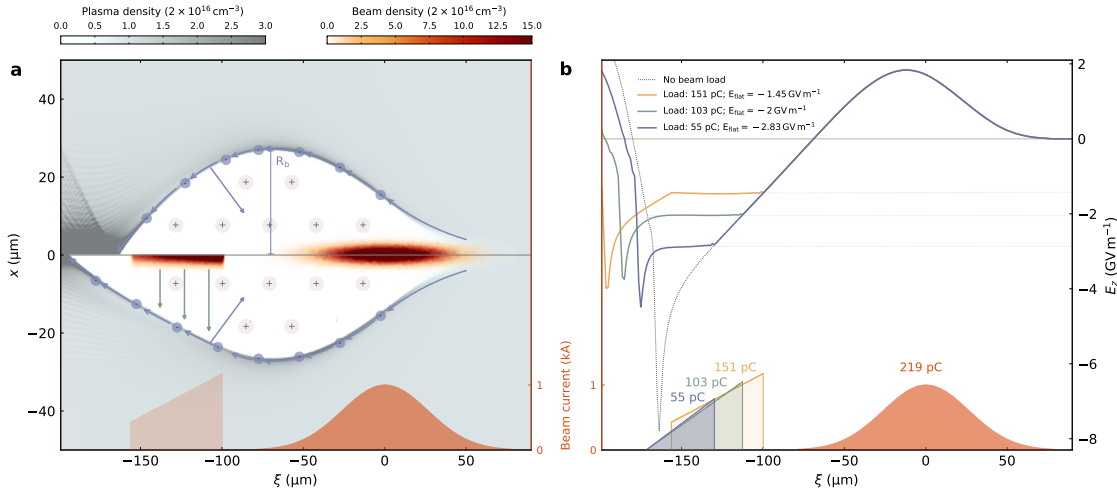
Figure 1.7: Beam loading in the non-linear regime. **a,** Spliced PIC-simulation frames showing a blowout of an unloaded (top) and loaded (bottom) plasma cavity. By virtue of the injected space charge, the trajectory of the sheath electrons is modified, the blowout elongated and the effective wakefield modified (quasi-static PIC simulation, $n_p = 2 \times 10^{16}$ cm^{-3}). **b,** By loading a suitably shaped bunch, the wakefield can be flattened over the extent of the injected bunch, thus preserving the energy distribution for a selectable acceleration gradient. The maximum loadable bunch charge, however, is thereby fundamentally limited.

Transformer ratio

In order to maximise the overall energy transfer from a drive bunch to a trailing bunch, one must first maximise the energy extracted from the drive bunch. In order to have a stable acceleration process, it must be ended before the first particle in the driver bunch has lost all of its energy and the wake-driving process changes as a result. As the wakefield gradually

builds up over the length of the drive bunch, the particles in the drive bunch are generally decelerated at different rates. A parameter suitable to describe the effectiveness of energy transfer is the *transformer ratio*, T, defined as the ratio of the peak accelerating electric field E_{min}, to the maximum decelerating electric field E_{max}: $T = E_{min}/E_{max}$. Those particles in a mono-energetic drive bunch that experience the maximum deceleration field deplete their energy the fastest and therefore determine the maximum length L of the plasma stage. This particle that experiences the maximum acceleration field over the same length L has a maximum energy gain of $T\Delta\gamma mc^2 = T\mathcal{E}_{drive}$ [84, 111].

In the linear regime, the transformer ratio of a bunch of finite length and symmetrical current distribution is limited to $T \leq 2$ [110, 116]—known as the *fundamental beam loading theorem*, while the upper limit of $T = 2$ corresponds to the 1D approximation of a wide and infinitesimally short bunch[1] ($\sigma_r \gg c/\omega_p, \delta(\mathbf{r}) = 1, \nabla_\perp = 0$) [117, 118].

Ideally, the energy in the drive bunch would be extracted at a lower but for each individual particle identical rate, so that the acceleration process can last for a longer distance. While this cannot be entirely achieved, drive bunches with a properly shaped current profile can evade the basic transformer ratio limitation ($T = 2$) [110–112]. This is to be understood in analogy to maximising the energy-transfer efficiency for the injected bunch by means of beam loading as explained in the previous section. When the beam density increases gradually from the head to the tail, the plasma electrons can follow the dynamics and move out of the way as the bunch charge increases—the fields within the bunch can thus be kept small. When the bunch charge suddenly terminates at the bunch tail, large plasma oscillations are generated behind the drive bunch [84].

In the non-linear regime, the transformer ratio is less restricted and scales with the length of the decelerating phase and inversely with the length of the accelerating phase of the plasma cavity: $T \sim \Delta\xi_{dec}/\Delta\xi_{acc}$. A long ramped bunch slowly drives the plasma sheath off-axis resulting in a correspondingly long ξ_{dec}. In contrast to the linear regime, ξ_{acc} only depends on the maximum radius of the plasma cavity R_b and not on how the cavity was created.

Maximising the accelerating gradient while minimising the accelerator structure requires the maximisation of the overall energy efficiency of the acceleration process, which is given by the product of the wall-plug efficiency for drive-bunch generation, the energy-transfer efficiency from the drive bunch to the wake and the energy-transfer efficiency from the wake to the injected bunch. The energy transfer of the drive bunch to the plasma is found to be severely limited by the energy per particle of the drive bunch rather than its overall energy [116]. Maximising the transformer ratio by enabling a uniform energy depletion of the particles in the drive bunch thus ultimately leads to an increase in the overall efficiency. This way of increasing the transformer ratio essentially means loading longer drive bunches, which is prone to undesirable instabilities. A compromise needs to be found between idealised optimisation scenarios and practical solutions that allow for eventual beam instabilities and deviations from theoretical assumptions.

---

1   This can be understood in a simplified picture, taking causality into account: an ultra-relativistic particle is only subject to the field that originates from the charges in front of it. The first particle in the drive bunch therefore experiences no field at all, while the "last" particle in the drive bunch experiences the field caused by the full drive charge. Overall, the drive bunch experiences only half of its own wakefield. The injected bunch, on the other hand, experiences the field driven by the full drive bunch, resulting in $T = 2$.

1.3 Towards high-quality beam-driven plasma wakefield acceleration

Research has come a long way since the first proposal for beam-driven plasma wakefield acceleration [31, 32]. From the very beginning, the progress in this field was based on strong synergies between theory, simulations and experiments as well as the interdisciplinary cooperation of the most diverse disciplines of physics. It was only through intensive theoretical work on one-dimensional high-amplitude plasma waves [81, 119–123] and corresponding simulation models that the initial idea of a plasma-based particle accelerator was given greater attention and more specific proposals [33, 124] were made for such an accelerator [125, 126].

First proof-of-principle experiments were carried out, which demonstrated the excitation of strong plasma waves that generated relativistic electrons in the forward direction [127–129]. The next hurdle was to demonstrate acceleration gradients far beyond conventional possibilities—an anticipated $GeV\,m^{-1}$-limit was drawn to be referred to as "high-gradient" acceleration. However, the laser systems available at the time could not generate pulses that were intense enough to stimulate strong enough waves, and eventually *P. Chen et al.* proposed wave excitation via a short, ultra-relativistic particle bunch instead[1] [124].

In 1988, first beam-driven plasma wakefield experiments [34] were carried out at the Argonne Wakefield Accelerator facility (AWA) at the Argonne National Laboratory (ANL), the prevailing wakefields being estimated by means of a variable time delay between an injected probe bunch and the wake-driving bunch [130]. However, these experiments were carried out in the linear regime of wave excitation and the acceleration gradient ($\sim MeV\,m^{-1}$) was severely limited due to the low-energy electron bunches with several picoseconds ($\sim$20 ps) bunch duration and the low plasma density of 10^{13} cm^{-3}. At the same time, *J. Rosenzweig et al.* were working out the limits of the linear regime of plasma wakefield acceleration and simulation-based studies eventually revealed the enormous advantages of the non-linear regime [95, 96, 131, 132]. Finally, the first experiments in the non-linear regime were carried out at AWA [133] in 1998.

Meanwhile, the control and stability in laser-driven schemes were significantly improved and first externally injected bunches were accelerated [35, 134] and finally the $GeV\,m^{-1}$-scale acceleration gradient aimed for was reached [135]. These results are now seen to have "heralded the dawn of relativistic wave-particle interactions and overcame tremendous scepticism" [44, 125] regarding the suitability of plasma-based acceleration for high-energy applications.

In 2000, a beam-driven plasma wakefield acceleration experiment was installed at the Stanford Linear ACcelerator (SLAC) Final Focus Test Beam (FFTB) beam line [136]. The linac provided 20–40 GeV electron bunches with picosecond length to excite linear plasma waves at plasma densities of 10^{14} cm^{-3}. Moderate acceleration gradients of $\sim$300 MeV m^{-1} were achieved. At this setup, an extremely uniform and reproducible plasma source was developed [137] that finally allowed the acceleration of a matched beam in a meter-scale plasma channel [138]. With the installation of a bunch compressor in the linac in 2003, operation in the blowout regime was finally enabled by 50 fs-bunches with peak currents up to 20 kA. In plasma densities of 10^{17} cm^{-3}, the $GeV\,m^{-1}$-gradient scale was finally

---

[1] Nowadays, state-of-the-art laser systems generate such high wakefields too. Although beam-driven plasma wakefield acceleration is mostly limited to large laboratories, it is still a vigorous research area as the high-average power as well as the high wall-plug efficiency provided by conventional particle beams can still not be achieved by today's lasers systems.

achieved also in beam-driven plasma acceleration. An energy gain of 3.7 GeV was achieved over an acceleration length of 10 cm [36]. With the installation of a longer 85 cm plasma channel, fields of over 50 GV m^{-1} were measured where the drive bunch extended over the full length of the cavities and the energy of the particles in the rear was doubled from 42 GeV to 85 GeV [37]. In this experiment, the acceleration process was not limited by pump depletion, i.e. the energy of the drive bunch, but by head erosion [97, 98]. The first external injection experiment where a drive bunch excited the wake and a trailing bunch was accelerated in the wake was carried out in 2008 [139]. Following the successes of the FFTB experiment, another beam-driven plasma wakefield experiment, Facility for Advanced Accelerator Experimental Tests (FACET), was implemented after reconstruction of the Linac Coherent Light Source (LCLS). Taking advantage of beam loading, ultimately a significant fraction of about 20% of the energy was extracted from the wake by an externally injected electron bunch [38]. Later on, a 9 GeV energy gain in 1.3 m was achieved for 28 pC accelerated bunches, whereas the growth in energy spread was kept below 5% [39]. Another major accomplishment at this experiment was the mapping of the longitudinal field structure of a non-linear plasma wake driven by an unmatched beam using the Panowsky-Wenzel Theorem [140]. Transformer ratios well above the fundamental beam-loading limit were demonstrated in the non-linear regime at The Photo Injector Test Facility at DESY, Zeuthen (PITZ) (R=4.6) [141] and just recently AWA (R=7.8) [142].

Research on positron acceleration was particularly promoted at SLAC, the only facility with an ultra-relativistic positron beam that is available for dedicated beam-driven plasma wakefield acceleration experiments. The first interactions with plasma and the transport through meter-scale plasma were demonstrated at FFTB [143–145] and eventually high-gradient positron acceleration ($\sim$4 GeV m^{-1}) was achieved at FACET [146].

While plasma-based electron acceleration has emerged as an entirely new paradigm for building high-gradient accelerators over the past 40 years, many fundamental and technological problems remain to be solved. Electron beams for these high-energy applications such as colliders and free-electron lasers must have exceptional beam parameters, the preservation of which in each individual acceleration stage is therefore of utmost importance. Therefore, the community is currently addressing the overarching goal of developing a self-consistent plasma-accelerator stage that simultaneously provides highly efficient and beam-quality-preserving acceleration. To reach this goal, beam loading must be used through detailed bunch shaping. The acceleration scheme with an externally injected bunch is the most appropriate approach for such a demonstration, as the parameters of the injected bunch are well defined (and easily tunable) and the bunch is already of "high-energy application quality".

Research on the beam-driven plasma wakefield scheme began rather slowly, as only very few suitable facilities were available. Based on the above-described successes of the experiments carried out at FFTB and FACET, further beam-driven plasma wakefield experiments have recently been commissioned (including e.g. FLASHFoward, AWAKE, SPARC_Lab, PITZ) to supplement this comprehensive research effort with different approaches. The work described in this thesis took place at the facility Future Oriented Wakefield Acceleration Research and Development at FLASH (FLASHForward) at DESY, from its first beam–plasma interaction and made significant contributions to the goal of a self-consistent plasma stage with acceleration gradients at the GV m^{-1}-level. A novel method for convenient focus positioning was implemented [3]. The method for generating two synchronised electron bunches with picosecond separation was adopted from the FACET implementation

and further developed [2] in such a way that eventually the wakefield could be flattened by means of optimal beam loading. Consequently, energy-spread preservation of the injected bunch and a record energy-transfer efficiency of 42% was simultaneously achieved for the first time [4]. An unprecedented dechirping strength of 1.8 GeV mm^{-1} m^{-1} was demonstrated [5]. Finally, a new method for measuring the effective longitudinal wakefield with femtosecond resolution was invented, which allows the acceleration process to be optimised with a previously unattainable level of precision [1].

CHAPTER 2

The FLASHForward facility

Beam-driven plasma wakefield acceleration places stringent demands on the beam source. Efficient excitation of strong plasma wakes requires an ultra-relativistic drive bunch much denser than the plasma ($n_b \gg n_p$) and shorter than the corresponding plasma wavelength (λ_p). For plasma densities ($\geq 10^{16}$ cm^{-3}) that enable GeV m^{-1}-level acceleration gradients, a kilo-Ampère peak current and a sub-picosecond bunch duration are required (Equ. 1.25). Stable and high-quality acceleration relies on a stable plasma and depends fundamentally on the stability and quality of the drive bunch as well as the injected bunch. Of particular importance are the stability of the bunch charge, the 6D phase-space beam properties and their stability in the focus at the plasma, and the synchronisation of the bunches with the generation of the plasma. Optimised plasma wakefield acceleration with regard to its efficiency, transformer ratio and the control of the energy spectrum of the accelerated bunch additionally requires the ability to precisely shape the current profiles of both bunches.

In 2010, J. Osterhoff and E. Elsen proposed the linac of the Free-Electron-Laser Hamburg (FLASH) as a suitable electron source for beam-driven plasma acceleration, whereupon the FLASHForward project was launched [147]. An additional, third beam line (FLASH3) was eventually installed in the FLASH facility, which is dedicated to studies on beam-driven plasma wakefield acceleration. The first electron-bunch transmission through the FLASH3 beam line was achieved in February 2018, and was followed by a phase of rigorous beam-based commissioning of the individual beam-line components. First beam–plasma interaction was observed in June 2018 after the plasma channel was installed. With the successful installation of a collimator device [2] which generates a finely tunable and highly synchronised double-bunch from a single FLASH bunch, the external injection experiment eventually went into operation in August 2018. In recent years, FLASHForward has grown into a large project that encompasses a broad field of fundamental research on plasma-based acceleration and the development of associated diagnostic and instrumentation tools.

The infrastructure of the FLASHForward facility, including the FLASH linac and the plasma-dedicated FLASH3 beam line, is described to the extent that is specifically relevant for the experiments carried out in the scope of this thesis. The chapter concludes with a classification of the experimental characteristics of the beam-driven external injection experiment in comparison to the capabilities at other operational facilities around the world.
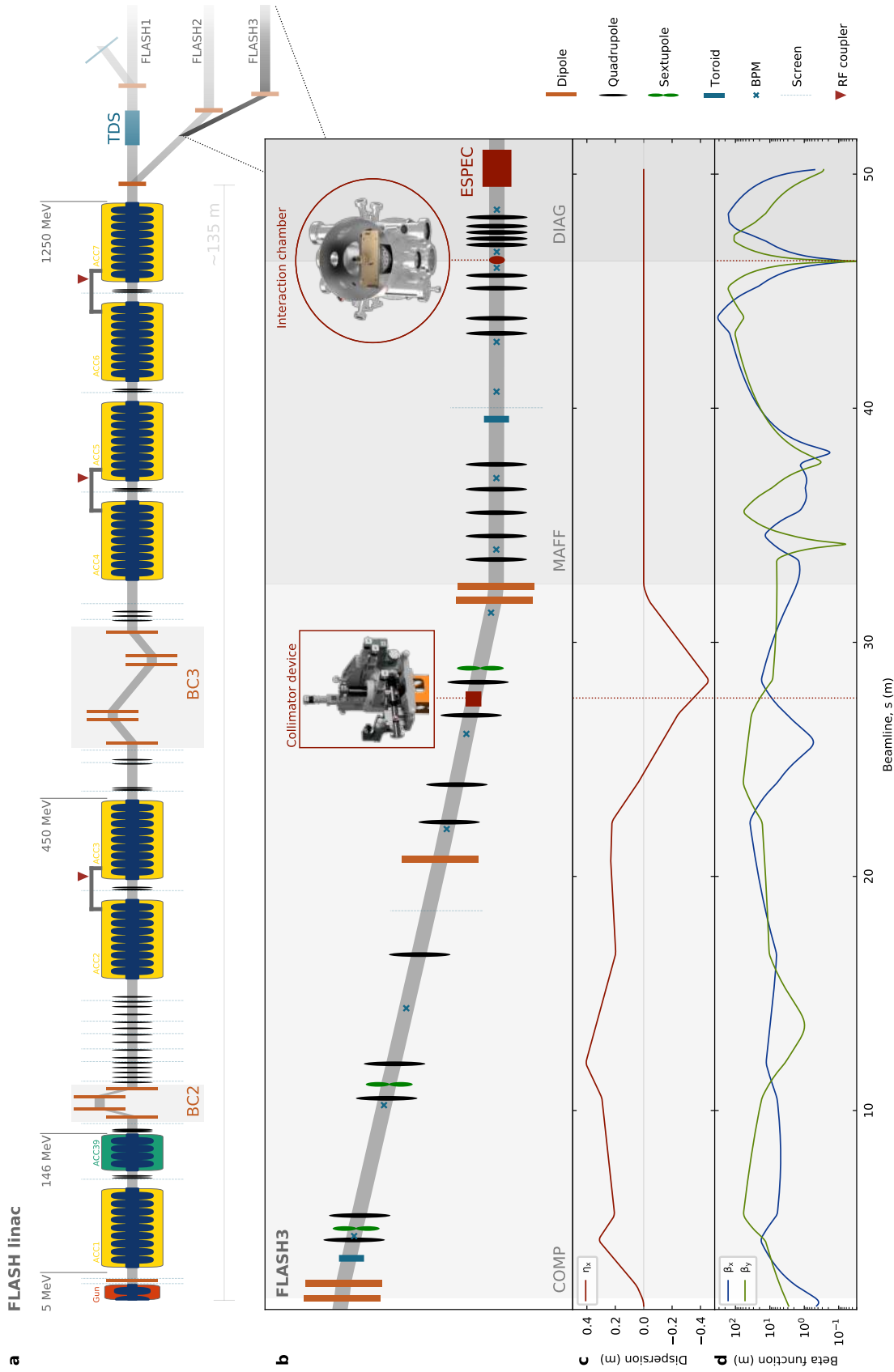
Figure 2.1: Schematic of the FLASHForward facility. a, The electron bunch is generated in a RF gun and accelerated in a three-staged scheme of super-conducting RF modules alternated with magnetic chicanes for longitudinal bunch compression. A third-harmonic RF module (ACC39) allows for flexible longitudinal phasespace shaping, which can be measured using a Transverse Deflecting Structure (TDS) located in the FLASH1 beam line. **b,** The FLASH3 beam line conceptually consists of three sections. The dispersive extraction section (COMP) features a collimator device for tunable two-bunch generation. The bunches are then tightly focused to the entrance of a plasma channel (MAFF), which is housed in a vacuum interaction chamber. Several diagnostic tools are available for beam monitoring (Toroids, Beam-Position Monitors (BPM), Screens) and eventually inspect the acceleration process with a dipole spectrometer (ESPEC). **c,** Theory horizontal dispersion. **d,** Theory beta functions.

2.1 FLASH linac—the electron bunch source

The FLASH linac developed from a test stand for a future linear collider, the TeV Super-conducting Linear Accelerator (TESLA) [148], and ultimately became the first free-electron laser in the soft X-ray regime [149]. Today, FLASH is an FEL user facility whose laser wavelength reaches into the water window (~3 nm) [150], and has two parallel photon beam lines that are accessible by both industry and research.

The sophisticated beam control and femtosecond synchronisation systems of a running FEL together with the available electron-beam parameters make the FLASH linac an excellent electron-bunch source for research on beam-driven plasma wakefield acceleration. The beam line of the FLASH linac is illustrated in Figure 2.1a, the main components of which and their usage for plasma wakefield acceleration experiments are described below; more detailed information on the FLASH linac can be found in the References [151, 152].

Radio-frequency photo-injector

An ultraviolet laser pulse generates an electron bunch through photo-electric emission from an Cs_2Te substrate, whereby a bunch charge of up to 2 nC can be achieved. This substrate is embedded in a normal-conducting 1.3 GHz RF cavity consisting of 1.6 cells, which in turn is arranged in a transversely focusing solenoid magnet (180 mT). With this overall structure, called "*gun*", detrimental effects from Coulomb repulsion are mitigated through immediate bunch acceleration and transverse bunch focusing.

Three independent laser systems are available with Gaussian longitudinal profiles and pulse lengths of 4.5, 6.5 and 0.8–1.2 ps (rms). The transverse profile of the lasers is essentially a flat-top profile. In order to fine-tune the achievable transverse emittance for a given bunch charge, the space charge in the gun can be modified by adjusting the spot size of the laser on the substrate.

Accelerating RF-modules

The electron bunch is accelerated to a final energy up to 1250 MeV in a total of seven TESLA-type super-conducting modules. Each accelerating module is about 12 m long and consists of eight 9-cell, 1 m-long standing-wave cavities and is operated at a fundamental mode frequency (f_{ACC}) of 1.3 GHz. The cavities are made of ultra-pure Niobium (Nb) and cooled to 2 K for super-conducting operation. A maximum acceleration gradient of about $25 \, \mathrm{MV \, m^{-1}}$ is achieved and can be sustained with a flat-top over 800 µs. The net energy gain of an electron bunch over the length of the cavities L is given by:

$$\Delta E(z) = A \cos\left(\frac{2\pi f_{ACC}}{c} z + \varphi\right) \cdot L, \tag{2.1}$$

where A is the average gradient experienced in a cavity. The energy gain can be adjusted by the amplitude and the phase φ of the RF-signal. The RF-power is generated in klystrons, which are driven by modulators, and eventually directed to the acceleration modules via waveguides. Some of the accelerator modules (as indicated in Figure 2.1a) are fed by a common klystron, their RF signal can thus be only changed in common.

Linearisation of the longitudinal phase space and bunch compression

The sinusoidal shape of the RF-signal in the accelerating cavities (see Equ. 2.1) imparts an energy chirp (i.e., an energy–time correlation) on an electron bunch of finite length $\Delta z \neq 0$. The shape of the resulting energy chirp is determined by the superposition of the RF-signals, which can be adjusted via their amplitude A and phase φ, but are generally not linear. In conjunction with subsequent bunch compression in magnetic chicanes, a non-linear energy chirp may lead to a partially over-compressed bunch where the initial core of the bunch is overtaking the head of the bunch. Such over-compression is inevitably associated with a deterioration in bunch quality due to collective effects. To compensate for this non-linearity, a *third-harmonic RF-module* (ACC39) with a fundamental mode frequency $f_{ACC} = 3.9$ GHz is implemented downstream of the first acceleration stage where the bunch is not yet compressed. The third-harmonic module consists of four RF cavities which are operated in decelerating mode with a gradient of 15 MV m^{-1}. The superposition of the fundamental mode with the third harmonic mode enables flexible tuning of the first, second and third derivatives of the longitudinal phase space and, to a good approximation, its linearisation. The linearisation of the longitudinal phase space is an essential part of the two-bunch generation for the external injection experiment, as will be explained later.

Coulomb-repulsion forces in the photo-injector inhibit bunch lengths shorter than a few millimetres and peak currents above tens of Ampère. Achieving sub-picosecond bunch duration and kilo-Ampère peak current require *longitudinal bunch compression* at relativistic beam energies, which is realised in two magnetic chicanes: a C-shaped chicane, which moderately compresses the bunch by a factor of 4–5 ($R_{56} = {\sim}180$ mm) at a bunch energy of 146 MeV, and an S-shaped chicane, which compresses the bunch by a factor up to 25 ($R_{56} = 43$ mm) at a bunch energy of 450 MeV. In addition to the magnetic chicanes, the extraction section to the FLASH3 beam line compresses the bunch by a factor of up to 1.2.

Bunch compression in magnetic chicanes is inevitably associated with undesirable collective effects such as Coherent Synchrotron Radiation (CSR) and Longitudinal Space Charge (LSC), which affect the stability and quality of the electron beam and thus can significantly impair the plasma wakefield acceleration. A careful choice must therefore be made between the initial bunch charge and the compression strength to achieve maximum peak current, sub-picosecond bunch duration and a linear phase space.

Bunch-train scheme and parallel beam line operation

The klystrons supply the accelerating modules with a power signal at a repetition rate of 10 Hz. A flat-top profile can be maintained for a maximum duration of 800 µs. The gun laser operates in a 1–10 Hz burst mode, with an adjustable micro-pulse spacing of 0.33–25 µs. At full capacity, this bunch-train scheme (see Figure 2.2a) corresponds to an average power of 30 kW. For reasons of radiation safety regulations, FLASHForward experiments are currently limited to two electron bunches per bunch train with a macro-pulse repetition rate of up to 10 Hz. The external injection bunch requires only a single bunch from FLASH.

The FLASH1 and FLASH3 beam line can be operated in parallel, with the dedicated bunch-train fractions being distributed to the different beam lines via a fast-rising kicker magnet (see Figure 2.2b). In order to supply the beam lines with different beam parameters with regard to the longitudinal phase space or the bunch energy, the klystrons can deliver RF signals of different amplitude and phase within the same macro-pulse.
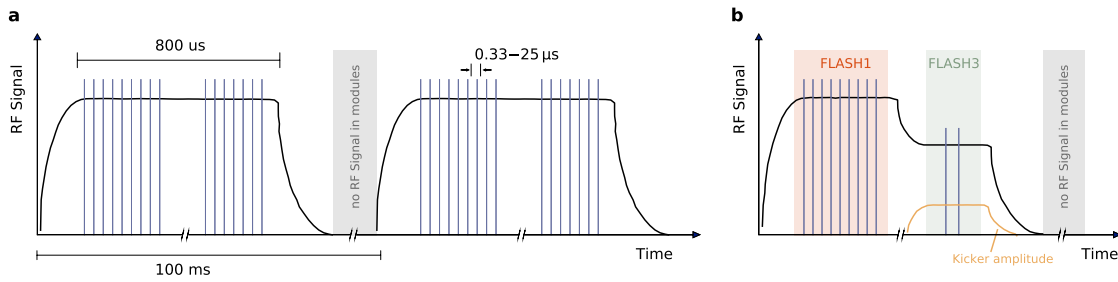
Figure 2.2: Bunch-train scheme. **a**, The FLASH macro-pulse has a flat-top duration of 800 μs and a maximum repetition rate of 10 Hz. The macro-pulse can be filled with electron bunches separated by a minimum of 0.33 μs. **b**, A step-like RF-signal enables parallel beam line operation with independent beam parameters.

Beam set-up and monitoring

Prior to the dedicated plasma-wakefield research program on external injection, the electron bunch is prepared for the special requirements in an 8–12 hour campaign. To give an impression of this pain-staking set-up procedure of the FLASH linac, a brief step-by-step description and the desired beam specification is given below.

1. *Bunch generation at the gun laser*
   The laser power is adjusted according to the desired bunch charge. The timing of the laser is set to one bunch per macro-pulse. In order to minimise radiation damage, the beam set-up procedure is conducted with 1 Hz macro-pulse repetition rate and later raised to 10 Hz for data taking.

2. *Acceleration in the RF modules*
   The beam energy is set by the combination of the RF phase and amplitude settings of each accelerator module. Those acceleration modules that are located upstream of the two bunch compressors (BC2 & BC3) are used for flexible longitudinal-phase-space shaping. The target beam energy is adjusted through the RF amplitudes of the last four acceleration modules (ACC4-7), which are operated on-crest (i.e., $\varphi_{ACC} = 0$).

3. *Beam guidance*
   Magnet settings of a previous experimental campaign with comparable beam parameters are restored as a starting point for the subsequent optimisation of the transverse phase space of the beam.

   Beam Position Monitors (BPMs), corrector dipoles, and toroids distributed along the beamline help optimise the orbit through the centre of the beamline components and achieve full charge transmission.

4. *Beam matching*
   The transverse phase space of the beam is matched to the design optics of the beam line on the basis of multi-screen emittance measurements downstream of the first bunch compressor (BC2). This is an iterative process of emittance measurements and changes in magnet currents, as well as potentially needed orbit corrections.

5. *Bunch compression and longitudinal-phase-space shaping*
   The RF phases and amplitudes of the accelerating modules ACC1-3 are adjusted in combination with the third harmonic RF-module ACC39. The fine-tuning of the bunch compression and linearisation of the longitudinal phase space is observed on a Transverse Deflecting Structure (TDS), which is installed in the FLASH1 beam line [153, 154]. The maximum achievable bunch compression is aimed for while maintaining a strictly monotonic—ideally linear—phase space. The resulting longitudinal phase space is measured with femtosecond resolution (see Figure 2.3).

6. *Dispersion minimisation*
   Magnet misalignment, a non-optimal beam orbit, and collective beam effects can result in a non-zero dispersion at the point of beam extraction. For a bunch with a strongly correlated energy spread, this produces a tilted beam centroid that is highly undesirable for plasma wakefield acceleration, where small deviations from the axis of the wake can lead to harmful beam oscillations, which must be minimised.

7. *Activation of feedback control*
   From the point at which no further changes need to be made to the linac, all available feedback loops are activated, which compensate for drifts in beam orbit, bunch charge and compression. The stabilisation of those parameters is essential for the following experiments, which must rely on similar beam conditions over several hours or up to days.

8. *Beam extraction to the FLASH3 beam line*
   A pulsed kicker magnet is activated to extract the beam into the FLASH2 beam line and the static dipole is activated to extract the beam further into the FLASH3 beam line. The usage of a static dipole precludes parallel operation of the FLASH2 and FLASH3 beam lines.

   Typical beam parameters delivered from the FLASH linac for the external injection plasma wakefield experiment are listed in Table 2.1.

Q (nC)	E (MeV)	σ_t (fs)	I_{max} (kA)	$\Delta p/p$ (rms) %	$\varepsilon_{x/y}$ (mm mrad)
0.3–1	600–1200	170–250	~ 1	0.7–1	~ 1.5

Table 2.1: Desired bunch parameters delivered to FLASH3. Particular attention is paid to achieve maximum peak current while maintaining a linear longitudinal phase space.

2.2 FLASH3—a beam line dedicated to plasma wakefield acceleration

The FLASH3 beam line conceptually consists of three sectors (see Figure 2.1b): the dispersive extraction section (COMP), which features a *collimator device* for tunable two-bunch generation; a matching and final-focusing section (MAFF) in which the bunch is tightly focused into the plasma; the post-plasma diagnostic section where the beam–plasma interaction is observed (DIAG). The plasma target is mounted on a finely adjustable table which is housed in a special vacuum *interaction chamber*. The characterisation of the plasma density profile is carried out in a test stand, which imitates the gas supply and plasma generation system of the FLASH3 beam line.

Extraction and final compression

The beam is guided via the transversely dispersive section (COMP) at a deflection angle of $8°$ to a transverse distance of 4 m to the parallel FLASH2 beam line, which is located in the same tunnel. A reverse-bend dipole within this section allows the final bunch compression factor to be adjusted (R_{56}: -4–5 mm), which typically has a value of 1.1–1.2 . The horizontal dispersion can be observed on a screening station, as can any vertical dispersion or a cross-correlation of the dispersion in the transverse planes, which are undesirable and should be corrected. By means of energy collimation [155], the current profile of the bunch is fine-tuned and, in particular, the bunch pair, which is required for the external injection experiment (the wake-driving bunch and the trailing bunch) is generated out of a single bunch with a strongly correlated longitudinal phase space.

Tunable two-bunch generation via energy collimation

In a transversely dispersive section, an energy deviation from the reference particle translates into a horizontal offset. A bunch with a strictly monotonic, e.g. a linear longitudinal phase space, is therefore transversely sheared. A vertically inserted metallic mask can then effectively separate the electron bunch into two consecutive bunches by scattering the particles of middle energies (see Figure 2.3), which are then outside the acceptance of the beam line and are lost.

Three collimators (see Figure 2.4a) allow the current profile of the two bunches to be fine-tuned in four independent ways: separation width, separation position and length of the drive bunch and the trailing bunch. A vertically and horizontally adjustable wedge-shaped collimator is used to adjust the separation width and separation position. The vertical wedge position deter-

Figure 2.3: Two-bunch generation. a, Energy collimation of a bunch with a linear longitudinal phase space **b**, effectively bi-sects the bunch (solid) into two consecutive bunches (dashed).

mines the collimator width at beam height and thereby also the bunch separation. The wedge position in the dispersive plane (horizontal) determines the collimated energies that correlate to a particular temporal bunch part, i.e. the separation position. Two horizontally adjustable block-shaped collimators act on the bunch head or tail.

In addition to pure two-bunch generation, these collimators proved to be of great importance as a diagnostic tool. The complete blocking of one or the other bunch allows *separate characterisation of the driver and the trailing bunch.* In case of a sufficiently small slice energy-spread, the simultaneous movement of the block collimators—so that only a small energy range can pass—allows a *temporally resolved characterisation of the bunches* and the investigation of the dynamics of individual bunch slices through the beam line. The simple capability of modifying the beam charge over *pC*-scales allows the *charge calibration* of downstream beam-line elements such as screen stations.

Figure 2.4: Collimator device for tunable two-bunch generation. a, A set of three finely adjustable collimators are implemented in the transversely dispersive COMP section. Two oppositely transversely adjustable block collimators effectively manipulate the bunch head and tail. A vertically and transversely adjustable wedge-shaped collimator generates two consecutive bunches with adjustable separation width and separation position. **b**, Side view and partially cut 3D CAD model of the collimator device. Six remotely controllable stepper motors are available for finely tunable two-bunch generation (M5, M6), initial alignment control of the wedge collimator (M3, M4) and bunch tail (M1) as well as bunch head modifications (M2).

This collimator device (see Figure 2.4b) was conceived in the scope of this thesis and is further discussed in Section 3.1.2 and in the related Publication, Reference [2].

Beam matching and focusing

The extraction and final compression section is followed by the 15 m long MAFF section. A set of five quadrupoles matches the transverse phase space to the beam-line optics according to multi-quadrupole current-scan emittance measurements. Another set of four quadrupoles focuses the beam in both planes to beta functions on the order of ~ 10 mm at the entrance of the plasma channel. For beam alignment, the interaction chamber is enclosed by two cavity-type BPMs, which are also used for a novel beam-focus adjustment technique [3]. The beam line is designed such that a beam position jitter below 10 μm and an angle jitter below 0.5 mrad can be achieved at the plasma channel [156].

Interaction chamber

The interaction chamber is a patented construction [157] consisting of two vertically stacked cylindrical vacuum chambers with diameters of 500 mm (see Figure 2.5a). The electron beam passes through the upper chamber, which is directly connected to the Ultra-High Vacuum (UHV) environment of the linac ($\sim 10^{-9}$ mbar). The plasma cell and various diagnostic tools (e.g. screens for beam-alignment and beam-size measurements) are mounted there on an adjustable base plate (see Figure 2.5b). The base plate is controlled by a parallel manipulator (hexapod), which is located in the lower chamber in a 10^{-3} mbar-level vacuum. The movement of the manipulator is transferred to the upper chamber via a feedthrough and

bellows system—precision adjustments can be made in all six dimensions (three translation coordinates and three angles of rotation). Several side ports in the upper chamber provide clear lines of sight for alignment control as well as additional optical diagnostic systems.
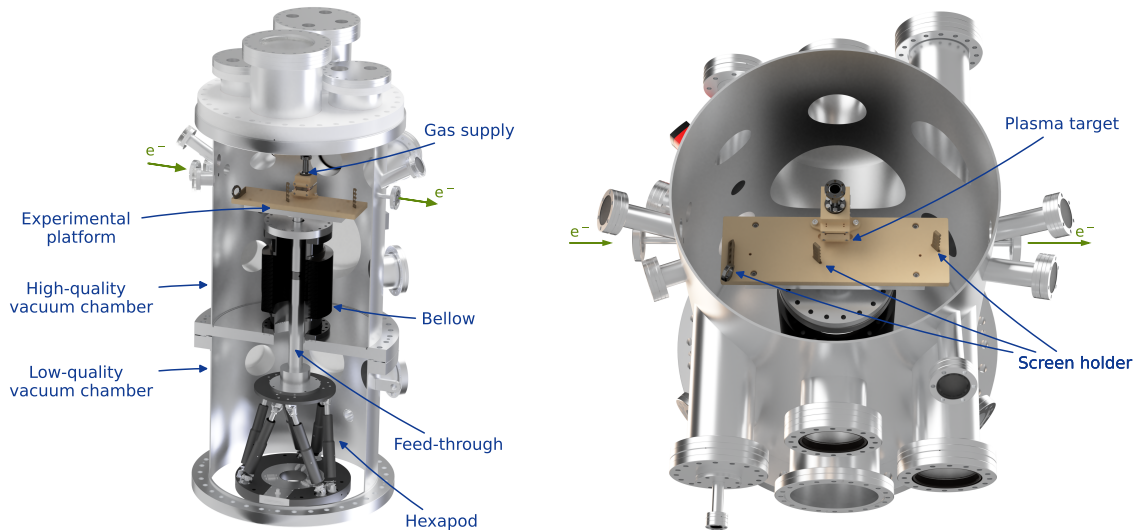
Figure 2.5: Interaction vacuum chamber. a, Side view of the patented double-vacuum chamber (CAD model). The experimental platform is located in the upper vacuum chamber and is adjustable in six dimensions through a parallel manipulator in the lower chamber. **b,** Top view into the upper vacuum chamber (CAD model) with the experimental platform comprising the plasma target and various screens for beam diagnostic. Several view ports allow free sight views and are equipped with cameras for additional optical diagnostics tools.
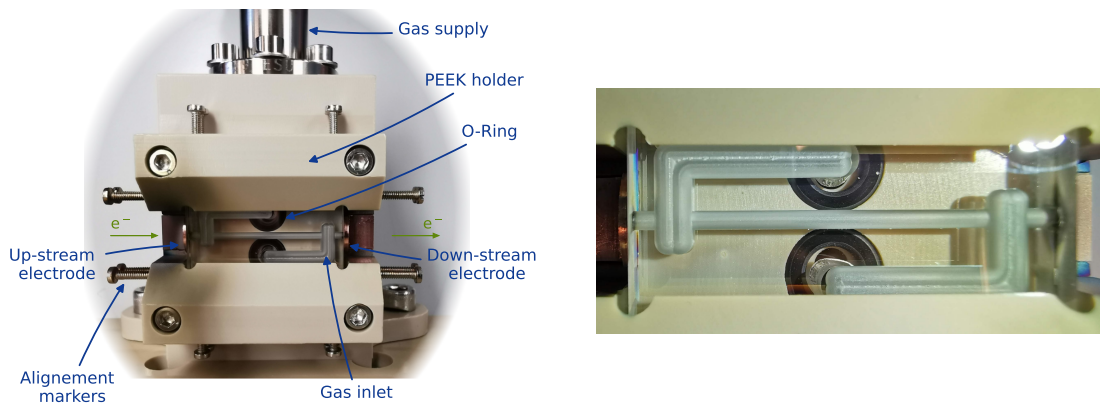
Figure 2.6: Plasma target. a, Two sapphire slabs with channels drilled into them are held together in a PEEK target holder. The gas is fed into the central channel through two gas inlet lines and ionised by a high-voltage discharge between the two electrodes. Screws are mounted to the PEEK holder as markings for aligning the plasma target. **b**, Microscope image of the plasma channel after one year in operation. No major damage of the plasma channel and gas supply lines were observed.

Plasma source

The plasma is generated by discharge ignition of a gas that is transversely confined by a channel drilled into sapphire, into which the gas constantly flows. This channel is created by milling a thin 1.5 mm-diameter and 33 mm-long capillary with two gas inlets in two sapphire slabs, each half milled and held together with a high-temperature-resistant PEEK plastic holder (see Figure 2.6).

A constant argon gas flow is supplied from a buffer volume at a backing pressure of 40 mbar. The gas escapes through the perforated copper electrodes into the interaction vacuum chamber, the ambient pressure of which is kept at 4.3×10^{-3} mbar. The absence of end caps allows the electron beam to be injected into the plasma without any deterioration in quality. In order to nevertheless adhere to the stringent UHV requirements [158] for the super-conducting RF cavities in the linac, the interaction chamber is embedded in a differential pumping system, which achieves a 10^{-9} mbar-level vacuum within ∼16 m. The discharge ignition is triggered by a 25 kV high-voltage pulse with 400 ns duration and a current of 500 A, which is supplied by a high-voltage thyratron switch connected to a pulse-forming network. The plasma density right after the discharge reaches ∼3×10^{17} cm^{-3} and decays exponentially with a decay constant of 6.5 µs. The plasma density is adjusted by delaying the discharge ignition with respect to beam arrival.

The plasma density in the capillary was characterised in a replica-cell in a dedicated test stand [160]. Two complementary diagnostic techniques were used: two-colour laser interferometry measures the plasma density integrated in the longitudinal direction; Stark broadening of the H-alpha line in 5% hydrogen-doped Ar–H gas mixture, measured with a side view camera, provides information about the longitudinally resolved plasma-density profile along the plasma channel. For the trigger-delay timings used in the experiment (5–10 µs) a Gaussian profile was found (see Figure 2.7). This Gaussian longitudinal plasma density profile was not intentionally chosen for a physical purpose in the experiment, but was found later during the data analysis when the experimental environment needed to be realistically modelled for comparing data with PIC simulations. Starting from an initially flat-top gas-density profile, this change in the longitudinal density profile is mainly attributed to gas expulsion[1].
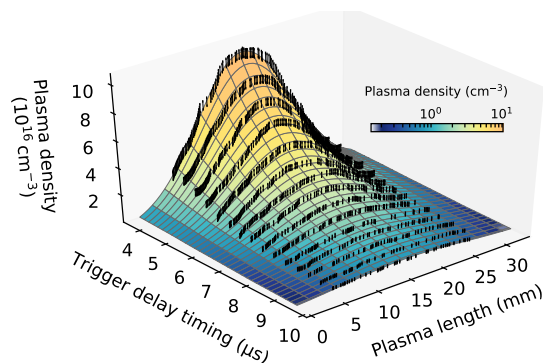
Figure 2.7: Plasma density profile characterisation. Temporal evolution of the longitudinally resolved plasma density (black error bars) in a 95–5% argon–hydrogen mixture measured for times between 4–10 µs after the discharge ignition. A surface function is fitted to the data, which describes the one-dimensional diffusion equation for an initially uniform source [159]. The plasma density profile at the particular discharge trigger delay timing of the measurement is estimated via linear interpolation.

---

1   The data was mainly recorded by Jimmy Garland.
    The analytic model of the evolution of the plasma density profile was derived by Gregory Boyle.
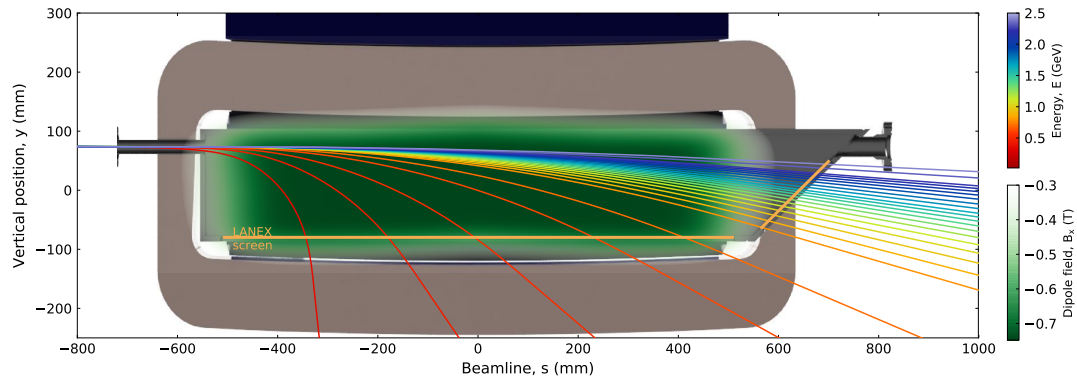
Figure 2.8: Model of dipole spectrometer. A dipole vertically disperses the incoming electron bunches onto a LANEX screen. According to CST simulations that use measured field maps, an energy range of up to 2.5 GeV can be imaged for a typical dipole current of 200 A.

Post-plasma electron-beam diagnostics

To investigate the beam–plasma interaction, the outgoing electron bunches must be well characterised in terms of its energy spectrum, charge, divergence, pointing, and emittance. A suite of single-shot diagnostic tools is available in the DIAG section, in particular two cavity BPMs and an electromagnetic dipole spectrometer (see Figure 2.8), which allow for the measurement of the energy spectrum, charge, divergence and pointing. A set of five quadrupoles, which act as a triplet, capture the typically strongly divergent bunches after interaction with the plasma and enable point-to-point imaging of the plasma exit plane to the dipole spectrometer screen. In the spectrometer, the bunches are dispersed vertically and their scintillation light, which is excited on a LANEX (fine) screen mounted outside the 1 mm thick stainless-steel vacuum-chamber wall, is recorded by a collection of cameras with objective lenses via a mirror (see Figure 2.9). When imaging bunches with a large energy spread, chromatic effects must be taken into account, since the energy resolution deteriorates as a function of the vertical divergence of the particles. In that case, the energy that is focused by the quadrupoles must be scanned in order to achieve a uniform energy resolution. The calibration of the optical system to an energy scale is done via a dipole current scan supported by CST simulations based on measured field maps of the dipole. The optical resolution of the camera system is about 2 pixels, which corresponds to 50 μm. The corresponding energy resolution depends on the exact position of the electron bunch on the screen as well as the dipole current and was typically on the order of 0.05 MeV.
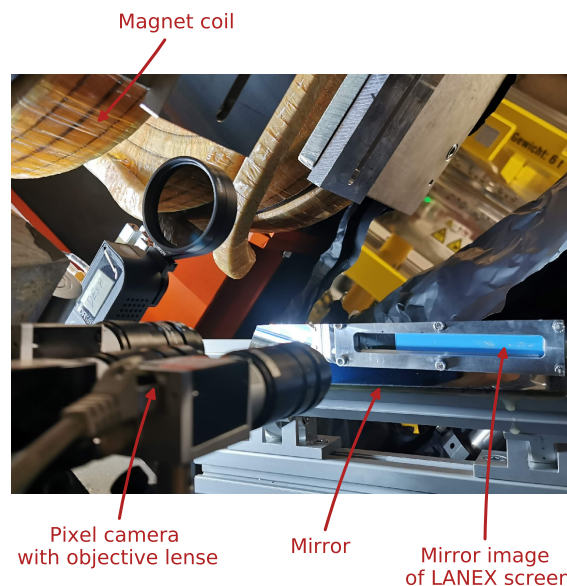
Figure 2.9: Imaging setup of the dipole spectrometer. The scintillating light excited on the LANEX screen is collected with a suite of cameras with objective lenses via a mirror.

2.3 Comparison of facilities in operation worldwide

The possible scientific contribution of an individual beam-driven plasma wakefield experiment to the research field is largely determined by the exact implementation of the experiment and, in particular, by the available beam parameters of the drive bunch. Until machines are built that are exclusively dedicated to beam-driven plasma wakefield acceleration, the need for an ultra-relativistic particle beam and thus a pre-accelerator limit this research field to a few suitable facilities. In recent years, unique experiments have been established in such existing accelerator facilities, which based on the characteristics of their beam sources deal with beam-driven plasma acceleration using very different approaches. In order to put the scientific endeavours of FLASHForward in a broader context, a tabular overview of the facilities currently in operation is provided in Table 2.2 and elaborated in the following.

On a broader perspective, FLASHForward and FACET-II share their preliminary goals to demonstrate a beam-quality-preserving plasma-wakefield-accelerator stage with beam parameters already relevant to a high-energy application such as an FEL. Both facilities benefit from the beam quality at FEL level, which represents an enormous improvement in acceleration stability compared to previous experiments and raises the research field to a new level of precision. In the more far-reaching goals, however, clear differences can be discerned.

FLASHForward operates at comparably modest beam energies of 1 GeV but stands out as the only facility in the world with the potential to explore high-average-power operation. With this, FLASHForward provides the capability of cutting-edge studies of high-precision plasma wakefield acceleration and may eventually turn into a high-repetition rate test-bed. Limits of this plasma acceleration scheme can be investigated and the applicability to future high-intensity photon science and high-energy-physics facilities can be tested.

FACET-II at SLAC stands out due to the immense energy that is stored in the beam (energy: ∼10 GeV, peak current: ∼15 kA, charge: 2–5 nC) [161]. With that, the acceleration process in meter-scale plasma channels and therewith associated instabilities (e.g. ion motion, head erosion, beam ionisation) can be investigated in greater detail. The planned future availability of high-energy positrons would be another unique feature of indispensable value in this facility, as the acceleration of high-gradient electrons is only half of a compact future e^+e^- collider—a solution for high-gradient positron acceleration is imperative. In contrast to all other beam-driven plasma wakefield accelerator facilities, FACET-II is organised as a user facility at which external research groups can conduct their experiments.

SPARC_Lab at INFN in Frascati particularly contributes to new technical approaches for a future plasma-based 1 GeV FEL, which is to be built as part of the European Plasma Research Accelerator with eXcellence In Applications (EuPRAXIA) initiative [162].

AWA at ANL as well as further (smaller) test-bed facilities operate at relatively low energies. These facilities mainly contribute to the development of new technologies to cope with technical challenges, such as the design of robust plasma sources or novel tools for bunch diagnostic and beam preparation, e.g. Emittance EXchange (EEX) [163].

The Advanced Proton Driven Plasma Wakefield Acceleration Experiment (AWAKE) with a proton driver pursues a conceptually completely different approach of beam-driven plasma acceleration, the detailed discussion of which is far beyond the scope of this thesis. The immense beam energy of the drive bunch with 400 GeV allows to investigate the scaleability of the acceleration scheme to collider-like parameters in tens of meter long plasma channels. AWAKE is the first beam-driven plasma wakefield facility that is increasingly concerned with the integration of high-energy physics experiments (e.g. search for dark matter) [164].

Facility	FLASHForward	FACET-II	SPARC_Lab	AWA	AWAKE
References	[147, 165]	[161, 166, 167]	[168–172]	[142]	[173–176]
Particles	e^-	e^- (e^+)	e^-	e^-	p^+ (d) / e^- (w)
Energy, E (GeV)	0.4–1.25	**4–13**	0.03–0.18	0.05	**400** (d) / 0.02 (t)
Energy spread, $\sigma_{\Delta p/p}$ (rms) %	**0.1–0.5**	0.1–1.6	0.1–1	1	0.03 (d) / 0.5 (t)
Emittance (norm.), $\varepsilon_{N,x/y}$ (mm mrad)	1–3	3	< 2	500	3.5 (t)
Focal spot size, $\sigma_{x/y}$ (μm)	5–20	5–20	20	200	200 (d / t)
Bunch charge, Q (nC)	0.1–1.2	2–5	0.01–1	**0.01–100**	0.1–1 (t)
Peak current, I_{max} (kA)	< 2.5	**2–10** (**→200**)	0.02–0.5	3	-
Bunch length (d+w), σ_z (rms) (μm)	50–100	20–100	10–100	$2e^3$	~ 100 (d)
Plasma density, n_p (e^-cm^{-3})	$5e^{15}$–$1e^{17}$	$1e^{14}$–$1e^{19}$	$1e^{15}$–$1e^{16}$	0.3–$1.3e^{14}$	$1e^{14}$–$1e^{15}$
Macro-pulse rep. rate, f_{macro} (Hz)	10	30	10	10	0.03–0.14
Micro-pulse rep. rate, f_{micro} (MHz)	0.04–3	-	-	-	-
Average power, P_{avg} (kW)	**0.01** (**→ 10**)	<1.5	<1	<1	0.6–1.3
Longitudinal phase space shaping capability	RF & BC	RF & BC	**Velocity buncher**	**EEX**	-

Table 2.2: Specifications of external injection beam-driven plasma wakefield acceleration experiments. The uniqueness of every operational facility around the world manifests itself in its parameter space and thus describes its mission in the research field of external-injection beam-driven plasma wakefield acceleration. FLASHForward stands out in terms of the generally FEL-quality beams and the potentially high average power in future. Note: The specified values are to be understood as a parameter space that can be found in the literature for typical operation—deviations for certain applications may be possible.

CHAPTER 3

External injection plasma wakefield acceleration at FLASHForward

Following the demonstration of the basic principle of externally injecting an electron bunch into plasma wakefields, the focus is now on preserving the properties of the injected electron bunch, stabilising the acceleration process and precisely controlling its parameters. The FEL-quality electron bunches, the high flexibility of the beam parameters and the presence of advanced diagnostic devices make the FLASHForward facility a suitable test bench to contribute to this comprehensive goal. One of the main pillars of the FLASHForward research programme is the demonstration of a self-consistent single plasma stage for high-gradient, high-efficiency and quality-preserving acceleration of an externally injected electron bunch. This thesis was carried out within the scope of the so-called X-2 experiment, which deals with the external injection beam-driven plasma wakefield acceleration. The development of the experiment over the past few years is illustrated in Figure 3.1.

A first phase of the experiment was dedicated to beam-line commissioning and the development of operational tools (data acquisition, diagnostic calibration, online monitoring). After first observations of the beam–plasma interaction with wakefields up to 12 GeV m^{-1} [177], the wakefields were then used to demonstrate a plasma-based dechirper with a strength of 1.8 GeV mm^{-1} m [5], which reduced the correlated energy spread of the incident electron bunch from 1.3% to 0.33% in 33 mm of plasma. The installation and commissioning of the collimator device [2] gave the ability to generate consecutive femtosecond-spaced wake-driving and trailing bunches and allowed the external-injection experiment to begin. After observing first acceleration, with a modest acceleration gradient of about 100 MeV m^{-1}, optimisation of the beam parameters led to a successively increased acceleration gradient that reached 1 GeV m^{-1}—achieving a FLASHForward-internal milestone. In a second phase, new tools to precisely control the acceleration process were developed. A new method to adjust the beam focus at the entrance of the plasma cell in a quasi-online manner was implemented [3]. The outstanding development, however, was a new method to measure the effective longitudinal plasma wakefield that acts on the electron bunches with femtosecond resolution [1]. This method gives unprecedented insights into the acceleration process and its dependencies on individual components of the experiment and ultimately enables the acceleration process to be optimised. A first step towards the demonstration of beam quality preservation in the longitudinal as well as transverse plane of a highly efficiently accelerated, externally injected electron bunch has been made by the demonstration of the preservation of the energy spread and simultaneous high-efficiency (42%) acceleration via optimal beam loading [4].
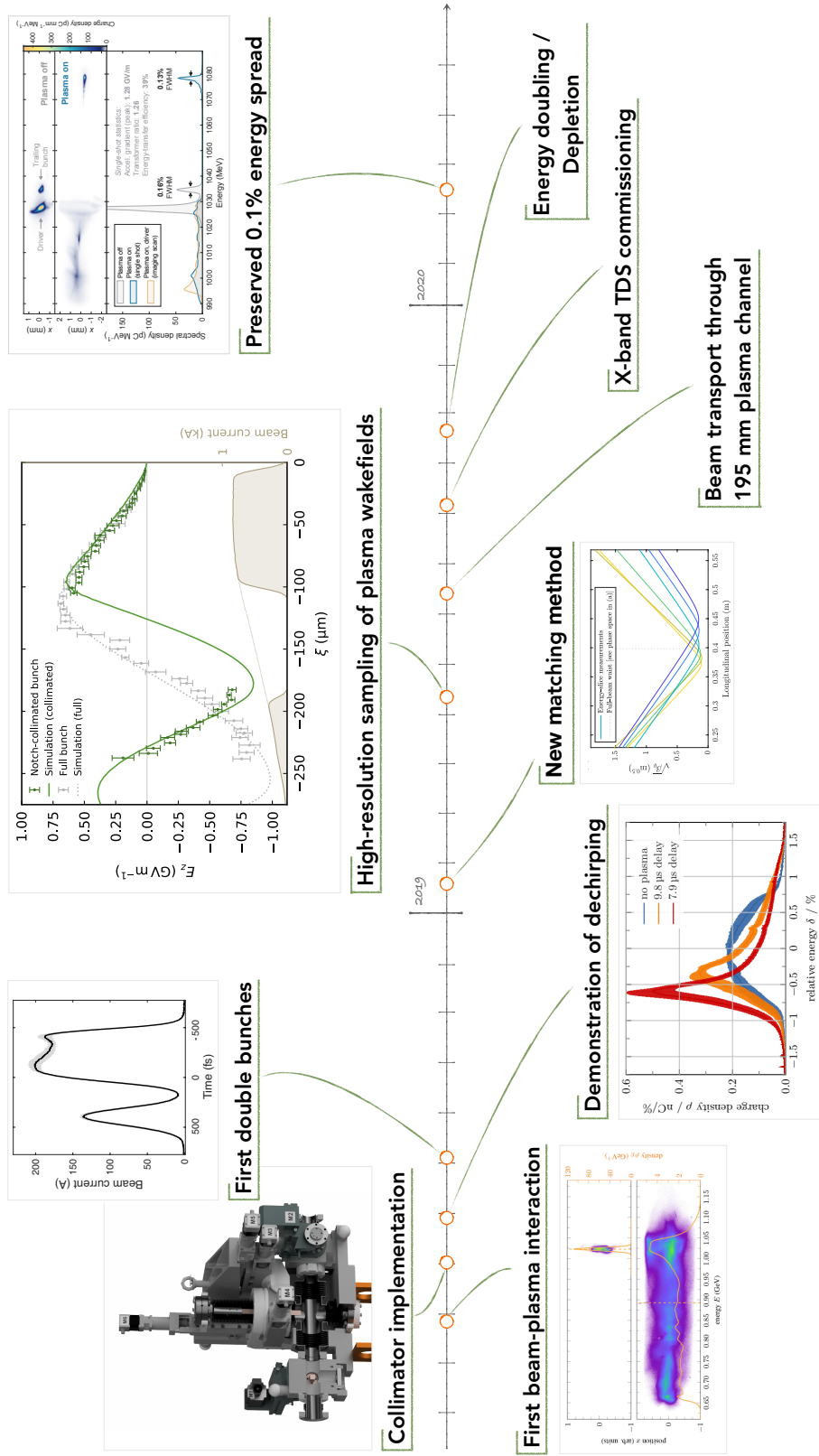
Figure 3.1: Development of the external injection experiment at FLASHForward. In the scope of this work, the external injection (X-2) experiment was accompanied from its early commissioning phase. Those achievements highlighted above the timeline have been substantially pushed forward by the author and form the backbone of this thesis. A collimator device for tunable two-bunch generation was developed and commissioned. This device lead to the invention of a novel method for high-resolution sampling of plasma wakefields and eventually enabled the preservation of the energy spread via optimal beam loading. In addition, a plasma-based dechirper was demonstrated and a novel focus-measurement technique was implemented. The experiment is now progressing towards its ultimate goal of demonstrating a self-consistent single plasma stage that simultaneously enables high-gradient, high-efficiency and beam quality-preserving electron acceleration.

3.1 Electron beam preparation

Controlling and optimising the acceleration process in plasma ultimately requires precise control of the wake-driving and beam-injection mechanisms, both of which depend largely on the properties of the plasma and the incident bunches. The capability to accurately measure and manipulate the beam parameters of both bunches—the wake-driving and the injected bunch—is therefore essential. Strong electromagnetic fields in the plasma wake, as well as the small geometric scale of the wake, place demands on the beam control that go far beyond conventional accelerator tools and therefore also require new methods and diagnostics. In the scope of this work, two additional tools for preparing the electron bunch for the interaction with the plasma were implemented to the FLASHForward beam line, which address the following important beam parameters:

- *Beam focus*: The beta function of the incident beam must be matched to the focusing fields in the plasma in order to avoid undesired oscillations of the beam size during acceleration that may lead to an increase in emittance.

- *Current profile*: In order to efficiently extract the energy from the plasma wake, it must be strongly loaded over a large range of phases. The optimisation of this beam load with regard to the energy-transfer efficiency, the transformer ratio and the preservation of the energy spread, requires a detailed shaping of the current profile of both bunches.

3.1.1 Beam matching

High-quality plasma acceleration relies on matching the transverse phase space of the incident beam to the strong radial focusing forces in the plasma wake. The beam waist must be positioned at the entrance of the plasma channel with an accuracy of the order of magnitude of the waist beta function, which, according to the matching condition Equ. (1.41), is only a few millimetres for plasma densities in the range of $\sim$10^{16}–10^{18} cm^{-3} and a beam energy of 1 GeV. Assuming an emittance of $\sim$mm mrad, the beam has to be focused to spot sizes of a few micrometers—achieving, positioning and monitoring such small beam foci is a nontrivial procedure. Conventional beam-focus diagnostics rely on time-consuming, destructive parameter scans (e.g., phase advance or object plane scans) that require detailed data analysis. Setting up a plasma accelerator is a complex task based on the optimisation of many parameters, making a simple and fast-feedback control of the beam-waist beta function and waist position a critical tool for beam preparation in the transverse plane. In order to more conveniently estimate the beam-waist position and the associated beta function at the entrance of the plasma cell, a new non-invasive method was developed using two BPMs.

The technique is based on the similarity of the Twiss parameters determined from the phase space of the beam jitter with those Twiss parameters of the actual beam phase space. This similarity allows the Twiss parameters to be estimated from the beam jitter in the two BPMs that enclose the free drift space around the plasma channel (i.e., focus position). Although this method is only approximate in nature, it is found to be a good assumption for a well commissioned beamline where the sources of jitter (e.g., magnets, cavities) are distributed over a range of several phase advances. In order to adjust the waist position and the waist beta function iteratively, time-consuming quadrupole scans can be replaced by quasi-online monitoring of the beam jitter within a few seconds.
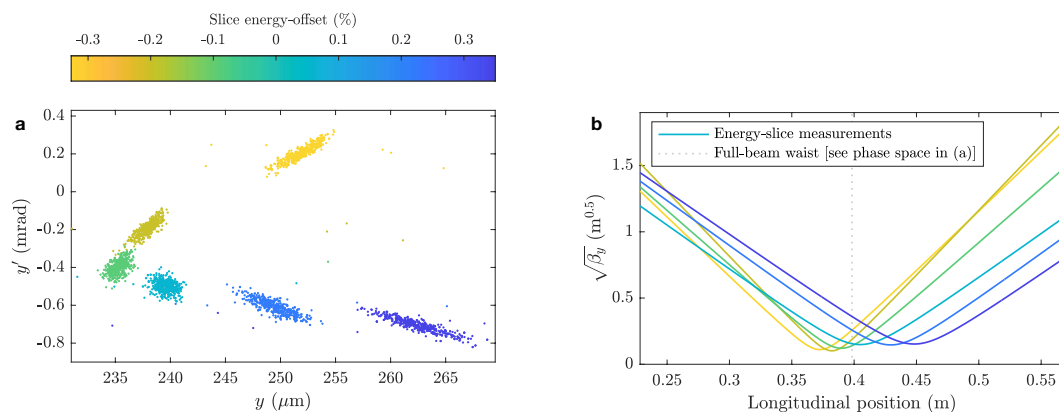
Figure 3.2: Energy-sliced focus measurement. a, By combining the new two-BPM focus-measurement method with a simultaneous scan of the two block collimators, the jitter phase space of 0.1% (rms) energy slices of a chirped bunch is measured. **b**, The resulting focus position of the individual energy slices indicate a strong chromatic effect; the bunch head is focused 80 mm ahead of the bunch tail. (Source: [3]; graph produced by C.A. Lindstrøm)

This method is now routinely integrated in the plasma-acceleration setup procedure. The comparison with a conventional quadrupole scan showed a 35% deviation in the beta function and an error in the focus position of 15 mm. These deviations are within the expected error, which is determined by the beta function itself and the resolution limit of the BPMs, lending credibility to the value of this method.

Tightly focused beams with a finite energy spread are subject to chromatic effects, i.e. high-energy particles have a longer focal length than less energetic particles—the overall beam-waist position is consequently smeared out. The use of the new focus diagnostic and the ability to perform energy-sliced beam measurements by simultaneously moving the two block collimators enabled a direct measurement of this effect. Figure 3.2 presents such a measurement for the vertical plane of the beam. The head of the bunch is focused approximately 80 mm prior to the tail of the bunch. This is of great importance for the external injection experiment where the drive and the trailing bunch are generated from a single chirped bunch, which implies that the difference in mean energy of the two bunches can be of the order of 1%. This reveals the difficulty of simultaneously matching both bunches to the focusing forces in the plasma wake, and underlines the necessary care with which this must be carried out in order to preserve the beam quality of the accelerated bunch.

3.1.2 Tunable and precise two-bunch generation

The acceleration scheme of externally injecting an electron bunch into a beam-driven plasma wakefield requires consecutive electron bunches synchronised to each other on the sub-femtosecond-level and with an adjustable bunch spacing of the order of tens of femtoseconds. Beyond the pure generation of the bunch pairs, the ability to shape the current profiles of both bunches is an essential prerequisite for precision control of the acceleration process in plasmas. The current profiles largely determine the shape of the resulting beam-loaded wakefield, whereby fundamental acceleration properties such as the acceleration gradient, the energy-transfer efficiency, the transformer ratio as well as important beam parameters such as the resulting energy spectrum and the amount of charge that can be loaded into the wakefields are determined. At FLASH, such a pair of bunches can in principle be generated directly at the gun using a tunable laser-pulse split-and-delay system [178]. However, the strong space-charge force prevalent in the photo-injector greatly complicates the beam setup routine and the independent tuning of the individual bunch parameters. In addition, experimental tests showed that this approach can lead to machine settings that are incompatible with parasitic operation. Another approach was therefore pursued, which is based on a corresponding implementation at FACET [155] and whose further development formed an essential part of this thesis: a single electron bunch with a strongly correlated longitudinal phase space is bisected by a notch collimator in a dispersive section (see Section 2.2).

Publication   [2]

Tunable and precise two-bunch generation at FLASHForward

S. Schröder, K. Ludwig, A. Aschikhin, R. D'Arcy, M. Dinter, P. Gonzalez, S. Karstensen, A. Knetsch, V. Libov, C.A. Lindstrøm, F. Marutzky, P. Niknejadi, A. Rahali, L. Schaper, A. Schleiermacher, B. Schmidt, S. Thiele, A. de Zubiaurre Wagner, S. Wesch and J. Osterhoff

---

The current profile of the bunches originating from the FLASH linac typically has a trapezoidal or Gaussian shape, an energy chirp of 0.7 % (rms) and is compressed to a duration of about 150–250 fs in order to carry out external injection experiments at plasma densities between 10^{15}–10^{17} cm^{-3}. Realistic start-to-end simulations were carried out for these plasma densities in order to determine the required capabilities of the collimators to precisely shape the wakefield, which determined the design of the collimator device that is further described in the accompanying publication [2]. On the basis of these simulations, it was found that an adjustment of the beam lengths at the femtosecond level is necessary in order to efficiently flatten the wakefield via optimal beam loading (see Section 1.2.3), which translates into a required µm-precision control of the collimators, which are located at a dispersion of −340 mm. The surface roughness of the collimators must correspondingly be below the µm level, which was achieved by eroding a copper-tungsten alloy, which material ensures the necessary energy absorption and heat transfer.
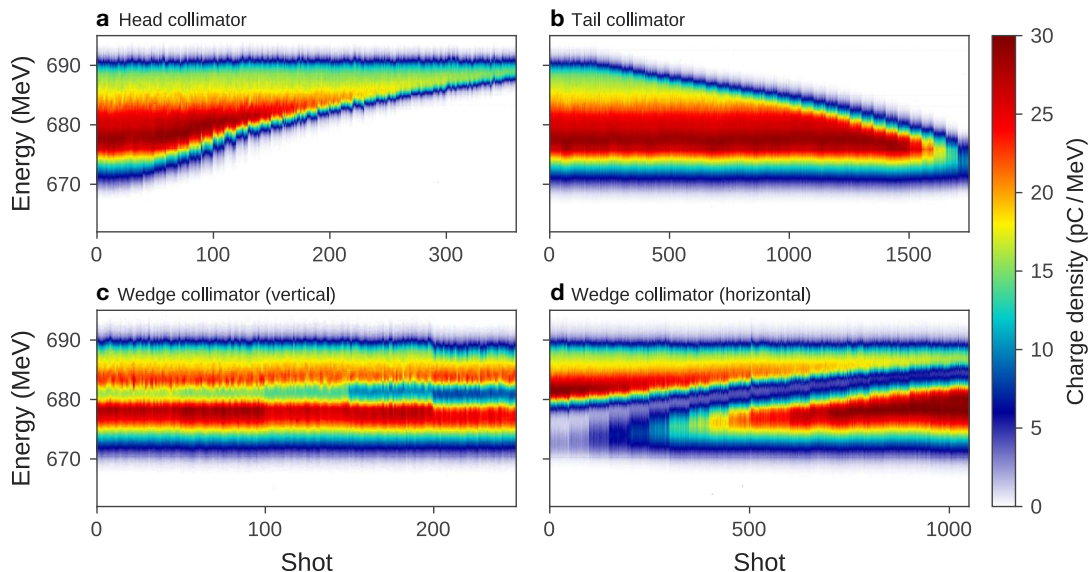
Figure 3.3: Energy projection waterfall of collimator position scans. The available beam modifications via the two block collimators (upper diagrams) and the wedge collimator (lower diagrams) are observed on the electron spectrometer while the collimator moved to discrete collimator positions. The measured energy projection (y-axis) is plotted against time (x-axis). **a**, A block collimator removing the low-energy part, which corresponds to the bunch *head*. **b**, A block collimator removing the high-energy part, which corresponds to the bunch *tail*. **c**, The wedge-shaped collimator is gradually inserted vertically into the beam line. The resulting increasing width of the collimator scatters a larger proportion of particle energies within the bunch and thereby determines the separation width of the generated consecutive bunches. **d**, Adjusting the wedge-shaped collimator horizontally determines the charge distribution among the two bunches. (Source: [2])

The initial beam-based commissioning consisted of collimator position scans of the four main adjustments: head removal, tail removal, bunch separation width, bunch separation position, i.e. charge distribution between the drive and trailing bunch (see Figure 3.3). Consecutive shots at discrete collimator positions on the electron spectrometer were recorded and distinct energy collimation was observed. Since a X-band TDS was commissioned downstream of the plasma cell in 2019 [179], the two-bunch generation can also be directly observed in the time domain (see Figure 3.4).

This method inherently ensures the best possible synchronisation of the two bunches, but at the expense of a limited flexibility to tailor the current profiles of the two bunches independently of one another and the need for detailed shaping of the longitudinal phase space. In addition, the practicability of this method is largely limited to bunches with a strictly monotonic longitudinal phase space and to operation with a low average power in order not to damage the collimators. Despite these restrictions, the simplicity of generating the drive and trailing bunch quickly and finely tunable with inherent time synchronisation makes this method particularly attractive. The large variability of possible bunch adjustments eventually enabled unique insights into the interaction of beam parameters and the acceleration process (see Sections 3.2 and 3.4). The collimator device has also proven itself in a large number of applications (e.g. wakefield measurement, longitudinally sliced bunch characterisation, charge calibration) and is used well beyond the external-injection experiment.
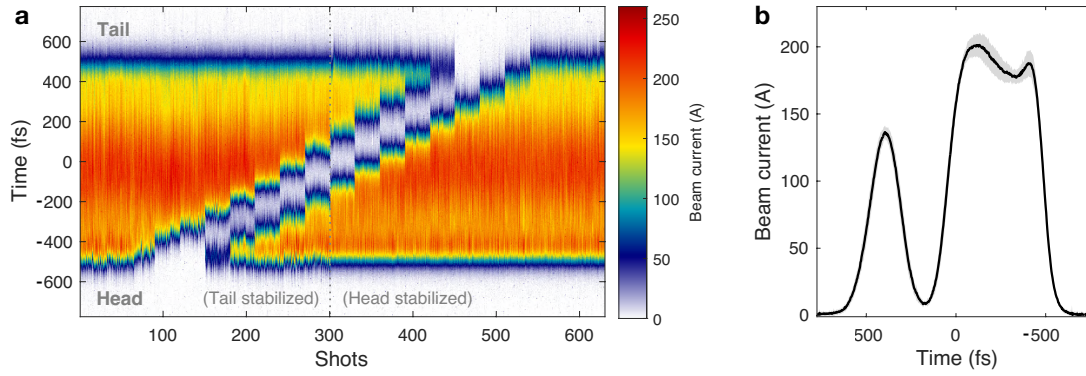
Figure 3.4: Two-bunch measurement in time domain with the TDS. a, Projection of the current profile (y-axis), measured with the PolariX X-band TDS, plotted against sot number (x-axis) while a horizontal wedge position scan is carried out. The single shots are phase corrected with a threshold for the bunch tail (first ∼ 300 shots) and then for the bunch head. **b**, Average current profile and its uncertainty (gray band) at one particular collimator position. (Source: [2])

3.2 Energy-spread preservation and high-efficiency acceleration

Efficient operation of each and every single component of an accelerator is of fundamental importance in order to reduce the power consumption of large high-energy physics facilities. The transient nature of plasma wakefields requires the immediate transfer of the energy from the driving bunch to the plasma and from the plasma to the injected bunch. High-efficiency acceleration while preserving beam quality is therefore one of the most important milestones that still have to be achieved with plasma accelerators. Special attention is here placed on the energy-transfer efficiency from the plasma wake to the injected electron bunch, which, together with the resulting energy spectrum of the accelerated bunch and the transformer ratio, depends on the exact structure of the wakefield. By using the beam-loading effect (see Section 1.2.3) to modify the wakefield shape by precisely tuning the current profiles, the acceleration can ultimately be optimised in such a way that high energy-transfer efficiency, preservation of the energy spread and a relatively high transformer ratio can be achieved simultaneously. In order to preserve a per-mill energy spread that is required for high luminosity colliders or FELs, the wakefield must be flattened along the extent of the injected bunch such that all particles experience the same acceleration. In section 1.2.3, a flattened wakefield was achieved by precisely shaping the current profile of the accelerated bunch. In this approach, the achievable acceleration gradient and charge of the accelerated bunch are inevitably linked. In order to obtain more flexibility with regard to bunch (charge, peak current) and acceleration properties (gradient, efficiency, transformer ratio), a more complex concept of acceleration optimisation must be pursued by not only adapting the current profile of the accelerated bunch but also that of the drive bunch and the plasma density. Using the capabilities of the newly installed collimator device, such an optimally beam-loaded operating point was experimentally demonstrated for the first time in a non-linear beam-driven plasma wakefield accelerator. A bunch of 100 pC charge was accelerated with a gradient of $1.3 \, \text{GeV} \, \text{m}^{-1}$ while an energy-transfer efficiency of $(42 \pm 4)\%$ was achieved and the per-mill energy spread as well as the total charge was preserved.
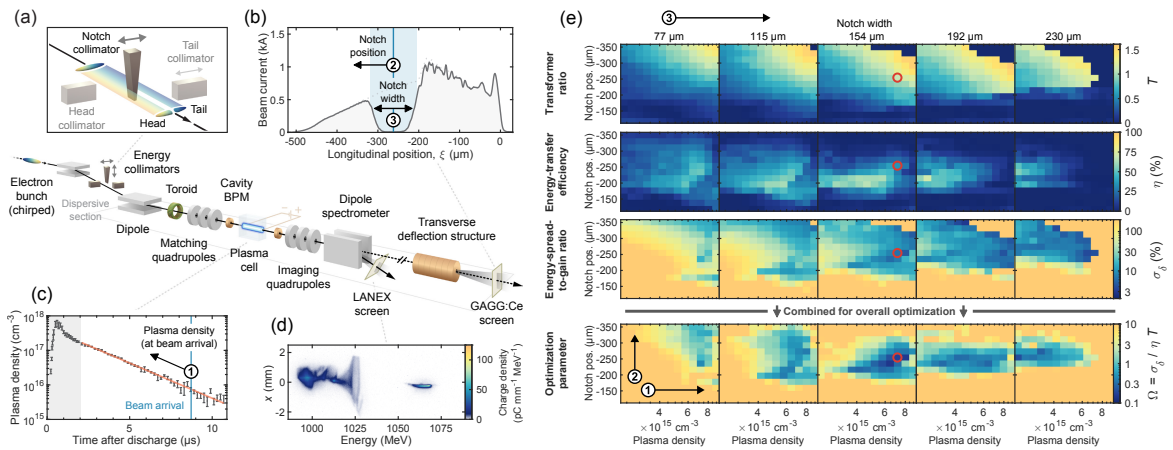
Figure 3.5: Multi-dimensional notch-collimator position and plasma density scan. a, Three collimators in a dispersive section allow tunable two-bunch generation from a chirped bunch. **b**, Vertical and transverse position of the wedge-shaped collimator determines the charge configuration of the two bunches. **c**, The plasma density in a 5 cm long discharge capillary is varied by adjusting the trigger-delay timing. **d**, The energy spectrum at the plasma-exit plane is point-to-point imaged on the dipole spectrometer screen. **e**, A parameter scan of plasma density (1) and notch position (2) as a function of notch width (3) is performed. At each scan point the transformer ratio (T), energy-transfer efficiency (η), energy-spread-to-gain ratio (σ_δ) and a combined optimisation parameter (Ω) are determined with the overall optimal operating point being marked with a red circle. (Source: [4]; graph produced by C.A. Lindstrøm)

To find this optimal operating point, a complex three-dimensional scan of the plasma density, the bunch-separation position and the corresponding bunch-separation width was carried out (see Figure 3.5). With this complex, multidimensional parameter scan, all available configurations for generating the two bunches from the given current profile of the incident electron bunch were examined, whereby the position of the injected bunch inside the wake, the peak currents of both bunches, the charge ratio between the two bunches as well as the wake strength are varied in an interdependent manner. In order to evaluate the overall performance of the acceleration process at each of these sampling points, three critical wakefield parameters were extracted from the recorded energy spectra, which all need

to eventually be optimised at the same time: the transformer ratio (T), the energy-transfer efficiency (η), and the energy-spread-to-gain ratio (σ_δ). A new parameter $\Omega = \sigma_\delta/(\eta T)$ as a simplified overall figure of merit was introduced, the minimisation of which helps to simultaneously minimise the energy-spread-to-gain ratio while maximising the energy-transfer efficiency and the transformer ratio. The optimal operating point found on the basis of this figure-of-merit parameter differs from the corresponding minima (σ_δ) and maxima (η, T) of the individual parameters [highest transformer ratio: 1.61 ± 0.01; highest energy-transfer efficiency: $71 \pm 4\%$; lowest energy-spread-to-gain ratio: $3.1 \pm 0.2\%$ Full Width at Half Maximum (FWHM)] and thus underlines the need for a complex multi-dimensional approach in order to achieve a holistic optimisation of the acceleration.

At the overall optimal operating point (minimum Ω), a 5000-shot high-statistics data set was taken (see Figure 3.6). The trailing bunch was accelerated by 45.4 ± 1.4 MeV with an energy-transfer efficiency of $42 \pm 4\%$. Preservation of the energy spread or even its reduction was found in 6.4% of the data set; the rest had a median energy spread of 0.2% (FWHM), which corresponds to a relative increase of 28%. The instabilities in energy gain $\sim$3% and energy spread can be understood as a sensitivity to jitters in beam and plasma parameters. This parameter set constitutes a major advance for beam-driven plasma wakefield accelerators.

The demonstration of high-gradient acceleration of an externally injected electron bunch, for which the energy distribution could be preserved and at the same time a high energy-transfer efficiency was achieved, represents a major step towards the comprehensive goal of efficient and beam-quality-preserving acceleration in the field of beam-driven plasma wakefield acceleration. In order to find this optimised operating point, the interdependent relation between the beam parameters and the acceleration performance required a complicated multi-dimensional parameter scan, which illustrates the complexity of controlling a plasma-based accelerator compared to

Figure 3.6: Optimally beam-loaded acceleration operation point. a, Spectrometer images with and without plasma interaction and the corresponding energy spectra. The initial energy spread of the trailing bunch is preserved. **b**, Across 5000 consecutive shots, the energy gain is stable within 3% (rms). **c**, The energy spread is preserved or even reduced in 6.4% of these shots (dotted line). **d**, At the same time, the energy-transfer efficiency is between 30% and 50%. (Source: [4]; graph produced by C.A. Lindstrøm)

conventional acceleration modules and the need for novel beam-optimisation methods. In order to optimise a plasma-based accelerator without restrictions for certain target beam parameters such as energy or charge, complete control over the current profile is necessary, which was only possible to a limited extent here. In future this could be achieved through more advanced two-bunch generation that uses a combination of the laser-pulse split-and-delay stage in the gun in combination with the collimators for the fine adjustment.

3.3 Plasma-based energy chirp correction

A finite energy spread in the form of a correlated longitudinal phase space is on the one hand a useful and often unavoidable feature, on the other hand a limiting factor for many applications of particle accelerators. As in the FLASH linac, such an energy chirp is often used for longitudinal bunch compression, but leads to chromatic effects, especially in the case of tight foci, and may limit the useful luminosity in colliders or the brilliance in FELs.

In plasma-based acceleration concepts, the injected electron bunch typically spans a large range of wakefield phases and develops an energy chirp over the acceleration distance if no special measures are taken. By cleverly exploiting the beam-loading effect, the energy spread can be reduced or even preserved, as described in the previous section, but the concept of beam loading may not always be applicable. Optimal beam loading requires a high degree of control over the current profile and thereby reduces flexibility with regard to key properties of the accelerated bunch (charge, bunch length, peak current)—a flexibility that may be necessary in specific applications that normally depend on the tunability of beam parameters, such as FELs. In addition, optimised beam loading for several staged plasma modules is becoming increasingly difficult, since the current profile of the accelerated bunch can only be optimised for the first plasma module. The conditions for optimised beam loading, however, can change due to deviations in the bunches during beam transport. Apart from these technical aspects, there may also be physical advantages to accelerating deliberately chirped bunches and only subsequently correcting the chirp for final use in colliders or FELs. One such case is to mitigate detrimental transverse beam instabilities resulting from the strong focusing forces in the plasma by means of Balakin-Novokhatsky-Smirnov (BNS)-type damping through a head-to-tail variation [180–183]. An independent tool for efficient chirp correction may therefore be indispensable for future high-gradient acceleration techniques.

The strong electric field ($\sim$GeV m^{-1}) that exists in plasma wakefields and varies greatly across the small structure of the plasma wave ($\sim$100µm) can be also used to reduce a correlated energy spreads with a strength on the order of GeV mm^{-1} m^{-1}. In order to reduce a negative chirp, the plasma density is chosen such that the bunch experiences the monotonically increasing and decelerating wakefield (see Figure 3.7). The wakefield shape that acts on the bunch depends on the beam and plasma parameters, with the plasma density ultimately lending the concept of plasma-based energy dechirping a high degree of adjustability. The mismatch between the exact wakefield shape and the bunch chirp is ultimately the limiting factor of this method. A positive energy chirp is inherently reduced by the acceleration process, provided the wakefield is not overloaded. [184]. The ease of adjustment and the sheer strength of a plasma-based dechirper, make this concept an interesting alternative to state-of-the-art techniques in corrugated metallic pipes [185] or dielectric structures [186], which operate with sub-MeV/mm level fields.
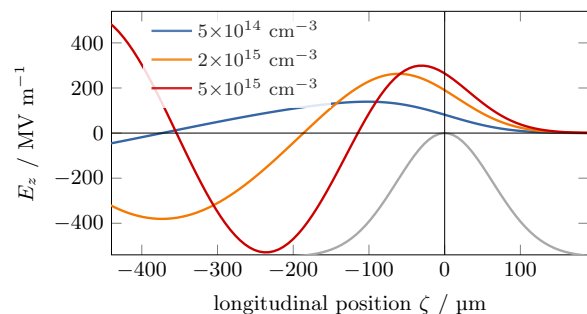

Figure 3.7: Plasma-based dechirping. An electron bunch (grey) excites a plasma wake. The wakefield gradually builds up along the bunch. A negative chirping of the incident bunch is thus reduced, with the plasma density determining the dechirping strength. (Source: [5]; graph produced by A. Martinez de la Ossa)

At FLASHForward, such a plasma-based energy chirp correction was demonstrated (see Figure 3.8). The energy spread of a negatively chirped electron bunch was reduced by interaction with the plasma from an initial FWHM 1.3% to 0.33%, which corresponds to a dechirping strength of $1.8\ \mathrm{GeV\,mm^{-1}\,m}$ in a 33 mm long plasma channel. The plasma density was optimised via the time delay between plasma generation and bunch arrival. The uncertainty in the energy spectrum was not affected by the interaction with the plasma (compare the error band of the blue with the red and orange spectra). For most applications, however, the transverse beam parameters must also be preserved, which has not yet been shown in this experimental campaign but remains to be demonstrated in order to finally evaluate the applicability of this dechirping method.

Figure 3.8: Dechirped energy spectra. A change in plasma density clearly shows a reduction in the FWHM energy spread compared to the non-interacted electron bunch (blue). The error ranges represent the standard deviation over 50 consecutive shots—showing no degradation. (Source: [5]; graph produced by Richard D'Arcy)

This result shows up an approach for subsequent chirp correction in plasma accelerators, in which a resulting large energy spread is often viewed as a limiting factor. In addition, this method can also be understood as a simple and low-cost addition to conventional accelerators whose functionality may be limited by remnant energy chirps.

3.4 High-resolution sampling of plasma wakefields

Controlling the beam parameters is of utmost importance for high-energy applications. While the energy spread has to be on the sub-percent level, the operation of free-electron lasers, in particular, is governed by the additional ability to tune beam parameters such as the beam charge and energy. In plasma wakefield accelerators, due to the typically strong beam-loading effect, all these parameters have a complex dependency that is determined by

the shape of the wakefield. Precision control over the wakefield shape is therefore crucial to produce the required beam-parameter settings and requires a technology that provides a quick feedback on the wakefield shape. As a core part of this thesis, a new method for sampling beam-driven plasma wakefields with femtosecond resolution was invented (Figure 3.9).

In principle, the complete information about the longitudinal wakefield with which the beam has interacted is imprinted on the longitudinal phase space of the incident beam. The effective wakefield that acts on the bunch integrated over the entire acceleration length can thus be obtained from the difference in the longitudinal phase space before and after the interaction with the plasma. While determining the energy spectrum of an electron bunch is a comparatively simple measurement, the femtosecond-resolved measurement in the time domain required here is anything but trivial and requires advanced diagnostic tools such as a TDS. In addition, beams that have interacted with plasma in a non-optimal manner are typically highly divergent and have a large energy spread, which complicates their transport through the beamline. In the plasma wakefield sampling method described here, these difficulties are circumvented by making the measurements in the energy and time domains of the longitudinal phase space independent of one another and replacing the post-plasma femtosecond-resolved time measurement with a collimator calibration with the non-interacted bunch.

By causality, removing the tail of the bunch does not alter the wakefield in front of this modification. Thus, gradually removing the bunch tail and observing the corresponding change in the energy spectrum of the outgoing bunch reveals the longitudi-

Figure 3.9: Sampling of plasma wakefield through energy collimation. a, Energy collimation of a linearly chirped bunch effectively allows the bunch tail slices to be progressively removed. **b**, The interaction with plasma imprints an energy spectrum onto the phase space of the incident bunch, which is characteristic for the wakefield shape (3D particle-in-cell simulation). **c**, The wakefield experienced by the bunch remains unaltered by removing the bunch tail. By subtracting the final energy spectrum of consecutive collimator positions, the energy change of each longitudinal slice can be determined——revealing the effective wakefield at the associated longitudinal position. (Source: [1])
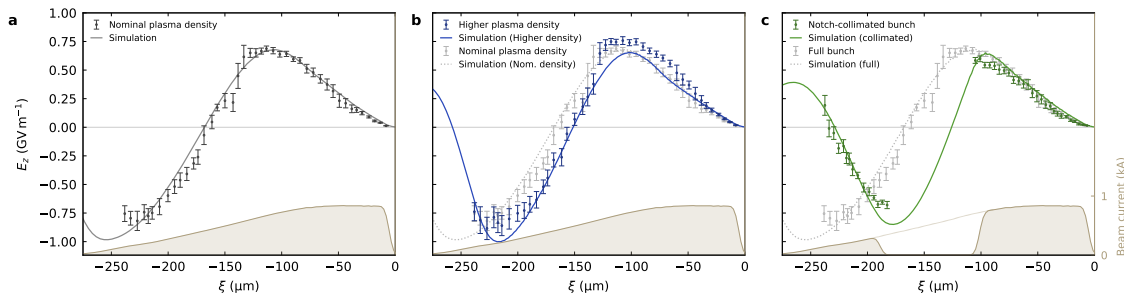
nally resolved wakefield shape. The hereby achievable time resolution depends on the ability to precisely remove the bunch tail, which is here limited by the monotonicity of the incident longitudinal phase space, the slice energy spread and the precision of the collimator adjustment. The temporal measurement of the wakefield is now reduced to a high-resolution calibration of the collimator position to an effective longitudinal intra-bunch position, which must be carried out only once and prior to the wakefield optimisation campaign. For this, the TDS in the parallel beam line FLASH1 was used.

Figure 3.10: Measured wakefields for various beam and plasma parameters. a, The wakefield of the nominal plasma density is sampled with a 6 μm granularity. Error bars represent the shot-to-shot standard deviation. The solid line shows the corresponding PIC simulated wakefield. **b**, The measurement is repeated with the same beam current profile and an 80% higher plasma density (the beam arrives 1.7 μs earlier), producing a shorter wavelength wakefield. **c**, At the nominal density (as in a), the beam current is notch-collimated into a double-bunch profile, producing a wakefield which is identical at the head, but strongly altered at the tail. The end point of $\xi = -240$ μm is determined by signal-to-noise ratio. (Source: [1])

Using this method, longitudinal electric fields of order gigavolts-per-meter ($0.8\,\mathrm{GV\,m^{-1}}$) were measured with 15 fs resolution (see Figure 3.10). To measure the plasma wakefield in its entirety a bunch was used that spans all phases of the plasma wake. Furthermore, the direct effect of plasma and beam parameters on the beam-loaded longitudinally integrated plasma wakefield are examined. Qualitatively, the increase in plasma density leads to an expected decrease of the plasma wavelength (Figure 3.10b). The separation of the bunch into two—a wake-driving bunch and a trailing bunch—results in a reduction in charge load inside the wake (Figure 3.10c) and consequently changes the wakefield shape. The wakefield at the location of the unmodified bunch part—the drive bunch—remains the same, while the total size of the plasma cavity reduces drastically. This measurement constitutes the first direct observation of the underlying effect of beam loading in plasma wakefields, where the trajectory of the sheath electrons forming the plasma cavity is modified by the space charge inside the cavity that is consequently elongated. A more quantitative evaluation of these results is done through a comparison with PIC simulations, in which the experimental environment is accurately modelled. The plasma density profile along the acceleration path

is examined in a test stand [160]; the full 6D phase space of the electron bunch at the entrance of the plasma channel is inferred by a combination of different diagnostic tools: the TDS measurement, a longitudinally resolved object plane scan with the imaging quadrupoles for the energy spectrometer and the longitudinally resolved two-BPM method discussed above. As a result of this detailed characterisation of the beam and plasma parameters, a good agreement between simulation and measurement is achieved—verifying to the accuracy of the method. This study of wakefield measurements over a large range of beam and plasma parameters exemplifies on one hand the achieved understanding of the experimental setup via the agreement with simulations and on the other hand the robustness of the wakefield measurement technique—a feature that is absolutely necessary for a diagnostic that is intended to support an optimisation process.

At FLASHForward, this newly developed wakefield measurement technique is now used as a key diagnostic for simple and quick feedback on the qualitative status of the acceleration process. It accompanies the routinely performed process of acceleration optimisation, and is ultimately used to precisely characterise the plasma wakefield. As such an optimisation diagnostic, this wakefield measurement method was used for the first time to support the search for the optimal operating point via beamloading as discussed in Section 3.2. Preserving the energy spread ultimately requires a constant electric field along the injected bunch. In order to find this optimal operating point, the wakefield measurement was carried out repeatedly during the entire optimisation campaign and the wakefield of the acceleration process that was ultimately determined

Figure 3.11: Optimally beam-loaded wakefield. Wakefield of uncollimated bunch (gray) and optimally collimated bunch (blue) with corresponding PIC simulations. An additional simulation without the trailing bunch (blue dotted line) indirectely proves the flattening of the wakefield through optimal beam loading. (Source: [4]; graph produced by C. A. Lindstrøm)

to be optimal was finally characterised with a high-resolution measurement (see Figure 3.11). This result constitutes the first measurement of a plasma wakefield flattened to the %-level.

The developed method is by no means restricted to the use at FLASHForward. Most facilities satisfy its prerequisites of a linear longitudinal phase space and a dispersive section, such that a collimator in the dispersive section is a low-cost addition and is easy to implement, if not already available. As in this case, the time calibration of the collimators with a TDS does not have to be carried out in the same beam line, but can also be done with a time-resolved bunch diagnostic at a different location—provided that the optics of the beam line is sufficiently understood. This is of great advantage, since femtosecond-resolved beam diagnostics such as a TDS are expensive devices and are not widely available.

This method enables a new level of control over the acceleration process achieved in the field of beam-driven plasma wakefield acceleration. The developed wakefield sampling method bridges a gap between theoretical predictive models and the experiment, it enables a direct insight into the actual acceleration process in experiments and thus points the way towards a precise tailoring of the wakefield shape to the needs of future demanding applications of beam-driven plasma wakefield accelerators.
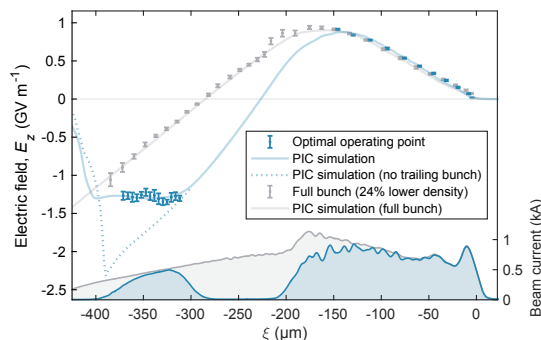
CHAPTER 4

Conclusion

Plasma wakefields, driven by intense and ultra-relativistic particle beams, can provide acceleration gradients on the order of hundreds of $\mathrm{GeV\,m^{-1}}$ as well as efficiencies of tens of percent, and are therefore a promising avenue to significantly reduce the size and cost of future accelerators for high-energy, high-average-power facilities such as FELs and particle colliders. Despite these extraordinary acceleration gradients, reaching the TeV energy-frontier still requires the in- and out-coupling of an electron bunch in successive acceleration stages. Research into the external injection of electron bunches into beam-driven plasma wakefields is therefore vital to the envisaged paradigm shift in acceleration technology.

Since the proof of the fundamental suitability of beam-driven plasma wakefields for high-gradient acceleration at FFTB and FACET, calls for the demonstration of usable electron bunches and the development of first applications of such plasma-based accelerators have become louder. The immediate research focus has therefore shifted to improved stability of the acceleration process as well as precision control and, in particular, the preservation of the beam parameters. With one and the same goal of contributing to the development of an ultimate beam-driven plasma wakefield accelerator for high-energy-physics experiments, various test-bench facilities were built which, with their unique specifications, contribute to this common goal from very different perspectives and with different aspects—including FLASHForward at Deutsches Elektronen-SYnchrotron (DESY), where this thesis was carried out. At FLASHForward, the high-quality wakefield-driving and injected electron bunches coming from an FEL (FLASH) enable an unprecedented stability and make this facility an excellent place for high-precision studies of the beam–plasma interaction. However, the small size of plasma wakefields, their sheer strength, and their transient nature create a slew of complications that go well beyond those of conventional acceleration techniques. The small structures put tight tolerances on synchronisation and misalignment; the high field strengths require careful beam matching; the transient nature of the plasma wakefields require rapid and efficient energy extraction. In addition, in plasma wakefield accelerators, acceleration, manipulation of the longitudinal phase space and strong transverse beam focusing happen simultaneously and in an interdependent manner—tasks that in a conventional accelerator are deliberately distributed among different devices. A holistic optimisation of plasma accelerators is therefore a complex multi-dimensional problem that eventually requires the development of new creative approaches. This thesis discussed recent achievements within the active research field of external injection into beam-driven plasma wakefield accelerators, which have been described in peer-reviewed publications.

A new method has been implemented that enables convenient adjustment of the beam focus based on the measurement of the beam jitter in two BPMs [3]. Even though this method is only approximate, the gained quasi-online feedback on the beam focus represents a massive simplification of the time-consuming process of beam matching into the strong transverse focusing fields prevalent in a plasma wake, which requires millimetre-scale beta functions and precision in focus positioning on the same order of magnitude.

The overall optimisation of beam-driven plasma wakefield accelerators is fundamentally linked to the concept of beam loading, by means of which the wakefield shape can be advantageously altered in order to simultaneously achieve high-gradient, high-efficiency, energy-spread-preserving acceleration with a relatively high transformer ratio. A precise adjustment of the beam load in the wake, i.e. the current profiles of the wake-driving and trailing bunch, is essential for this; this has been given special attention in this work. A collimator device that enables beam-current-profile manipulations by means of energy collimation of an electron bunch with a strictly monotonic longitudinal phase space in a dispersive section was designed [2]. This device enables the current profiles of the driving as well as the accelerated bunch to be fine-tuned with femtosecond precision within the restrictions of the incoming beam parameters. By utilising all the degrees of freedom of this fine adjustment, it was ultimately possible to find an optimal operating point of the plasma accelerator at which the bunch was accelerated with a $1.3\,\text{GeV}\,\text{m}^{-1}$ gradient, while for the first time the energy spread as well as the charge of the accelerated bunch were preserved and at the same time a high degree of efficiency of 42% was achieved [4].

Plasma wakefields are also known as an useful tool beyond pure particle acceleration in order to take over other tasks in an accelerator. A correction of a correlated energy spread with an outstanding strength of $1.8\,\text{GeV}\,\text{mm}^{-1}\,\text{m}^{-1}$ was demonstrated here. Such a plasma-based chirp correction shows a potential solution to a typically large energy spread that results from a plasma accelerator, if optimised beam loading is not applicable. This induced energy spread is often remarked as a fundamental limitation for high-quality beams from plasma-based accelerators.

Investigating the plasma–beam interaction in depth requires a detailed understanding of the acceleration process, with the shape of the longitudinal wakefield playing a pivotal role. Ultimately, the optimisation of the acceleration through wakefield shaping necessitates a tool to precisely measure the wakefields. As a central part of this thesis, a plasma-wakefield sampling technique was invented that enables unique femtosecond-resolved insights to the plasma acceleration process [1]. For the first time the effect of beam loading on the wakefield could be directly measured and an optimally flattened wakefield was achieved. Excellent agreement with the characteristics of the data was achieved with PIC simulations. Given the extreme sensitivity of the wakefield to only small modifications in beam or plasma parameters, the agreement of data and simulations achieved for considerably different beam and plasma parameters, each of which was carefully measured, constitutes a new level of understanding and precision for beam-driven plasma wakefield acceleration operation.

Despite the contribution to the research field made in this thesis, the construction of a plasma-based collider is still far from the horizon, and many fundamental and technological problems still need to be solved. The studies pursued in this work concentrated largely on the control and quality of those beam parameters that are influenced through the interaction with the longitudinal plasma wakefields. For a complete preservation of the beam quality, however, the interaction of the beam with the transverse wakefields is also of importance. Next steps are to also preserve the transverse beam parameters (in the optimal case directly

together with the longitudinal beam parameters) or to measure and suppress the extent of the emittance growth.

On a more distant time scale, the staging of several plasma modules in order to reach the energy-frontier of today's colliders, the demonstration of high-average-power operation, the scaling of the entire acceleration process to higher energies and longer plasma channels and all of these also for positrons, are crucial future tasks.

While the construction of a collider is the most demanding, and therefore distant, application of the plasma-based particle-acceleration technology, there are others that would be conceivable in the next decade or two and that are seen as essential for the further funding of the research field. In particular, the implementation of a single plasma stage as an energy amplifier for existing or planned facilities can be an attractive first high-energy application [187, 188], on the one hand to convince the last sceptics of the potential of this acceleration technology through its use in a proper high-energy facility and on the other hand to enrich the physics carried out in these facilities.

The FLASHForward project follows precisely this path with the endeavour to demonstrate a fully beam-quality-preserving, self-consistent single plasma stage in a first step, which is then planned to be scaled to high-average-power operation.

APPENDIX A

Author contribution and publications

The author of this thesis, referred to as "the author" in the following, contributed to the initial commissioning and further development of the beamline and played a key role in the experimental campaign of the external injection experiment at FLASHForward. The author was instrumental in planning the experimental campaigns, setting up the experiment and data collection for each publication discussed in this thesis. Contributions that go beyond this are elaborated below, with the publications listed in chronological order.

1. **Tunable plasma-based energy dechirper** [5] (page 62)
   The author supported the data analysis with a detailed energy calibration of the dipole energy spectrometer based on CST simulations.

2. **Tunable and precise two-bunch generation at FLASHForward** [2] (page 68)
   The author led the project. The author determined the required specifications of the collimator device for a precisely tunable two-bunch generation that enables optimal beam loading based on first start-to-end simulations of the experiment. The author coordinated the process of construction, assembly and commissioning, wrote the associated conference proceeding as part of an invited plenary talk at the 4th European Advanced Accelerator Concepts workshop 2019 and coordinated the process of publication.

3. **Matching small β functions using centroid jitter and two beam position monitors** [3] (page 75)
   The author contributed to the conceptual idea and paper writing.

4. **High-resolution sampling of beam-driven plasma wakefields** [1] (page 83)
   The author conceived the idea of the wakefield sampling method and lead the project. The author performed the data analysis and PIC simulations, coordinated the required precise plasma density characterisation (carried out by others), mainly wrote the paper and coordinated the publication process.

5. **Energy-spread preservation and high efficiency in a plasma-wakefield accelerator** [4] (page 89)
   The author proposed this measurement, enabled it through the design of the collimator device and played a leading role in the planning and execution. The increased understanding of the experimental setup gained through the meticulously carried out data–simulation comparison from the wakefield-sampling paper have made a fundamental contribution to the data analysis for this publication.

Tunable Plasma-Based Energy Dechirper

R. D'Arcy,[1,*] S. Wesch,[1] A. Aschikhin,[1,2] S. Bohlen,[1,2] C. Behrens,[1] M. J. Garland,[1] L. Goldberg,[1,2] P. Gonzalez,[1,2]
A. Knetsch,[1] V. Libov,[1,2] A. Martinez de la Ossa,[1,2] M. Meisel,[1,2] T. J. Mehrling,[1,3] P. Niknejadi,[1] K. Poder,[1]
J.-H. Röckemann,[1,2] L. Schaper,[1] B. Schmidt,[1] S. Schröder,[1,2] C. Palmer,[1,4] J.-P. Schwinkendorf,[1,2] B. Sheeran,[1,2]
M. J. V. Streeter,[1,5] G. Tauscher,[1,2] V. Wacker,[1] and J. Osterhoff[1]

[1]*Deutsches Elektronen-Synchrotron DESY, Notkestraße 85, 22607 Hamburg, Germany*
[2]*Universität Hamburg, Luruper Chaussee 149, 22761 Hamburg, Germany*
[3]*Lawrence Berkeley National Laboratory, University of California, Berkeley, California 94720, USA*
[4]*University of Oxford, Wellington Square, Oxford OX1 2JD, United Kingdom*
[5]*Imperial College London, Kensington, London SW7 2AZ, United Kingdom*

A tunable plasma-based energy dechirper has been developed at FLASHForward to remove the correlated energy spread of a 681 MeV electron bunch. Through the interaction of the bunch with wakefields excited in plasma the projected energy spread was reduced from a FWHM of 1.31% to 0.33% without reducing the stability of the incoming beam. The experimental results for variable plasma density are in good agreement with analytic predictions and three-dimensional simulations. The proof-of-principle dechirping strength of 1.8 GeV/mm/m significantly exceeds those demonstrated for competing state-of-the-art techniques and may be key to future plasma wakefield-based free-electron lasers and high energy physics facilities, where large intrinsic chirps need to be removed.

The wakefield structure in a plasma-based particle accelerator [1,2] offers distinct advantages for future free-electron laser (FEL) and high energy physics (HEP) applications [3], such as strong intrinsic focusing and high accelerating gradients [4]. These, in principle, allow for the stable propagation and acceleration of an injected bunch to required energies over distances orders of magnitude shorter than those possible in conventional accelerator designs. A challenge of plasma-based concepts, however, is the development of the longitudinal phase space of the beam, accelerated in an environment that may imprint a large linear energy-time dependency—the so-called "chirp"—on the beam up to the GeV/mm level. Upon exit of the plasma section this large negative remanent chirp will halt FEL gain or lead to a beam size increase limiting luminosity in HEP experiments. Ideally the chirp ought to be mitigated in order to utilize plasma wakefield acceleration techniques in future facilities.

Beam loading [5]—in which the steep accelerating plasma wakefield gradient observed by the electron beam is flattened due to high bunch charges, either by shaping of the bunch [6] or through the injection of a second bunch [7]—has been experimentally demonstrated to minimize production of chirps in plasma [8]. Other concepts, such as modulated plasma densities [9], have also been proposed to prevent the generation of these chirps. However, recent studies indicate that it is advantageous for a beam propagating through plasma to feature a finite correlated energy spread in order to mitigate, for example, the instability that

seeds hosing [10,11]. This effect is analogous to Balakin-Novokhatsky-Smirnov damping [12], where a correlated energy spread mitigates transverse instabilities in linacs and storage rings. Its utilization may be necessary in future plasma-based FEL and HEP applications to conserve the required beam characteristics in the acceleration process. Allowing the generation of chirps within plasma would therefore be beneficial, with dechirping of the beam occurring in a separate section.

Removal of energy chirps using corrugated pipes [13] and dielectric-based slab structures [14] has been experimentally demonstrated. To date, these structures have been shown to remove chirps on the sub-MeV/mm level, with current theoretical estimates indicating potential for growth [15–17]. To compensate the extreme energy chirps generated in plasma-based accelerators within distances comparable or shorter than the accelerator size, a technique capable of removing chirps far exceeding those experimentally demonstrated is required. This can be achieved by taking advantage of the large electric fields inherent to the plasma acceleration process.

One such mitigation strategy, based on the observation that a beam driving a plasma wakefield—a so-called "driver"—will be subjected to a decelerating longitudinal field with a particular longitudinal dependency, is explored. By carefully matching the electron plasma density to the longitudinal beam properties it is possible to reduce, and potentially remove, an initial energy chirp of a driver beam. In this Letter the utilization of such a plasma-based energy

chirp compensator at the FLASHForward experiment [18] is described, whereby an electron bunch produced by the gun of the FLASH water-window FEL facility [19,20], and linearly chirped using the accelerating modules and bunch compressors in the linac, is dechirped in plasma.

The time-averaged profile of the electric field in plasma E_z leading to the reduction of the energy chirp, ultimately depends on the beam phase space distribution and the plasma profile. Here we regard a flat-top plasma with a plasma electron density of n_p and electron beams with densities n_b on the order of n_p. The FEL-quality beams have an emittance smaller or equal to the matched emittance in a homogeneous plasma channel such that the relation $k_p\sigma_x \ll 1$ for the rms width, σ_x can be maintained during the whole interaction with the plasma, where $k_p = \omega_p/c$ is the inverse plasma skin depth, $\omega_p = \sqrt{n_p e^2/m\epsilon_0}$ the plasma frequency, e the elementary charge, m the electron mass, ϵ_0 the vacuum permittivity, and c the speed of light.

For underdense beams, where $n_b < n_p$, linear plasma waves are driven with an on-axis electric field, given by [21]

$$\frac{E_z(\zeta)}{E_0} = k_p^2 \int_\infty^\zeta d\zeta' \cos\left[k_p(\zeta - \zeta')\right]$$
$$\times \int_0^\infty dr' k_p r' K_0(k_p r') \frac{n_b(\zeta', r')}{n_p}, \quad (1)$$

where $\zeta = z - ct$ is the comoving variable, r' the radius, $E_0 = \omega_p mc/e$ the cold nonrelativistic wave-breaking field, and K_0 the modified Bessel function of the second kind.

For beams with a transverse Gaussian profile with $k_p\sigma_x \ll 1$,

$$\frac{E_z(\zeta)}{E_0} \simeq -\log(k_p\sigma_x)k_p \int_\infty^\zeta d\zeta' \cos\left[k_p(\zeta-\zeta')\right]\frac{2I_b(\zeta')}{I_A}, \quad (2)$$

where $I_b(\zeta')$ is the beam current profile and I_A the Alfvén current. Such field profiles generated from a 3D Gaussian beam are illustrated in Fig. 1. A characteristic beam length of $k_p l_z \lesssim 1$ ensures that the beam quasiresonantly excites the plasma wave and that E_z is monotonically increasing from the head to the tail for the majority of the beam. This electric field will, therefore, reduce the correlated energy spread of a beam with a linearly increasing energy profile from head to tail, i.e., a negative energy chirp.

For the blow-out regime, with $n_b \gg n_p$, similar considerations can be made. If, furthermore, $k_p\sigma_x \ll 1$ the majority of the beam is embedded in the generated blowout, such that E_z is constant within a beam slice and, to a good approximation, only depends on I_b and n_p (cf., e.g., Refs. [22,23]). While the profile of E_z in the blowout
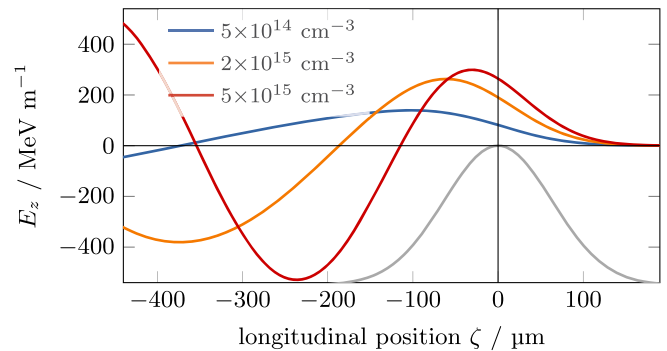

FIG. 1. Lineouts of the analytical electric fields E_z of three plasma wakefields (with differing electron densities) as driven by a 3D Gaussian beam. The longitudinal distribution of the electron beam is shown in gray in arbitrary units with the head of the bunch located towards the right.

regime differs from that of the quasilinear regime, the dechirping mechanism is analogously effective.

Assuming a constant transverse rms beam size during propagation in the flat-top plasma target with length L_p, the energy change along the beam is given by

$$\Delta\gamma(\zeta) = -k_p L_p E_z(\zeta)/E_0, \quad (3)$$

where $\Delta\gamma$ denotes the change of the relativistic Lorentz factor. Hence, for a known current profile, the plasma density and target length can be experimentally tuned in order to optimize the dechirping process with the goal of minimizing the final energy chirp. Since the impact of the dechirper linearly scales with the length of the device it is convenient to characterize the dechirper strength in units of MeV/mm/m, i.e., the chirp compensated over a meter-long dechirping length. These considerations determined the design of the experimental set up as described in the following methodology.

The schematic in Fig. 2 shows the layout of the FEL facility FLASH, with its 1.3 GHz superconducting accelerating structures, third harmonic cavity, magnetic bunch compressor chicanes, and S-band transverse deflection system (TDS) for longitudinal phase space characterization [24,25]. For this experiment the electron bunch was accelerated off crest in the linac to 681 MeV and compressed in the chicanes from an initial rms bunch length of 1.95 mm. The TDS was used to establish a stable and reproducible machine working point where the required negative linear energy chirp in longitudinal phase space (typical for a PWFA scheme) was met. Using the TDS a beam with a rms bunch length of 63 μm and rms energy spread of 0.56% was measured. This corresponds to a chirp of 60.5 MeV/mm. The longitudinal profile of the beam can be seen in the upper right inset of Fig. 2.

Once longitudinal characterization of the bunch with the TDS was complete the beam was transported to the FLASHForward beam line through a series of magnetic
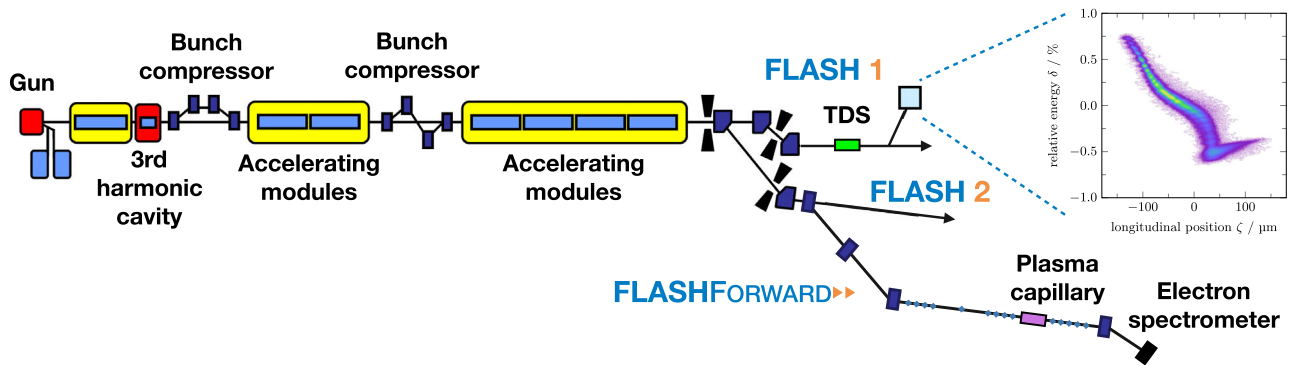
FIG. 2.   Beam line schematic of the FLASH water-window FEL facility illustrating the radiofrequency gun and linac components used to accelerate, compress, and chirp the electron beams. The magnetic dipoles deflecting the beam into FLASHForward, as well as some components of the FLASHForward beam line itself, are also shown. The linearly chirped longitudinal phase space of the beam used in this experiment, as measured by the transverse deflection structure, is shown in the upper right inset.

doglegs, with the optics set to maintain the longitudinal bunch properties. The transverse beam size of the electron beam at the interaction point (IP) was minimized using a quadrupole scan matching routine whereby optics upstream of the IP were varied, with the resulting change in beam size observed using a yttrium aluminium garnet (YAG) profile screen. For the matching routine the profile screen was moved to the position of the plasma capillary by a mover system with a total of six degrees of freedom in translation and rotation. The matching routine minimized the beam to a transverse size of $60~\mu m \times 20~\mu m$.

For the measured longitudinal and transverse beam parameters Eq. (1) can be used to estimate the electron plasma density required to fully dechirp the beam. The head-to-tail energy difference of the beam is $\approx$7 MeV and, therefore, a decelerating field magnitude of $\approx$210 MV/m at the rear of the beam is required to compensate the energy difference in a 33 mm long plasma capillary [cf. Eq. (3)]. Figure 1 shows E_z along the beam for three different plasma density values, calculated using Eq. (1) for a wakefield driven by a bunch with the measured beam parameters. According to the quasilinear plasma excitation model a density value of 2×10^{15} cm^{-3} approximately fulfils this condition. The peak electron bunch density for these measured beam parameters is $\approx 1.6 \times 10^{15}$ cm^{-3}; therefore the beam is underdense compared to the plasma density estimated to provide maximum dechirping. As such it is reasonable to use the quasilinear relation of Eq. (1) to estimate the wakefield magnitude.

A plasma capillary, 33 mm in length and with a 1.5 mm diameter, was driven to the IP using the mover. Lossless transmission of the chirped bunch was confirmed by measuring a consistent charge of 300 ± 2 pC upstream and downstream of the IP. The chirped bunch was then captured by a quadrupole triplet immediately downstream of the IP and transported to a dipole spectrometer, used to disperse the chirped bunch in energy. The dispersed beam then impinged on a fluorescence screen (of Lanex Fine

type) with the emitted light captured and imaged on a high resolution CCD camera with 1 Hz repetition rate. The energy spectrum of the chirped driver bunch with no plasma interaction can be seen in Fig. 3, the rms of which is comparable to that measured by the TDS in FLASH1.

The chirped bunch was then injected into a plasma with a fixed average density. The plasma was generated by filling the capillary with argon gas with a flow rate of 10 mbar l/s and then igniting the gas to create a plasma using a 400 ns long, nearly flat-top current pulse from a 4.1 nF capacitance pulse forming network charged to 25 kV and switched by a thyratron. Once the discharge pulse ends the density of plasma electrons exponentially decays due to plasma recombination and expansion into vacuum with a lifetime on the μs level [26,27]. The plasma density can, therefore, be controlled by delaying the arrival time of the electron beam relative to the discharge, with the electron beam experiencing lower densities at ever longer times after
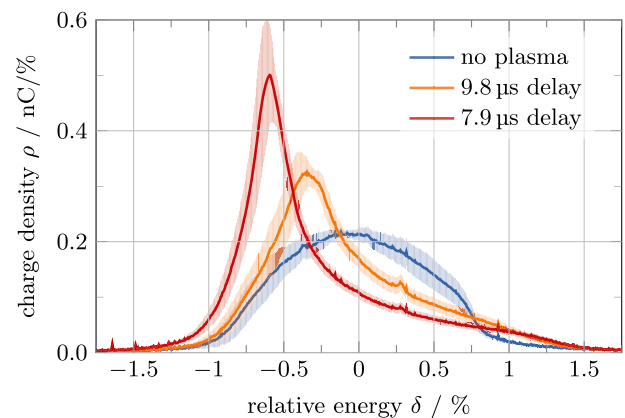

FIG. 3.   A series of energy spectra, as recorded by the optical system surrounding the dipole spectrometer, for no interaction with plasma as well as two dechirping plasma densities. The standard deviation for each energy slice—an average over 50 consecutive shots—is shown by the error ranges.

discharge. By observing a reduction of beam width on the dipole spectrometer for variable delay a maximum dechirping effect was seen at approximately 8 μs after discharge, at which point the electron plasma density is optimal for dechirping. In addition to the energy distribution after no plasma interaction, Fig. 3 shows two spectra for differing discharge delay times demonstrating the tunable plasma dechirping effect. For each delay time 50 consecutive shots were recorded in order to provide a sample size large enough to quantify the stability of the incoming beam.

Using the experimentally derived electron beam parameters it is possible to calculate the expected dechirping effect for this driver for plasma densities corresponding to the delay times in Fig. 3. These calculations were performed using the quasistatic three-dimensional particle-in-cell code HiPACE [28], whereby a 3D Gaussian representation of the bunch was propagated over a 33 mm flat-top plasma length. The plasma density was varied and the resulting longitudinal phase spaces, and therefore the energy spectra, were numerically simulated. The maximum dechirping effect in simulation was observed at a density of approx. 2×10^{15} cm^{-3}, in agreement with that of Eq. (1). The simulated spectrum for this maximum dechirping density, as well as that of an intermediate dechirping density, can be seen in Fig. 4. These spectra are analogous to the experimental spectra shown in Fig. 3 and demonstrate good agreement with data.

The discharge delay time was then scanned over a wide range in steps of 92.3 ns, starting at a time before the discharge and ending when no further perturbative effect was observed on the chirped bunch. The results of this experimental scan around the delay time region of interest can be seen in Fig. 5. The dechirping effect is indicated by a decrease in the FWHM of the bunch energy spectra (chosen over the rms due to the asymmetric nature of the distributions) as a function of time after discharge. The effect reaches a maximum at ≈8 μs. The dechirping magnitude at this delay time reduces the projected energy spread of the chirped bunch from 1.31% to 0.33% over 33 mm of plasma. This reduction corresponds to a field strength of 202 ± 18 MeV/m at the rear of the bunch, in agreement with the magnitude of the electric field observed by the tail of the bunch as derived using the analytic formalism of Eq. (1) to be 210 MeV/m. At this time after discharge the plasma density is much smaller than the length-matched density of 7×10^{16} cm^{-3}, i.e., when $k_p \sigma_z = 1$, at which point maximum electric field gradients are expected. In the experimental density regime the bunch length is short compared to the plasma wavelength, resulting in the majority of the bunch experiencing the linear and monotonically increasing part of the electric field as originally suggested in Fig. 1. In this case the linear chirp over the bunch centroid, previously measured as 60.5 MeV/mm, was fully compensated over a 33 mm plasma length for the 300 pC bunch, implying a dechirping strength of 1.8 GeV/mm/m. The utilization of plasma waves to
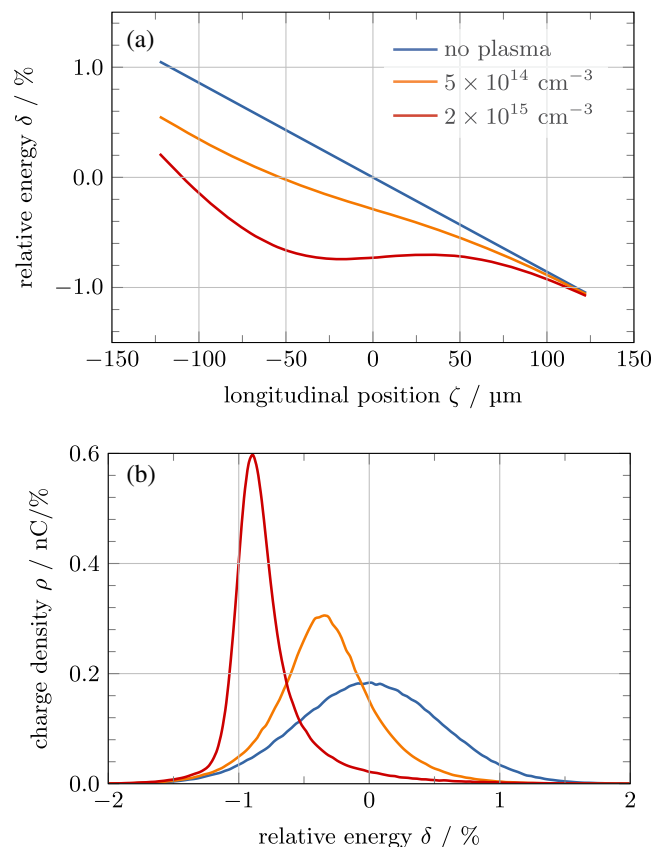

FIG. 4. Simulations of (a) longitudinal phase space centroids, and (b) collapsed energy spectra for no plasma interaction as well as two dechirping plasma densities. The three simulated spectra are equivalent to the experimental spectra shown in Fig. 3.

compensate for chirps in our experiment enabled a dechirping strength significantly greater than previously demonstrated and has the potential to compensate even greater chirps in shorter distances in future experiments.

An additional observation from the data of Fig. 5 is that the standard deviation from 50 consecutive shots, indicated by the error range, decreases towards a minimum at maximum dechirping. This suggests that the implementation of the plasma dechirper in the experimental setup does not decrease the stability of the incoming beam. This stability most likely stems from the full decoherence within a few betatron periods of the beam when resonantly driving a plasma wave in the quasilinear regime [11,29], suppressing any hosing effects. As such it is implied that there will be no further growth of transverse instability for longer plasma capillaries.

Simulations of the chirped bunch interacting with plasma over the entire density range in Fig. 5 were then performed in HiPACE. The results of these simulations are displayed in Fig. 5. A comparison between the profile and absolute values of dechirping for both the experimental and simulated data sets shows excellent agreement within both errors and the energy resolution of the dipole spectrometer,
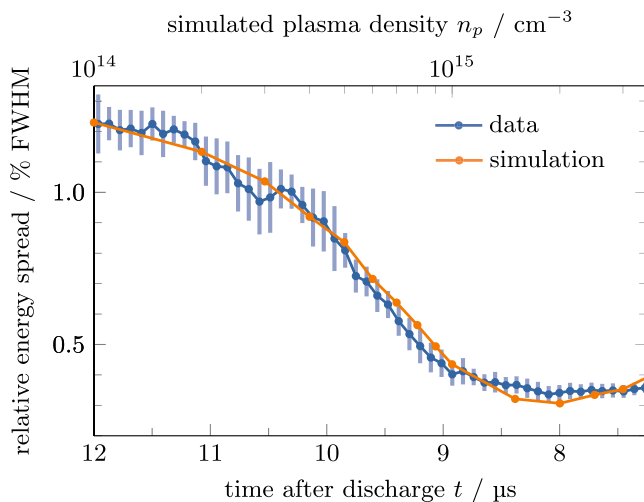
FIG. 5. The FWHM of the chirped bunch energy as a function of discharge time relative to the arrival time of the electron bunch. The standard deviation, representing the shot-to-shot fluctuations per delay step, is plotted. Simulated FWHM of the chirped bunch energy spectra as a function of electron plasma density over the identical range are shown for comparison.

supporting the interpretation that the effect observed in data is indeed a plasma-induced dechirping of the bunch. The less pronounced inflexion point in the experimental data at higher plasma densities is likely due to a variable uncorrelated energy spread over the length of the bunch saturating the dechirping effect around its maximum.

In summation, a tunable plasma dechirper with a maximum dechirping strength of 1.8 GeV/mm/m was successfully implemented in an experiment carried out at FLASHForward, DESY. By carefully selecting a plasma density at which the majority of the bunch sees a monotonically increasing E_z the initial negative energy chirp of the bunch was completely removed over the centroid with a global reduction of projected energy spread from 1.31% to 0.33% FWHM. This result constitutes the first observation of its type, describing a proof-of-principle tunable plasma dechirper. If a larger integrated dechirping effect is required the technique may be scaled up by increasing the dechirping length. Furthermore, this dechirping scheme was found to not measurably affect the stability of the incoming beam. As such it may be applied to future FEL and HEP facilities where remanent chirps lead to limited functionality. In addition, this principle may be used to mitigate the large energy chirps of electron bunches generated in plasma, thus drastically improving the applicability of plasma wakefield schemes to future experiments where a negligible correlated energy spread is required.

[*] richard.darcy@desy.de
[1] V. I. Veksler, in *Proceedings of the CERN Symposium on High-Energy Accelerators, Pion Physics* (unpublished), p. 80.
[2] P. Chen, J. M. Dawson, R. W. Huff, and T. Katsouleas, Phys. Rev. Lett. **54**, 693 (1985).
[3] E. Adli, J.-P. Delahaye, S. J. Gessner, M. J. Hogan, T. Raubenheimer, W. An, C. Joshi, and W. Mori, arXiv:1308.1145.
[4] I. Blumenfeld *et al.*, Nature (London) **445**, 741 (2007).
[5] T. C. Katsouleas, S. Wilks, P. Chen, J. M. Dawson, and J. J. Su, Part. Accel. **22**, 81 (1987).
[6] M. Tzoufras, W. Lu, F. S. Tsung, C. Huang, W. B. Mori, T. Katsouleas, J. Vieira, R. A. Fonseca, and L. O. Silva, Phys. Plasmas **16**, 056705 (2009).
[7] G. G. Manahan *et al.*, Nat. Commun. **8**, 15705 (2017).
[8] M. Litos *et al.*, Nature (London) **515**, 92 (2014).
[9] R. Brinkmann *et al.*, Phys. Rev. Lett. **118**, 214801 (2017).
[10] T. J. Mehrling, R. A. Fonseca, A. Martinez de la Ossa, and J. Vieira, Phys. Rev. Lett. **118**, 174801 (2017).
[11] R. Lehe, C. B. Schroeder, J.-L. Vay, E. Esarey, and W. P. Leemans, Phys. Rev. Lett. **119**, 244801 (2017).
[12] V. E. Balakin, A. V. Novokhatsky, and V. P. Smirnov, eConf. Proc. **C830811**, 119 (1983).
[13] K. L. F. Bane and G. Stupakov, Nucl. Instrum. Methods Phys. Res., Sect. A **690**, 106 (2012).
[14] S. Antipov, S. Baturin, C. Jing, M. Fedurin, A. Kanareykin, C. Swinson, P. Schoessow, W. Gai, and A. Zholents, Phys. Rev. Lett. **112**, 114801 (2014).
[15] D. Mihalcea, P. Piot, and P. Stoltz, Phys. Rev. ST Accel. Beams **15**, 081304 (2012).
[16] C. Wang and J. L. Hirshfield, Phys. Rev. ST Accel. Beams **9**, 031301 (2006).
[17] S. S. Baturin, I. L. Sheinman, A. M. Altmark, and A. D. Kanareykin, Phys. Rev. ST Accel. Beams **16**, 051302 (2013).
[18] A. Aschikhin *et al.*, Nucl. Instrum. Methods Phys. Res., Sect. A **806**, 175 (2016).
[19] K. Tiedtke *et al.*, New J. Phys. **11**, 023029 (2009).
[20] W. Ackermann *et al.*, Nat. Photonics **1**, 336 (2007).
[21] R. Keinigs and M. E. Jones, Phys. Fluids **30**, 252 (1987).
[22] W. Lu, C. Huang, M. Zhou, W. B. Mori, and T. Katsouleas, Phys. Rev. Lett. **96**, 165002 (2006).
[23] S. A. Yi, V. Khudik, C. Siemon, and G. Shvets, Phys. Plasmas **20**, 013108 (2013).
[24] P. Emma, J. Frisch, and P. Krejcik, SLAC LCLS Technical Report No. LCLS-TN-00-12, 2000.
[25] C. Behrens, N. Gerasimova, Ch. Gerth, B. Schmidt, E. A. Schneidmiller, S. Serkez, S. Wesch, and M. V. Yurkov, Phys. Rev. ST Accel. Beams **15**, 030707 (2012).

[26] G. Loisch *et al.*, Phys. Rev. Lett. **121**, 064801 (2018).

[27] E. Kallos, T. Katsouleas, W. D. Kimura, K. Kusche, P. Muggli, I. Pavlishin, I. Pogorelsky, D. Stolyarov, and V. Yakimenko, Phys. Rev. Lett. **100**, 074802 (2008).

[28] T. J. Mehrling, C. Benedetti, C. B. Schroeder, and J. Osterhoff, Plasma Phys. Controlled Fusion **56**, 084012 (2014).

[29] A. Martinez de la Ossa, T. J. Mehrling, and J. Osterhoff, Phys. Rev. Lett. **121**, 064803 (2018).

Tunable and precise two-bunch generation at FLASHForward

S Schröder[1,2]**, K Ludwig**[1]**, A Aschikhin**[1,2]**, R D'Arcy**[1]**, M Dinter**[1]**, P Gonzalez**[1,2]**, S Karstensen**[1]**, A Knetsch**[1]**, V Libov**[1,2]**, C A Lindstrøm**[1]**, F Marutzky**[1]**, P Niknejadi**[1]**, A Rahali**[1]**, L Schaper**[1]**, A Schleiermacher**[1]**, B Schmidt**[1]**, S Thiele**[1]**, A de Zubiaurre Wagner**[1]**, S Wesch**[1] **and J Osterhoff**[1]

[1] Deutsches-Elektronen Synchrotron (DESY), Notkestraße 85, 22607 Hamburg, Germany
[2] University of Hamburg, Luruper Chaussee 149, 22761 Hamburg, Germany

E-mail: `sarah.schroeder@desy.de`

Abstract. Beam-driven plasma-wakefield acceleration based on external injection has the potential to significantly reduce the size of future accelerators. Stability and quality of the acceleration process substantially depends on the incoming bunch parameters. Precise control of the current profile is essential for optimising energy-transfer efficiency and preserving energy spread. At the FLASHForward facility, driver–witness bunch pairs of adjustable bunch length and separation are generated by a set of collimators in a dispersive section, which enables fs-level control of the longitudinal bunch profile. The design of the collimator apparatus and its commissioning is presented.

1. Introduction

High acceleration gradients inherent in a plasma wakefield make it a compelling technique for compact particle accelerators [1, 2, 3], potentially reducing costs of future free-electron lasers (FELs) or colliders [4, 5, 6]. For such applications, beam-driven plasma-wakefield acceleration (PWFA) is a promising approach, as it can supply high wall-plug efficiencies and MW-scale average power. Studies on the external-injection scheme, where the energy is transferred from a driver to a witness bunch, are crucial for staging plasma channels to achieve the required energies (GeV–TeV). High-gradient as well as high-efficiency acceleration using the external-injection PWFA method have successfully been demonstrated [7, 8].

The next milestone of external-injection PWFA is high-efficiency acceleration while preserving the beam quality, including emittance and energy spread. The energy-transfer efficiency contributes largely to the overall efficiency of the acceleration process [9, 10, 11, 12]. For high-energy applications, also the transformer ratio—the limitation on the energy being transferred from the wakefield-driving bunch to the accelerated bunch—must be optimised. Asymmetric longitudinal bunch profiles can lead to an increased transformer ratio [14]. Furthermore, the resulting energy spread of the accelerated bunch is determined by the wakefield structure, which also changes with the current profiles of the driver and witness bunches. Current profile shaping of the incoming bunches can thus achieve high efficiency as well as energy-spread preservation
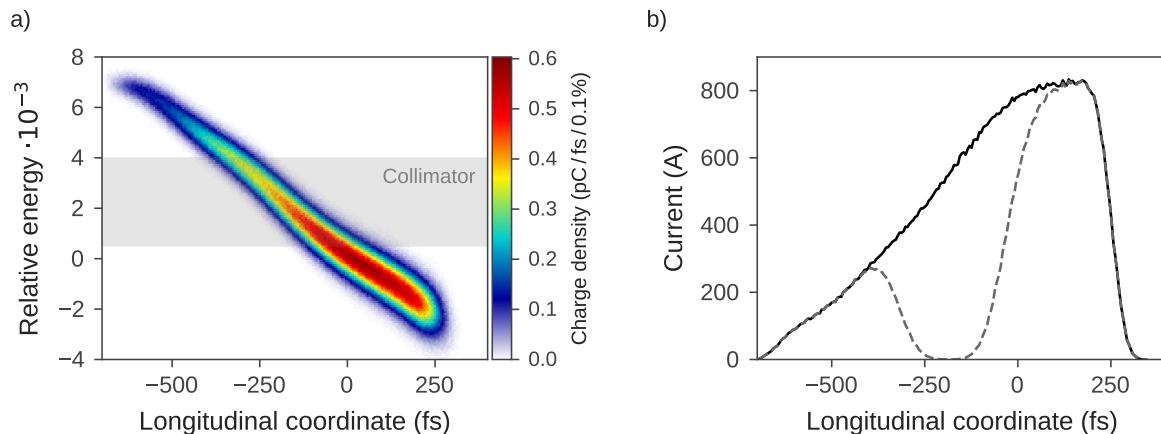
Figure 1. Two-bunch generation using a collimator in a dispersive section. The longitudinal phase space is linearised in the FLASH accelerator and measured by a transverse deflecting structure in a photon beamline parallel to FLASHForward (a). A collimator in a dispersive section effectively cuts the original bunch (solid) in a driver–witness bunch pair (dashed) (b).

via optimised beam loading [15].

Several different techniques for longitudinal bunch shaping have already been explored. Laser pulse stacking at the photo-cathode [16, 17, 18, 19, 20] as well as emittance exchange [21, 22, 23] can be used to tailor the current profile of the electron bunches as it is generated. Both techniques have independent control of the driver and witness current profiles. Partial beam masking with a collimator is also a well established method for two-bunch generation [24, 8]. Owing to a strong energy–time correlation of the electron bunch, a collimator in a dispersive section acts effectively also on the longitudinal bunch profile (see Figure 1b). Thus, this method relies on longitudinal-phase-space shaping of a chirped bunch in a pre-accelerator.

At future high-energy accelerators, the drive bunch must be generated independently from the witness bunch before each plasma stage. The collimation two-bunch generation method can thus only be applied for single plasma channels. Nevertheless, the intrinsic synchronisation of the two bunches and the simple implementation to pre-existing beamlines make it a convenient option for underlying single-stage studies and is, as such, also implemented at FLASHForward.

FLASHForward is an experimental test facility dedicated to beam-driven plasma-wakefield research [25] and is located in an extension beamline to the X-ray Free-electron LASer in Hamburg (FLASH) at DESY [26, 27]. Primary scientific goals are high-brightness electron-bunch generation from the plasma (X-1: Internal injection) and beam-quality-preserving acceleration of pre-existing bunches (X-2: External injection). Furthermore, the access to 3 MHz micro-pulse repetition rate makes FLASHForward a unique facility for high-average-power (up to 30 kW) studies on beam-driven PWFA (X-3: High average power).

2. Longitudinal phase-space shaping at FLASHForward

In the FLASH accelerator, electron bunches of up to 1 nC are produced at 10 Hz in a laser-driven photoinjector and subsequently accelerated up to 1.2 GeV in seven 1.3 GHz superconducting radio-frequency (SRF) cavities. Two magnetic compressor chicanes can reduce the bunch length to 150 fs (rms) with peak currents on the order of 1-2 kA.

A series of SRF cavities and bunch compressors in the FLASH linear accelerator allows for flexible longitudinal phase-space shaping [28]. Off-crest acceleration in the SRF cavities imprints a correlation between the particle energy and the longitudinal bunch coordinate—an energy chirp. The chirped bunch is then longitudinally compressed in the magnetic chicanes of FLASH and in the FLASHForward extraction line. A third-harmonic SRF cavity in the FLASH accelerator gives control over the first and second derivative of the chirp. This allows in particular linearisation of the longitudinal phase space (see Figure 1a).

The generation of driver-witness bunch pairs for external-injection PWFA is not directly supplied as a standard operation mode at FLASH. The two-bunch generation for FLASHForward can either be realised at the gun by two delayed laser pulses or by a set of collimators in a dispersive section blocking the middle part of a single bunch. This paper reports on the two-bunch generation by collimation, which in particular provides high tunability and precision within the restriction of the original beam profile.

3. Collimator design
At FLASHForward, a three-collimator device is implemented (see Figure 2 and Figure 3), which allows the beam to be manipulated in four distinct and independent ways: separation width, separation position, driver and witness length.

The width and position of the driver–witness separation is determined by a wedge-shaped collimator that can be adjusted by stepper motors vertically (M6) and horizontally (M5). The vertical movement determines the width of the collimator and thus the separation width. The horizontal movement determines the separation position and thus the charge distribution and bunch lengths. For alignment, the wedge collimator can additionally be rotated about the vertical (M4) and the longitudinal (beam) axis (M3).

The required wedge geometry is given by the typical energy spread (0.1–0.5% rms) of the incoming electron bunch and the horizontal dispersion at the location of the collimators (-340 mm). This results in a transverse bunch size of 1.5×0.1 mm rms (x × y). At the plasma channel the bunches typically have a bunch length of 150–300 fs rms, which is suitable for external injection experiments at plasma densities between 10^{15}–10^{17} cm^{-3}.

The wedge-shape allows stepless and precise separation-width adjustment. The available width of 0.6–3 mm ensures considerable cutting of the bunch, resulting in 30–120 μm bunch separations. The wedge height of 125 mm makes the vertical cutting across the bunch negligible (below 1%). The depth of 15 mm ensures sufficient particle scattering, structure stability and limited energy deposition in the material. The multi-dimensional tension from wedge adjustments (two linear axles, a goniometer, and a circle segment) is decoupled from the beam pipe with a cross-shaped bellow construction.

In front of and behind the wedge collimator two block-shaped collimators are installed, which are adjustable in the dispersive (horizontal) plane. For the standard FLASH operation mode with a negatively chirped bunch, the upstream collimator acts on high energies—the bunch tail (M1)—and the downstream collimator acts on low energies—the bunch head (M2). The block collimators are produced in a simple rectangular solid shape ($10 \times 10 \times 15$ mm). This geometry also allows for blocking the entire bunch.

These block collimators also have the capability of individual characterisation of the drive and witness bunch by blocking one or the other bunch. Furthermore, in case of a sufficiently small slice energy spread, the simultaneous movement of the block collimators—so that only a small energy range can pass—enables *temporally sliced bunch characterisation*.
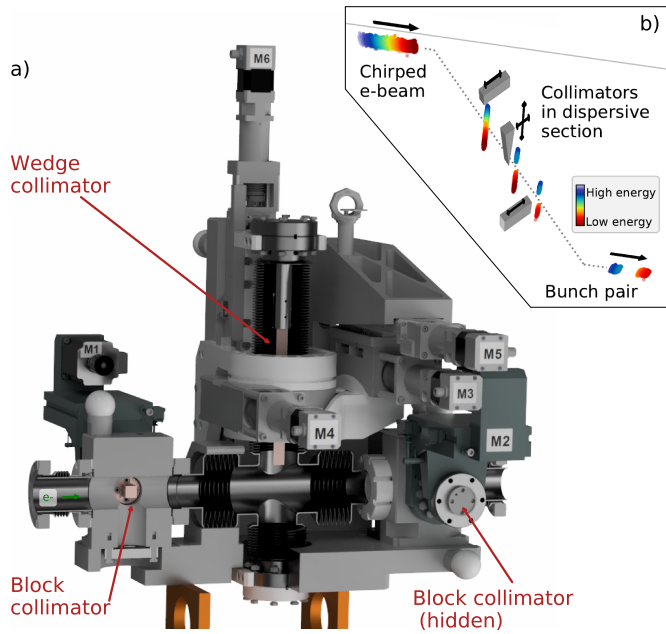
Figure 2. 3D CAD model of the three collimator device. (a) The block collimators are adjustable in the horizontal plane (M1, M2) and act on the head and tail of the bunch. The wedge determines the bunch separation width (M6) and position (M5). Further alignment of the wedge is available by rotation about the vertical (M4) and the longitudinal (beam) axis (M3). (b) Schematic layout of bunch collimation in dispersive section.
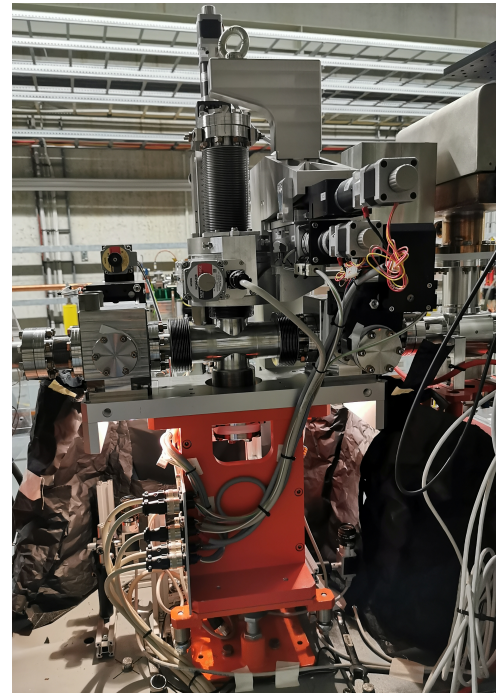
Figure 3. Installed collimator device. An adjustable support allows precision alignment to the beamline. Cameras observe the collimator position through window flanges from underneath. All collimators can be adjusted remotely.

Collimator	Motor	Sledge type, DOF	Range	Accuracy
Block	M1	lin. axle, hor. translation	30 mm	10 µm
Block	M2	lin. axle, hor. translation	30 mm	10 µm
Wedge	M3	Circle segment, long. rotation	$\pm 1°$	$0.001°$
	M4	Goniometer, vert. rotation	$\pm 1°$	$0.001°$
	M5	linear axle, hor. translation	± 3 mm	20 µm
	M6	linear axle, vert. translation	120 mm	20 µm

Table 1. Technical specification of collimators. Six remotely controllable motors are available for tunable two-bunch generation. The µm-precision control of the linear feedthroughs ensure the required fs-precision of bunch lengths.

An emphasis was placed on *beam loading control* and the capability of *acceleration optimisation precision studies* when designing the device. Start-to-end simulations [29, 30] suggest µm-precision control of all collimators to control bunch lengths on the fs-level. Table 1 summarises the available collimator motors, their technical realisation and control accuracy.

All three collimators are made of copper-tungsten alloy (50:50). This material is compatible with ultra-high-vacuum operation and can be eroded to manufacture the sophisticated wedge geometry. Tungsten enhances the absorption, copper improves the heat transfer to the outside. A single shot 1 GeV beam shows in Geant4 [31] simulations 5% and 15% energy deposition, for a typical two-bunch separation at the wedge and a complete beam blocking with a block collimator, respectively. Heat generation in the collimators limits their use for high-average-power studies.

The collimator apparatus approximately weighs 120 kg and has a total beamline length of 0.5 m. All collimator adjustments can be remotely controlled, with their positions observed by cameras through window flanges.

4. Commissioning of the collimators

The beam-based commissioning comprised of collimator position scans (see Figure 4), which were recorded on a vertically-dispersive electron spectrometer. The horizontal collimator positions were scanned over the entire dimension of the bunch (Figure 4 a, b, d). Driver-witness bunch separations were recorded for 5 different vertical wedge positions (Figure 4 c). At each collimator position, about 20–50 consecutive shots were taken.

All collimator scans show a clean beam removal in the energy plane. The stability of the energy profiles at each collimator position relies on a high beam stability and especially a high pointing stability at the collimators. The combination of fine energy-profile tunability and a strongly correlated longitudinal phase space (see Figure 1) allow precise two-bunch generation at FLASHForward.

The conceptual method could be verified with a recently commissioned transverse deflecting structure [32] in the FLASHForward beamline (see Figure 5). The depicted stability of bunch separation width and separation position underpins the ability of adjustable and precise two-bunch generation at FLASHForward.

5. Conclusion and outlook

The presented two-bunch generation at FLASHForward with a set of collimators in a dispersive section demonstrate for high tunablity and flexibility of the driver–witness parameters. This method allows high-precision studies of the plasma acceleration as a function of the incoming bunch parameters.

The applicability of this method is limited by the slice energy spread of the original bunch, the available dispersion of the beamline, and the monotonicity of the energy chirp. Furthermore, the longitudinal-phase-space shape of the original bunch restricts the achievable bunch parameters. Consequently the longitudinal phase-space shape of the original bunch must be set up to the demands of the experiment.

First driver–witness bunch pairs for external injection PWFA at FLASHForward have been generated. Stability of the bunch charge and beam pointing at the collimator resulted in a repeatable and stable two-bunch structure, that is highly controllable. Precision studies of the plasma wakefield acceleration utilising the tunability and precision of the driver–witness bunch pair settings are ongoing.
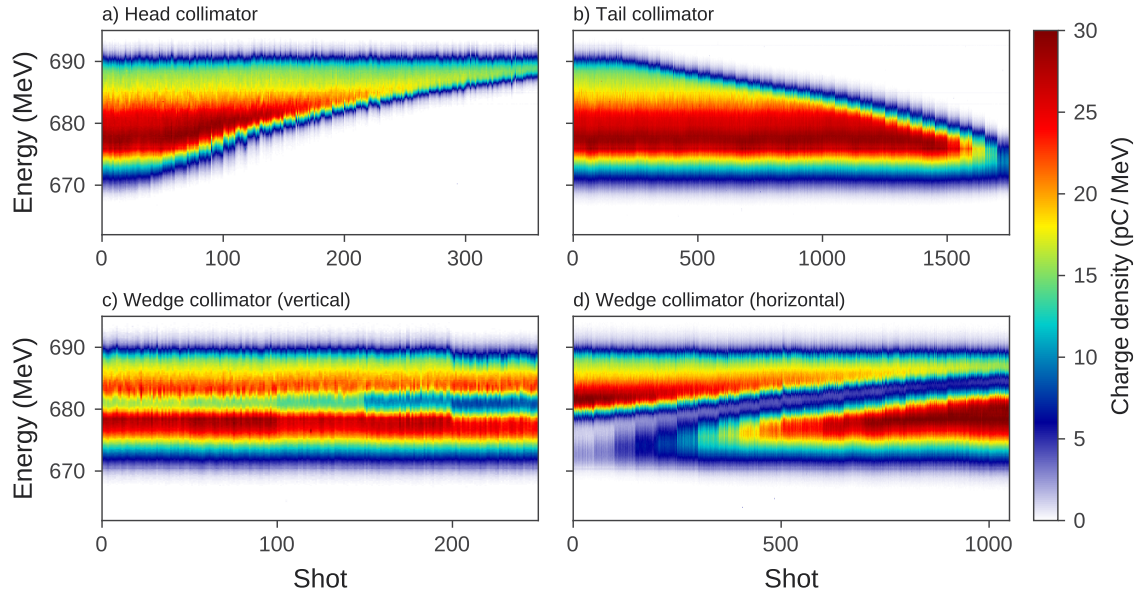
Figure 4. Energy projection waterfall of collimator position scans. Two blocks can be used to remove the low-energy head (a) or the high-energy tail (b) of the bunch. Separation width (c) and position (d) is adjusted by a wedge-shaped collimator, which can be positioned in the vertical and horizontal (dispersive) plane.
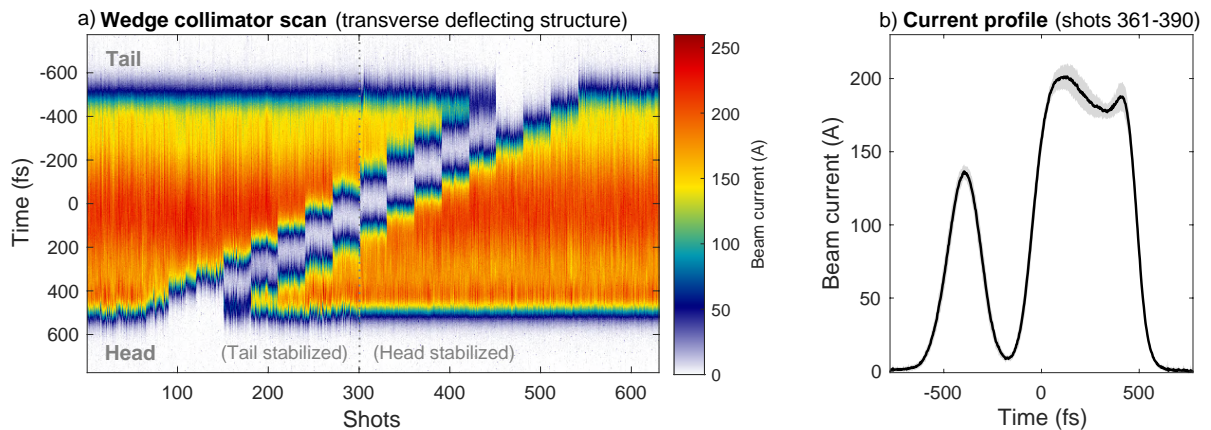

Figure 5. Two-bunch measurement in a transverse deflecting structure. Current profile waterfall of horizontal wedge position scan with a moderately compressed beam (a). The single shots are phase corrected with a threshold for the bunch tail (first ~ 300 shots) and then for the bunch head. Mean current profile and its root mean square (gray band) of one particular collimator position (b).

References

[1] Tajima T, Dawson J M 1979 *Phys. Rev. Lett.* **43**, 267

[2] Ruth R D, Chao A W, Morton P L and Wilson P W 1985 *Part.Acceler.* **17**, 171
[3] Chen P, Dawson J M, Huff R W and Katsouleas T 1985 *Phys. Rev. Lett.* **54**, 693-696
[4] Schroeder C B *et al* 2010 *Phys. Rev. ST Accel. Beams* **13** 101301
[5] Adli E *et al* 2013 *Proceedings of the Snowmass Process CSS2013*; arXiv:1308.1145
[6] Schroeder C B *et al* 2016 *Nucl. Instrum. Meth. A* **829** 113-116
[7] Blumenfeld I *et al* 2007 *Nature* **445**, 7129
[8] Litos M *et al* 2014 *Nature* **515**, 7525
[9] Ruth R, Chao A, Morton P and Wilson P 1985 *Part. Accel.* **17**, 171
[10] Chen P, Su J J, Dawson J M, Bane K L F and Wilson P B 1986 *Phys. Rev. Lett.* **56** (12), 1252
[11] Chiou T C and Katsouleas T 1998 *Phys. Rev. Lett.* **81**, 16
[12] Lotov K V 2005 *Phys. Plasmas* **12**, 053105
[13] Bane K L F *et al* 1985 *IEEE Trans. Nucl. Sci.* **32**, 3524
[14] Loisch G *et al* 2018 *Phys. Rev. Lett.* **121**, 064801
[15] Katsouleas T C, Su J J, Wilks S, Dawson J M and Chen P 1987 *Part. Accel.* **22**, 81-99
[16] Will I and Klemz G 2008 *Opt. Express* **16**, 14922
[17] Ferrario M *et al* 2011 *Nucl. Instrum. Methods Phys. Res. A* **637.1**: S43-S46
[18] Ronsivalle C *et al* 2014 *New Journal of Physics* **16.3**: 033018.
[19] Pompili R *et al* 2016 *Nucl. Instrum. Methods Phys. Res. A* **829**, 17-23
[20] Loisch G *et al* 2018 *Nucl. Instrum. Methods Phys. Res. A* **909**
[21] Emma P, Huang Z, Kim K-J and Piot P 2006 *Phys. Rev. ST Accel. Beams* **9**, 100702
[22] Piot P, Sun Y-E, Power J G and Rihaoui M 2011 *Phys. Rev. ST Accel. Beams* **14**, 022801
[23] Gao Q *et al* 2018 *Phys. Rev. Lett.* **120**, 114801
[24] Muggli P *et al* 2008 *Phys. Rev. Lett.* **101**, 054801
[25] D'Arcy R *et al* 2019 *Phil. Trans. R. Soc. A* **377**: 20180392
[26] Ayvazyan V *et al* 2006 *Eur. Phys. J. D* **37**, 297–303
[27] Ackermann W *et al* 2007 *Nat. Photonics* **1**, 336–342
[28] Piot P *et al* 2012 *Phys. Rev. Lett.* **108**, 034801
[29] Floettmann K `www.desy.de/~mpyflo` (A Space Charge Tracking Algorithm)
[30] Borland M 2000 ANL Advanced Photon Source Report No. LS-287
[31] Allison J *et al* 2016 *Nucl. Instrum. Methods A* **835**
[32] Gonzalez Caminal P *et al* 2020 *Paper in preparation*

Matching small β functions using centroid jitter and two beam position monitors

C. A. Lindstrøm[1,*] R. D'Arcy,[1] M. J. Garland,[1] P. Gonzalez,[1,2] B. Schmidt[1] S. Schröder[1,2]
S. Wesch[1] and J. Osterhoff[1]

[1]*Deutsches Elektronen-Synchrotron DESY, Notkestraße 85, 22607 Hamburg, Germany*
[2]*Universität Hamburg, Luruper Chaussee 149, 22761 Hamburg, Germany*

Matching to small beta functions is required to preserve emittance in plasma accelerators. The plasma wake provides strong focusing fields, which typically require beta functions on the mm-scale, comparable to those found in the final focusing of a linear collider. Such beams can be time consuming to experimentally produce and diagnose. We present a simple, fast, and noninvasive method to measure Twiss parameters in a linac using two beam position monitors only, relying on the similarity of the beam phase space and the jitter phase space. By benchmarking against conventional quadrupole scans, the viability of this technique was experimentally demonstrated at the FLASHForward plasma-accelerator facility.

I. INTRODUCTION

Plasma-wakefield accelerators [1–3] can provide accelerating gradients in the GV/m-range [4,5], promising smaller and cheaper accelerators [6,7]. Reaching high energies, needed for x-ray free-electron lasers [8,9] and linear colliders [10–13] in particular, will require multiple accelerator stages [14,15] and hence some form of external beam injection into the plasma wake.

Since the focusing field from an exposed ion column in a plasma accelerator is typically very strong, beams must be tightly focused for the beam size not to oscillate, as this would lead to significant and unacceptable emittance growth [16]. In terms of Twiss or Courant-Snyder parameters [17], the beta function needs to be matched to

$$\beta_m = \sqrt{\frac{2E\epsilon_0}{ne^2}} \qquad (1)$$

where E is the beam energy, n is the plasma density, ϵ_0 is the vacuum permittivity, and e is the electron charge. Injecting a GeV-level beam into a typical plasma accelerator requires beta functions on the mm-scale. While plasma density ramps [18–20] can relax the matching condition by increasing β_m at the entry and exit of the accelerator stage, it will nevertheless be challenging and

time-consuming to experimentally produce and diagnose the required tightly focused beams.

Conventional beam-focus diagnostics include wire scanners and high-resolution screens around the focal point, or downstream quadrupoles that point-to-point image the beam onto a screen—all of which require nontrivial experimental setups and careful data analysis. This can be inconvenient when matching beams into a plasma accelerator—a slow multiparameter optimization process where fast feedback will be crucial.

In this paper, we present an alternative method for simple, fast, and noninvasive measurement of small beta functions by using two beam position monitors (BPMs) to measure the centroid jitter. The technique is based on the observation that the phase space of the jitter often has similar Twiss parameters to that of the beam, and can therefore be used as a proxy. While the method is approximate in nature, it allows online monitoring and iterative adjustment of the waist location and beta function. This technique was successfully implemented and experimentally demonstrated at the FLASHForward [21,22] plasma-accelerator facility at DESY.

II. BEAM AND JITTER PHASE SPACES

The phase space of a beam consists of its particle distribution in x–x' space (in one transverse plane). Similarly, the phase space of the beam centroid jitter—the *jitter phase space*—is the distribution of beam centroid offsets in x–x' space when integrated over a large number of shots. Therefore, the jitter has its own Twiss parameters and emittance.

The central assumption underpinning this technique is that the Twiss parameters of the jitter are similar to those
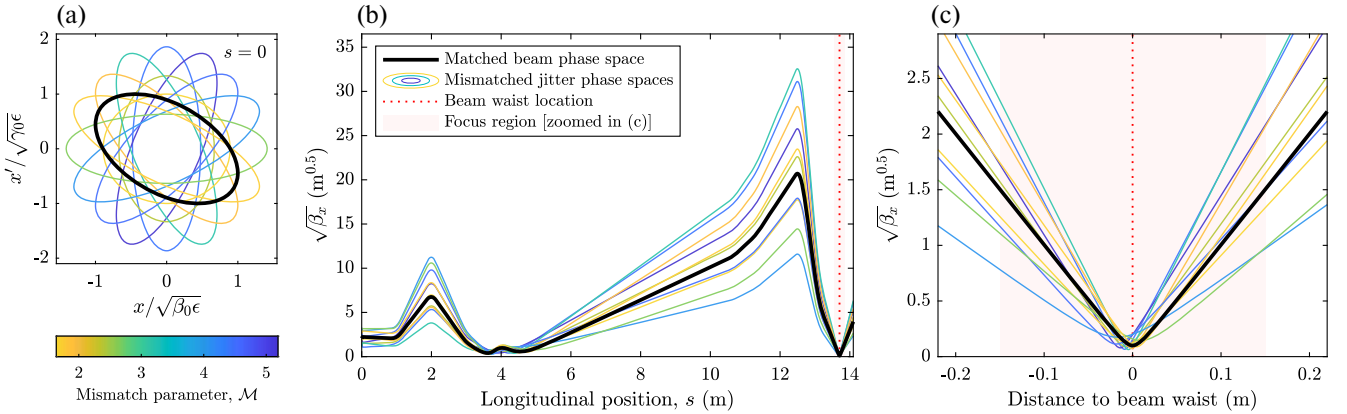
[*]carl.a.lindstroem@desy.de

FIG. 1.   Evolution of a matched beam phase space and various possible mismatched jitter phase spaces through a strong-focusing lattice. Starting out moderately mismatched (a), the jitter beta functions evolve (b) and appear to diverge from that of the matched beam beta function. Nevertheless, in the focus region (c) the mismatched jitter phase spaces are all focused to a similar waist beta function and waist location as the beam.

of the beam. A significant consequence of this connection is that it is possible to simply and noninvasively measure the phase space of the jitter using BPMs, which then acts as an approximate measurement of Twiss parameters of the beam. It should be noted that this technique is generally not suitable for measuring the beam emittance, but this is also not required for matching [see Eq. (1)].

While the similarity of the beam and the jitter is not guaranteed, it is motivated by both experimental observation and theoretical considerations. Linear accelerators usually have long FODO-like lattices with beta functions on the 1–10 m scale. This means that magnets and accelerating cavities—sources of jitter—are typically distributed across a range of phase advances. As a consequence, the jitter-phase-space ellipse gradually expands while it rotates to acquire a similar shape to the beam-phase-space ellipse. Conversely, if there were only a few dominant jitter sources—such as the gun or a single vibrating quadrupole—the jitter-phase-space ellipse would be disproportionately stretched in the x'-dimension at these phases. Similar beam and jitter-phase-space ellipses can therefore be expected in any well-commissioned machine where such dominant jitter sources have been removed. Even if the beam and jitter phase spaces are moderately mismatched, both will evolve and be focused similarly in a linear-optics lattice—also in the case of strong focusing, as demonstrated by the example in Fig. 1. It should be noted that in the presence of strong focusing, the final-focusing quadrupoles can contribute disproportionately to the jitter phase space due to large beta functions—special care therefore needs to be taken to ensure their stability [23,24].

The most interesting quantities in the context of matching are the location and beta function of the focus waist. How inaccurate should we expect the jitter-based measurement to be? Consider a lattice that focuses the beam to a small waist, where the beam size is demagnified by a factor B. Starting from matched Twiss parameters β_0 and α_0, the

resulting waist beta function would be β_0/B^2. The transfer matrix of such a lattice [17] can be expressed as

$$R = \begin{bmatrix} \frac{\cos\psi + \alpha_0 \sin\psi}{B} & \frac{\beta_0}{B}\sin\psi \\ \frac{B}{\beta_0}(\alpha_0\cos\psi - \sin\psi) & B\cos\psi \end{bmatrix}, \qquad (2)$$

where the phase advance ψ is a free parameter. Consider then a mismatched jitter with an initial betatron amplitude matrix

$$\Sigma_0 = \begin{bmatrix} \beta & -\alpha \\ -\alpha & \gamma \end{bmatrix}, \qquad (3)$$

where $\gamma = (1 + \alpha^2)/\beta$ is the Twiss gamma function. The overall mismatch can be quantified by the *mismatch parameter* [25]

$$\mathcal{M} = \frac{1}{2}\left(\tilde{\beta}_e + \tilde{\gamma}_e + \sqrt{(\tilde{\beta}_e + \tilde{\gamma}_e)^2 - 4}\right), \qquad (4)$$

where $\tilde{\beta}_e = \beta/\beta_0$, $\tilde{\alpha}_e = \alpha - \alpha_0\beta/\beta_0$ and $\tilde{\gamma}_e = (1 + \tilde{\alpha}_e^2)/\tilde{\beta}_e$ quantify the normalized error of each Twiss parameter. The mismatch parameter $\mathcal{M}$ is invariant in a linear-optics lattice, whereas the individual Twiss errors are not.

We can transport the mismatched jitter to the beam waist location (i.e., the end of the lattice) using

$$\Sigma = R\Sigma_0 R^T. \qquad (5)$$

The Σ_{11} element corresponds to the jitter beta function at the beam waist location. However, the beam waist does not generally coincide with the jitter waist, and therefore Σ_{11} does not correspond to the waist beta function of the jitter. Instead, assuming that the focus region consists only of a drift, the waist beta function equates to the inverse gamma function $(1/\Sigma_{22})$, which can be expressed as

$$\beta_w = \frac{\beta_0}{B^2} \left(\frac{1}{\tilde{\alpha}_e \sin 2\psi + \tilde{\beta}_e \sin^2\psi + \tilde{\gamma}_e \cos^2\psi} \right). \quad (6)$$

Similarly, the shift of the jitter waist location is given by the ratio of the alpha and the gamma function $(-\Sigma_{12}/\Sigma_{22})$, which is derived to be

$$\delta s_w = \frac{\beta_0}{B^2} \left(\frac{\tilde{\alpha}_e \cos 2\psi + \frac{1}{2}(\tilde{\beta}_e - \tilde{\gamma}_e) \sin 2\psi}{\tilde{\alpha}_e \sin 2\psi + \tilde{\beta}_e \sin^2\psi + \tilde{\gamma}_e \cos^2\psi} \right). \quad (7)$$

Although lengthy, it is easy to see that if the Twiss errors $\tilde{\alpha}_e$, $\tilde{\beta}_e$, and $\tilde{\gamma}_e$ are all of order one (i.e., moderately mismatched), the brackets in both Eqs. (6) and (7) become numerical factors also of order one, regardless of the free parameter ψ. This means that the waist beta function of the mismatched jitter remains similar to the waist beta function β_0/B^2 of the matched beam. Moreover, it implies that the offset of the waist location is also approximately β_0/B^2—of the order of the waist beta function itself.

In a plasma accelerator, this mismatch leads to an emittance growth for beams of finite energy spread, as the phase-space ellipse of each energy slice rotates at a different rate. Fully decohered, the relative emittance growth saturates at [16]

$$\frac{\epsilon_{\text{sat}}}{\epsilon_0} = \frac{1}{2}\left(\mathcal{M} + \frac{1}{\mathcal{M}}\right), \quad (8)$$

which also agrees with simulations. This implies that for a moderate mismatch ($\mathcal{M}$ of order one) the emittance growth is relatively small—e.g., a mismatch of $\mathcal{M} = 2$ leads to an emittance growth of only 25%. Using the jitter as a proxy is therefore appropriate for a quick first-pass matching to the plasma, before a final in-situ optimization using the beam.

III. TWO-BPM MEASUREMENT METHOD

Having connected the phase space of the beam to that of the jitter, the problem has been reduced to measuring the jitter phase space. This can be done quickly and noninvasively with a multishot measurement using two BPMs—see Fig. 2 for a conceptual setup. Correlated offset data is required to measure the position and angle of each shot, which for a ballistic orbit (i.e., no magnets between the BPMs) is given by

$$x' = \frac{x_2 - x_1}{\Delta s}, \quad (9)$$

where x_1 and x_2 are the upstream and downstream centroid offsets, respectively, and Δs is the separation of the two BPMs. Both transverse planes can be measured simultaneously. As the number of shots increases, the jitter phase space will gradually build up, assuming that the optics remains unchanged. Whenever the optics *does* change, the measurement must be restarted.
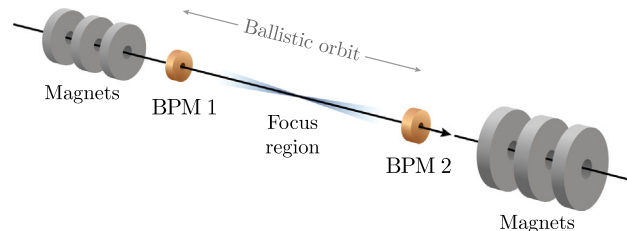

FIG. 2. Basic experimental setup, with two BPMs surrounding the focus region, separated by a ballistic orbit. The measurement can also be generalized to nonballistic orbits, where there are magnets also between the BPMs.

Given that no scan is performed, the data can be analyzed immediately from the start of the measurement, then reanalyzed with every additional shot, gradually increasing the precision. As the number of shots N increases, the relative measurement error of Twiss parameters and jitter emittance will be approximately $1/\sqrt{N}$. Since the connection between the beam and the jitter phase space is only approximate, it will rarely be necessary to require better than about 10% precision (corresponding to 50–500 shots). In a typical accelerator with a 1–10 Hz repetition rate, this allows quasionline monitoring on a few-tens-of-seconds timescale.

The measurement can also be generalized to nonballistic orbits (i.e., with magnets between the BPMs), as is relevant to for instance plasma accelerators with strong permanent quadrupoles close to the plasma entrance [26]. In this case, the angle at the upstream BPM can be calculated using

$$x_1' = \frac{x_2 - M_{11}x_1}{M_{12}}, \quad (10)$$

where M is the transfer matrix between the two BPMs. However, predicting the evolution of beta functions with mm-level accuracy then requires very accurate (per-mille-level) measurements of monitor locations, quadrupole locations, field strengths and beam energy—just like for a quadrupole scan. A ballistic measurement is comparatively simple, and hence always preferable if possible, as only an accurate measurement of BPM locations (and relative-offset calibrations) is required. For the remainder of this paper we will, therefore, assume that the BPMs are separated by only a drift space in order to facilitate ballistic measurements.

IV. RESOLUTION LIMITS

The main limitation of this technique stems from the finite resolution of BPMs. In measuring the jitter-phase-space ellipse, the width of each angle-slice (i.e., the position jitter at the waist) must be well resolved, which limits how small a waist beta function can be measured.

A. Analytic model

To calculate this resolution limit, we consider the apparent covariance matrix of the jitter at the upstream BPM location

$$\text{cov}(x, x') = \begin{bmatrix} \langle x^2 \rangle + \sigma^2 & \langle xx' \rangle - \frac{\sigma^2}{\Delta s} \\ \langle xx' \rangle - \frac{\sigma^2}{\Delta s} & \langle x'^2 \rangle + 2\frac{\sigma^2}{\Delta s^2} \end{bmatrix}, \quad (11)$$

where σ is the BPM resolution. The true covariances of the jitter can be expressed in terms of its waist parameters as $\langle x^2 \rangle = \epsilon(\beta_w + s_w^2/\beta_w)$, $\langle xx' \rangle = -\epsilon s_w/\beta_w$, and $\langle x'^2 \rangle = \epsilon/\beta_w$, where ϵ is the geometric jitter emittance and s_w is the distance from the upstream BPM to the jitter waist.

The measured jitter emittance for this finite BPM resolution is given by the determinant of Eq. (11)

$$\hat{\epsilon}^2 = \epsilon^2 + \frac{\sigma^2}{\Delta s^2}\frac{\epsilon}{\beta_w}\left(s_w^2 + (\Delta s - s_w)^2 + 2\beta_w^2\right) + \frac{\sigma^4}{\Delta s^2}. \quad (12)$$

Employing the same logic as in Sec. II [for Eqs. (6) and (7)], we can find the measured waist beta function from the inverse of the measured gamma function

$$\hat{\beta}_w = \frac{\hat{\epsilon}\beta_w}{\epsilon + 2\frac{\beta_w\sigma^2}{\Delta s^2}}, \quad (13)$$

where $\hat{\epsilon}$ can be substituted from Eq. (12), as well as the measured waist location from the ratio of the measured alpha and gamma functions

$$\hat{s}_w = \frac{s_w + \frac{\beta_w\sigma^2}{\epsilon\Delta s}}{1 + 2\frac{\beta_w\sigma^2}{\epsilon\Delta s^2}}. \quad (14)$$

Equations (12)–(14) establish three resolution regimes: (1) well-resolved, (2) distorted, and (3) fully saturated. To avoid any distortion whatsoever, the BPM resolution must be better than

$$\sigma \ll \sqrt{\frac{\epsilon\beta_w\Delta s^2}{s_w^2 + (\Delta s - s_w)^2 + 2\beta_w^2}}, \quad (15)$$

found by requiring the quadratic σ^2-term in Eq. (12) to be smaller than the constant ϵ^2-term. To avoid saturation (i.e., noise dominating the signal), the resolution should be better than

$$\sigma \ll \sqrt{\frac{\epsilon\Delta s^2}{2\beta_w}}, \quad (16)$$

found by demanding the σ^2-term in the denominator of Eq. (13) be smaller than the ϵ-term. Encouragingly, the measurement of the waist location is not affected by the distortion limit, and instead only by the significantly larger saturation limit. This is because the waist location is only related to the phase-space correlation and not its area. These regimes are demonstrated by the example in Fig. 3, which also shows exact agreement with Monte Carlo simulations of two finite-resolution BPMs.
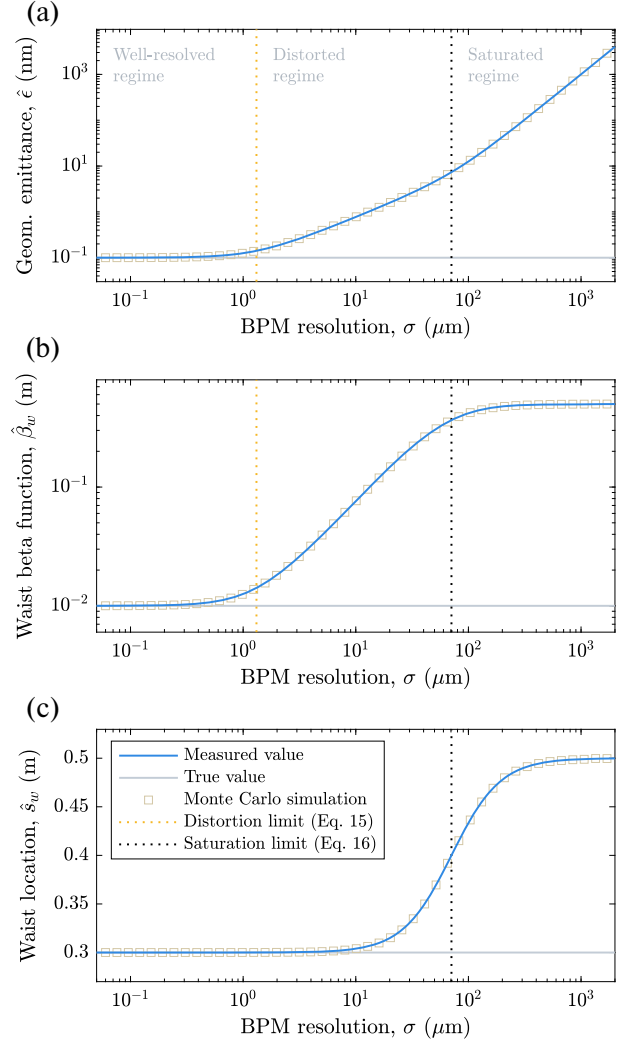

FIG. 3. Simulated two-BPM measurements over a large range of finite BPM resolutions. The BPMs are spaced 1 m apart and the jitter is focused 0.3 m from the upstream BPM with a 10 mm beta function and 0.1 mm mrad normalized emittance. Monte Carlo simulations (average of 10^7 shots per resolution) demonstrate that this analytic model is exact.

In a typical case where the waist beta function is small compared to the BPM separation ($\beta_w \ll \Delta s$) and the waist is approximately half way between the BPMs ($s_w \approx \Delta s/2$), Eq. (15) simplifies to $\sigma \ll \sqrt{2\epsilon\beta_w}$—therefore the BPM resolution should be smaller than the position jitter at the waist. This limit informs the choice of BPM technology required for the application in question.

B. Overcoming the resolution limit

For matching into a plasma accelerator with mm-scale beta functions and sub-μm jitter emittances, a very high BPM resolution is required. Ideally, this is achieved using state-of-the-art cavity BPMs, which can provide sub-100 nm resolution (depending on the charge distribution) [27,28]. However, if such BPMs are not available, measuring the

waist beta function may require going beyond the resolution limit. This is in principle possible to do, if the emittance of the jitter is already known.

Just like the emittance of the beam, the jitter emittance is preserved in a linear-optics lattice (assuming it contains no significant jitter sources). Therefore one of two alternative measurement techniques can be utilized: (1) Relax the strength of the focusing until the jitter waist is well resolved—giving different Twiss parameters, but the same emittance. (2) Simultaneously perform a similar measurement with two other BPMs just upstream or just downstream, where the focusing is relaxed compared to the focus region. The first method requires the jitter emittance to persist in time, whereas the second requires it to persist in space. Both methods assume negligible chromaticity or that energy slices are measured separately (see Sec. V B).

When the jitter emittance is known, the analysis simplifies greatly. The waist beta function can be calculated using

$$\beta_w = \frac{\epsilon \Delta s^2}{\langle (x_2 - x_1)^2 \rangle}, \qquad (17)$$

based on the variance of the angle jitter [Eq. (9)], and the waist location is simply

$$s_w = \frac{\Delta s}{1 - \frac{\partial x_2}{\partial x_1}}, \qquad (18)$$

where $\frac{\partial x_2}{\partial x_1}$ is the slope of the correlation between the two BPM readings.

V. MEASUREMENTS AT FLASHFORWARD

Experimental demonstration of the two-BPM method was performed at the FLASHForward facility at DESY, which uses a 1 GeV electron beam from the FLASH free-electron-laser facility [29]. FLASH provides high-charge (up to 1 nC), low-emittance (1 mm mrad) bunches with relatively small centroid jitter. After an approximately 150 m long linac, the bunches are diverted into the FLASHForward beamline. Here, a dispersive section allows for advanced energetic collimation [30], then a final-focusing section [depicted in Fig. 1(b)] tightly focuses the beam into a plasma accelerator. Downstream of the plasma is a suite of beam diagnostics, in particular a dipole spectrometer with quadrupoles for point-to-point beam imaging.

A. Comparison to quadrupole scans

To test the assumptions in Sec. II and the applicability of the method, a detailed comparison of the measured jitter and beam phase spaces was performed. A strong-focusing optic was set up to focus bunches with an energy of 678 MeV and charge 290 pC down to a cm-scale beta
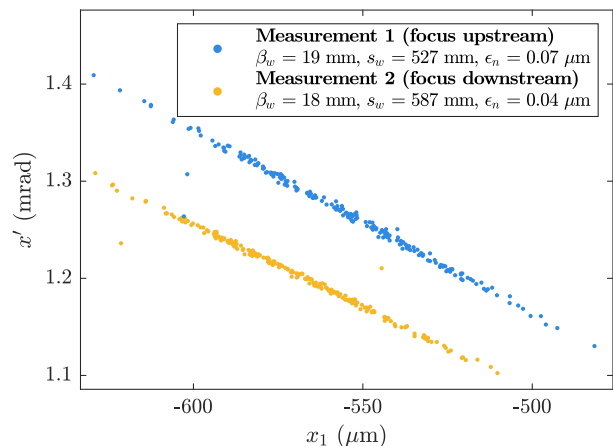

FIG. 4. Measured jitter phase spaces at the location of the upstream BPM for two different optics settings, indicating cm-scale waist beta functions focused at two waist locations 60 mm apart. A small distortion from a finite BPM resolution was taken into account when calculating the jitter parameters. These measurements should be compared to the corresponding quadrupole scans in Fig. 5. Each dataset consists of 210 shots, giving an estimated relative error of 7%.

function at the location of the plasma accelerator module (which had been removed from the beam path). Surrounding this focus region were two cavity BPMs [31,32] with a resolution of 0.9 μm, separated by 1.073 m, and approximately equidistant from the nominal focus point.

Two datasets were collected, using slightly different final-focusing optics with the beam focused at two locations 60 mm apart. Figure 4 shows the measured jitter phase space for each of these two settings using the two-BPM method. The presence of outliers (as seen in Fig. 4) can significantly skew the calculation of phase-space parameters, and thus an outlier-cleaning method was applied: (i) translate the jitter to the waist location from the BPM correlation [Eq. (18)], (ii) perform Gaussian fits of both the x and x' distributions, (iii) remove all shots beyond $\pm 5\sigma$, and then (iv) undo the translation from (i). Finally, a small distortive effect from the finite BPM resolution was removed by numerically solving Eqs. (12)–(14) for the true jitter-phase-space parameters.

At the same time, an object-plane scan was performed with the downstream quadrupoles (after the second BPM), imaging the beam onto a LANEX screen with a resolution of 57 μm. Figure 5 shows the corresponding measurement of the beam waist. Note that the spectrometer limits the measurement to the horizontal plane, as the dipole disperses vertically. No chromaticity was observed on the screen.

The two-BPM measurement agrees with the quadrupole scan measurement to an acceptable level. The waist beta function of the jitter (18–19 mm) differs from that of the beam (27–29 mm) by about 35%, and the jitter waist location is offset from the beam waist location by 15 mm—on the same scale as the waist beta function, as expected.
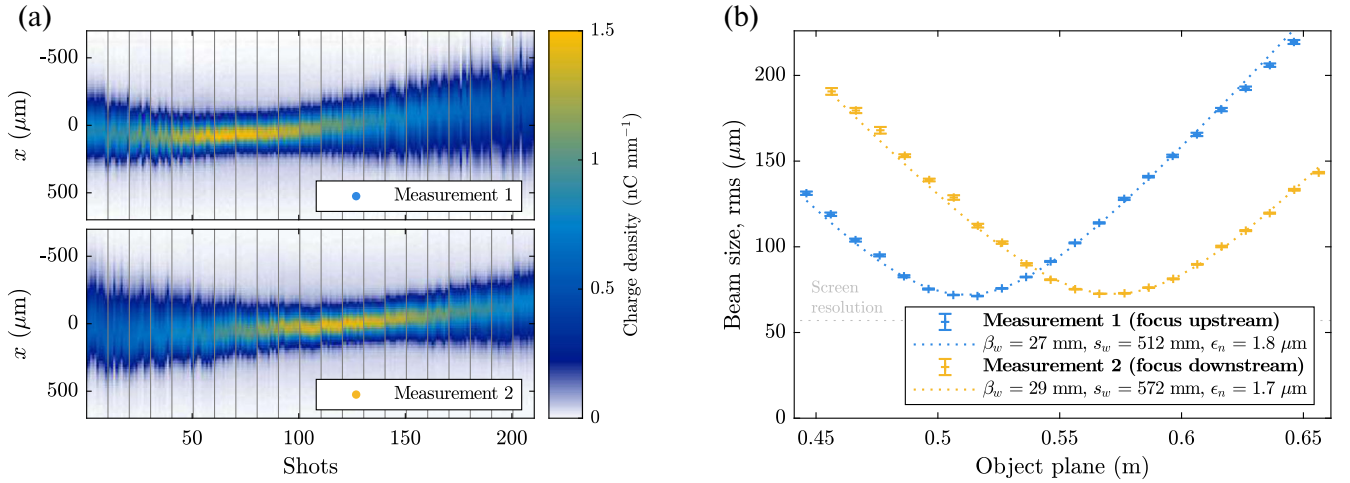
FIG. 5.   Quadrupole scans on a downstream spectrometer screen performed during the two-BPM measurements in Fig. 4, (a) imaging the beam from a range of object planes around the beam waist. (b) The variation of horizontally projected beam size for each object plane indicates that the beam was focused to a small waist beta function (27–29 mm) close to the center of the focus region—only moderately mismatched from measured jitter. The screen resolution was accounted for in the calculation of beam parameters. Error bars represent the standard error of the mean.

Based on these numbers, the beam–jitter mismatch parameter was calculated to be $\mathcal{M} = 2.1$–2.2, implying that the phase space of the jitter was indeed closely matched to that of the beam. If used to match into a plasma accelerator (where the jitter phase space would be matched), the expected emittance growth of the beam from mismatching [Eq. (8)] would be 28%–33%.

As an additional cross-check of the jitter measurements, the centroid jitter was also measured directly on the spectrometer (see Fig. 6). This was used to verify the accuracy of the distances and quadrupole field strength calibrations used for the quadrupole scans, as well as to fine-tune the value of the BPM resolution and calibrations.
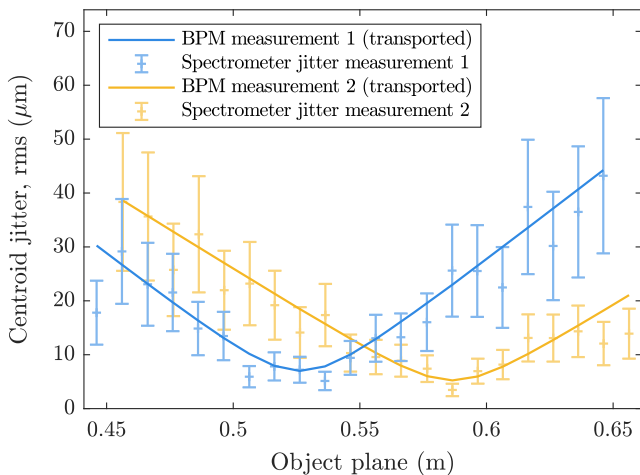
B. Slice-by-slice measurements

Chromaticity, where Twiss parameters change with energy [33,34], can be a concern when tightly focusing beams of finite energy spread [35]. This is especially important in energy-chirp-based two-bunch experiments where a trailing bunch needs to be exactly matched into the plasma wake behind a different-energy driver bunch.

Measuring chromaticity with the two-BPM technique requires it to be combined with an energy filter—each energy slice sufficiently narrow to have an achromatic focus. At FLASHForward this is accomplished using an energetic collimator [30]. Moving both the high- and low-energy collimators together, thin slices with 0.1% root-mean-square (rms) energy spread could be made. Figure 7 shows the result of such an energy-slice scan around a mean energy of 1120 MeV, indicating a highly chromatic focus in the vertical plane. The waist beta functions are relatively consistent (10–20 mm) across all slices, whereas the waist location shifted significantly between the highest and lowest energy slice (by 80 mm). In the horizontal plane (not shown in Fig. 7), the waist location spanned only 10 mm—considerably less chromatic. This asymmetric chromaticity is expected in a quadrupole-based final-focus system, where the beam is more strongly defocused in one plane (typically the vertical plane) before being focused to a waist.

Taking into account all the information gathered in an energy-slice scan, we can extract a partial 5D beam tomography. As seen in Fig. 7(a), the average position and angle of each individual energy slice is also measured,

FIG. 6.   Comparison of the centroid jitter measured on the spectrometer screen and with the two-BPM method (artificially transported through the quadrupoles to the spectrometer location). Error bars represent the standard error of the mean. A statistically significant agreement is observed, verifying the accuracy of both measurement methods.
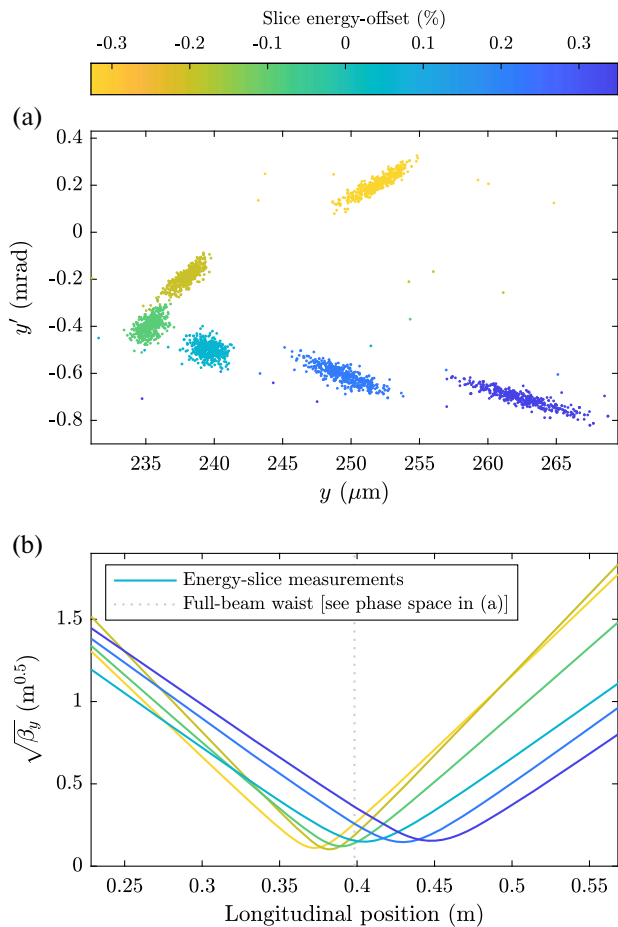
FIG. 7. Chromaticity measurement using an energy-slice scan. (a) Jitter phase space for a range of energy slices. Significant dispersion (energy-dependent offsets) can also be observed. Each step consists of 500 shots. (b) The corresponding evolution of the beta function for each slice in the focus region, indicating a highly chromatic focus.

and therefore both the beam centroid and the (emittance-normalized) beam size of each slice is known in both planes. This in-situ tomography allows not only slice-specific matching, but also measurement and removal of any bunch dispersion. For a linearized longitudinal phase space, dispersion corresponds to a bunch tilt or curvature, which in a plasma wake leads to emittance growth [36,37] and potentially a hosing instability [38–40]. Finally, combining such a two-BPM tomography with longitudinal-phase-space data from a transverse-deflecting cavity allows a 6D phase space to be reconstructed—important for realistic simulations and detailed optimization of the external injection process.

VI. CONCLUSIONS

We have shown that centroid jitter measured by two BPMs can be used to quickly estimate Twiss parameters in a region of strong focusing. While being an approximate

measurement, it can significantly speed up the complex and delicate beam setup procedure needed to properly match into a plasma accelerator, and allows noninvasive online monitoring of the beam focus. Experiments were successfully performed at FLASHForward to verify this technique, by comparing the two-BPM measurement to a conventional quadrupole scan. Already in routine use for plasma-wakefield experiments at FLASHForward, it is clear that the power of this method lies in its simplicity.

ACKNOWLEDGMENTS

[1] T. Tajima and J. M. Dawson, Laser Electron Accelerator, Phys. Rev. Lett. **43**, 267 (1979).

[2] P. Chen, J. M. Dawson, R. W. Huff, and T. Katsouleas, Acceleration of Electrons by the Interaction of a Bunched Electron Beam with a Plasma, Phys. Rev. Lett. **54**, 693 (1985).

[3] R. D. Ruth, A. W. Chao, P. L. Morton, and P. W. Wilson, A plasma wake field accelerator, Part. Accel. **17**, 171 (1985).

[4] I. Blumenfeld, C. E. Clayton, F.-J. Decker, M. J. Hogan, C. Huang, R. Ischebeck *et al.*, Energy doubling of 42 GeV electrons in a metre-scale plasma wakefield accelerator, Nature (London) **445**, 741 (2007).

[5] M. Litos, E. Adli, W. An, C. I. Clarke, C. E. Clayton, S. Corde *et al.*, High-efficiency acceleration of an electron beam in a plasma wakefield accelerator, Nature (London) **515**, 92 (2014).

[6] C. Joshi and T. Katsouleas, Plasma accelerators at the energy frontier and on tabletops, Phys. Today **56**, 47, (2003).

[7] W. P. Leemans and E. Esarey, Laser-driven plasma-wave electron accelerators, Phys. Today **62**, No. 3, 44 (2009).

[8] J. M. J. Madey, Stimulated emission of bremsstrahlung in a periodic magnetic field, J. Appl. Phys. **42**, 1906 (1971).

[9] M. E. Couprie, A. Loulergue, M. Labat, R. Lehe, and V. Malka, Towards a free electron laser based on laser plasma accelerators, J. Phys. B **47**, 234001 (2014).

[10] J. Rosenzweig, N. Barov, A. Murokh, E. Colby, and P. Colestock, Towards a plasma wake-field acceleration-based linear collider, Nucl. Instrum. Methods Phys. Res., Sect. A **410**, 532 (1998).

[11] C. B. Schroeder, E. Esarey, C. G. R. Geddes, C. Benedetti, and W. P. Leemans, Physics considerations for laser-plasma linear colliders, Phys. Rev. Accel. Beams **13**, 101301 (2010).

[12] E. Adli, J.-P. Delahaye, S. J. Gessner, M. J. Hogan, T. O. Raubenheimer, W. An, C. Joshi, and W. B. Mori, A beam driven plasma-wakefield linear collider: from Higgs factory to multi-TeV, SLAC Report No. SLAC-PUB-15426, 2013.

[13] C. A. Lindstrøm, Emittance growth and preservation in a plasma-based linear collider, Ph.D. Thesis, University of Oslo, 2019.

[14] S. Steinke, J. van tilborg, C. Benedetti, C. G. R. Geddes, C. B. Schroeder, J. Daniels *et al.*, Multistage coupling of independent laser-plasma accelerators, Nature (London) **530**, 190 (2016).

[15] C. A. Lindstrøm, E. Adli, J. M. Allen, J. P. Delahaye, M. J. Hogan, C. Joshi, P. Muggli, T. O. Raubenheimer, and V. Yakimenko, Staging optics considerations for a plasma wakefield acceleration linear collider, Nucl. Instrum. Methods Phys. Res., Sect. A **829**, 224 (2016).

[16] T. Mehrling, J. Grebenyuk, F. S. Tsung, K. Floettmann, and J. Osterhoff, Transverse emittance growth in staged laser-wakefield acceleration, Phys. Rev. Accel. Beams **15**, 111303 (2012).

[17] E. D. Courant and H. S. Snyder, Theory of the alternating-gradient synchrotron, Ann. Phys. (N.Y.) **3**, 1 (1958).

[18] K. A. Marsh, C. E. Clayton, D. K. Johnson, C. Huang, C. Joshi, W. Lu *et al.*, Beam matching to a plasma wake field accelerator using a ramped density profile at the plasma boundary, *Proceedings of PAC2005, Knoxville, TN, USA* (JACoW, Geneva, 2005), p. 2702.

[19] I. Dornmair, K. Floettmann, and A. R. Maier, Emittance conservation by tailored focusing profiles in a plasma accelerator, Phys. Rev. Accel. Beams **18**, 041302 (2015).

[20] Y. Zhao, W. An, X. Xu, F. Li, L. Hildebrand, M. J. Hogan, V. Yakimenko, C. Joshi, and W. B. Mori, Emittance preservation through density ramp matching sections in a plasma wakefield accelerator, Phys. Rev. Accel. Beams **23**, 011302 (2020).

[21] A. Aschikhin, C. Behrens, S. Bohlen, J. Dale, N. Delbos, L. di Lucchio *et al.*, The FLASHForward facility at DESY, Nucl. Instrum. Methods Phys. Res., Sect. A **806**, 175 (2016).

[22] R. D'Arcy, A. Aschikhin, S. Bohlen, G. Boyle, T. Brümmer, J. Chappell *et al.*, FLASHForward: plasma wakefield accelerator science for high-average-power applications, Phil. Trans. R. Soc. A **377**, 20180392 (2019).

[23] G. Balik, B. Aimard, L. Brunetti, and B. Caron, Proof of concept of CLIC final focus quadrupoles stabilization, in *Proceedings of IPAC2017, Copenhagen, Denmark* (JACoW, Geneva, 2017), p. 1290.

[24] D. R. Bett, C. Charrondière, M. Pateckia, J. Pfingstner, D. Schulte, R. Tomás *et al.*, Compensation of orbit distortion due to quadrupole motion using feed-forward control at KEK ATF, Nucl. Instrum. Methods Phys. Res., Sect. A **895**, 10 (2018).

[25] M. Sands, A beta mismatch parameter, SLAC Report No. SLAC-AP-85, 1991.

[26] S. Yamin, R. W. Assmann, U. Dorda, F. Lemery, B. Marchetti, E. Panofski, and P. A. Walker, Design considerations for permanent magnetic quadrupole triplet for matching into laser driver wake field acceleration

[27] experiment at SINBAD, in *Proceedings of IPAC2019, Melbourne, Australia* (JACoW, Geneva, 2019), p. 143.

Y. I. Kim, R. Ainsworth, A. Aryshev, S. T. Boogert, G. Boorman, J. Frisch *et al.*, Cavity beam position monitor system for the Accelerator Test Facility 2, Phys. Rev. Accel. Beams **15**, 042801 (2012).

[28] D. R. Bett, N. B. Kraljevic, R. M. Bodenstein, T. Bromwich, P. N. Burrows, G. B. Christian *et al.*, Performance of nanometre-level resolution cavity beam position monitors at ATF2, in *Proceedings of IPAC2018, Vancouver, BC, Canada* (JACoW, Geneva, 2018), p. 1212.

[29] W. Ackermann, G. Asova, V. Ayvazyan, A. Azima, N. Baboi, J. Bähr *et al.*, Operation of a free-electron laser from the extreme ultraviolet to the water window, Nat. Photonics **1**, 336 (2007).

[30] S. Schröeder, K. Ludwig, A. Aschikhin, R. D'Arcy, M. Dinter, P. Gonzalez *et al.*, Tunable and precise two-bunch generation at FLASHForward, arXiv:2005.12071 [J. Phys.: Conf. Ser. (to be published)].

[31] D. Lipka, N. Baboi, D. Noelle, G. Petrosyan, S. Vilcins, R. Baldinger *et al.*, FLASH undulator BPM commissioning and beam characterization results, in *Proceedings of IBIC2014, Monterey, CA, USA* (JACoW, Geneva, 2015), p. 315.

[32] D. Nölle *et al.*, The diagnostic system at the European XFEL; commissioning and first user operation, in *Proceedings of IBIC2018, Shanghai, China* (JACoW, Geneva, 2019), p. 162.

[33] H. Zyngier, Strategy for correcting for chromaticity, Report No. LAL-77/35, Laboratoire de l'Accélérateur Linéaire, Orsay, 1977.

[34] B. W. Montague, Linear optics for improved chromaticity correction, LEP Note No. 165, CERN, Geneva, 1979.

[35] C. A. Lindstrøm and E. Adli, Design of general apochromatic drift-quadrupole beam lines, Phys. Rev. Accel. Beams **19**, 071002 (2016).

[36] R. Assmann and K. Yokoya, Transverse beam dynamics in plasma-based linacs, Nucl. Instrum. Methods Phys. Res., Sect. A **410**, 544 (1998).

[37] C. A. Lindstrøm, E. Adli, J. Pfingstner, E. Marín, and D. Schulte, Transverse tolerances of a multi-stage plasma wakefield accelerator, in *Proceedings of IPAC2016, Busan, Korea* (JACoW, Geneva, 2016), p. 2561.

[38] D. H. Whittum, W. M. Sharp, S. S. Yu, M. Lampe, and G. Joyce, Electron-Hose Instability in the Ion-Focused Regime, Phys. Rev. Lett. **67**, 991 (1991).

[39] C. Huang, W. Lu, M. Zhou, C. E. Clayton, C. Joshi, W. B. Mori *et al.*, Hosing Instability in the Blow-out Regime for Plasma-Wakefield Acceleration, Phys. Rev. Lett. **99**, 255001 (2007).

[40] T. J. Mehrling, R. A. Fonseca, A. M. de la Ossa, and J. Vieira, Mitigation of the Hose Instability in Plasma-Wakefield Accelerators, Phys. Rev. Lett. **118**, 174801 (2017).

ARTICLE

Check for updates

High-resolution sampling of beam-driven plasma wakefields

S. Schröder [1,2✉], C. A. Lindstrøm [1], S. Bohlen [1,2], G. Boyle [1], R. D'Arcy[1], S. Diederichs [1,2], M. J. Garland[1], P. Gonzalez [1,2], A. Knetsch [1], V. Libov[1], P. Niknejadi [1], Kris Põder [1], L. Schaper [1], B. Schmidt[1], B. Sheeran[1,2], G. Tauscher[1,2], S. Wesch [1], J. Zemella[1], M. Zeng [1] & J. Osterhoff [1]

Plasma-wakefield accelerators driven by intense particle beams promise to significantly reduce the size of future high-energy facilities. Such applications require particle beams with a well-controlled energy spectrum, which necessitates detailed tailoring of the plasma wakefield. Precise measurements of the effective wakefield structure are therefore essential for optimising the acceleration process. Here we propose and demonstrate such a measurement technique that enables femtosecond-level (15 fs) sampling of longitudinal electric fields of order gigavolts-per-meter (0.8 GV m^{-1}). This method—based on energy collimation of the incoming bunch—made it possible to investigate the effect of beam and plasma parameters on the beam-loaded longitudinally integrated plasma wakefield, showing good agreement with particle-in-cell simulations. These results open the door to high-quality operation of future plasma accelerators through precise control of the acceleration process.

[1] Deutsches Elektronen-Synchrotron DESY, Notkestraße 85, 22607 Hamburg, Germany. [2] Universität Hamburg, Mittelweg 177, 20148 Hamburg, Germany. ✉email: sarah.schroeder@desy.de

ARTICLE

Plasma wakefields[1] can accelerate charged particle beams with gradients in excess of gigavolts-per-meter, promising more compact accelerators for high energy physics and photon science[2,3]. In a beam-driven plasma-wakefield accelerator[4,5], a high-density charged-particle beam interacts with plasma electrons to form an electron density wake, in which trailing particles can rapidly gain energy from strong electric fields[6]. The resulting energy spectrum of the accelerated particles is determined by the detailed structure of this plasma wakefield, which again depends on the exact distributions of plasma density and beam charge[7]. Free-electron lasers[8] and particle colliders[9] have strict demands for precise control of the energy spectrum (e.g., low spread of energies), which have not yet been met by plasma accelerators. To reach this level of precision, it is first necessary to measure the wakefield with high resolution—highly nontrivial at the required plasma densities. Here we present a method that enables such a high-resolution sampling of the effective wakefield in a beam-driven plasma accelerator. The method is based on separating the energy and time measurements of the longitudinal phase space of particle beams by energy collimation of chirped bunches, thereby overcoming the practical challenges faced by previous methods of temporally resolving bunches after plasma interaction. Using this technique, we demonstrate experimentally how beam and plasma parameters affect the wakefield. The method enables a new level of precision optimisation of the plasma acceleration process necessary to attain the lower energy spread, higher efficiency[10], and higher transformer ratios[11,12] desired for future applications.

Various techniques exist for measuring the structure of a plasma wake[13]. The electron density distribution can be imaged using laser-based methods like shadowgraphy[14] and frequency domain holography[15]. Also the magnetic fields inside the wake can be measured using lasers via the Faraday effect[16,17]. However, a direct measurement of the electric fields requires the use of charged particles. This can be done by traversing the wake perpendicular to its direction of motion with a short probe electron bunch, such that the transversely-integrated wakefield is imprinted on the transverse profile of the probe[18]. Alternatively, in a beam-driven plasma accelerator the beam itself can be used to measure the longitudinal wakefield, by comparing the longitudinal phase space (i.e., a time-resolved energy spectrum) of bunches with and without plasma interaction. This gives access to the effective wakefield, longitudinally integrated over the full plasma accelerator module—ultimately the quantity that needs to be optimised. The longitudinal phase space is typically measured using a magnetic spectrometer in combination with either a streak camera or an RF transverse deflecting structure (TDS)[19,20]. Both methods have been used to measure wakefields[11,12,21] in plasmas with densities of order 10^{13}–10^{14} cm^{-3}, requiring picosecond resolution—close to the resolution limit of a streak camera, whereas a TDS can, in principle, provide time resolution down to the femtosecond-scale.

Reaching high gradients for compact acceleration requires operating at plasma densities of 10^{16}–10^{17} cm^{-3}. In this range, prior to being optimised, the plasma wakefield can generate large energy spreads and complex, slice-dependent distributions in transverse phase space—highly divergent beams that are difficult to transport. As a result, measuring the longitudinal phase space of the plasma-interacted bunches becomes very challenging. The energy spectrum is therefore commonly measured close to the plasma module to avoid excessive chromaticity. This makes conventional use of a TDS highly impractical: the required ultrahigh-vacuum conditions cannot easily be met in the vicinity of a gas load such as a high-density plasma cell; the structure can be damaged by irradiation; and the diverging beams can sample off-axis longitudinal RF fields[22]. Alternative methods for providing the required

time resolution are therefore needed. The first example of this was presented by Clayton et al.[23], who were able to use correlations within the complex energy transverse phase space measured on a spectrometer screen to measure the wakefield indirectly at high density. However, this particular method works only for mismatched beams (causing emittance growth[24]) and the temporal resolution is highly restricted.

In this paper, we propose and demonstrate a more general solution to measuring beam-driven plasma wakefields—by fully separating the time and energy measurements of the longitudinal phase space. The method works by linking the two measurements using an energy collimator and bunches with a highly correlated (chirped) longitudinal-phase-space distribution. This chirp allows slice-by-slice collimation of the incoming beam-current profile (see Fig. 1), which can be used to progressively remove thin tail slices from the energy spectrum after plasma-interaction. Full time-resolvability necessitates a detailed temporal calibration of the collimators prior to the measurement (see Methods) and is then achieved by comparing the spectra as the collimator position is varied to find the energy of the charge that disappears between steps. Crucially, the measurement of the longitudinal slice position within the bunch for each collimator step can now be entirely
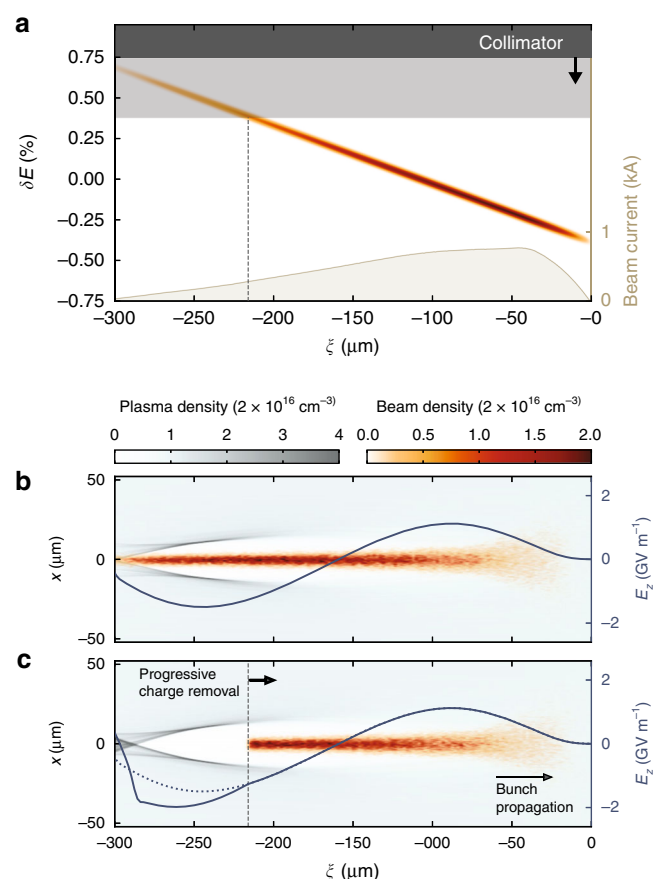

Fig. 1 Plasma wakefield sampling by energy collimation. a A strongly correlated longitudinal phase space allows tail slices to be progressively removed from the bunch, e.g., by collimation in a dispersive section. **b** An electron bunch interacts with a plasma and excites a density wake with strong longitudinal electric fields (3D particle-in-cell simulation). **c** Removing charge from the bunch tail alters the wakefield (compared to the original field, dotted line), but does not alter the wakefield experienced by the remaining bunch charge. By subtracting the final energy spectrum of consecutive collimator steps, the energy change of each longitudinal slice can be determined—revealing the effective wakefield.

ARTICLE

disentangled from the energy-spectrum measurement. As a consequence, this temporal measurement (e.g., using a TDS) can be performed elsewhere in the beamline, where conditions such as beam optics and vacuum requirements can be optimised for maximum time resolution, and not for the operation of a plasma accelerator. The measurement can even be performed in a parallel beamline if the difference in the longitudinal phase space can be accurately determined.

While bunch-tail removal does affect the wakefield, it does not influence the part being sampled—the wakefield experienced by the removed tail slice is identical to that experienced within an uncollimated bunch (see Fig. 1c). This is because the beam and the plasma wake both travel at approximately the speed of light, and therefore (by causality) cannot be affected by changes behind the cut. By using energy collimation to manipulate the current profile, some constraints are imposed—in particular, a strictly monotonic longitudinal-phase-space distribution is required. In general, a linear monotonic correlation will result in an equidistant sampling of the wakefield for a constant collimator step size. Non-linear correlations are applicable, but sample non-equidistantly. Moreover, the accuracy of the measurement will be limited by the sliced energy spread of the chirped bunches relative to their overall energy spread, as well as the beam-size-to-dispersion ratio at the location of the collimator.

Results

Experimental setup. This wakefield sampling measurement technique was implemented and experimentally demonstrated at the FLASHForward plasma accelerator facility[25] at DESY. High-quality electron bunches were generated with a photocathode at a repetition rate of 10 Hz and accelerated to 1.1 GeV using super-conducting RF cavities in the FLASH linac[26]. The bunches were linearised in longitudinal phase space and compressed to a bunch length of 285 ± 2 fs rms, characterised using an S-band TDS in a beam line parallel to the FLASHForward experimental area. The beam was then extracted into a dispersive section with a set of energy collimators for advanced shaping of the current profile[27]. The bunch head was collimated throughout the experiment to optimise the plasma interaction. A downstream toroid measured

the total delivered charge to be 460 ± 5 pC. Two sets of quadrupoles were used to focus the beam tightly at the interaction point, where the beam orbit was measured using two cavity-based beam-position monitors (BPMs). The plasma was generated by a high-voltage discharge in a 1.5-mm-diameter, 33-mm-long sapphire capillary filled with argon at a backing pressure of 40 mbar. The plasma cell was separated from the accelerator vacuum by three (windowless) differential pumping stations. After exiting the plasma cell, the energy spectrum of the electron beam was measured with a beam-imaging spectrometer, consisting of a vertically-dispersive dipole magnet and a set of quadrupoles for point-to-point beam imaging from the plasma exit plane to a scintillating LANEX screen. Figure 2 shows the experimental setup (see Methods for more details).

Experimental campaign. The wakefield sampling measurement consisted of a set of tail-collimator scans, progressively removing the rear part of the bunch until no charge was left. The plasma density was chosen such that the first oscillation of the plasma wake could be probed by the full length of the current profile (a density of $\sim 2 \times 10^{16}$ cm^{-3}). The evolution of the energy spectrum of the collimated bunches is shown in Fig. 3. The scan was repeated at three different imaging energies to ensure good energy resolution over the entire spectrum. The final energy of each longitudinal slice was then determined by the spectral difference between consecutive collimator steps (see Fig. 3c), resulting in a distinct signal that can be programmatically extracted (see Methods). The tail-collimator scan was then repeated with the plasma turned off, in order to accurately determine the energy change of each longitudinal slice. Some noise appears in the difference measurement due to imperfect stability of the plasma acceleration process, but this does not significantly hinder the extraction of the wakefield signal.

Time calibration of the tail-collimator steps was performed by direct comparison to the longitudinal phase space measured by the TDS. The cumulative charge below each energy in the longitudinal phase space was compared to the charge readings of the toroid downstream of the tail collimator (see Methods). Additionally, a known compression factor of 1.09 (i.e., 9% shorter
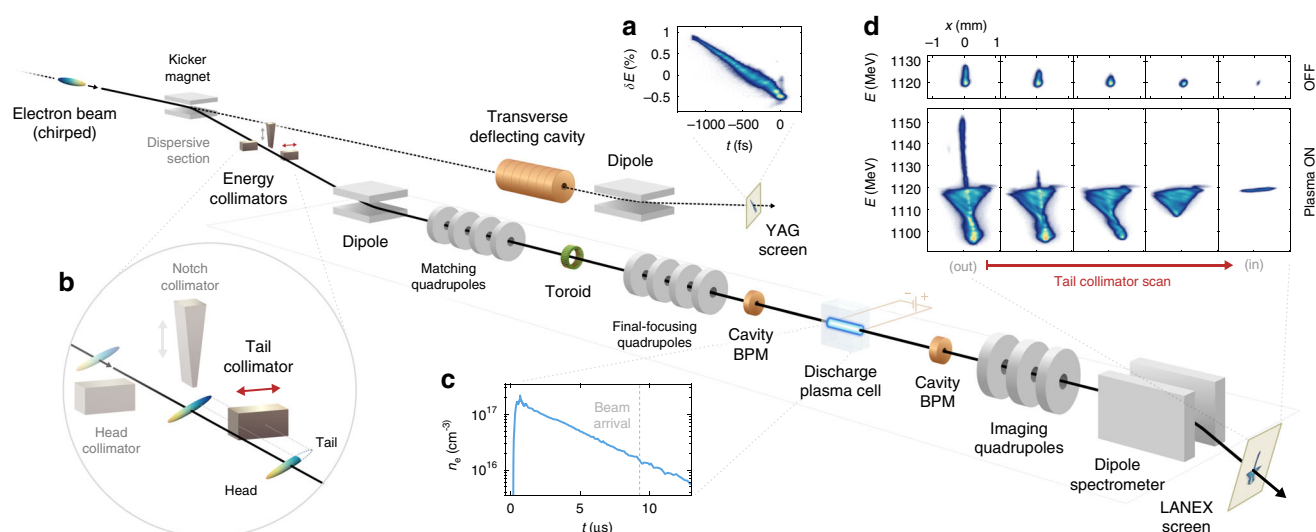

Fig. 2 Experimental setup. a An electron beam with a linearly chirped longitudinal phase space is characterised in a parallel beam line using a TDS. **b** A beam enters a dispersive section with energy collimators for optional removal of the tail (high energy), the head (low energy), and the centre (for two-bunch generation). The beam charge is measured with a toroid after collimation and before the beam is focused into a discharge plasma cell. **c** The relative time-of-arrival of the beam is adjusted to reach the desired plasma density: the temporal evolution of the average density was measured using two-colour interferometry in a test stand with a replica cell. **d** Finally, the beam following plasma interaction passes through a quadrupole triplet and is vertically dispersed by a spectrometer dipole to form a point-to-point image on a scintillating LANEX screen.
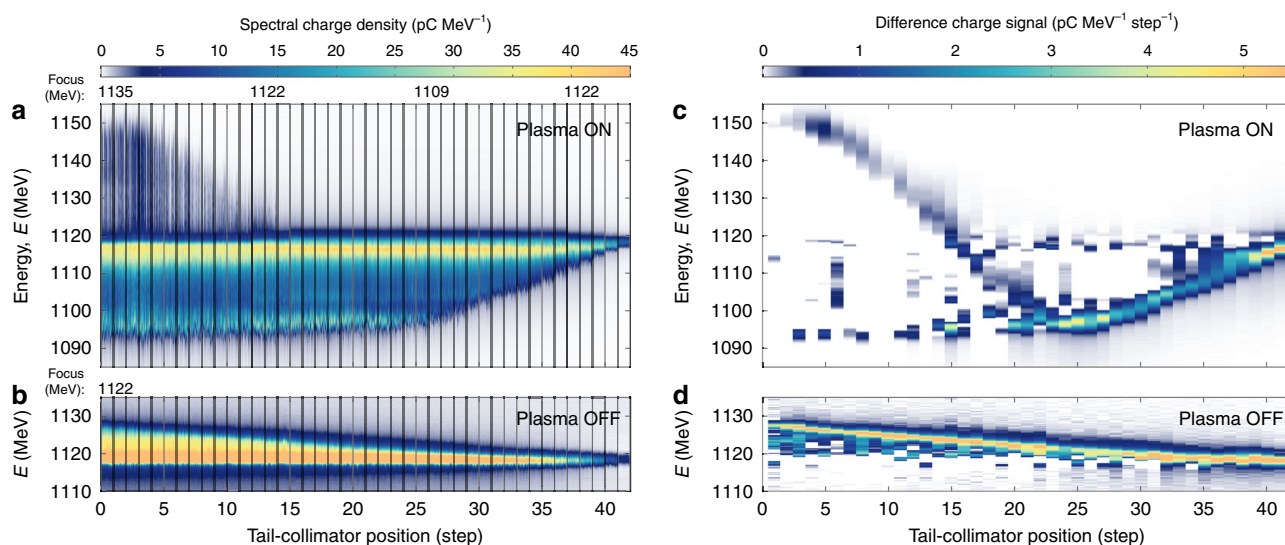
ARTICLE

Fig. 3 Evolution of the tail-collimated energy spectrum. a As the tail collimator is moved in (horizontal axis), the tail particles are progressively removed from the plasma-interacted energy spectrum; 70 shots are collected per step. **b** The same scan is repeated with no plasma (20 shots per step), demonstrating the energy collimation of the incoming bunch. **c** The difference of (averaged) spectra at consecutive collimator steps reveals the energy of each slice of the plasma-interacted bunch. **d** By subtracting the plasma-off energy of each slice, the wakefield signal can be extracted.

bunches) from the calculated longitudinal dispersion R_{56} of the extraction sections was taken into account.

Interpretation of experimental data. Figure 4a shows the resulting time-resolved wakefield measurement, sampled with more than 40 data points separated by ~6 μm. The electric field is calculated as the slice energy change normalised by the full 33-mm length of the cell—giving the effective wakefield of the plasma module. The wakefield is observed to have a zero-crossing at −165 μm (behind the bunch head), and reaches a maximum average accelerating gradient of 0.82 ± 0.08 GV m^{-1} at the bunch tail.

Given that the effective wakefield is longitudinally averaged, understanding the full evolution of the beam and the wakefield requires a 3D particle-in-cell (PIC) simulation (see Methods). Since the measurement is precise to the few-percent level, a similarly detailed understanding of every aspect of the simulated system is required—in particular the 6D phase space of the beam, as well as the longitudinal density profile of the plasma. Using quadrupole scans and a two-BPM technique for determining the transverse phase space[28], sliced transverse beam parameters were estimated (see Methods). Additionally, a longitudinally resolved measurement of the plasma density was performed in a replica cell using Stark broadening[29], where the argon was doped with hydrogen (see Methods). Due to the Gaussian-like longitudinal plasma-density profile, the wakefield and, as such, the peak electric-field amplitude evolve along the length of the plasma channel. The simulations indicate that the largest instantaneous accelerating field observed was −1.8 GV m^{-1} at a plasma density of 2.6×10^{16} cm^{-3}, 7 mm after the peak of the Gaussian-like longitudinal density profile. This implies that the plasma accelerator was operating in a quasi-linear regime, reaching ~12% of the wave-breaking field. As a result of this detailed characterisation of the beam and plasma parameters, a good agreement between simulation and measurement was achieved (as seen in Fig. 4)—lending credibility to the accuracy of the method.

Having demonstrated the precise measurement of plasma wakefields, we can now investigate the effects of changing key parameters: (1) the plasma density, and (2) the current profile. Figure 4b shows the measured wakefield for a 80% higher plasma

density. The wavelength is observed to decrease (zero-crossing at −155 μm) and the wakefield amplitude increases, as expected. Figure 4c shows the effect of introducing a notch collimator (see Fig. 2b) to remove the central part of the bunch—producing a double-bunch current profile. This does not alter the wakefield ahead of the notch, but drastically changes the shape of the wakefield experienced by the trailing charge. In this case, the zero-crossing of the wakefield occurs much earlier (at around −130 μm) because the lack of beam current allows the expelled plasma electrons to start returning to the axis earlier (the wakefield is proportional to the radial velocity of the plasma-sheath electrons[7]). This latter measurement is a direct demonstration of the physics of beam loading[30], where the presence or absence of beam electrons alters the shape of the plasma wakefield.

Discussion

The precise measurement of the plasma wakefield is an essential precursor to its optimisation. By using an energy-collimation technique, we have demonstrated that the necessary precision can be achieved—overcoming the practical challenges faced in a beam-driven plasma accelerator operating at high densities. Combined with an ability to fine-tune beam and plasma parameters, this innovative method opens the door to achieving milestones that require precisely tailored wakefields—such as optimised beam loading[31] for energy-spread preservation and high efficiency—while operating at the plasma densities and accelerating gradients necessary for many applications in high energy physics and photon science.

Methods

Generation of electron bunches. The superconducting linear accelerator FLASH was used to accelerate electron bunches of 600 pC total charge to a mean particle energy of 1122 MeV. The bunches were compressed in two magnetic bunch-compressor chicanes to a peak current of 750 A. The longitudinal phase space of the bunch was measured by a transverse deflecting structure in a beam line parallel to the FLASHForward experimental area. The measured energy spread spans ~1%, with slice energy spreads well below 0.1% (the measurement is limited by the transverse beam size inside the TDS and on the screen). A kicker magnet was used to extract the beam into a dispersive section where a set of three collimators[27] were used for energy profile manipulation, which due to the strongly correlated longitudinal phase space also allows precise manipulation of the bunch current profile.
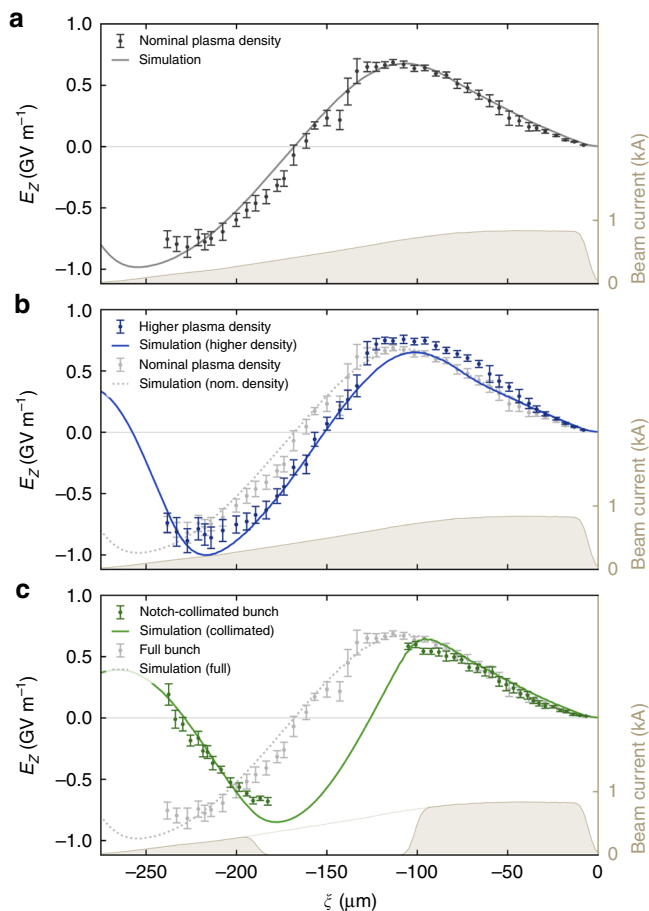
Fig. 4 Measured longitudinally averaged plasma wakefields. a The wakefield of the nominal beam and plasma is sampled with a 6 μm granularity. Error bars represent the shot-to-shot standard deviation. The solid line shows the corresponding PIC simulated wakefield. **b** The measurement is repeated with the same beam current profile and an 80% higher plasma density (the beam arrives 1.7 μs earlier), producing a shorter wavelength wakefield. **c** At the nominal density (same as in **a**), the beam current is notch-collimated into a double-bunch profile, producing a wakefield which is identical at the head, but strongly altered at the tail. The end point of $\xi = -240\,\mu m$ is determined by signal-to-noise ratio.

Owing to collective effects during bunch compression, it was found that collimating the bunch head (down to a total charge of 460 pC) increases the stability of beam–plasma interaction. This setting was chosen prior to the measurement campaign and kept throughout it. Toroids were used to measure the beam charge before and after the energy collimation. The bunches were further compressed by an estimated 9% in the dispersive extraction line. A set of nine quadrupoles was used to tightly focus the beam at the location of the plasma cell. Two cavity-based beam-position monitors (50 cm upstream and 50 cm downstream of the plasma) were used for beam alignment. Three differential pumping stations enabled a windowless vacuum-to-plasma transition—ensuring high beam quality while also meeting the ultrahigh vacuum requirements of the superconducting FLASH accelerator.

Plasma source. A discharge plasma source was used to create the plasma, ignited by a high-voltage thyratron supplying ~500 A of current at 25 kV for a duration of 400 ns. A thin 1.5-mm-diameter, 33-mm-long capillary was milled from two slabs of sapphire, mounted in a PEEK plastic holder, again mounted on a hexapod platform for high-precision alignment. A continuous flow of argon was supplied through two internal gas inlets from a buffer volume at a 40 mbar backing pressure. The gas escaped the open-ended capillary through holed copper electrodes (cathode upstream, anode downstream) into a large 500-mm-diameter vacuum chamber pumped to an ambient pressure of 4.3×10^{-3} mbar.

Electron imaging spectrometer. A dipole magnet was used to perform energy dispersion of the beam vertically onto a LANEX (fine) screen mounted just outside

the 1-mm-thick stainless-steel vacuum chamber wall, ~3 m downstream of the plasma cell. Five quadrupoles (acting as a triplet) located just upstream of the dipole were used to point-to-point image the beam from the plasma cell exit (the object plane) to the screen (the image plane) with a magnification of $R_{11} = -5$ (horizontally) and $R_{33} = -0.43$ (vertically), where R is the object-to-image-plane transfer matrix. The spatial resolution of the optical system was ~50 μm (i.e., ~2 pixels), corresponding to an energy resolution of 0.05% for particles close to the imaged energy. Away from this imaged energy, the energy resolution degrades depending on the vertical divergence of the bunch.

Wakefield signal extraction. The wakefield signal of a bunch slice is given by the difference in the energy spectrum between two consecutive collimator steps. All energy spectra (shots i) at collimator step $s + 1$ are subtracted from all energy spectra (shots j) at collimator step s, and subsequently fitted with a Gaussian distribution. Difference signals with a Gaussian peak μ_{ij} further away than 10 MeV from an initial peak estimate are rejected. Each event i of collimator step s has an attributed mean signal at $E_i = \frac{1}{n}\sum_{j=1}^{n}\mu_{ij}$, where n is the number of shots per step. The resulting energy signal between collimator steps s and $s + 1$ is given by the mean energy $E_{s+1/2} = \frac{1}{n}\sum_{i=1}^{n}E_i$. The standard deviation of E_s is used as the uncertainty of the signal. This uncertainty represents statistical fluctuations and is connected to the stability of the beam–plasma interaction. The same wakefield-signal extraction routine is used for all datasets. The presented wakefields are spliced from three datasets imaging at low, middle and high energies onto the spectrometer screen (1109, 1122 and 1135 MeV, respectively).

Temporal calibration of collimator steps. The collimator position scan is mimicked by a virtual energy-collimation scan on the reconstructed longitudinal-phase-space measurement (Supplementary Fig. 1a). The subtraction signal of two current profiles of consecutive collimator positions is fitted with a Gaussian distribution, where the peak position is used for the collimator-to-longitudinal-position calibration. Comparing the remaining charge measured in both the real and the virtual collimator scans (Supplementary Fig. 1b) can then be used to determine the corresponding longitudinal position within the bunch at each individual collimator step (Supplementary Fig. 1c). An additional compression factor of 1.09 from the extraction line is also taken into account—this factor is determined by the lattice configuration ($R_{56} = -3$ mm) in the dispersive section of the beamline.

Transverse beam characteristics. The transverse phase space of the beam was measured using a two-BPM tomography technique[28]. The phase space of the centroid jitter measured with two BPMs (upstream and downstream of the plasma chamber) allows the Twiss parameters of the beam to be estimated—a measurement based on the observation that the Twiss parameters of the jitter phase space are similar to those of the beam phase space. Combining this measurement with a head-and-tail-collimator position scan, which allows passage of 0.1% rms energy slices, enables an energetically resolved (and because of the strong chirp also temporally resolved) characterisation of the transverse phase space. The sliced emittance in the horizontal plane was determined using a quadrupole scan on the electron spectrometer, indicating a normalised emittance between 1 mm mrad (tail) and 10 mm mrad (head)—a variation likely to be caused by transverse kicks from coherent synchrotron radiation (CSR). The emittance in the vertical plane could not be measured directly, but was estimated to be 0.5–1 mm mrad—a typical value measured directly at the gun, not expected to be affected by CSR during transport. The beam was focused to beta functions of $\sim 10 \times 10$ mm^2, with a waist close to the plasma entrance, with a relatively large chromaticity (correlation between slice energy and waist location) in the vertical plane caused by asymmetric focusing in the final-focusing quadrupoles.

Longitudinal plasma density profile. Two complimentary diagnostics techniques were used to characterise the density profile evolution of the argon plasma[29]. Two-colour laser interferometry was used to measure the longitudinally integrated average plasma density (see Fig. 2c), and Stark broadening allowed the density to be longitudinally resolved. This was performed with a replica cell in a dedicated test laboratory. Supplementary Figure 2 shows the profile and evolution of the plasma density between 4 and 10 μs after the discharge, where the argon was doped with 5% hydrogen to enable Stark broadening of the H-alpha line. The density measurements were fitted (see Supplementary Fig. 2a) to obtain longitudinal profiles at 7.5 and 9.3 μs, which were then scaled to the corresponding absolute average density in pure argon (shown in Supplementary Fig. 2b).

Particle-in-cell simulations. The 3D quasistatic particle-in-cell code HIPACE[32] was used to simulate the full evolution of the beam–plasma interaction. The input beam was generated based on the 6D-phase-space information of the experimentally characterised beam. It was modeled with 0.2×10^6 constant-weight numerical particles. Similarly, a 33-mm-long longitudinally tailored plasma-density profile was implemented based on density measurements (see above). The plasma was sampled with 4 particles per cell. A simulation box of size $20 \times 20 \times 7\,k_p^{-3}$ (in $x \times y \times \xi$) was resolved by a grid of $1024 \times 1024 \times 200$ cells, evolved with a

ARTICLE

constant time step of 3.5 ω_p^{-1}, where k_p and ω_p are the plasma wavenumber and frequency, respectively. The resulting longitudinally averaged, on-axis electric fields were used for comparison to the experimentally measured wakefields (see Fig. 4).

Data availability

The data that support the findings of this study are available from the corresponding author upon reasonable request.

References

1. Tajima, T. & Dawson, J. M. Laser electron accelerator. *Phys. Rev. Lett.* **4**, 267–270 (1979).
2. Joshi, C. & Katsouleas, T. C. Plasma accelerators at the energy frontier and on tabletops. *Phys. Today* **56**, 47–53 (2003).
3. Couprie, M. E., Loulergue, A., Labat, M., Lehe, R. & Malka, V. Towards a free electron laser based on laser plasma accelerators. *J. Phys. B* **47**, 234001 (2014).
4. Chen, P., Dawson, J. M., Huff, R. W. & Katsouleas, T. Acceleration of electrons by the interaction of a bunched electron beam with a plasma. *Phys. Rev. Lett.* **54**, 693–696 (1985).
5. Ruth, R. D., Chao, A. W., Morton, P. L. & Wilson, P. B. A plasma wake field accelerator. *Part. Accel.* **17**, 171 (1985).
6. Blumenfeld, I. et al. Energy doubling of 42 GeV electrons in a metre-scale plasma wakefield accelerator. *Nature* **445**, 741 (2007).
7. Lu, W., Huang, C., Zhou, M., Mori, W. B. & Katsouleas, T. Nonlinear theory for relativistic plasma wakefields in the blowout regime. *Phys. Rev. Lett.* **96**, 165002 (2006).
8. Madey, J. M. J. Stimulated emission of bremsstrahlung in a periodic magnetic field. *J. Appl. Phys.* **42**, 1906–1913 (1971).
9. Adli, E. et al. A beam driven plasma-wakefield linear collider: from higgs factory to multi-tev. SLAC Internal Report SLAC–PUB–15426. Preprint at http://arxiv.org/abs/1308.1145 (2013).
10. Litos, M. et al. High-efficiency acceleration of an electron beam in a plasma wakefield accelerator. *Nature* **515**, 92 (2014).
11. Loisch, G. et al. Observation of high transformer ratio plasma wakefield acceleration. *Phys. Rev. Lett.* **121**, 693–696 (2018).
12. Roussel, R. et al. Single shot characterization of high transformer ratio wakefields in nonlinear plasma acceleration. *Phys. Rev. Lett.* **124**, 044802 (2020).
13. Downer, M. C., Zgadzaj, R., Debus, A., Schramm, U. & Kaluza, M. C. Diagnostics for plasma-based electron accelerators. *Rev. Mod. Phys.* **90**, 035002 (2018).
14. Sävert, A. et al. Direct observation of the injection dynamics of a laser wakefield accelerator using few-femtosecond shadowgraphy. *Phys. Rev. Lett.* **115**, 055002 (2015).
15. Matlis, N. H. et al. Snapshots of laser wakefields. *Nat. Phys.* **2**, 749 (2006).
16. Kaluza, M. C. et al. Measurement of magnetic-field structures in a laser-wakefield accelerator. *Phys. Rev. Lett.* **105**, 115002 (2010).
17. Buck, A. et al. Real-time observation of laser-driven electron acceleration. *Nat. Phys.* **7**, 543–548 (2011).
18. Zhang, C. J. et al. Femtosecond probing of plasma wakefields and observation of the plasma wake reversal using a relativistic electron bunch. *Phys. Rev. Lett.* **119**, 064801 (2017).
19. Altenmueller, O. H., Larsen, R. R. & Loew, G. A. Investigations of traveling-wave separators for the stanford two-mile linear accelerator. *Rev. Sci. Instrum.* **35**, 438–442 (1964).
20. Emma, P., Frisch, J. & Krejcik, P. A transverse RF deflecting structure for bunch length and phase space diagnostics. SLAC LCLS Technical Report No. LCLS–TN–00–12, SLAC, California, USA (2000).
21. Muggli, P. et al. Meter-scale plasma-wakefield accelerator driven by a matched electron beam. *Phys. Rev. Lett.* **93**, 014802 (2004).
22. Behrens, C. & Gerth, C. Measurement of the slice energy spread induced by a transverse deflecting rf structure at flash. in *Proc. DIPAC2011* (JACoW, Hamburg, Germany, 2011).
23. Clayton, C. E. et al. Self-mapping the longitudinal field structure of a nonlinear plasma accelerator cavity. *Nat. Commun.* **7**, 12483 (2016).
24. Mehrling, T. et al. Transverse emittance growth in staged laser-wakefield acceleration. *Phys. Rev. ST Accel. Beams* **15**, 111303 (2012).
25. D'Arcy, R. et al. FLASHForward: plasma wakefield accelerator science for high-average-power applications. *Phil. Trans. R. Soc. A* **377**, 20180392 (2019).
26. Ayvazyan, V. et al. First operation of a free-electron laser generating GW power radiation at 32 nm wavelength. *Eur. Phys. J. D* **37**, 297–303 (2006).
27. Schröder, S. et al. Tunable and precise two-bunch generation at FLASHForward. *J. Phys. Conf. Ser.* **1596**, 012002 (2020).
28. Lindstrøm, C. A. et al. Matching small β functions using centroid jitter and two beam position monitors. *Phys. Rev. Accel. Beams* **23**, 052802 (2020).
29. Garland, J. M. et al. Evolution of longitudinal plasma-density profiles in discharge capillaries for plasma wakefield accelerators. Preprint at http://arxiv.org/abs/2010.02567 (2020).
30. Katsouleas, T. et al. Beam loading in plasma accelerators. *Part. Accel.* **18**, 81–99 (1987).
31. Tzoufras, M. et al. Beam loading in the nonlinear regime of plasma-based acceleration. *Phys. Rev. Lett.* **101**, 145002 (2008).
32. Mehrling, T. et al. HiPACE: a quasi-static particle-in-cell code. *Plasma Phys. Control. Fusion* **56**, 84012 (2014).

Author contributions

S.S. and J.O. conceived the idea of the wakefield sampling method. S.S and C.A.L. carried out the experiments with the assistance of S.W., J.Z, P.G. and V.L., S.S. performed the data analysis with the assistance of J.O. and C.A.L., C.A.L. determined the transverse beam characteristics. S.S. performed the simulations with assistance of S.D. and M.Z. L.S., G.T. and M.J.G. set up the plasma density diagnostics with the assistance of S.B. and K.P. M.J.G. measured the longitudinal plasma density profile. G.B. developed the model for the plasma density extrapolation. S.S. and C.A.L. prepared the paper with the assistance of J.O., R.D., B.Schmidt and G.B.. C.A.L. created the equipment diagram Fig. 2. S.W., V.L., S.S., J.Z., R.D., P.N., L.S., A.K. and B.Sheeran contributed to the commissioning of the beam line. J.O., R.D. and B.Schmidt supervised the project. All authors discussed the results presented in the paper.

Competing interests

The authors declare no competing interests.

Energy-Spread Preservation and High Efficiency in a Plasma-Wakefield Accelerator

C. A. Lindstrøm[ORCID],[1,*] J. M. Garland,[1] S. Schröder[ORCID],[1,2] L. Boulton,[1,3,4] G. Boyle,[1] J. Chappell,[5] R. D'Arcy,[1] P. Gonzalez,[1,2] A. Knetsch[ORCID],[1,†] V. Libov,[1] G. Loisch[ORCID],[1] A. Martinez de la Ossa,[1] P. Niknejadi[ORCID],[1] K. Põder,[1] L. Schaper,[1] B. Schmidt,[1] B. Sheeran,[1,2] S. Wesch[ORCID],[1] J. Wood[ORCID],[1] and J. Osterhoff[1]

[1]*Deutsches Elektronen-Synchrotron DESY, Notkestraße 85, 22607 Hamburg, Germany*
[2]*Universität Hamburg, Luruper Chaussee 149, 22761 Hamburg, Germany*
[3]*SUPA, Department of Physics, University of Strathclyde, Glasgow, United Kingdom*
[4]*The Cockcroft Institute, Daresbury, United Kingdom*
[5]*University College London, London, United Kingdom*

Energy-efficient plasma-wakefield acceleration of particle bunches with low energy spread is a promising path to realizing compact free-electron lasers and particle colliders. High efficiency and low energy spread can be achieved simultaneously by strong beam loading of plasma wakefields when accelerating bunches with carefully tailored current profiles [M. Tzoufras *et al.*, Phys. Rev. Lett. **101,** 145002 (2008)]. We experimentally demonstrate such optimal beam loading in a nonlinear electron-driven plasma accelerator. Bunches with an initial energy of 1 GeV were accelerated by 45 MeV with an energy-transfer efficiency of $(42 \pm 4)\%$ at a gradient of 1.3 GV/m while preserving per-mille energy spreads with full charge coupling, demonstrating wakefield flattening at the few-percent level.

Plasma wakefields [1] driven by intense particle beams [2,3] can provide accelerating gradients in the multi-GV/m range [4–6], promising more compact accelerators for high energy physics and photon science [7–10]. Delivering bunches with low energy spread is a key requirement for realizing high-brilliance free-electron lasers [11] and high luminosity with a narrow energy spectrum in linear colliders [12]. Simultaneously, high energy-transfer efficiency is crucial for minimizing the energy consumption of such machines. The solution to both of these problems is strong beam loading, where the presence of a high-current trailing bunch changes the trajectory of in-flowing plasma-wake electrons expelled by the driver, thereby altering the longitudinal wakefield and efficiently extracting the kinetic energy of the wake [13–16]. By precisely shaping the current profile of this trailing bunch, the longitudinal wakefield can be locally flattened such that all particles experience the same accelerating gradient. Beam loading has already been experimentally demonstrated in a beam-driven plasma accelerator [17,18], resulting in high energy-transfer efficiency (up to 30%), but so far with relatively large energy spreads compared to the energy gain. To reach the sub-percent-level energy spread required for

applications, the wakefield must be shaped with a similar level of precision. Tzoufras *et al.* [19] showed that in the nonlinear regime [20,21] optimal beam loading requires the use of trailing bunches with a trapezoidal current profile, precisely tailored according to the bunch location and the strength of the wakefield. Nontrapezoidal (e.g., Gaussian) current profiles can also partially flatten the wakefield, but will result in tails in the accelerated energy spectrum.

In this Letter, we experimentally demonstrate optimal beam loading of a nonlinear plasma wakefield, resulting in simultaneous preservation of per-mille energy spreads, high energy-transfer efficiency, and full charge coupling. The optimized acceleration regime was reached by employing quasitrapezoidal trailing bunches and performing a large multidimensional scan of beam and plasma parameters. Direct measurement of field flattening within the trailing bunch was performed with a novel high-resolution wakefield-sampling technique [22]. While the energy gain was modest, preservation of the small initial energy spread implies that the wakefield was flattened at the few-percent level.

The experiment was performed at the FLASHForward plasma-accelerator facility at DESY [23]. Electron bunches were provided by the FLASH linac [24]; generated with a photoelectron gun and accelerated to 1 GeV using superconducting radio-frequency (rf) cavities. The bunches were compressed by two magnetic chicanes and linearized in longitudinal phase space by a third-harmonic cavity. Three energy collimators in a dispersive section were used for detailed shaping of the current profile [25]: low- and
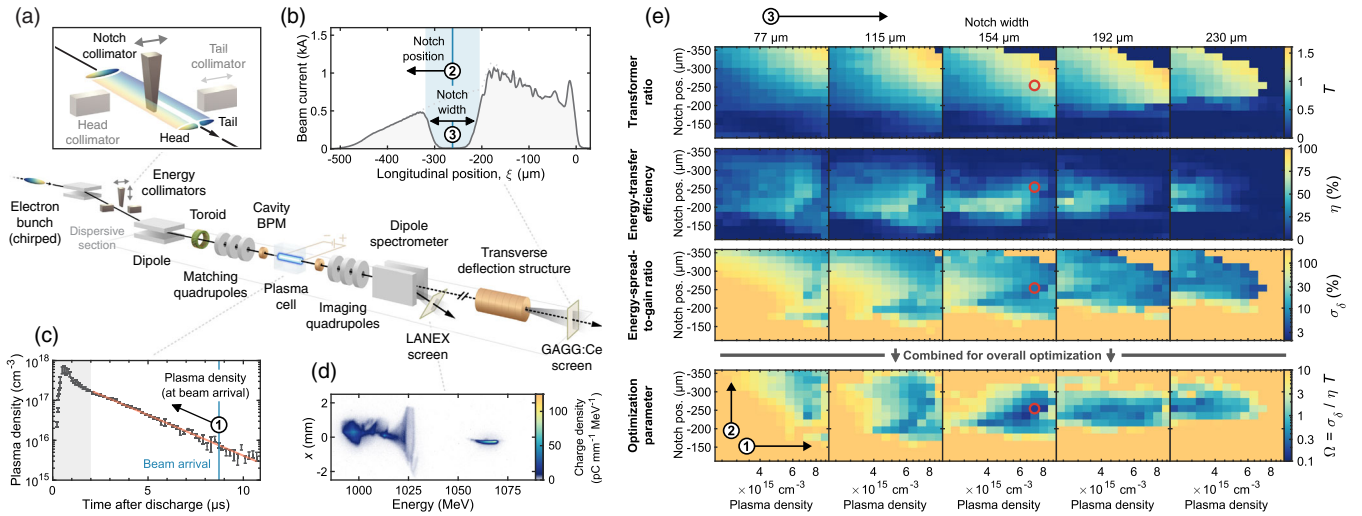
FIG. 1.   (a) A notch collimator with an adjustable width and position, located in a dispersive section, was used to create two bunches from a chirped electron bunch. (b) The resulting current profiles were measured with a downstream TDS. (c) A discharge capillary was used to form a plasma channel. The plasma density was measured to decay exponentially (orange trendline) after the initial discharge—the density was varied by adjusting the beam arrival time. Measurements shortly after the discharge (shaded area) may be inaccurate due to temperature effects [28]. (d) Energy spectra were measured with a dipole spectrometer and a set of quadrupoles for point-to-point imaging. (e) 3D parameter scan of plasma density (1) versus notch position (2) as a function of notch width (3). Each row of plots shows, from the top, measurements at each step of the transformer ratio (T), energy-transfer efficiency (η) and energy-spread-to-gain ratio (σ_δ), which were combined into an overall optimization parameter Ω [Eq. (2)]. A full characterization was performed at the optimal operating point (red circle).

high-energy collimators for removing the bunch head and tail, respectively, and a wedge-shaped notch collimator for creating a double-bunch profile with an adjustable separation [Figs. 1(a) and 1(b)]. The bunch charge was measured before and after collimation with toroidal current transformers—the uncollimated charge was (1018 ± 1) pC. A set of quadrupole magnets was used to tightly focus the electron beam at the entrance of the plasma cell. Two cavity-based beam-position monitors (BPMs) [26], placed directly upstream and downstream of the cell, were used to measure the beam trajectory. The plasma cell consisted of a discharge capillary [27] with a 50 mm-long, 1.5 mm-diameter channel milled from two blocks of sapphire, filled with argon through two gas inlets (placed 2.5 mm from the ends) at a backing pressure of 20 mbar, and discharged with short (400 ns), high-voltage (25 kV), high-current (500 A) pulses. The evolution of the plasma density at the cell center [Fig. 1(c)] was measured in an identical setup where the argon was doped with 3% hydrogen to observe spectral-line broadening of the H-alpha line [28,29]. The electron bunches were diagnosed downstream of the plasma cell with a dipole spectrometer, using five quadrupoles for point-to-point imaging of the beam from the plasma exit to a LANEX screen [Fig. 1(d)]. Further downstream, an X-band rf transverse deflection structure (TDS) [30,31] was used to streak the bunch onto a cerium-doped gadolinium aluminium gallium garnet (GAGG:Ce) screen for measurements of the current profile—the full length of the bunch was approximately 500 μm with a peak current of 1 kA.

The TDS was only operated with non-plasma-interacted bunches and relaxed beam focusing due to the complexity of transporting high-divergence bunches the full distance (33 m) from the plasma to the TDS measurement screen.

High-quality plasma acceleration requires precise control of the transverse phase space of the incoming beam. The matching quadrupoles were set to focus the beam to a waist close to the plasma entrance with a beta function [32] of approximately 10 mm in both planes. The waist location and beta function were then measured and fine-tuned with mm precision using a novel jitter-based measurement technique [33]. An object-plane scan was performed with the imaging quadrupoles, verifying the location of the waist and measuring the horizontal divergence to be (0.23 ± 0.03) mrad in the tail and up to 1 mrad in the head (higher due to coherent-synchrotron-radiation effects [34]). These measurements imply minimum beam sizes of 2–10 μm and normalized slice emittances of 1–20 mm mrad (tail to head, respectively). The vertical divergence could not be measured, but is expected to be similar to the horizontal divergence of the tail. In order to inject charge in the very back of the plasma cavity, the bunch was straightened by adjusting quadrupoles and sextupoles in the dispersive section to cancel beam tilts and curvatures, respectively [35]. A plasma density of approximately 6×10^{15} cm^{-3} was found to best match the plasma-cavity length to the full (uncollimated) bunch length.

A multidimensional scan of beam and plasma parameters was performed to locate the optimal-beam-loading

operating point. Three important parameters were identified: (1) the plasma density, adjusted by changing the beam arrival time after the discharge; (2) the longitudinal position of the current-profile notch, adjusted by transverse movements of the wedge-shaped notch collimator; and (3) the width of the notch, adjusted by vertical movements of the notch collimator. While the current profile prior to collimation remained constant, the plasma density was used to change the normalized bunch length (relative to the plasma-cavity length), and the two notch parameters were used to change the separation distance and charge ratio between the two bunches. Each parameter was scanned across the full range of values where acceleration could be observed, with a total of $5 \times 13 \times 13$ steps averaged over 15 shots per step; 12 675 shots in total.

At each step, three wakefield properties were calculated from the resulting spectra to evaluate the shape of the longitudinally averaged wakefield: the transformer ratio, the energy-transfer efficiency, and the energy-spread-to-gain ratio. The longitudinally averaged transformer ratio T is calculated as the mean energy gain of the trailing bunch normalized by the maximum energy loss within the driver [36]; the longitudinally averaged energy-transfer efficiency is calculated as

$$\eta = -\frac{\Delta\langle E\rangle_{\mathrm{acc}}Q_{\mathrm{acc}}}{\Delta\langle E\rangle_{\mathrm{dec}}Q_{\mathrm{dec}}}, \qquad (1)$$

where $\Delta\langle E\rangle$ denotes the mean energy change of each bunch, Q_{acc} is the final accelerated charge, and Q_{dec} is the average of the initial and final decelerated charge—the best estimate of the wake-driving charge in case of charge loss from the driver. Finally, the energy-spread-to-gain ratio, σ_δ, is calculated as the full width at half maximum (FWHM) of the accelerated spectrum normalized by the mean energy gain. All three properties (T, η, and σ_δ) are dimensionless and instantaneous representations of the wakefield, and therefore allow the quality of the beam-loading process to be evaluated independently of acceleration length and gradient.

Figure 1(e) shows the measurement of the three wakefield properties. This complex parameter space has multiple optima based on the desired objective: the highest transformer ratio was measured to be (1.61 ± 0.01), the highest efficiency was $(71 \pm 4)\%$ (subject to systematic errors discussed below), and the lowest energy-spread-to-gain ratio was $(3.1 \pm 0.2)\%$ FWHM, where the quoted uncertainty represents the root-mean-square (rms) variation at the optimum step. However, a useful operating point requires all properties to be simultaneously optimized. It is therefore helpful to define a new wakefield optimization parameter,

$$\Omega = \frac{\sigma_\delta}{\eta T}, \qquad (2)$$

as an overall figure of merit. Minimizing this quantity simultaneously minimizes the energy-spread-to-gain ratio

σ_δ, while maximizing the energy-transfer efficiency η and the transformer ratio T. Measurements of this optimization parameter show a distinct minimum in the parameter space. A careful characterization was performed at this optimal operating point [red circle in Fig. 1(e)], where the value of Ω was measured to be (0.077 ± 0.012)—between 1 and 2 orders of magnitude lower than in previous experiments [17,18].

Figure 2(a) shows spectrometer images and spectra for a single shot at the optimal operating point: a (490 ± 10) pC driver accelerates a 100 pC trailing bunch while preserving (and slightly dechirping [37–39]) the 0.16% FWHM initial energy spread. A small negative skewness (i.e., a low-energy tail) is introduced in the accelerated spectrum, caused by imperfections in the trailing-bunch current profile compared to the ideal shape described by Tzoufras *et al.* [19]. To ensure good energy resolution, the spectrometer was configured to form a point-to-point image for the mean energy of the trailing bunch in spectrum measurements both with and without plasma interaction.
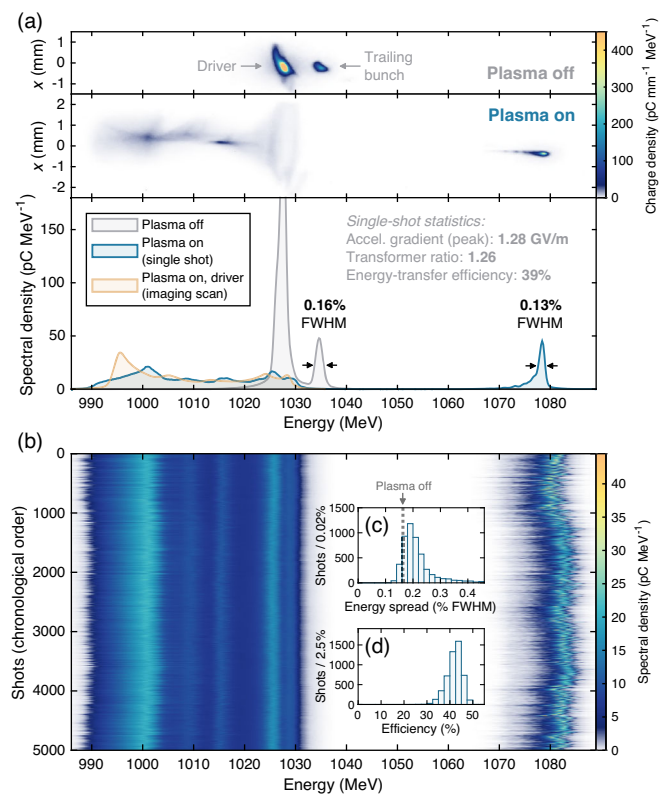
FIG. 2. (a) Spectrometer images at the optimal operating point [red circle in Fig. 1(e)], as well as the corresponding energy spectra, for shots with and without plasma interaction. The initial energy spread of the trailing bunch is preserved. (b) High stability is observed across 5000 consecutive shots—the energy gain is stable to within 3% rms. (c) In 6.4% of these shots, the energy spread is lower than or equal to the initial energy spread (dotted line). (d) Simultaneously, high energy-transfer efficiency is observed, distributed between 30% and 50%.

A 5000-shot high-statistics dataset [Fig. 2(b)] shows that the energy gain was (45.4 ± 1.4) MeV—stable to 3% rms. The energy spread was fully preserved in 6.4% of these shots [Fig. 2(c)], while the rest had a median energy spread of 0.2% FWHM (a relative increase of 28%), indicating that the optimal operating point is highly sensitive to even low-level jitters in beam or plasma parameters.

The energy-transfer efficiency at the optimal operating point was measured to be $(42 \pm 4)\%$ [Fig. 2(d)]. This measurement depends on the accuracy of the charge distribution across the full energy spectrum, which cannot be measured everywhere simultaneously with good resolution—the spectrum is distorted away from the imaging energy due to nonzero divergence and angular misalignments. Therefore, an imaging-energy scan was performed to measure the driver spectrum in 0.5% energy steps—the resulting spliced spectrum is shown in Fig. 2(a). This leads to an energy-efficiency correction of −3.6 percentage points (already accounted for in the efficiency quoted above) compared to single-shot spectra where only the accelerated bunch is imaged. This systematic effect is expected to be similar for the efficiency measurements in Fig. 1(e). Furthermore, only 94% of the initial driver charge is measured in the spectrometer. Given that the energy loss of the missing driver charge is unknown, this introduces a systematic uncertainty on the efficiency of ± 1.3 percentage points.

Energy-spread preservation is only strictly meaningful if no charge is lost. Figure 3 shows a tail-collimator scan of the trailing bunch at the optimal operating point, demonstrating that full charge coupling could be achieved with appropriate collimation of the bunch tail. When the collimator is fully extracted, only (98 ± 9) pC of the initial (176 ± 3) pC of charge is accelerated. As the tail of the trailing bunch gets progressively removed, the accelerated charge remains approximately constant until the incoming charge equals the accelerated charge—this is caused by strong defocusing of the trailing bunch as the plasma-sheath electrons return to the axis. Beyond this point, both the incoming and accelerated charge decrease identically, showing an approximately 100% charge-coupling efficiency. Note that the charge jitter decreases significantly (from 10% to 4% rms) when transitioning into the full charge-coupling regime, indicating that if the tail of the trailing bunch reaches the back of the plasma cavity, its coupling is highly sensitive to variations of the cavity length (determined by the plasma density and driver parameters).

Direct measurement of the wakefield flattening was performed using a newly developed wakefield-sampling technique (see Ref. [22] for a complete description). The measurement consisted of a tail-collimation scan of the incoming driver and trailing bunch from tail to head, observing the energy spectrum of each slice as they are removed from the overall spectrum. This scan was
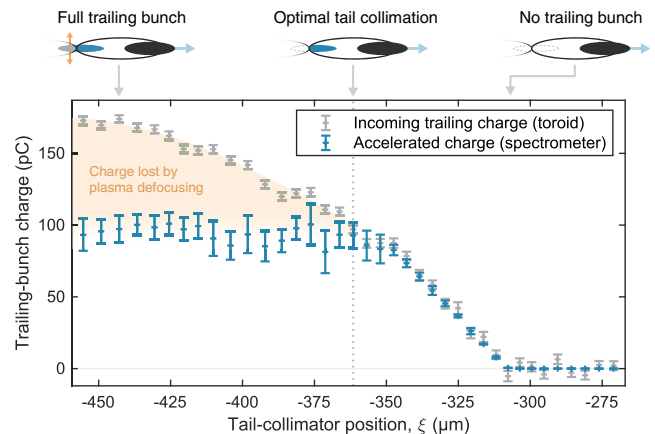

FIG. 3. Comparison of incoming trailing-bunch charge (gray points) and accelerated charge (blue points) in a tail-collimator scan. Charge is lost until position $\xi \lesssim -360$ μm, after which full charge coupling is observed. This transition is caused by the defocusing field of plasma electrons crossing the axis: beam particles behind the axis crossing are lost, whereas particles ahead remain focused. The incoming trailing charge is calculated by subtracting the mean driver charge from the total charge, as measured by a toroid, where the error bars represent the standard error of the mean. The accelerated charge is measured on the spectrometer, where the error bars represent the standard deviation. Data in Fig. 2 were taken at the optimal tail-collimator position (dotted line).

performed both with and without plasma interaction in order to calculate the energy change of each slice, and repeated at the TDS to measure the longitudinal position within the current profile of each collimator position (without plasma interaction to allow the beam to be transported). Figure 4(a) shows the measured wakefield for the optimal operating point, demonstrating that it has been locally flattened by the trailing bunch at −1.29 GV/m, with a variation of 2.8% rms across the 60 μm where the signal-to-noise ratio was sufficiently high. For comparison, a measurement was also performed for the full bunch (i.e., no notch collimator) at a slightly lower density. Calculating the longitudinally averaged wakefield from the overall energy gain requires knowledge of the plasma length. Since the longitudinal plasma density profile is not known in detail, an effective length of 34.2 mm is assumed, slightly shorter than the distance between the two gas inlets (39 mm).

Beam loading can be demonstrated indirectly by comparison of the measured wakefield with an unloaded wakefield from a particle-in-cell (PIC) simulation. For this, accurate modeling of the plasma acceleration process is required. Using longitudinal-phase-space measurements from the TDS and transverse-phase-space measurements from the spectrometer and the BPMs [33], a detailed reconstruction of the 6D beam phase space was possible. The vertical slice emittance was the only parameter that could not be measured and was assumed to be similar to the
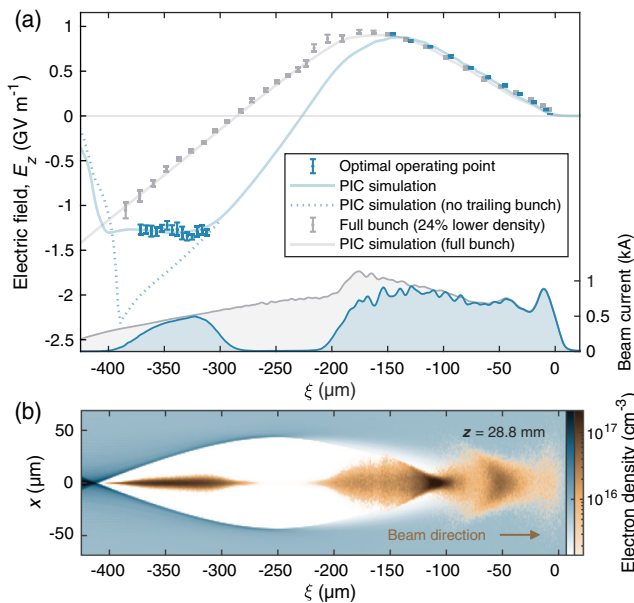
FIG. 4. (a) Longitudinally averaged wakefield measured using a tail-collimator scan, both for optimal beam loading (blue points) and for a full bunch (gray points)—in excellent agreement with PIC simulations (blue and gray solid lines). A simulation with no trailing bunch (blue dotted line) indicates that the wakefield was flattened by beam loading. The beam currents of the collimated and the full bunch (blue and gray areas) were measured with a TDS. (b) Snapshot showing cross sections of beam (orange) and plasma electron density (blue) for a simulation of the optimal operating point, on a logarithmic color scale. The simulated flat-top plasma density is 7.2×10^{15} cm^{-3}.

horizontal slice emittance of the tail. A flattop plasma density 4% lower than the measured central density [Fig. 1(c)] was found to best match the wakefield measurement, suggesting that any density ramps present had an effect small enough to justify a flat-top model. Simulations were performed with the 3D quasistatic code HiPACE [40] in a grid of $512 \times 512 \times 512$ cells, 4 plasma particles per cell in the wake region, a spatial resolution of 1.18 μm in all dimensions, 4.2×10^6 beam particles, and a time step of 5 ω_p^{-1}, where ω_p is the angular plasma frequency. The simulated longitudinally averaged wakefield is consistent with the sampling measurement for both the optimal operating point and the full bunch. Repeating the optimal-operating-point simulation without a trailing bunch clearly shows that the unloaded wakefield would not have been flat, and that strong beam loading was needed to flatten the field—consistent with the high energy-transfer efficiency observed in the measurement. Simulations indicate that while the initial energy spread would also be preserved for trailing bunches with a similar Gaussian current profile, the accelerated spectrum would have longer tails compared to the quasitrapezoidal bunches used in the experiment. The spread in wakefield amplitude across the trailing bunch (weighted by charge) was reduced by approximately 40%

(from 9.3% to 5.8% rms) as a result of this current-profile shaping.

In conclusion, we have experimentally demonstrated optimal beam loading in a plasma-wakefield accelerator. Optimization of the combined wakefield parameter Ω [Eq. (2)] resulted in simultaneous preservation of per-mille energy spreads, $(42 \pm 4)\%$ energy-transfer efficiency and full charge coupling for 100 pC bunches accelerated with high stability (3% rms) at a gradient of 1.3 GV/m—all in excellent agreement with simulations. This represents a major step towards precise and application-relevant plasma-wakefield accelerators. Reaching per-mille-level control of the wakefield will enable energy-spread preservation also for larger energy gains, which, combined with emittance preservation, can open the door to a new generation of free-electron lasers and particle colliders.

[*]Present address: LOA, ENSTA ParisTech, CNRS, Ecole Polytechnique, Université Paris-Saclay, 91762 Palaiseau, France.
[†]carl.a.lindstroem@desy.de

[1] T. Tajima and J. M. Dawson, Laser Electron Accelerator, Phys. Rev. Lett. **43**, 267 (1979).

[2] P. Chen, J. M. Dawson, R. W. Huff, and T. Katsouleas, Acceleration of Electrons by the Interaction of a Bunched Electron Beam with a Plasma, Phys. Rev. Lett. **54**, 693 (1985).

[3] R. D. Ruth, A. W. Chao, P. L. Morton, and P. B. Wilson, A plasma wake field accelerator, Part. Accel. **17**, 171 (1985).

[4] M. J. Hogan, C. D. Barnes, C. E. Clayton, F. J. Decker, S. Deng, P. Emma *et al.*, Multi-GeV Energy Gain in a Plasma-Wakefield Accelerator, Phys. Rev. Lett. **95**, 054802 (2005).

[5] I. Blumenfeld, C. E. Clayton, F.-J. Decker, M. J. Hogan, C. Huang, R. Ischebeck *et al.*, Energy doubling of 42 GeV electrons in a metre-scale plasma wakefield accelerator, Nature (London) **445**, 741 (2007).

[6] S. Corde, E. Adli, J. Allen, W. An, C. I. Clarke, B. Clausse *et al.*, High-field plasma acceleration in a high-ionization-potential gas, Nat. Commun. **7**, 11898 (2016).

[7] C. Joshi and T. Katsouleas, Plasma accelerators at the energy frontier and on tabletops, Phys. Today **56**, 6, 47 (2003).

[8] E. Adli, J.-P. Delahaye, S. J. Gessner, M. J. Hogan, T. O. Raubenheimer, W. An, C. Joshi, and W. B. Mori, A beam driven plasma-wakefield linear collider: From Higgs factory to multi-TeV, SLAC Report No. SLAC-PUB-15426, 2013.

[9] M. E. Couprie, A. Loulergue, M. Labat, R. Lehe, and V. Malka, Towards a free electron laser based on laser plasma accelerators, J. Phys. B **47,** 234001 (2014).

[10] A. R. Maier, M. Kirchen, and F. Grüner, Brilliant light sources driven by laser-plasma accelerators, *Synchrotron Light Sources and Free-Electron Lasers: Accelerator Physics, Instrumentation and Science Applications* (Springer, Cham, 2020), p. 245.

[11] J. M. J. Madey, Stimulated emission of bremsstrahlung in a periodic magnetic field, J. Appl. Phys. **42,** 1906 (1971).

[12] *The International Linear Collider Technical Design Report*, edited by T. Behnke *et al.*, Volume 1: Executive Summary (2013).

[13] S. van der Meer, Improving the power efficiency of the plasma wakefield accelerator, CLIC Note No. 3, 1985.

[14] T. Katsouleas, S. Wilks, P. Chen, J. M. Dawson, and J. J. Su, Beam loading in plasma accelerators, Part. Accel. **22,** 81 (1987).

[15] P. Chen, J. J. Su, J. M. Dawson, K. L. F. Bane, and P. B. Wilson, Energy Transfer in the Plasma Wake-Field Accelerator, Phys. Rev. Lett. **56,** 1252 (1986).

[16] K. V. Lotov, Efficient operating mode of the plasma wakefield accelerator, Phys. Plasmas **12,** 053105 (2005).

[17] M. Litos, E. Adli, W. An, C. I. Clarke, C. E. Clayton, S. Corde *et al.*, High-efficiency acceleration of an electron beam in a plasma wakefield accelerator, Nature (London) **515,** 92 (2014).

[18] M. Litos, E. Adli, J. M. Allen, W. An, C. I. Clarke, S. Corde *et al.*, 9 GeV energy gain in a beam-driven plasma wakefield accelerator, Plasma Phys. Controlled Fusion **58,** 034017 (2016).

[19] M. Tzoufras, W. Lu, F. S. Tsung, C. Huang, W. B. Mori, T. Katsouleas, J. Vieira, R. A. Fonseca, and L. O. Silva, Beam Loading in the Nonlinear Regime of Plasma-Based Acceleration, Phys. Rev. Lett. **101,** 145002 (2008).

[20] J. B. Rosenzweig, Nonlinear Plasma Dynamics in the Plasma Wake-Field Accelerator, Phys. Rev. Lett. **58,** 555 (1987).

[21] W. Lu, C. Huang, M. Zhou, W. B. Mori, and T. Katsouleas, Nonlinear Theory for Relativistic Plasma Wakefields in the Blowout Regime, Phys. Rev. Lett. **96,** 165002 (2006).

[22] S. Schröder, C. A. Lindström, G. Boyle, R. D'Arcy, S. Diedrichs, M. J. Garland *et al.*, High-resolution sampling of beam-driven plasma wakefields, Nat. Commun. **11,** 5984 (2020).

[23] R. D'Arcy, A. Aschikhin, S. Bohlen, G. Boyle, T. Brümmer, J. Chappell *et al.*, FLASHForward: Plasma wakefield accelerator science for high-average-power applications, Phil. Trans. R. Soc. A **377,** 20180392 (2019).

[24] S. Schreiber and B. Faatz, The free-electron laser FLASH, High Power Laser Sci. Eng. **3,** e20 (2015).

[25] S. Schröder, K. Ludwig, A. Aschikhin, R. D'Arcy, M. Dinter, P. Gonzalez *et al.*, Tunable and precise two-bunch generation at FLASHForward, J. Phys. Conf. Ser. **1596,** 012002 (2020).

[26] D. Lipka, Cavity BPM designs, related electronics and measured performances, *Proceedings of DIPAC'09, Basel, Switzerland, 2009* (CERN, Geneva, 2009), p. 280.

[27] D. J. Spence and S. M. Hooker, Investigation of a hydrogen plasma waveguide, Phys. Rev. E **63,** 015401(R) (2000).

[28] M. A. Gigosos, M. A. González, and V. Cardeñoso, Computer simulated Balmer-alpha, -beta and -gamma Stark line profiles for non-equilibrium plasmas diagnostics, Spectrochim. Acta B Atom. Spectros. **58,** 1489 (2003).

[29] J. M. Garland, G. Tauscher, S. Bohlen, G. J. Boyle, R. D'Arcy, L. Goldberg, K. Põder, L. Schaper, B. Schmidt, and J. Osterhoff, Evolution of longitudinal plasma-density profiles in discharge capillaries for plasma wakefield accelerators, arXiv:2010.02567.

[30] A. Grudiev, Design of compact high power RF components at X-band, CLIC Note No. 1067, 2016.

[31] R. D'Arcy, A. Aschikhin, P. Gonzalez Caminal, J. Osterhoff, and V. Libov, Longitudinal phase space reconstruction at FLASHForward using a novel X-band transverse deflection cavity (XTDC), *Proceedings of IPAC'18, Vancouver, Canada* (JACoW, Geneva, 2018), p. 1567.

[32] E. D. Courant and H. S. Snyder, Theory of the alternating-gradient synchrotron, Ann. Phys. (N.Y.) **3,** 1 (1958).

[33] C. A. Lindström, R. D'Arcy, M. J. Garland, P. Gonzalez, B. Schmidt, S. Schröder, S. Wesch, and J. Osterhoff, Matching small β functions using centroid jitter and two beam position monitors, Phys. Rev. Accel. Beams **23,** 052802 (2020).

[34] E. L. Saldin, E. A. Schneidmiller, and M. V. Yurkov, On the coherent radiation of an electron bunch moving in an arc of a circle, Nucl. Instrum. Methods Phys. Res., Sect. A **398,** 373 (1997).

[35] M. W. Guetg, B. Beutner, E. Prat, and S. Reiche, Optimization of free electron laser performance by dispersion-based beam-tilt correction, Phys. Rev. Accel. Beams **18,** 030701 (2015).

[36] G. Loisch, G. Asova, P. Boonpornprasert, R. Brinkmann, Y. Chen, J. Engel *et al.*, Observation of High Transformer Ratio Plasma Wakefield Acceleration, Phys. Rev. Lett. **121,** 064801 (2018).

[37] R. D'Arcy, S. Wesch, A. Aschikhin, S. Bohlen, C. Behrens, M. J. Garland *et al.*, Tunable Plasma-Based Energy Dechirper, Phys. Rev. Lett. **122,** 034801 (2019).

[38] V. Shpakov, M. P. Anania, M. Bellaveglia, A. Biagioni, F. Bisesto, F. Cardelli *et al.*, Longitudinal Phase-Space Manipulation with Beam-Driven Plasma Wakefields, Phys. Rev. Lett. **122,** 114801 (2019).

[39] Y. P. Wu, J. F. Hua, Z. Zhou, J. Zhang, S. Liu, B. Peng *et al.*, Phase Space Dynamics of a Plasma Wakefield Dechirper for Energy Spread Reduction, Phys. Rev. Lett. **122,** 204804 (2019).

[40] T. Mehrling, C. Benedetti, C. B. Schroeder, and J. Osterhoff, HiPACE: a quasi-static particle-in-cell code, Plasma Phys. Controlled Fusion **56,** 084012 (2014).

Bibliography

[1] S. Schröder, C. A. Lindstrøm, S. Bohlen, G. Boyle, R. D'Arcy, S. Diederichs, M. J. Garland, P. Gonzalez, A. Knetsch, V. Libov, P. Niknejadi, K. Põder, L. Schaper, B. Schmidt, B. Sheeran, G. Tauscher, S. Wesch, J. Zemella, M. Zeng, and J. Osterhoff, 'High-resolution sampling of beam-driven plasma wakefields', Nature Communications **11**, 5984 (2020) (cit. on pp. 27, 43, 54, 55, 58, 61).

[2] S. Schröder, K. Ludwig, A. Aschikhin, R. D'Arcy, M. Dinter, P. Gonzalez, S. Karstensen, A. Knetsch, V. Libov, C. A. Lindstrøm, F. Marutzky, P. Niknejadi, A. Rahali, L. Schaper, A. Schleiermacher, B. Schmidt, S. Thiele, A. d. Z. Wagner, S. Wesch, and J. Osterhoff, 'Tunable and precise two-bunch generation at FLASHForward', Journal of Physics: Conference Series **1596**, 012002 (2020) (cit. on pp. 27, 29, 36, 43, 47–49, 58, 61).

[3] C. A. Lindstrøm, R. D'Arcy, M. J. Garland, P. Gonzalez, B. Schmidt, S. Schröder, S. Wesch, and J. Osterhoff, 'Matching small β functions using centroid jitter and two beam position monitors', Physical Review Accelerators and Beams **23**, 52802 (2020) (cit. on pp. 26, 36, 43, 46, 58, 61).

[4] C. A. Lindstrøm, J. M. Garland, S. Schröder, L. Boulton, G. Boyle, J. Chappell, R. D'Arcy, P. Gonzalez, A. Knetsch, V. Libov, G. Loisch, A. Martinez de la Ossa, P. Niknejadi, K. Põder, L. Schaper, B. Schmidt, B. Sheeran, S. Wesch, J. Wood, and J. Osterhoff, 'Energy-spread preservation and high efficiency in a plasma-wakefield accelerator', Physical Review Letters **126**, 014801 (2021) (cit. on pp. 27, 43, 50, 51, 56, 58, 61).

[5] R. D. Arcy, S. Wesch, A. Aschikhin, S. Bohlen, C. Behrens, M. J. Garland, L. Goldberg, P. Gonzalez, A. Knetsch, V. Libov, A. M. D. Ossa, M. Meisel, T. J. Mehrling, P. Niknejadi, K. Poder, J.-H. H. Röckemann, L. Schaper, B. Schmidt, S. Schröder, C. Palmer, J.-P. P. Schwinkendorf, B. Sheeran, M. J. V. Streeter, G. Tauscher, V. Wacker, and J. Osterhoff, 'Tunable Plasma-Based Energy Dechirper', Physical Review Letters **122**, 34801 (2019) (cit. on pp. 27, 43, 52, 53, 61).

[6] F. Braun, 'Über ein Verfahren zur Demonstration und zum Studium des zeitlichen Verlaufes variabler Ströme', Annalen der Physik und Chemie **296**, 552–559 (1897) (cit. on p. 1).

[7] J. Thomson, 'Cathode Rays', The London, Edinburgh, and Dublin Philosophical Magazine and Journal of Science **44**, 293–316 (1897) (cit. on p. 1).

[8] J. Thomson, 'On the structure of the atom: an investigation of the stability and periods of oscillation of a number of corpuscles arranged at equal intervals around the circumference of a circle; with application of the results to the theory of atomic structure', The London,

Edinburgh, and Dublin Philosophical Magazine and Journal of Science **7**, 237–265 (1904) (cit. on p. 1).

[9]E. Rutherford, 'The scattering of α and β particles by matter and the structure of the atom', The London, Edinburgh, and Dublin Philosophical Magazine and Journal of Science **21**, 669–688 (1911) (cit. on p. 1).

[10]N. Bohr, 'On the constitution of atoms and molecules', The London, Edinburgh, and Dublin Philosophical Magazine and Journal of Science **26**, 1–25 (1913) (cit. on p. 1).

[11]S. Weinberg, 'A Model of Leptons', Physical Review Letters **19**, 1264–1266 (1967) (cit. on p. 1).

[12]G. Aad et al., 'Observation of a new particle in the search for the Standard Model Higgs boson with the ATLAS detector at the LHC', Physics Letters, Section B: Nuclear, Elementary Particle and High-Energy Physics **716**, 1–29 (2012) (cit. on p. 1).

[13]S. Chatrchyan et al., 'Observation of a new boson at a mass of 125 GeV with the CMS experiment at the LHC', Physics Letters, Section B: Nuclear, Elementary Particle and High-Energy Physics **716**, 30–61 (2012) (cit. on p. 1).

[14]F. Englert and R. Brout, 'Broken symmetry and the mass of gauge vector mesons', Physical Review Letters **13**, 321–323 (1964) (cit. on p. 1).

[15]P. W. Higgs, 'Broken symmetries and the masses of gauge bosons', Physical Review Letters **13**, 508–509 (1964) (cit. on p. 1).

[16]L. Evans and P. Bryant, 'LHC Machine', Journal of Instrumentation **3**, 8001 (2008) (cit. on p. 1).

[17]V. Shiltsev, 'High-energy particle colliders: past 20 years, next 20 years, and beyond', Physics-Uspekhi **55**, 965–976 (2012) (cit. on p. 1).

[18]*2020 update of the european strategy for particle physics* (2020) (cit. on pp. 1, 2, 12).

[19]D. Iwanenko and I. Pomeranchuk, 'On the Maximal Energy Attainable in a Betatron', Physical Review **65**, 343–343 (1944) (cit. on p. 1).

[20]F. R. Elder, A. M. Gurewitsch, R. V. Langmuir, and H. C. Pollock, 'Radiation from Electrons in a Synchrotron', Physical Review **71**, 829–830 (1947) (cit. on p. 1).

[21]J. M. Madey, 'Stimulated emission of bremsstrahlung in a periodic magnetic field', Journal of Applied Physics **42**, 1906–1913 (1971) (cit. on p. 1).

[22]P. G. O'Shea, 'Free-Electron Lasers: Status and Applications', Science **292**, 1853–1858 (2001) (cit. on p. 1).

[23]S. Grundmann, D. Trabert, K. Fehre, N. Strenger, A. Pier, L. Kaiser, M. Kircher, M. Weller, S. Eckart, L. P. H. Schmidt, F. Trinter, T. Jahnke, M. S. Schöffler, and R. Dörner, 'Zeptosecond birth time delay in molecular photoionization', Science **370**, 339–341 (2020) (cit. on p. 1).

[24]R. Neutze, R. Wouts, D. van der Spoel, E. Weckert, and J. Hajdu, 'Potential for biomolecular imaging with femtosecond X-ray pulses', Nature **406**, 752–757 (2000) (cit. on p. 1).

[25] H. N. Chapman, P. Fromme, A. Barty, T. A. White, R. A. Kirian, A. Aquila, M. S. Hunter, J. Schulz, D. P. Deponte, U. Weierstall, R. B. Doak, F. R. Maia, A. V. Martin, I. Schlichting, L. Lomb, N. Coppola, R. L. Shoeman, S. W. Epp, R. Hartmann, D. Rolles, A. Rudenko, L. Foucar, N. Kimmel, G. Weidenspointner, P. Holl, M. Liang, M. Barthelmess, C. Caleman, S. Boutet, M. J. Bogan, J. Krzywinski, C. Bostedt, S. Bajt, L. Gumprecht, B. Rudek, B. Erk, C. Schmidt, A. Hömke, C. Reich, D. Pietschner, L. Ströder, G. Hauser, H. Gorke, J. Ullrich, S. Herrmann, G. Schaller, F. Schopper, H. Soltau, K. U. Kühnel, M. Messerschmidt, J. D. Bozek, S. P. Hau-Riege, M. Frank, C. Y. Hampton, R. G. Sierra, D. Starodub, G. J. Williams, J. Hajdu, N. Timneanu, M. M. Seibert, J. Andreasson, A. Rocker, O. Jönsson, M. Svenda, S. Stern, K. Nass, R. Andritschke, C. D. Schröter, F. Krasniqi, M. Bott, K. E. Schmidt, X. Wang, I. Grotjohann, J. M. Holton, T. R. Barends, R. Neutze, S. Marchesini, R. Fromme, S. Schorb, D. Rupp, M. Adolph, T. Gorkhover, I. Andersson, H. Hirsemann, G. Potdevin, H. Graafsma, B. Nilsson, and J. C. Spence, 'Femtosecond X-ray protein nanocrystallography', Nature **470**, 73–78 (2011) (cit. on p. 1).

[26] T. Kierspel, A. Morgan, J. Wiese, T. Mullins, A. Aquila, A. Barty, R. Bean, R. Boll, S. Boutet, P. Bucksbaum, H. N. Chapman, L. Christensen, A. Fry, M. Hunter, J. E. Koglin, M. Liang, V. Mariani, A. Natan, J. Robinson, D. Rolles, A. Rudenko, K. Schnorr, H. Stapelfeldt, S. Stern, J. Thøgersen, C. H. Yoon, F. Wang, and J. Küpper, 'X-ray diffractive imaging of controlled gas-phase molecules: Toward imaging of dynamics in the molecular frame', Journal of Chemical Physics **152** (2020) (cit. on p. 1).

[27] E. F. Haussecker and A. W. Chao, 'The influence of accelerator science on physics research', Physics in Perspective **13**, 146–160 (2011) (cit. on p. 1).

[28] V. Shiltsev, 'Particle beams behind physics discoveries', Physics Today **73**, 32–39 (2020) (cit. on pp. 2, 11).

[29] O. Barbalat, *Applications of particle accelerators*, tech. rep. (CERN, 1994) (cit. on p. 2).

[30] R. W. Hamm and M. E. Hamm, 'The beam business: Accelerators in industry', Physics Today **64**, 46–51 (2011) (cit. on p. 2).

[31] V. I. Veksler, 'Coherent principle of acceleration of charged particles', in Cern symposium on high energy accelerators and pion physics (1956), pp. 80–83 (cit. on pp. 2, 14, 25).

[32] G. J. Budker, 'Relativistic stabilized electron beam', The Soviet Journal of Atomic Energy **1**, 673–686 (1965) (cit. on pp. 2, 14, 25).

[33] T. Tajima and J. M. Dawson, 'Laser Electron Accelerator', Physical Review Letters **43**, 267–270 (1979) (cit. on pp. 2, 14, 25).

[34] J. B. Rosenzweig, D. B. Cline, B. Cole, H. Figueroa, W. Gai, R. Konecny, J. Norem, P. Schoessow, and J. Simpson, 'Experimental Observation of Plasma Wake-Field Acceleration', Physical Review Letters **61**, 98–101 (1988) (cit. on pp. 2, 25).

[35] C. Clayton, K. A. Marsh, A. Dyson, M. Everett, A. Lal, W. P. Leemans, R. Williams, C. Joshi, R. Williams, and C. Joshi, 'Ultrahigh-gradient acceleration of injected electrons by laser-excited relativistic electron plasma waves', Physical Review Letters **70**, 37–40 (1993) (cit. on pp. 2, 25).

[36] M. J. Hogan, C. D. Barnes, C. E. Clayton, F. J. Decker, S. Deng, P. Emma, C. Huang, R. H. Iverson, D. K. Johnson, C. Joshi, T. C. Katsouleas, P. Krejcik, W. Lu, K. A. Marsh, W. B. Mori, P. Muggli, C. L. O'connell, E. Oz, R. H. Siemann, D. Walz, C. L. O'Connell, E. Oz, R. H. Siemann, and D. Walz, 'Multi-GeV Energy Gain in a Plasma-Wakefield Accelerator', Physical Review Letters **95**, 054802 (2005) (cit. on pp. 2, 26).

[37] I. Blumenfeld, C. Clayton, F.-J. J. F. Decker, M. J. M. Hogan, C. Huang, R. Ischebeck, R. Iverson, C. Joshi, T. C. Katsouleas, N. Kirby, W. Lu, K. K. A. Marsh, W. B. Mori, P. Muggli, E. Oz, R. H. R. Siemann, D. Walz, and M. Zhou, 'Energy doubling of 42 GeV electrons in a metre-scale plasma wakefield accelerator', Nature **445**, 741–744 (2007) (cit. on pp. 2, 26).

[38] M. Litos, E. Adli, W. An, C. I. Clarke, C. Clayton, S. Corde, J. P. Delahaye, R. J. England, A. S. Fisher, J. Frederico, S. J. Gessner, S. Z. Green, M. J. Hogan, C. Joshi, W. Lu, K. A. Marsh, W. B. Mori, P. Muggli, N. Vafaei-Najafabadi, D. Walz, G. White, Z. Wu, V. E. Yakimenko, and G. Yocky, 'High-efficiency acceleration of an electron beam in a plasma wakefield accelerator', Nature **515**, 92–95 (2014) (cit. on pp. 2, 26).

[39] M. Litos, E. Adli, J. M. Allen, W. An, C. I. Clarke, S. Corde, C. Clayton, J. Frederico, S. J. Gessner, S. Z. Green, M. J. Hogan, C. Joshi, W. Lu, K. A. Marsh, W. B. Mori, M. Schmeltz, N. Vafaei-Najafabadi, and V. E. Yakimenko, '9 GeV energy gain in a beam-driven plasma wakefield accelerator', Plasma Physics and Controlled Fusion **58**, 34017 (2016) (cit. on pp. 2, 26).

[40] K. Wille, *The Physics of Particle accelerators - an introduction* (Clarendon Press, 2000) (cit. on pp. 3, 7).

[41] H. Wiedemann, *Particle Accelerator Physics*, Graduate Texts in Physics (Springer International Publishing, 2015) (cit. on pp. 3, 7).

[42] D. A. Edwards and M. J. Syphers, *An Introduction to the Physics of High Energy Accelerators* (Wiley, 1993) (cit. on p. 3).

[43] E. Esarey, C. B. Schroeder, and W. P. Leemans, 'Physics of laser-driven plasma-based electron accelerators', Reviews of Modern Physics **81**, 1229–1285 (2009) (cit. on pp. 3, 15).

[44] C. Joshi, S. Corde, and W. B. Mori, 'Perspectives on the generation of electron beams from plasma-based accelerators and their near and long term applications', Physics of Plasmas **27**, 070602 (2020) (cit. on pp. 3, 25).

[45] A. Antognini, F. Nez, K. Schuhmann, F. D. Amaro, F. Biraben, J. M. R. Cardoso, D. S. Covita, A. Dax, S. Dhawan, M. Diepold, L. M. P. Fernandes, A. Giesen, A. L. Gouvea, T. Graf, T. W. Hansch, P. Indelicato, L. Julien, C.-Y. Kao, P. Knowles, F. Kottmann, E.-O. Le Bigot, Y.-W. Liu, J. A. M. Lopes, L. Ludhova, C. M. B. Monteiro, F. Mulhauser, T. Nebel, P. Rabinowitz, J. M. F. dos Santos, L. A. Schaller, C. Schwob, D. Taqqu, J. F. C. A. Veloso, J. Vogelsang, and R. Pohl, 'Proton Structure from the Measurement of 2S-2P Transition Frequencies of Muonic Hydrogen', Science **339**, 417–420 (2013) (cit. on p. 3).

[46] H. A. Kramers, 'On the theory of X-ray absorption and of the continuous X-ray spectrum', The London, Edinburgh, and Dublin Philosophical Magazine and Journal of Science **46**, 836–871 (1923) (cit. on p. 3).

[47]L. de Broglie, 'The reinterpretation of wave mechanics', Foundations of Physics **1**, 5–15 (1970) (cit. on p. 4).

[48]A. Einstein, 'Ist die Trägheit eines Körpers von seinem Energieinhalt abhängig?', Annalen der Physik **323**, 639–641 (1905) (cit. on p. 4).

[49]A. Einstein, 'Über die vom Relativitätsprinzip geforderte Trägheit der Energie', Annalen der Physik **328**, 371–384 (1907) (cit. on p. 4).

[50]J. Clerk Maxwell, 'A dynamical theory of the electromagnetic field', Philosophical Transactions of the Royal Society of London **155**, 459–512 (1865) (cit. on p. 4).

[51]O. Heaviside, 'On the electromagnetic effects due to the motion of electrification through a dielectric', The London, Edinburgh, and Dublin Philosophical Magazine and Journal of Science **27**, 324–339 (1889) (cit. on p. 5).

[52]H. A. Lorentz, 'Versuch Einer Theorie der Electrischen und Optischen Erscheinungen in Bewegten Körpern', in *Collected papers* (Springer Netherlands, Dordrecht, 1937), pp. 1–138 (cit. on p. 5).

[53]W. K. H. Panofsky and W. A. Wenzel, 'Some considerations concerning the transverse deflection of charged particles in radio-frequency fields', Review of Scientific Instruments **27**, 967 (1956) (cit. on p. 5).

[54]J.-A. Serret, 'Sur quelques formules relatives à la théorie des courbes à double courbure.', Journal de Mathématiques Pures et Appliquées, 193–207 (1851) (cit. on p. 6).

[55]F. Frenet, 'Sur les courbes à double courbure.', Journal de Mathématiques Pures et Appliquées, 437–447 (1852) (cit. on p. 6).

[56]S. Wesch, 'Echtzeitbestimmung longitudinaler Elektronenstrahlparameter mittels absoluter Intensitäts- und Spektralmessung einzelner kohärenter THz Strahlungspulse', PhD thesis (2012) (cit. on p. 8).

[57]E. Courant and H. Snyder, 'Theory of the alternating-gradient synchrotron', Annals of Physics **3**, 1–48 (1958) (cit. on p. 9).

[58]T. P. Wangler, *RF Linear Accelerators* (Wiley, 2008) (cit. on p. 10).

[59]D. Schulte, 'Application of advanced accelerator concepts for colliders', Reviews of Accelerator Science and Technology **9**, 209–233 (2017) (cit. on p. 10).

[60]F. Amman and D. Ritson, 'Space-charge effects in electron-electron and positron-electron colliding or crossing beam rings', in 3rd international conference on high-energy accelerators (1961), pp. 471–475 (cit. on p. 10).

[61]A. W. Chao, *2001 Snowmass Accelerator R and D Report*, tech. rep. (SLAC National Accelerator Laboratory (SLAC), Menlo Park, CA (United States), 2002) (cit. on p. 12).

[62]H. Greinacher, 'Über eine Methode, Wechselstrom mittels elektrischer Ventile und Kondensatoren in hochgespannten Gleichstrom umzuwandeln', Zeitschrift für Physik **4**, 195–205 (1921) (cit. on p. 12).

[63]R. J. Van de Graaff, K. T. Compton, and L. C. Van Atta, 'The Electrostatic Production of High Voltage for Nuclear Investigations', Physical Review **43**, 149–157 (1933) (cit. on p. 12).

[64] B. Aune, R. Bandelmann, D. Bloess, B. Bonin, A. Bosotti, M. Champion, C. Crawford, G. Deppe, B. Dwersteg, D. A. Edwards, H. T. Edwards, M. Ferrario, M. Fouaidy, P. D. Gall, A. Gamp, A. Gössel, J. Graber, D. Hubert, M. Hüning, M. Juillard, T. Junquera, H. Kaiser, G. Kreps, M. Kuchnir, R. Lange, M. Leenen, M. Liepe, L. Lilje, A. Matheisen, W. D. Möller, A. Mosnier, H. Padamsee, C. Pagani, M. Pekeler, H. B. Peters, O. Peters, D. Proch, K. Rehlich, D. Reschke, H. Safa, T. Schilcher, P. Schmüser, J. Sekutowicz, S. Simrock, W. Singer, M. Tigner, D. Trines, K. Twarowski, G. Weichert, J. Weisend, J. Wojtkiewicz, S. Wolff, and K. Zapfe, 'Superconducting TESLA cavities', Physical Review Special Topics - Accelerators and Beams **3**, 21–45 (2000) (cit. on p. 12).

[65] D. Reschke, V. Gubarev, J. Schaffran, L. Steder, N. Walker, M. Wenskat, and L. Monaco, 'Performance in the vertical test of the 832 nine-cell 1.3 GHz cavities for the European X-ray Free Electron Laser PERFORMANCE in the VERTICAL TEST D. RESCHKE et al.', Physical Review Accelerators and Beams **20**, 042004 (2017) (cit. on p. 12).

[66] T. Behnke, J. E. Brau, B. Foster, J. Fuster, M. Harrison, J. M. Paterson, M. Peskin, M. Stanitzki, N. Walker, and H. Yamamoto, 'The International Linear Collider Technical Design Report - Volume 1: Executive Summary', (2013) (cit. on p. 12).

[67] CLIC collaboration, 'A Multi-TeV Linear Collider Based on CLIC Technology : CLIC Conceptual Design Report', CERN, Geneva, Switzerland, Rep. CERN-2012-007 (2012) (cit. on p. 12).

[68] A. Grassellino, A. Romanenko, D. Sergatskov, O. Melnychuk, Y. Trenikhina, A. Crawford, A. Rowe, M. Wong, T. Khabiboulline, and F. Barkov, 'Nitrogen and argon doping of niobium for superconducting radio frequency cavities: A pathway to highly efficient accelerating structures', Superconductor Science and Technology (2013) (cit. on p. 13).

[69] A. Grassellino, A. Romanenko, Y. Trenikhina, M. Checchin, M. Martinello, O. S. Melnychuk, S. Chandrasekaran, D. A. Sergatskov, S. Posen, A. C. Crawford, S. Aderhold, and D. Bice, 'Unprecedented quality factors at accelerating gradients up to 45 MVm-1 in niobium superconducting resonators via low temperature nitrogen infusion', Superconductor Science and Technology **30**, 094004 (2017) (cit. on p. 13).

[70] S. Posen, A. Romanenko, A. Grassellino, O. S. Melnychuk, and D. A. Sergatskov, 'Ultralow Surface Resistance via Vacuum Heat Treatment of Superconducting Radio-Frequency Cavities', Physical Review Applied **13**, 14024 (2020) (cit. on p. 13).

[71] A. Gurevich, 'Enhancement of rf breakdown field of superconductors by multilayer coating', Applied Physics Letters **88**, 012511 (2006) (cit. on p. 13).

[72] 'IEEE Standard Letter Designations for Radar-Frequency Bands', IEEE Std 521-2019 (Revision of IEEE Std 521-2002), 1–15 (2020) (cit. on p. 13).

[73] T. Argyropoulos, N. Catalan-Lasheras, A. Grudiev, G. Mcmonagle, E. Rodriguez-Castro, I. Syrachev, R. Wegner, B. Woolley, W. Wuensch, H. Zha, V. Dolgashev, G. Bowden, A. Haase, T. G. Lucas, M. Volpi, D. Esperante-Pereira, and R. Rajamäki, 'Design, fabrication, and high-gradient testing of an X-band, traveling-wave accelerating structure milled from copper halves', Physical Review Accelerators and Beams **21**, 061001 (2018) (cit. on p. 13).

[74]R. J. England, R. J. Noble, K. Bane, D. H. Dowell, C.-K. Ng, J. E. Spencer, S. Tantawi, Z. Wu, R. L. Byer, E. Peralta, K. Soong, C.-M. Chang, B. Montazeri, S. J. Wolf, B. Cowan, J. Dawson, W. Gai, P. Hommelhoff, Y.-C. Huang, C. Jing, C. McGuinness, R. B. Palmer, B. Naranjo, J. Rosenzweig, G. Travish, A. Mizrahi, L. Schachter, C. Sears, G. R. Werner, and R. B. Yoder, 'Dielectric laser accelerators', Reviews of Modern Physics **86**, 1337–1389 (2014) (cit. on p. 13).

[75]S. Corde, E. Adli, J. M. Allen, W. An, C. I. Clarke, B. Clausse, C. E. Clayton, J. P. Delahaye, J. Frederico, S. Gessner, S. Z. Green, M. J. Hogan, C. Joshi, M. Litos, W. Lu, K. A. Marsh, W. B. Mori, N. Vafaei-Najafabadi, D. Walz, and V. Yakimenko, 'High-field plasma acceleration in a high-ionization-potential gas', Nature Communications **7**, 11898 (2016) (cit. on p. 13).

[76]J.-L. Delcroix and A. Bers, *Physique des plasmas* (1994) (cit. on p. 13).

[77]A. Bers, *Plasma Physics and Fusion Plasma Electrodynamics*, Vol. 1 (2016), p. 14 (cit. on p. 14).

[78]L. Rayleigh, 'On electrical vibrations and the constitution of the atom', The London, Edinburgh, and Dublin Philosophical Magazine and Journal of Science **11**, 117–123 (1906) (cit. on p. 14).

[79]L. Tonks and I. Langmuir, 'Oscillations in ionized gases', Physical Review **33**, 195–210 (1929) (cit. on p. 14).

[80]F. M. Penning, 'Scattering of Electrons in Ionised Gases', Nature **118**, 301–301 (1926) (cit. on p. 14).

[81]J. M. Dawson, 'One-dimensional plasma model', Phys. Fluids **5**, 445–459 (1962) (cit. on pp. 15, 25).

[82]M. J. Hogan, 'Electron and positron beam-driven plasma acceleration', Reviews of Accelerator Science and Technology **9**, 63–83 (2017) (cit. on p. 15).

[83]A. G. R. Thomas, 'Acceleration of Electrons in Plasma', CAS - CERN Accelerator School **4**, 7–13 (2020) (cit. on p. 15).

[84]P. Chen and J. M. Dawson, 'The plasma wake field accelerator', in Aip conference proceedings, Vol. 130, June (1985), pp. 201–212 (cit. on pp. 16, 24).

[85]T. C. Katsouleas, S. Wilks, P. Chen, J. M. Dawson, and J. J. Su, 'Beam loading in plasma accelerators', Particle Accelerators **22**, 81–99 (1987) (cit. on pp. 16, 21, 22).

[86]R. Keinigs and M. E. Jones, 'Two-dimensional dynamics of the plasma wakefield accelerator', Phys. Fluids **30**, 252 (1987) (cit. on p. 16).

[87]P. Sprangle, E. Esarey, and A. Ting, 'Nonlinear theory of intense laser-plasma interactions', Physical Review Letters **64**, 2011–2014 (1990) (cit. on p. 16).

[88]W. Lu, C. Huang, M. M. Zhou, W. B. Mori, and T. C. Katsouleas, 'Limits of linear plasma wakefield theory for electron or positron beams', Phys. Plasmas **12**, 1–8 (2005) (cit. on p. 17).

[89]J. M. Dawson, 'Nonlinear Electron Oscillations in a Cold Plasma', Physical Review **113**, 383–387 (1959) (cit. on p. 17).

[90] J. Vieira, R. A. Fonseca, and L. O. Silva, 'Multidimensional Plasma Wake Excitation in the Non-linear Blowout Regime', CAS - CERN Accelerator School **001**, 23–29 (2016) (cit. on p. 17).

[91] J. Albritton and P. Koch, 'Cold plasma wavebreaking: Production of energetic electrons', Phys. Fluids **18**, 1136–1139 (1975) (cit. on p. 17).

[92] A. Akhiezer and R. Polovin, 'Theory of Wave Motion of an Electron Plasma', Soviet Phys. JETP **Vol: 3**, 696–705 (1956) (cit. on p. 18).

[93] W. Lu, C. Huang, M. Zhou, M. Tzoufras, F. S. Tsung, W. B. Mori, and T. C. Katsouleas, 'A nonlinear theory for multidimensional relativistic plasma wave wakefields', Phys. Plasmas **13** (2006) (cit. on p. 18).

[94] W. Lu, C. Huang, M. Zhou, W. B. Mori, and T. C. Katsouleas, 'Nonlinear theory for relativistic plasma wakefields in the blowout regime', Physical Review Letters **96**, 165002 (2006) (cit. on p. 18).

[95] J. B. Rosenzweig, 'Nonlinear plasma dynamics in the plasma wake-field accelerator', Physical Review Letters **58**, 555–558 (1987) (cit. on pp. 19, 25).

[96] J. B. Rosenzweig, B. Breizman, T. Katsouleas, and J. J. Su, 'Acceleration and focusing of electrons in two-dimensional nonlinear plasma wake fields', Physical Review A **44**, R6189–R6192 (1991) (cit. on pp. 19, 21, 25).

[97] C. L. O'Connell, F. J. Decker, M. J. Hogan, R. Iverson, P. Raimondi, R. H. Siemann, D. Walz, B. Blue, C. Clayton, C. Joshi, K. A. Marsh, W. B. Mori, S. Wang, T. C. Katsouleas, S. Lee, and P. Muggli, 'Dynamic focusing of an electron beam through a long plasma', Physical Review Special Topics - Accelerators and Beams **5**, 17–24 (2002) (cit. on pp. 19, 26).

[98] I. Blumenfeld, C. E. Clayton, F. J. Decker, M. J. Hogan, C. Huang, R. Ischebeck, R. H. Iverson, C. Joshi, T. Katsouleas, N. Kirby, W. Lu, K. A. Marsh, W. B. Mori, P. Muggli, E. Oz, R. H. Siemann, D. R. Walz, and M. Zhou, 'Scaling of the longitudinal electric field and transformer ratio in a nonlinear plasma wakefield accelerator', Physical Review Special Topics - Accelerators and Beams **13**, 111301 (2010) (cit. on pp. 19, 26).

[99] W. An, M. Zhou, N. Vafaei-Najafabadi, K. A. Marsh, C. E. Clayton, C. Joshi, W. B. Mori, W. Lu, E. Adli, S. Corde, M. Litos, S. Li, S. J. Gessner, J. Frederico, M. J. Hogan, D. Walz, J. England, J. P. Delahaye, and P. Muggli, 'Strategies for mitigating the ionization-induced beam head erosion problem in an electron-beam-driven plasma wakefield accelerator', Physical Review Special Topics - Accelerators and Beams **16**, 1–8 (2013) (cit. on p. 19).

[100] C. A. Lindstrøm, 'Staging of plasma-wakefield accelerators', Physical Review Accelerators and Beams **24**, 014801 (2021) (cit. on p. 19).

[101] M. F. Gilljohann, H. Ding, A. Döpp, J. Götzfried, S. Schindler, G. Schilling, S. Corde, A. Debus, T. Heinemann, B. Hidding, S. M. Hooker, A. Irman, O. Kononenko, T. Kurz, A. Martinez De La Ossa, U. Schramm, and S. Karsch, 'Direct Observation of Plasma Waves and Dynamics Induced by Laser-Accelerated Electron Beams', Physical Review X **9**, 11046 (2019) (cit. on p. 20).

[102] A. G. Khachatryan, A. Irman, F. A. van Goor, and K.-J. Boller, 'Femtosecond electron-bunch dynamics in laser wakefields and vacuum', Physical Review Special Topics - Accelerators and Beams **10**, 121301 (2007) (cit. on p. 21).

[103]T. Mehrling, J. Grebenyuk, F. S. Tsung, K. Floettmann, and J. Osterhoff, 'Transverse emittance growth in staged laser-wakefield acceleration', Phys. Rev. ST Accel. Beams **15**, 1–7 (2012) (cit. on p. 21).

[104]N. Barov and J. B. Rosenzweig, 'Propagation of short electron pulses in underdense plasmas', Physical Review E **49**, 4407–4416 (1994) (cit. on p. 21).

[105]K. Marsh, C. Clayton, D. Johnson, C. Huang, C. Joshi, W. Lu, W. Mori, M. Zhou, C. Barnes, F.-J. Decker, M. Hogan, R. Iverson, P. Krejcik, C. O'Connell, R. Siemann, D. Walz, S. Deng, T. Katsouleas, P. Muggli, and E. Oz, 'Beam Matching to a Plasma Wake Field Accelerator using a Ramped Density Profile at the Plasma Boundary', Proceedings of the 2005 Particle Accelerator Conference, 2702–2704 (2005) (cit. on p. 21).

[106]I. Dornmair, K. Floettmann, and A. R. Maier, 'Emittance conservation by tailored focusing profiles in a plasma accelerator', Physical Review Special Topics - Accelerators and Beams **18**, 041302 (2015) (cit. on p. 21).

[107]R. Ariniello, C. E. Doss, K. Hunt-Stone, J. R. Cary, and M. Litos, 'Transverse beam dynamics in a plasma density ramp', Physical Review Accelerators and Beams **22**, 41304 (2019) (cit. on p. 21).

[108]Y. Zhao, W. An, X. Xu, F. Li, L. Hildebrand, M. J. Hogan, V. E. Yakimenko, C. Joshi, and W. B. Mori, 'Emittance preservation through density ramp matching sections in a plasma wakefield accelerator', Physical Review Accelerators and Beams **23**, 11302 (2020) (cit. on p. 21).

[109]S. van der Meer, *Improving the power efficiency of the plasma wakefield accelerator*, tech. rep. (CERN, 1985) (cit. on p. 21).

[110]K. L. F. Bane, P. Chen, and P. B. Wilson, 'On Collinear Wake Field Acceleration', IEEE Transactions on Nuclear Science **32**, 3524–3526 (1985) (cit. on pp. 21, 24).

[111]P. Chen, J. J. Su, J. M. Dawson, K. L. F. Bane, and P. B. Wilson, 'Energy Transfer in the Plasma Wake-Field Accelerator', Physical Review Letters **56**, 1252–1255 (1986) (cit. on pp. 21, 24).

[112]T. Katsouleas, 'Physical mechanisms in the plasma wake-field accelerator', Physical Review A **33**, 2056–2064 (1986) (cit. on pp. 21, 24).

[113]S. Wilks, T. C. Katsouleas, J. M. Dawson, and J. J. Su, 'Beam Loading Efficiency in Plasma Accelerators', Particle Accelerators **22**, 81–99 (1987) (cit. on p. 22).

[114]M. Tzoufras, W. Lu, F. S. Tsung, C. Huang, W. B. Mori, T. Katsouleas, J. Vieira, R. A. Fonseca, and L. O. Silva, 'Beam loading by electrons in nonlinear plasma wakes', Physics of Plasmas **16**, 056705 (2009) (cit. on pp. 22, 23).

[115]M. Tzoufras, W. Lu, F. S. Tsung, C. Huang, W. B. Mori, T. C. Katsouleas, J. M. Vieira, R. A. Fonseca, and L. O. Silva, 'Beam loading in the nonlinear regime of plasma-based acceleration', Physical Review Letters **101**, 145002 (2008) (cit. on p. 22).

[116]R. Ruth, A. W. Chao, P. L. Morton, and P. B. Wilson, 'A plasma wakefield accelerator', Particle Accelerators **17**, 171–189 (1985) (cit. on p. 24).

[117]P. B. Wilson and J. E. Griffin, 'High energy electron linacs; application to storage ring RF systems and linear colliders', AIP Conference Proceedings **87**, 450–555 (1982) (cit. on p. 24).

[118]A. W. Chao, 'Coherent instabilities of a relativistic bunched beam', in Aip conference proceedings, Vol. 105 (1983), pp. 353–523 (cit. on p. 24).

[119]R. E. Aamodt and W. E. Drummond, 'Resonant Wave—Wave Scattering of Plasma Oscillations', Phys. Fluids **7**, 1816 (1964) (cit. on p. 25).

[120]W. L. Kruer, J. M. Dawson, and R. N. Sudan, 'Trapped-particle instability', Physical Review Letters **23**, 838–841 (1969) (cit. on p. 25).

[121]T. P. Coffey, 'Breaking of large amplitude plasma oscillations', Phys. Fluids **14**, 1402–1406 (1971) (cit. on p. 25).

[122]J. F. Drake, P. K. Kaw, Y. C. Lee, G. Schmidt, C. S. Liu, and M. N. Rosenbluth, 'Parametric instabilities of electromagnetic waves in plasmas', Phys. Fluids **17**, 778–785 (1974) (cit. on p. 25).

[123]J. Weiland and H. Wilhelmsson, 'Coherent non-linear interaction of waves in plasmas', Oxford Pergamon Press International Series on Natural Philosophy **88** (1977) (cit. on p. 25).

[124]P. Chen, J. M. Dawson, R. W. Huff, and T. C. Katsouleas, 'Acceleration of electrons by the interaction of a bunched electron beam with a plasma', Physical Review Letters **54**, 693–696 (1985) (cit. on p. 25).

[125]C. Joshi, 'Plasma-based accelerators: then and now', Plasma Physics and Controlled Fusion **61**, 104001 (2019) (cit. on p. 25).

[126]J. M. Dawson, 'Personal recollections on the development of Plasma Accelerators and light sources', in Aip conference proceedings, Vol. 3, August 2001 (2003), pp. 3–22 (cit. on p. 25).

[127]C. Joshi, T. Tajima, J. M. Dawson, H. A. Baldis, and N. A. Ebrahim, 'Forward Raman Instability and Electron Acceleration', Physical Review Letters **47**, 1285–1288 (1981) (cit. on p. 25).

[128]C. Joshi, C. E. Clayton, and F. F. Chen, 'Resonant self-focusing of laser light in a plasma', Physical Review Letters **48**, 874–877 (1982) (cit. on p. 25).

[129]C. E. Clayton, C. Joshi, C. Darrow, and D. Umstadter, 'Relativistic Plasma-Wave Excitation by Collinear Optical Mixing', Physical Review Letters **54**, 2343–2346 (1985) (cit. on p. 25).

[130]J. B. Rosenzweig, P. Schoessow, B. Cole, W. Gai, R. Konecny, J. Norem, and J. Simpson, 'Experimental measurement of nonlinear plasma wake fields', Physical Review A **39**, 1586–1589 (1989) (cit. on p. 25).

[131]J. B. Rosenzweig, 'Trapping, thermal effects, and wave breaking in the nonlinear plasma wake-field accelerator', Physical Review A **38**, 3634–3642 (1988) (cit. on p. 25).

[132]J. B. Rosenzweig, 'Multiple-fluid models for plasma wake-field phenomena', Physical Review A **40**, 5249–5255 (1989) (cit. on p. 25).

[133]N. Barov, M. E. Conde, W. Gai, and J. B. Rosenzweig, 'Propagation of short electron pulses in a plasma channel', Physical Review Letters **80**, 81–84 (1998) (cit. on p. 25).

[134] Y. Kitagawa, T. Matsumoto, T. Minamihata, K. Sawai, K. Matsuo, K. Mima, K. Nishihara, H. Azechi, K. A. Tanaka, H. Takabe, and S. Nakai, 'Beat-wave excitation of plasma wave and observation of accelerated electrons', Physical Review Letters **68**, 48–51 (1992) (cit. on p. 25).

[135] M. Everett, A. Lal, D. Gordon, C. E. Clayton, K. A. Marsh, and C. Joshi, 'Trapped electron acceleration by a laser-driven relativistic plasma wave', Nature **368**, 527–529 (1994) (cit. on p. 25).

[136] M. J. Hogan, R. W. Assmann, F. J. Decker, R. Iverson, P. Raimondi, S. Rokni, R. H. Siemann, D. Walz, D. Whittum, B. Blue, C. Clayton, E. Dodd, R. Hemker, C. Joshi, K. A. Marsh, W. B. Mori, S. Wang, T. C. Katsouleas, S. Lee, P. Muggli, P. Catravas, S. Chattopadhyay, E. Esarey, and W. P. Leemans, 'E-157: A 1.4-m-long plasma wake field acceleration experiment using a 30 GeV electron beam from the Stanford Linear Accelerator Center Linac', Physics of Plasmas **7**, 2241–2248 (2000) (cit. on p. 25).

[137] P. Muggli, K. Marsh, S. Wang, C. Clayton, S. Lee, T. Katsouleas, and C. Joshi, 'Photo-ionized lithium source for plasma accelerator applications', IEEE Transactions on Plasma Science **27**, 791–799 (1999) (cit. on p. 25).

[138] P. Muggli, B. E. Blue, C. Clayton, S. Deng, F.-J. J. Decker, M. J. Hogan, C. Huang, R. Iverson, C. Joshi, T. C. Katsouleas, S. Lee, W. Lu, K. A. Marsh, W. B. Mori, C. L. O'Connell, P. Raimondi, R. Siemann, and D. Walz, 'Meter-Scale Plasma-Wakefield Accelerator Driven by a Matched Electron Beam', Physical Review Letters **93**, 14802 (2004) (cit. on p. 25).

[139] E. Kallos, T. C. Katsouleas, W. D. Kimura, K. Kusche, P. Muggli, I. Pavlishin, I. Pogorelsky, D. Stolyarov, and V. E. Yakimenko, 'High-Gradient Plasma-Wakefield Acceleration with Two Subpicosecond Electron Bunches', Physical Review Letters **100**, 74802 (2008) (cit. on p. 26).

[140] C. Clayton and C. Joshi, 'The energy-dependent betatron phase advance in the blowout regime-comparison of two methods for estimation', AIP Conference Proceedings **1777** (2016) (cit. on p. 26).

[141] G. Loisch, G. Asova, P. Boonpornprasert, R. Brinkmann, Y. Chen, J. Engel, J. Good, M. Gross, F. Grüner, H. Huck, D. Kalantaryan, M. Krasilnikov, O. Lishilin, A. M. De La Ossa, T. J. Mehrling, D. Melkumyan, A. Oppelt, J. Osterhoff, H. Qian, Y. Renier, F. Stephan, C. Tenholt, V. Wohlfarth, and Q. Zhao, 'Observation of High Transformer Ratio Plasma Wakefield Acceleration', Physical Review Letters **121**, 64801 (2018) (cit. on p. 26).

[142] R. Roussel, G. Andonian, W. Lynn, K. Sanwalka, R. Robles, C. Hansel, A. Deng, G. Lawler, J. B. Rosenzweig, G. Ha, J. Seok, J. G. Power, M. Conde, E. Wisniewski, D. S. Doran, and C. E. Whiteford, 'Single Shot Characterization of High Transformer Ratio Wakefields in Nonlinear Plasma Acceleration', Physical Review Letters **124**, 1–6 (2020) (cit. on pp. 26, 41).

[143] B. E. Blue, C. E. Clayton, C. L. O'Connell, F.-J. Decker, M. J. Hogan, C. Huang, R. Iverson, C. Joshi, T. C. Katsouleas, W. Lu, K. A. Marsh, W. B. Mori, P. Muggli, R. Siemann, and D. Walz, 'Plasma-Wakefield Acceleration of an Intense Positron Beam', Physical Review Letters **90**, 214801 (2003) (cit. on p. 26).

[144]M. J. Hogan, C. E. Clayton, C. Huang, P. Muggli, S. Wang, B. E. Blue, D. Walz, K. A. Marsh, C. L. O'Connell, S. Lee, R. Iverson, F.-J. Decker, P. Raimondi, W. B. Mori, T. C. Katsouleas, C. Joshi, and R. H. Siemann, 'Ultrarelativistic-Positron-Beam Transport through Meter-Scale Plasmas', Physical Review Letters **90**, 205002 (2003) (cit. on p. 26).

[145]P. Muggli, B. E. Blue, C. E. Clayton, F. J. Decker, M. J. Hogan, C. Huang, C. Joshi, T. C. Katsouleas, W. Lu, W. B. Mori, C. L. O'Connell, R. H. Siemann, D. Walz, and M. Zhou, 'Halo Formation and Emittance Growth of Positron Beams in Plasmas', Physical Review Letters **101**, 055001 (2008) (cit. on p. 26).

[146]S. Corde, E. Adli, J. M. Allen, W. An, C. I. Clarke, C. E. Clayton, J. P. Delahaye, J. Frederico, S. Gessner, S. Z. Green, M. J. Hogan, C. Joshi, N. Lipkowitz, M. Litos, W. Lu, K. A. Marsh, W. B. Mori, M. Schmeltz, N. Vafaei-Najafabadi, D. Walz, V. Yakimenko, and G. Yocky, 'Multi-gigaelectronvolt acceleration of positrons in a self-loaded plasma wakefield', Nature **524**, 442–445 (2015) (cit. on p. 26).

[147]A. Aschikhin, C. Behrens, S. Bohlen, J. Dale, N. Delbos, L. Di Lucchio, E. Elsen, J.-H. H. Erbe, M. Felber, B. Foster, L. Goldberg, J. Grebenyuk, J. N. .-.-N. Gruse, B. Hidding, Z. Hu, S. Karstensen, A. Knetsch, O. Kononenko, V. Libov, K. Ludwig, A. R. Maier, A. Martinez De La Ossa, T. J. Mehrling, C. A. J. Palmer, F. Pannek, L. F. Schaper, H. Schlarb, B. Schmidt, S. Schreiber, J.-P. P. Schwinkendorf, H. Steel, M. J. Streeter, G. Tauscher, V. Wacker, S. Weichert, S. Wunderlich, J. Zemella, J. Osterhoff, A. de la Ossa, T. J. Mehrling, J. Osterhoff, C. A. J. Palmer, F. Pannek, L. F. Schaper, H. Schlarb, B. Schmidt, S. Schreiber, J.-P. P. Schwinkendorf, H. Steel, M. J. Streeter, G. Tauscher, V. Wacker, S. Weichert, S. Wunderlich, and J. Zemella, 'The FLASHForward facility at DESY', Nucl. Instrum. Methods Phys. Res. A **806**, 175–183 (2016) (cit. on pp. 29, 41).

[148]T. Heinze, O. Hallonsten, and S. Heinecke, 'Turning the Ship: The Transformation of DESY, 1993–2009', Physics in Perspective **19**, 424–451 (2017) (cit. on p. 31).

[149]V. Ayvazyan, N. Baboi, J. Bähr, V. Balandin, B. Beutner, A. Brandt, I. Bohnet, A. Bolzmann, R. Brinkmann, O. I. Brovko, J. P. Carneiro, S. Casalbuoni, M. Castellano, P. Castro, L. Catani, E. Chiadroni, S. Choroba, A. Cianchi, H. Delsim-Hashemi, G. di Pirro, M. Dohlus, S. Düsterer, H. T. Edwards, B. Faatz, A. A. Fateev, J. Feldhaus, K. Flöttmann, J. Frisch, L. Fröhlich, T. Garvey, U. Gensch, N. Golubeva, H. J. Grabosch, B. Grigoryan, O. Grimm, U. Hahn, J. H. Han, M. V. Hartrott, K. Honkavaara, M. Hüning, R. Ischebeck, E. Jaeschke, M. Jablonka, R. Kammering, V. Katalev, B. Keitel, S. Khodyachykh, Y. Kim, V. Kocharyan, M. Körfer, M. Kollewe, D. Kostin, D. Krämer, M. Krassilnikov, G. Kube, L. Lilje, T. Limberg, D. Lipka, F. Löhl, M. Luong, C. Magne, J. Menzel, P. Michelato, V. Miltchev, M. Minty, W. D. Möller, L. Monaco, W. Müller, M. Nagl, O. Napoly, P. Nicolosi, D. Nölle, T. Nuñez, A. Oppelt, C. Pagani, R. Paparella, B. Petersen, B. Petrosyan, J. Pflüger, P. Piot, E. Plönjes, L. Poletto, D. Proch, D. Pugachov, K. Rehlich, D. Richter, S. Riemann, M. Ross, J. Rossbach, M. Sachwitz, E. L. Saldin, W. Sandner, H. Schlarb, B. Schmidt, M. Schmitz, P. Schmüser, J. R. Schneider, E. A. Schneidmiller, H. J. Schreiber, S. Schreiber, A. V. Shabunov, D. Sertore, S. Setzer, S. Simrock, E. Sombrowski, L. Staykov, B. Steffen, F. Stephan, F. Stulle, K. P. Sytchev, H. Thom, K. Tiedtke, M. Tischer, R. Treusch, D. Trines, I. Tsakov, A. Vardanyan, R. Wanzenberg, T. Weiland, H. Weise, M. Wendt, I. Will, A. Winter, K. Wittenburg, M. V. Yurkov, I. Zagorodnov, P. Zambolin,

and K. Zapfe, 'First operation of a free-electron laser generating GW power radiation at 32 nm wavelength', European Physical Journal D **37**, 297–303 (2006) (cit. on p. 31).

[150]W. Ackermann, G. Asova, V. Ayvazyan, A. Azima, N. Baboi, J. Bähr, V. Balandin, B. Beutner, A. Brandt, A. Bolzmann, R. Brinkmann, O. I. Brovko, M. Castellano, P. Castro, L. Catani, E. Chiadroni, S. Choroba, A. Cianchi, J. T. Costello, D. Cubaynes, J. Dardis, W. Decking, H. Delsim-Hashemi, A. Delserieys, G. Di Pirro, M. Dohlus, S. Düsterer, A. Eckhardt, H. T. Edwards, B. Faatz, J. Feldhaus, K. Flöttmann, J. Frisch, L. Fröhlich, T. Garvey, U. Gensch, C. Gerth, M. Görler, N. Golubeva, H. J. Grabosch, M. Grecki, O. Grimm, K. Hacker, U. Hahn, J. H. Han, K. Honkavaara, T. Hott, M. Hüning, Y. Ivanisenko, E. Jaeschke, W. Jalmuzna, T. Jezynski, R. Kammering, V. Katalev, K. Kavanagh, E. T. Kennedy, S. Khodyachykh, K. Klose, V. Kocharyan, M. Körfer, M. Kollewe, W. Koprek, S. Korepanov, D. Kostin, M. Krassilnikov, G. Kube, M. Kuhlmann, C. L. Lewis, L. Lilje, T. Limberg, D. Lipka, F. Löhl, H. Luna, M. Luong, M. Martins, M. Meyer, P. Michelato, V. Miltchev, W. D. Möller, L. Monaco, W. F. Müller, O. Napieralski, O. Napoly, P. Nicolosi, D. Nölle, T. Nũez, A. Oppelt, C. Pagani, R. Paparella, N. Pchalek, J. Pedregosa-Gutierrez, B. Petersen, B. Petrosyan, G. Petrosyan, L. Petrosyan, J. Pflüger, E. Plönjes, L. Poletto, K. Pozniak, E. Prat, D. Proch, P. Pucyk, P. Radcliffe, H. Redlin, K. Rehlich, M. Richter, M. Roehrs, J. Roensch, R. Romaniuk, M. Ross, J. Rossbach, V. Rybnikov, M. Sachwitz, E. L. Saldin, W. Sandner, H. Schlarb, B. Schmidt, M. Schmitz, P. Schmüser, J. R. Schneider, E. A. Schneidmiller, S. Schnepp, S. Schreiber, M. Seidel, D. Sertore, A. V. Shabunov, C. Simon, S. Simrock, E. Sombrowski, A. A. Sorokin, P. Spanknebel, R. Spesyvtsev, L. Staykov, B. Steffen, F. Stephan, F. Stulle, H. Thom, K. Tiedtke, M. Tischer, S. Toleikis, R. Treusch, D. Trines, I. Tsakov, E. Vogel, T. Weiland, H. Weise, M. Wellhöfer, M. Wendt, I. Will, A. Winter, K. Wittenburg, W. Wurth, P. Yeates, M. V. Yurkov, I. Zagorodnov, and K. Zapfe, 'Operation of a free-electron laser from the extreme ultraviolet to the water window', Nature Photonics **1**, 336–342 (2007) (cit. on p. 31).

[151]S. Schreiber and B. Faatz, 'The free-electron laser FLASH', High Power Laser Science and Engineering **3** (2015) (cit. on p. 31).

[152]P. Schmüser, M. Dohlus, J. Rossbach, and C. Behrens, 'Free-Electron lasers in the ultraviolet and x-ray regime: Physical principles, experimental results, technical realization', Springer Tracts in Modern Physics **258**, 3–5 (2014) (cit. on p. 31).

[153]O. H. Altenmueller, R. R. Larsen, and G. A. Loew, 'Investigations of Traveling-Wave Separators for the Stanford Two-Mile Linear Accelerator', Review of Scientific Instruments **35**, 438–442 (1964) (cit. on p. 34).

[154]M. Röhrs, C. Gerth, H. Schlarb, B. Schmidt, and P. Schmüser, 'Time-resolved electron beam phase space tomography at a soft x-ray free-electron laser', Physical Review Special Topics - Accelerators and Beams **12**, 050704 (2009) (cit. on p. 34).

[155]P. Muggli, V. Yakimenko, M. Babzien, E. Kallos, and K. P. Kusche, 'Generation of trains of electron microbunches with adjustable subpicosecond spacing', Physical Review Letters **101**, 1–4 (2008) (cit. on pp. 35, 47).

[156]C. Behrens, *LAOLA Technical Seminar Dec. 2014: 'FLASHForward—Beamline for plasma experiments at FLASH'*, tech. rep. (2014) (cit. on p. 36).

[157] J. Dale, K. Ludwig, L. Schaper, and J. Osterhoff, *Deutsche Patentanmeldung Nr. 10 2014.116 476.8*, 2014 (cit. on p. 36).

[158] *DESY technical specification No.: Vacuum 005/2008.* 2008 (cit. on p. 38).

[159] P. M. Morse, H. Feshbach, and E. L. Hill, 'Methods of Theoretical Physics', American Journal of Physics **22**, 410–413 (1954) (cit. on p. 38).

[160] J. M. Garland, G. Tauscher, S. Bohlen, G. J. Boyle, R. D'Arcy, L. Goldberg, K. Põder, L. Schaper, B. Schmidt, and J. Osterhoff, 'Combining laser interferometry and plasma spectroscopy for spatially resolved high-sensitivity plasma density measurements in discharge capillaries', Review of Scientific Instruments **92**, 013505 (2021) (cit. on pp. 38, 56).

[161] V. E. Yakimenko, L. Alsberg, E. Bong, G. Bouchard, C. Clarke, C. Emma, S. Z. Green, C. Hast, M. J. Hogan, J. Seabury, N. Lipkowitz, B. D. O'Shea, D. Storey, G. White, and G. Yocky, 'FACET-II facility for advanced accelerator experimental tests', Physical Review Accelerators and Beams **22**, 101301 (2019) (cit. on pp. 40, 41).

[162] M. K. Weikum, T. Akhter, P. D. Alesini, A. S. Alexandrova, M. P. Anania, N. E. Andreev, I. Andriyash, A. Aschikhin, R. W. Assmann, T. Audet, A. Bacci, I. F. Barna, A. Beaton, A. Beck, A. Beluze, A. Bernhard, S. Bielawski, F. G. Bisesto, F. Brandi, O. Bringer, R. Brinkmann, E. Bründermann, M. Büscher, M. Bussmann, G. C. Bussolino, A. Chance, J. C. Chanteloup, M. Chen, E. Chiadroni, A. Cianchi, J. Clarke, J. Cole, M. E. Couprie, M. Croia, B. Cros, P. Crump, G. Dattoli, N. Delerue, O. Delferriere, P. Delinikolas, S. De Nicola, J. Dias, U. Dorda, R. Fedele, A. F. Pousa, M. Ferrario, F. Filippi, J. Fils, G. Fiore, R. A. Fonseca, M. Galimberti, A. Gallo, D. Garzella, P. Gastinel, D. Giove, A. Giribono, L. A. Gizzi, F. J. Grüner, A. F. Habib, T. Heinemann, B. Hidding, B. J. Holzer, S. M. Hooker, T. Hosokai, M. Hübner, A. Irman, F. Jafarinia, D. A. Jaroszynski, S. Jaster-Merz, C. Joshi, M. C. Kaluza, M. Kando, O. S. Karger, S. Karsch, E. Khazanov, D. Khikhlukha, A. Knetsch, D. Kocon, P. Koester, O. Kononenko, G. Korn, I. Kostyukov, K. Kruchinin, L. Labate, C. Lechner, W. P. Leemans, A. Lehrach, F. Y. Li, X. Li, V. Libov, A. Lifschitz, V. Litvinenko, W. Lu, O. Lundh, A. R. Maier, V. Malka, G. G. Manahan, S. P. D. Mangles, B. Marchetti, A. Marocchino, A. M. de la Ossa, J. L. Martins, P. Mason, F. Massimo, F. Mathieu, G. Maynard, Z. Mazzotta, T. J. Mehrling, A. Y. Molodozhentsev, A. Mostacci, A. S. Müller, C. D. Murphy, Z. Najmudin, P. A. P. Nghiem, F. Nguyen, P. Niknejadi, J. Osterhoff, D. Papadopoulos, B. Patrizi, V. Petrillo, M. A. Pocsai, K. Poder, R. Pompili, L. Pribyl, D. Pugacheva, S. Romeo, P. P. Rajeev, M. R. Conti, A. R. Rossi, R. Rossmanith, E. Roussel, A. A. Sahai, G. Sarri, L. Schaper, P. Scherkl, U. Schramm, C. B. Schroeder, J. Schwindling, J. Scifo, L. Serafini, Z. M. Sheng, L. O. Silva, T. Silva, C. Simon, U. Sinha, A. Specka, M. J. V. Streeter, E. N. Svystun, D. Symes, C. Szwaj, G. Tauscher, D. Terzani, N. Thompson, G. Toci, P. Tomassini, R. Torres, D. Ullmann, C. Vaccarezza, M. Vannini, J. M. Vieira, F. Villa, C. .-.-G. Wahlström, R. Walczak, P. A. Walker, K. Wang, C. P. Welsch, J. Wolfenden, G. Xia, M. Yabashi, L. Yu, J. Zhu, and A. Zigler, 'EuPRAXIA – a compact, cost-efficient particle and radiation source', AIP Conference Proceedings **2160**, 040012 (2019) (cit. on p. 40).

[163] G. Ha, M. H. Cho, W. Namkung, J. G. Power, D. S. Doran, E. E. Wisniewski, M. Conde, W. Gai, W. Liu, C. Whiteford, Q. Gao, K.-J. Kim, A. Zholents, Y.-E. Sun, C. Jing, and P. Piot, 'Precision Control of the Electron Longitudinal Bunch Shape Using an Emittance-Exchange Beam Line', Physical Review Letters **118**, 104801 (2017) (cit. on p. 40).

[164]A. Caldwell, E. Gschwendtner, K. Lotov, P. Muggli, and M. Wing, *Physics of AWAKE Run 2*, tech. rep. (CERN, 2021) (cit. on p. 40).

[165]R. D'Arcy, A. Aschikhin, S. Bohlen, G. Boyle, T. Brümmer, J. Chappell, S. Diederichs, B. Foster, M. J. Garland, L. Goldberg, P. Gonzalez, S. Karstensen, A. Knetsch, P. Kuang, V. Libov, K. Ludwig, A. de la Ossa, F. Marutzky, M. Meisel, T. J. Mehrling, P. Niknejadi, K. Põder, P. Pourmoussavi, M. Quast, J. .-.-H. H. Röckemann, L. Schaper, B. Schmidt, S. Schröder, J. P. .-.-P. Schwinkendorf, B. Sheeran, G. Tauscher, S. Wesch, M. Wing, P. Winkler, M. Zeng, J. Osterhoff, A. Martinez de la Ossa, F. Marutzky, M. Meisel, T. J. Mehrling, P. Niknejadi, K. Põder, P. Pourmoussavi, M. Quast, J. .-.-H. H. Röckemann, L. Schaper, B. Schmidt, S. Schröder, J. P. .-.-P. Schwinkendorf, B. Sheeran, G. Tauscher, S. Wesch, M. Wing, P. Winkler, M. Zeng, and J. Osterhoff, 'FLASHForward: plasma wakefield accelerator science for high-average-power applications', Philosophical Transactions of the Royal Society A: Mathematical, Physical and Engineering Sciences **377**, 20180392 (2019) (cit. on p. 41).

[166]V. E. Yakimenko, Y. Cai, C. Clarke, S. Z. Green, C. Hast, M. J. Hogan, N. Lipkowitz, N. Phinney, G. White, and G. Yocky, 'FACET-II: Accelerator research with beams of extreme intensities', IPAC 2016 - Proceedings of the 7th International Particle Accelerator Conference, 1067–1070 (2016) (cit. on p. 41).

[167]*Technical Design Report for the FACET-II Project at SLAC National Accelerator Laboratory*, tech. rep. (SLAC National Accelerator Laboratory (SLAC), Menlo Park, CA (United States), 2016) (cit. on p. 41).

[168]M. Ferrario, D. Alesini, A. Bacci, M. Bellaveglia, R. Boni, M. Boscolo, M. Castellano, L. Catani, E. Chiadroni, S. Cialdi, A. Cianchi, A. Clozza, L. Cultrera, G. Di Pirro, A. Drago, A. Esposito, L. Ficcadenti, D. Filippetto, V. Fusco, A. Gallo, G. Gatti, A. Ghigo, L. Giannessi, C. Ligi, M. Mattioli, M. Migliorati, A. Mostacci, P. Musumeci, E. Pace, L. Palumbo, L. Pellegrino, M. Petrarca, M. Quattromini, R. Ricci, C. Ronsivalle, J. Rosenzweig, A. R. Rossi, C. Sanelli, L. Serafini, M. Serio, F. Sgamma, B. Spataro, F. Tazzioli, S. Tomassini, C. Vaccarezza, M. Vescovi, and C. Vicario, 'Direct Measurement of the Double Emittance Minimum in the Beam Dynamics of the Sparc High-Brightness Photoinjector', Physical Review Letters **99**, 234801 (2007) (cit. on p. 41).

[169]M. Ferrario, D. Alesini, A. Bacci, M. Bellaveglia, R. Boni, M. Boscolo, P. Calvani, M. Castellano, E. Chiadroni, A. Cianchi, L. Cultrera, G. Di Pirro, L. Ficcadenti, D. Filippetto, A. Gallo, G. Gatti, L. Giannessi, M. Labat, S. Lupi, B. Marchetti, C. Marrelli, M. Migliorati, A. Mostacci, D. Nicoletti, E. Pace, L. Palumbo, V. Petrillo, M. Quattromini, C. Ronsivalle, A. R. Rossi, J. Rosenzweig, L. Serafini, M. Serluca, B. Spataro, H. Tomizawa, C. Vaccarezza, and C. Vicario, 'Laser comb with velocity bunching: Preliminary results at SPARC', Nucl. Instrum. Methods Phys. Res. A **637**, S43–S46 (2011) (cit. on p. 41).

[170]M. Ferrario, D. Alesini, M. Anania, A. Bacci, M. Bellaveglia, O. Bogdanov, R. Boni, M. Castellano, E. Chiadroni, A. Cianchi, S. B. Dabagov, C. D. Martinis, D. D. Giovenale, G. D. Pirro, U. Dosselli, A. Drago, A. Esposito, R. Faccini, A. Gallo, M. Gambaccini, C. Gatti, G. Gatti, A. Ghigo, D. Giulietti, A. Ligidov, P. Londrillo, S. Lupi, A. Mostacci, E. Pace, L. Palumbo, V. Petrillo, R. Pompili, A. R. Rossi, L. Serafini, B. Spataro, P. Tomassini, G. Turchetti, C. Vaccarezza, F. Villa, G. Dattoli, E. D. Palma, L. Giannessi, A. Petralia, C. Ronsivalle, I. Spassovsky, V. Surrenti, L. Gizzi, L. Labate, T. Levato, and

J. V. Rau, 'SPARC-LAB present and future', Nucl. Instrum. Methods Phys. Res. B **309**, 183–188 (2013) (cit. on p. 41).

[171] A. R. Rossi, A. Bacci, M. Belleveglia, E. Chiadroni, A. Cianchi, G. Di Pirro, M. Ferrario, A. Gallo, G. Gatti, C. Maroli, A. Mostacci, V. Petrillo, L. Serafini, P. Tomassini, and C. Vaccarezza, 'The External-Injection experiment at the SPARC-LAB facility', Nucl. Instrum. Methods Phys. Res. A **740**, 60–66 (2014) (cit. on p. 41).

[172] A. Marocchino, E. Chiadroni, M. Ferrario, F. Mira, and A. R. Rossi, 'Design of high brightness Plasma Wakefield Acceleration experiment at SPARC_LAB test facility with particle-in-cell simulations', Nucl. Instrum. Methods Phys. Res. A **909**, 408–413 (2018) (cit. on p. 41).

[173] E. Gschwendtner, E. Adli, L. D. Amorim, R. Apsimon, R. W. Assmann, A. M. Bachmann, F. Batsch, J. Bauche, V. K. Berglyd Olsen, M. Bernardini, R. Bingham, B. Biskup, T. Bohl, C. Bracco, P. N. Burrows, G. Burt, B. Buttenschön, A. Butterworth, A. Caldwell, M. Cascella, E. Chevallay, S. Cipiccia, H. Damerau, L. Deacon, P. Dirksen, S. Doebert, U. Dorda, J. Farmer, V. Fedosseev, E. Feldbaumer, R. Fiorito, R. Fonseca, F. Friebel, A. A. Gorn, O. Grulke, J. Hansen, C. Hessler, W. Hofle, J. Holloway, M. Hüther, D. A. Jaroszynski, L. Jensen, S. Jolly, A. Joulaei, M. Kasim, F. Keeble, Y. Li, S. Liu, N. Lopes, K. V. Lotov, S. Mandry, R. Martorelli, M. Martyanov, S. Mazzoni, O. Mete, V. A. Minakov, J. Mitchell, J. Moody, P. Muggli, Z. Najmudin, P. Norreys, E. Öz, A. Pardons, K. Pepitone, A. Petrenko, G. Plyushchev, A. Pukhov, K. Rieger, H. Ruhl, F. Salveter, N. Savard, J. Schmidt, A. Seryi, E. Shaposhnikova, Z. M. Sheng, P. Sherwood, L. O. Silva, L. Soby, A. P. Sosedkin, R. I. Spitsyn, R. Trines, P. V. Tuev, M. Turner, V. Verzilov, J. M. Vieira, H. Vincke, Y. Wei, C. P. Welsch, M. Wing, G. Xia, and H. Zhang, 'AWAKE, The Advanced Proton Driven Plasma Wakefield Acceleration Experiment at CERN', Nucl. Instrum. Methods Phys. Res. A **829**, 76–82 (2016) (cit. on p. 41).

[174] A. Caldwell, E. Adli, L. D. Amorim, R. Apsimon, T. Argyropoulos, R. W. Assmann, A. M. Bachmann, F. Batsch, J. Bauche, V. K. Berglyd Olsen, M. Bernardini, R. Bingham, B. Biskup, T. Bohl, C. Bracco, P. N. Burrows, G. Burt, B. Buttenschön, A. Butterworth, M. Cascella, S. Chattopadhyay, E. Chevallay, S. Cipiccia, H. Damerau, L. Deacon, P. Dirksen, S. Doebert, U. Dorda, E. Elsen, J. Farmer, S. Fartoukh, V. Fedosseev, E. Feldbaumer, R. Fiorito, R. Fonseca, F. Friebel, G. Geschonke, B. Goddard, A. A. Gorn, O. Grulke, E. Gschwendtner, J. Hansen, C. Hessler, S. Hillenbrand, W. Hofle, J. Holloway, C. Huang, M. Hüther, D. A. Jaroszynski, L. Jensen, S. Jolly, A. Joulaei, M. Kasim, F. Keeble, R. Kersevan, N. Kumar, Y. Li, S. Liu, N. Lopes, K. V. Lotov, W. Lu, J. Machacek, S. Mandry, I. Martin, R. Martorelli, M. Martyanov, S. Mazzoni, M. Meddahi, L. Merminga, O. Mete, V. A. Minakov, J. Mitchell, J. Moody, A. S. Müller, Z. Najmudin, T. C. Noakes, P. Norreys, J. Osterhoff, E. Öz, A. Pardons, K. Pepitone, A. Petrenko, G. Plyushchev, J. Pozimski, A. Pukhov, O. Reimann, K. Rieger, S. Roesler, H. Ruhl, T. Rusnak, F. Salveter, N. Savard, J. Schmidt, H. von der Schmitt, A. Seryi, E. Shaposhnikova, Z. M. Sheng, P. Sherwood, L. O. Silva, F. Simon, L. Soby, A. P. Sosedkin, R. I. Spitsyn, T. Tajima, R. Tarkeshian, H. Timko, R. Trines, T. Tückmantel, P. V. Tuev, M. Turner, F. Velotti, V. Verzilov, J. M. Vieira, H. Vincke, Y. Wei, C. P. Welsch, M. Wing, G. Xia, V. E. Yakimenko, H. Zhang, and F. Zimmermann, 'Path to AWAKE: Evolution of the concept', Nucl. Instrum. Methods Phys. Res. A **829**, 3–16 (2016) (cit. on p. 41).

[175] P. Muggli, E. Adli, R. Apsimon, F. Asmus, R. Baartman, A.-M. Bachmann, M. Barros Marin, F. Batsch, J. Bauche, V. K. Berglyd Olsen, M. Bernardini, B. Biskup, E. B. Vinuela, A. Boccardi, T. Bogey, T. Bohl, C. Bracco, F. Braunmuller, S. Burger, G. Burt, S. Bustamante, B. Buttenschön, A. Butterworth, A. Caldwell, M. Cascella, E. Chevallay, M. Chung, H. Damerau, L. Deacon, A. Dexter, P. Dirksen, S. Doebert, J. Farmer, V. Fedosseev, T. Feniet, G. Fior, R. Fiorito, R. Fonseca, F. Friebel, P. Gander, S. Gessner, I. Gorgisyan, A. A. Gorn, O. Grulke, E. Gschwendtner, A. Guerrero, J. Hansen, C. Hessler, W. Hofle, J. Holloway, M. Hüther, M. Ibison, M. R. Islam, L. Jensen, S. Jolly, M. Kasim, F. Keeble, S.-Y. Kim, F. Kraus, A. Lasheen, T. Lefevre, G. LeGodec, Y. Li, S. Liu, N. Lopes, K. V. Lotov, M. Martyanov, S. Mazzoni, D. Medina Godoy, O. Mete, V. A. Minakov, R. Mompo, J. Moody, M. T. Moreira, J. Mitchell, C. Mutin, P. Norreys, E. Öz, E. Ozturk, W. Pauw, A. Pardons, C. Pasquino, K. Pepitone, A. Petrenko, S. Pitmann, G. Plyushchev, A. Pukhov, K. Rieger, H. Ruhl, J. Schmidt, I. A. Shalimova, E. Shaposhnikova, P. Sherwood, L. Silva, A. P. Sosedkin, R. Speroni, R. I. Spitsyn, K. Szczurek, J. Thomas, P. V. Tuev, M. Turner, V. Verzilov, J. Vieira, H. Vincke, C. P. Welsch, B. Williamson, M. Wing, G. Xia, and H. Zhang, 'AWAKE readiness for the study of the seeded self-modulation of a 400 GeV proton bunch', Plasma Physics and Controlled Fusion **60**, 014046 (2018) (cit. on p. 41).

[176] E. Adli, A. Ahuja, O. Apsimon, R. Apsimon, A.-M. A. A.-M. Bachmann, D. Barrientos, F. Batsch, J. Bauche, V. K. Berglyd Olsen, M. Bernardini, T. Bohl, C. Bracco, F. Braun-müller, G. Burt, B. Buttenschön, A. Caldwell, M. Cascella, J. Chappell, E. Chevallay, M. Chung, D. Cooke, H. Damerau, L. Deacon, L. H. Deubner, A. Dexter, S. Doebert, J. Farmer, V. N. Fedosseev, R. Fiorito, R. A. Fonseca, F. Friebel, L. Garolfi, S. J. Gessner, I. Gorgisyan, A. A. Gorn, E. Granados, O. Grulke, E. Gschwendtner, J. Hansen, A. Helm, J. R. Henderson, M. Hüther, M. Ibison, L. Jensen, S. Jolly, F. Keeble, S.-Y. S. S.-Y. Kim, F. Kraus, Y. Li, S. Liu, N. Lopes, K. V. Lotov, L. Maricalva Brun, M. Martyanov, S. Mazzoni, D. Medina Godoy, V. A. Minakov, J. Mitchell, J. C. Molendijk, J. T. Moody, M. Moreira, P. Muggli, E. Öz, C. Pasquino, A. Pardons, F. Peña Asmus, K. Pepitone, A. Perera, A. Petrenko, S. Pitman, A. Pukhov, S. Rey, K. Rieger, H. Ruhl, J. S. Schmidt, I. A. Shalimova, P. Sherwood, L. O. Silva, L. Soby, A. P. Sosedkin, R. Speroni, R. I. Spitsyn, P. V. Tuev, M. Turner, F. Velotti, L. Verra, V. A. Verzilov, J. M. Vieira, C. P. Welsch, B. Williamson, M. Wing, B. Woolley, G. Xia, D. Medina, and F. P. Asmus, 'Acceleration of electrons in the plasma wakefield of a proton bunch', Nature **561**, 363–367 (2018) (cit. on p. 41).

[177] *FLASHForward makes waves*, `https://www.desy.de/news/news_search/index_eng.html?openDirectAnchor=1424&two_columns=1`, accessed on 20.05.2021 (cit. on p. 43).

[178] C. Utrilla, *Erzeugung und Transport von Doppelpaket-Elektronenstrahlen im FLASH Linearbeschleuniger*, Master Thesis, 2014 (cit. on p. 47).

[179] B. Marchetti, A. Grudiev, P. Craievich, R. Assmann, H.-H. Braun, N. Catalan Lasheras, F. Christie, R. D'Arcy, R. Fortunati, R. Ganter, P. González Caminal, M. Hoffmann, M. Huening, S. M. Jaster-Merz, R. Jonas, F. Marcellini, D. Marx, G. McMonagle, J. Osterhoff, M. Pedrozzi, E. Prat Costa, S. Reiche, M. Reukauff, S. Schreiber, G. Tews, M. Vogt, S. Wesch, and W. Wuensch, 'Experimental demonstration of novel beam characterization using a polarizable X-band transverse deflection structure', Scientific Reports **11**, 3560 (2021) (cit. on p. 48).

[180] J. Vieira, W. B. Mori, and P. Muggli, 'Hosing Instability Suppression in Self-Modulated Plasma Wakefields', Physical Review Letters **112**, 205001 (2014) (cit. on p. 52).

[181] T. J. Mehrling, R. A. Fonseca, A. Martinez de la Ossa, and J. Vieira, 'Mitigation of the Hose Instability in Plasma-Wakefield Accelerators', Physical Review Letters **118**, 174801 (2017) (cit. on p. 52).

[182] R. Lehe, C. B. Schroeder, J.-L. Vay, E. Esarey, and W. P. Leemans, 'Saturation of the Hosing Instability in Quasilinear Plasma Accelerators', Physical Review Letters **119**, 244801 (2017) (cit. on p. 52).

[183] T. J. Mehrling, C. Benedetti, C. B. Schroeder, E. Esarey, and W. P. Leemans, 'Suppression of Beam Hosing in Plasma Accelerators with Ion Motion', Physical Review Letters **121**, 264802 (2018) (cit. on p. 52).

[184] R. Pompili, D. Alesini, M. P. Anania, M. Behtouei, M. Bellaveglia, A. Biagioni, F. G. Bisesto, M. Cesarini, E. Chiadroni, A. Cianchi, G. Costa, M. Croia, A. Del Dotto, D. Di Giovenale, M. Diomede, F. Dipace, M. Ferrario, A. Giribono, V. Lollo, L. Magnisi, M. Marongiu, A. Mostacci, L. Piersanti, G. Di Pirro, S. Romeo, A. R. Rossi, J. Scifo, V. Shpakov, C. Vaccarezza, F. Villa, and A. Zigler, 'Energy spread minimization in a beam-driven plasma wakefield accelerator', Nature Physics **17**, 499–503 (2021) (cit. on p. 52).

[185] K. Bane and G. Stupakov, 'Corrugated pipe as a beam dechirper', Nucl. Instrum. Methods Phys. Res. A **690**, 106–110 (2012) (cit. on p. 52).

[186] S. Antipov, S. Baturin, C. Jing, M. Fedurin, A. Kanareykin, C. Swinson, P. Schoessow, W. Gai, and A. Zholents, 'Experimental Demonstration of Energy-Chirp Compensation by a Tunable Dielectric-Based Structure', Physical Review Letters **112**, 114801 (2014) (cit. on p. 52).

[187] S. Lee, T. C. Katsouleas, P. Muggli, W. B. Mori, C. Joshi, R. Hemker, E. S. Dodd, C. Clayton, K. A. Marsh, B. Blue, S. Wang, R. W. Assmann, F. J. Decker, M. J. Hogan, R. Iverson, and D. Walz, 'Energy doubler for a linear collider', Physical Review Special Topics - Accelerators and Beams **5**, 8–11 (2002) (cit. on p. 59).

[188] T. O. Raubenheimer, 'An Afterburner at the ILC: The Collider Viewpoint', AIP Conference Proceedings **737**, 86–94 (2004) (cit. on p. 59).

Acronyms

ANL	Argonne National Laboratory
AWA	Argonne Wakefield Accelerator facility
AWAKE	Advanced Proton Driven Plasma Wakefield Acceleration Experiment
BNS	Balakin-Novokhatsky-Smirnov
BPM	Beam Position Monitor
CLIC	Compact Linear Collider
CSR	Coherent Synchrotron Radiation
DESY	Deutsches Elektronen-SYnchrotron
EEX	Emittance EXchange
EuPRAXIA	European Plasma Research Accelerator with eXcellence In Applications
FACET	Facility for Advanced Accelerator Experimental Tests
FEL	Free-Electron-Laser
FFTB	Final Focus Test Beam
FWHM	Full Width at Half Maximum
FLASH	Free-Electron-Laser Hamburg
FLASHForward	Future Oriented Wakefield Acceleration Research and Development at FLASH
ILC	International Linear Collider
IP	Interaction Point
LCLS	Linac Coherent Light Source
linac	linear accelerator
LSC	Longitudinal Space Charge
PIC	Particle-In-Cell
PITZ	The Photo Injector Test Facility at DESY, Zeuthen
RF	Radio-Frequency
rms	root-mean-square
SLAC	Stanford Linear ACcelerator
TDS	Transverse Deflecting Structure

TESLA   TeV Superconducting Linear Accelerator

UHV   Ultra-High Vacuum

List of Figures

List of Tables

Acknowledgements

This thesis emerged from the constant exchange with many generous and helpful people with whom I have enjoyed working in recent years and whom I would like to express my cordial thanks for their support.

First and foremost, I would like to thank my supervisor *Jens Osterhoff* for the opportunity to do my doctoral thesis in his great team and at this outstanding environment. The regular discussions were a great source of inspiration and gave me the scientific guidance through this exciting research field. I am deeply grateful for his active support, the permanent encouragement and the fundamental trust he has placed in my work and that has been of inestimable value for the success of this work.

Brian Forster kindly agreed to be my doctoral advisor and has always been a reliable source of help throughout the past years. I am grateful for your tireless patience to put all the hyphens where they belong, thank you very much!

I would like to thank *Prof. Dr. Olle Lundh* for his report on this thesis.

Thank you very much to *Daniela Pfannkuche*, *Gudrid Moortgat-Pick* and *Erika Garutti* for agreeing to be part of the examination committee.

I am very grateful for the support I received from *Bernhard Schmidt*, who has always been a reliable place to seek help or advice over the past few years and has kept me on track with numerous encouragements. Dankschee aa für dess klene bissel Kurpälzisch midde im hoe Nodde, dess waa ma allerid ä grees Freid!

I thank *Arik Willner* for the mentorship throughout the PhD programm.

In completely unexpected encounters on campus, *Erika Garutti*, *Robert Klanner* and *Hartwig Spitzer* triggered an avalanche of motivation several times. Your interest in my advancement, a "courage!" instead of a "goodbye" or an intensive discussion about the deeper meaning of science for society, have enriched me over the past few years.

Many thanks to the entire FLA Group. Above all, I would like to thank the "Beschleunigermannschaft" for the many unforgettable Kümmelmomente (more due to the moments and less the Kümmel) and the countless successful shifts. Without you I probably would have never learnt the Russian anthem and all the other peculiarities needed to know in order to work with the FLASH Linac. *Slava* introduced me to the fundamentals of accelerator physics and the FLASHForward facility. *Stephan* never left a question unanswered but rather intensively dealt with it and generously shared his immense experience and knowledge. I admire your clear thinking and your purposeful approach to any task or problem. *Carl* eventually introduced me to the physics of plasma wakefield accelerators and taught

me the art of deliberately bringing rare and precious shifts to success. Our meetings, which usually lasted several hours, have always been a great source of inspiration with all the physics I've learned, but also through the myriad of philosophical discussions we had. It is a pleasure to work with you! *Severin* always had an unwavering urge to not only find a working solution for a HiPACE simulations, but also to find a well-working solution at any day or night time. *Jimmy* and *Greg* put tremendous efforts into the characterisation of the plasma density profile, I thank you for the intensive collaboration and your support. Greg had also kindly agreed to take a first look at my first pages of this thesis—thank you for your time and generous help! *Theresa* was an excellent office mate with a great deal of Python wisdom and always interesting stories and discussions. I was glad to have the PhD-peer *Pau* around for plenty of discussions and collaborations. *Kai* and his team were always of great help concerning any technical issue. Your availability well beyond normal working hours, and your understanding for the time pressure in science are very special. Likewise, I'd like to thank *Antonio* from MVS, who was also of the utmost importance to finally get the X2 experiment started.

A wise man left me the words: "Die Familie ist das beste Forum zum Erleben von Glück" and as such I am cordially grateful for all the unconditional and extensive support I get from my family. I owe my dear siblings Christoph, Andreas and Christina the intensive training in assertiveness and perseverance from day one, but also the understanding of being stronger in a team. Christoph's patience in letting a small child run around in his lab sparked my curiosity about science early on, and taught me that even the most boring tasks must be done with dedication and care if one doesn't want to do it twice. The joy of discovery that connects me to Andreas regularly drives me away from my desk and into unexpected adventures together. Walking all the path so closely with your dearest sister is a huge stroke of luck, thank you very much for listening, consulting and encouraging me. Thank you also to my five lovely nephews for teaching me how little probability calculations have to do with life. I am sincerely grateful for the support my parents have given me. Your availability at all times and your active support in many respects were of great value on the path I ultimately embarked on.

Eidesstattliche Erklärung / Declaration on oath

Hiermit versichere ich an Eides statt, die vorliegende Dissertation selbst verfasst und keine anderen als die angegebenen Hilfsmittel und Quellen genutzt zu haben. Die eingereichte schriftliche Fassung entspricht der auf dem elektronischen Speichermedium. Die Dissertation wurde in der vorgelegten oder einer ähnlichen Form nicht schon einmal in einem früheren Promotionsverfahren eingereicht.

I hereby affirm, that I wrote the present dissertation myself and that I have not used any other sources than those given. The written version submitted corresponds to that on the electronic storage medium. The dissertation was not submitted in the present or in a similar form in an earlier doctoral procedure.

Hamburg, den 29. November, 2021   Sarah Schröder